Defining the role of Fibroblast growth factor 21 (FGF21) in the pathogenesis of growth hormone resistance and subsequent growth failure in chronic childhood conditions

Jayna Narendra Mistry

Submitted in partial fulfilment of the requirements of the

Degree of Doctor of Philosophy

2018

Centre for Endocrinology

William Harvey Research Institute

Barts and the London School of Medicine and Dentistry

Queen Mary University of London

Statement of Originality

I, Jayna Narendra Mistry, confirm that the research included within this thesis is my own work or that where it has been carried out in collaboration with, or supported by others, that this is duly acknowledged below and my contribution indicated. Previously published material is also acknowledged below.

I attest that I have exercised reasonable care to ensure that the work is original, and does not to the best of my knowledge break any UK law, infringe any third party's copyright or other Intellectual Property Right, or contain any confidential material.

I accept that the College has the right to use plagiarism detection software to check the electronic version of the thesis.

I confirm that this thesis has not been previously submitted for the award of a degree by this or any other university.

Signature: 

Date: 9th August 2018.

Collaborations:

For the recruitment of very pre-term infants as part of a clinical investigation.

Dr Ulla Sankilampi, M.D, PhD and Neonatologist.

Dr Sanna Silvennoinen, M.D and Clinical Educator.

Department of Pediatrics, Kuopio University Hospital, Kuopio, Finland.

For the collection for human growth plate tissue biopsies.

Professor Lars Sävendahl, M.D, PhD, Licenced physician, certified paediatrician and Professor of Pediatric Endocrinology.

Dr Farasat Zaman, PhD and Assistant professor.

Department of Women's and Children's Health, Karolinska Institutet, Stockholm, Sweden.

Sponsorship and PhD supervisors:

PhD sponsorship.

Merck Serono, Grant for Growth Innovation (GGI) 2014.

Merck KGaA, Darmstadt, Germany.

Primary supervisor.

Professor Leo Dunkel, M.D, PhD, Professor of Paediatric Endocrinology and Metabolism and Honorary Consultant in Paediatric Endocrinology.

Centre for Endocrinology, William Harvey Research Institute, Barts & the London Medical School, Queen Mary University of London, London, United Kingdom.

Co-supervisor.

Dr Leonardo Guasti, PhD, Senior Lecturer in Endocrinology.

Centre for Endocrinology, William Harvey Research Institute, Barts & the London Medical School, Queen Mary University of London, London, United Kingdom.

Acknowledgements

I would like to take this opportunity to express my sincere gratitude to the following people who have influenced and supported me throughout my PhD journey.

Firstly, to my primary supervisor Professor Leo Dunkel for giving me a chance to be a part of a truly exciting project which I have thoroughly enjoyed. It has been an honour to work with Professor Dunkel and I am grateful for his patience, encouragement, immense knowledge and for the opportunities which have led to the establishment of our collaborative partners. I am thankful for the experiences, skills and guidance during my project.

To Dr Leonardo Guasti for his invaluable advice and assistance during my experimental lab research and writing. I thank Dr Guasti for his expertise and experience in the research field and for his time in helping me throughout the project.

Merck Serono for the Grant for Growth Innovation (GGI) 2014 award for sponsoring the project for 3 years.

Our collaborators; Professor Lars Sävendahl and Dr Farasat Zaman at Karolinska Institutet for the opportunity to join their team and for their support, guidance and assistance with *ex vivo* experiments. The experience has been invaluable. To Dr Ulla Sankilampi and Dr Sanna Silvennoinen at Kuopio University for their help in the recruitment of paediatric patients for our clinical investigation. I thank all participants involved in this study.

To all members of staff in the Centre for Endocrinology, especially Dr Gerard Ruiz Babot, Dr Tözen Özkan and Alessandra Mancini for their support, direction and friendship. Thank you for making my time at the Centre of Endocrinology an enjoyable experience.

Lastly, to my parents (Narendra Mistry and Kalavati Mistry), my brother (Bhavin Mistry) and partner (Manit Pitroda). Your continuous positivity, guidance, love and care throughout my struggles and successes have pushed me further to reach my ambitious goals. Thank you for your support, motivation and patience throughout my education and life in general. I hope I've made you proud.

Abstract

Fibroblast growth factor 21 (FGF21) is an essential metabolic regulator, adapting to changes in nutritional status. Excessive undernutrition is suggested to elevate FGF21 levels, developing Growth hormone (GH) resistance and subsequent linear growth attenuation through unknown mechanisms. The aim of this PhD was to unravel *in vitro* the mechanistic interplay of FGF21 on GH receptor (GHR) signalling, further determining the association between nutrition induced chronic FGF21 using postnatal growth failure of very pre-term (VPT) infants as a model.

FGF21 and receptor complex (FGFR1/-IIIC/β-Klotho) expression was evaluated in newly established HEK-293 stably expressing human/ mouse GHR. Human growth plate tissue was examined for the localisation of FGF21 and co-receptors within growth plate zonation. Cell lines and/or human growth plate explants were tested for GHR half-life and key GHR signalling mediators; STAT5, SOCS2 and IGF-1 in the presence/ absence of recombinant GH and FGF21. Serially measured FGF21/ IGF-1 levels and nutritional intake were assessed for the association with linear growth trends in VPT infants.

The molecular integrity of GHR signalling and expression of *FGF21* and receptors; *FGFR1*/*-IIIC*/*β-KLOTHO* was confirmed in stable lines. FGF21 and co-receptors were localised within the proliferative and pre-hypertrophic zones of human growth plate tissue. FGF21 increased GH-induced GHR turnover and SOCS2 expression; leading to the inhibition of downstream GHR signalling events including; pSTAT5 and IGF-1 expression. VPT infants displayed an immediate growth failure after birth followed by catch-up. FGF21 levels were elevated during growth deflection compared to catch-up ($p<0.001$). A positive association of fat ($\beta=8.83$, $p=0.004$) and carbohydrate ($\beta=4.11$, $p=0.006$) intake after birth was associated with the change in SD score for length catch-up growth.

Chronic FGF21 inhibited GHR signalling events, playing a central role in GH resistance and growth failure. Nutrition did not regulate hormonal levels, having a direct effect on linear growth catch-up in VPT infants.

Contents

List of Figures

List of Tables

List of Abbreviations

ALS	Acid Labile Subunit
ATF4	Activating Transcription Factor 4
AgC1	Aggrecan
AP	Alkaline Phosphatase
aa	Amino Acid
APS	Ammonium Persulfate
ANOVA	Analysis of Variance
AB/AM	Anti-biotic Anti-mycotic
bp	Base Pairs
BCA	Bicinchoninic Acid
BMPs	Bone Morphogenetic Proteins
BSA	Bovine Serum Albumin
$Ca2^{+}$	Calcium
CREBH	cAMP-Responsive Element Binding Protein
ChoRE	Carbohydrate Response Element
ChREBP	Carbohydrate Response Element Binding Protein
CNS	Central Nervous System
Col1	Collagen Type I
Col2	Collagen Type II
Col2a1 IIb	Collagen Type II Alpa 1 IIb
Col10	Collagen Type 10
CI	Confidence Interval
CIS	SH2-Containing Protein
CHD	Coronary Heart Disease
CT	Cycle Threshold
CHX	Cycloheximide
Da	Dalton
dNTPs	Deoxyribonucleotide Triphosphate
DAG	Diacylglycerol
dH_2O	Distilled H_2O
DMEM	Dulbecco's Modified Eagle Medium

DMEM- F12HAM	Dulbecco’s Modified Eagle Medium/ Nutrient Mixture F-12 Ham
Endo-H	Endo-Glycosidase H
ER	Endoplasmic Reticulum
ER-α	Estrogen Receptor Alpa
ESPE	European Society for Paediatric Endocrinology
ECD	Extracellular Domain
ECM	Extracellular Matrix
FXR	Farnesoid X Receptor
FBS	Fetal Bovine Serum
FGF	Fibroblast Growth Factor
FGF2	Fibroblast Growth Factor 2
FGF21	Fibroblast Growth Factor 21
FGFR	Fibroblast Growth Factor Receptor
FGFR3	Fibroblast Growth Factor Receptor 3
FFA	Free Fatty Acid
GCN2	General Control Non-Derepressible 2
GWAS	Genome Wide Association Studies
GC	Glucocorticoids
GR	Glucocorticoid Receptor
GLUT-1	Glucose Transporter 1
GAPDH	Glyceraldehyde 3-Phosphate Dehydrogenase
GH	Growth Hormone
GHBP	GH Binding Protein
GHD	GH Deficiency
GHI	GH Insensitivity
GHRH	GH-Releasing Hormone
GHR	GH Receptor
GHRE	GH-Responsive Elements
G418	Neomycin
HBS	Heparin Binding Site
HSPG	Heparin Sulfate Proteoglycan
HCD	High Carbohydrate Diet

HFD	High Fat Diet
HDAC3	Histone Deacetylase 3
Hek-293	Human Embryonic Kidney Cell Line
Hek-293 hGHR	Hek-293 Human GHR
Hek-293 mGHR	Hek-293 Mouse GHR
ISS	Idiopathic Short Stature,
Ig-like	Immunoglobulin-Like
Ihh	Indian Hedgehog
ICP	Infancy-Childhood-Puberty Model
IBD	Inflammatory Bowel Disease
IGF-1	Insulin-Like Growth Factor 1
IGF-BP	IGF-Binding Protein
IGF-1R	IGF Receptor
IGFBP-RP	IGFBP-Related Proteins
IRS1	Insulin Receptor Substrate 1
IRS2	Insulin Receptor Substrate 2
IL-6	Interleukin 6
ICD	Intracellular Domain
JAK	Janus Kinase
kb	Kilo-Bases
kDa	Kilodatons
KLB	β-Klotho
KLPH	Klotho-LPH Related Protein
Lctl	Lactase-Like Klotho
LBM	Lean Body Mass
LID	Liver Deficient IGF 1
LXR	Liver X Receptor
LPD	Low-Protein Diet
LB	Luria Broth
MMP	Matrix Metalloproteinase
MAPK	Mitogen-Activated Protein Kinase
M-MLV	Moloney Murine Leukemia Virus

Ncad	Neural-Cadherin
Ncam1	Neural-Cell Adhesion Molecule 1
N-GF	N-Glycosidase F
Osx	Osterix
PTHrP-R	Parathyroid Hormone-Related Protein Receptor
P/S	Penicillin-Streptomycin
PPARα	Peroxisome Proliferator Activated Receptor Alpha
PPRE	Peroxisome Proliferator Response Elements
PPARγ	Peroxisome Proliferator Activated Receptor Gamma
PGC1α	PPARγ Coactivator 1 Alpha
PBS	Phosphate Buffered Saline
PI3K	Phosphatidylinositol-3-Phosphate-Kinase
PDGF	Platelet Derived Growth Factor
PKC	Protein Kinase C
PAGE	Polyacrylamide Gel Electrophoresis
PEI	Polyethylenimine
PCR	Polymerase Chain Reaction
PM	Postmenstrual
PTM	Post-Translational Modification
RIPA	Radio-Immunoprecipitation Assay
RT-qPCR	Real-Time Quantitative PCR
RTKs	Receptor Tyrosine Kinases
rFGF21	Recombinant Fibroblast Growth Factor 21
RNAsin	Ribonuclease Inhibitor
RT	Room Temperature
RUNX2	Runt-Related Transcription Factor 2
STAT	Signal Transducers and Activators of Transcription
SNPs	Single Nucleotide Polymorphisms
SP	Single Peptide
SDS	Sodium Dodecyl Sulfate
SH2	Src homology 2
SEM	Standard Error Mean

SOCS	Suppressor of Cytokine Signalling
TEMED	Tetramethylethylenediamine
TAE	Tris-Acetate-EDTA Buffer
TNF-α	Tumor Necrosis Factor α
Tyr	Tyrosine
T2D	Type 2 Diabetes
VEGFα	Vascular Endothelial Growth Factor Alpha
VPT	Very Pre-term
WAT	White Adipose Tissue
WHO	World Health Organisation

CHAPTER 1. Introduction

Growth is a fundamental process during childhood development, playing a vital role in the overall physical and psychosocial well-being of infants. An evaluation of growth after birth serves as an important screening tool and indicator for a child's health and is routinely measured universally as part of paediatric healthcare practice. Abnormalities in linear growth have overtime become a more frequent concern for families worldwide and today is considered the most common cause for referral to clinical endocrinologists (Doyle, 2015; Oostdijk et al., 2009; Yadav and Dabas, 2015).

Approximately 2.5% of children in the global population present with short stature (Stanley, 2012). Typically it is evaluated by comparing a child's height with that of a large cohort of a similar genetic background, further accounting for mid-parental target height and an assessment of individual growth rate patterns. Clinically, short stature is defined as having a height of more than 2 standard deviations (SDs) below the mean (or below the 2.5 percentile) for equivalent age and sex (Nichols, 2016; Oostdijk et al., 2009; Rogol et al., 2000). Familial short stature, constitutional delay of growth and development and severe chronic conditions (malnutrition, renal insufficiency, gastroenterological disorders, chronic infections/ inflammation, conditions associated with failure to thrive and premature birth) form the three broad categories describing a widely documented list of childhood growth failure (Wheeler et al., 2004). In addition, it is suggested that some individuals may experience psychosocial stress associated with shortness, affecting their ability to cope, increased anxiety and behavioural or emotional disturbance, however there is little evidence to support this phenomenon (Sandberg, 2011).

Preventing short stature is of particular importance for children with debilitating chronic conditions. Growth hormone (GH) therapy is considered as the foremost choice of medical treatment for growth failure (Harris et al., 2004). However, such treatment has proven to be ineffective in conditions of GH resistance, often triggered by a disruption in the growth hormone-insulin-like growth factor 1 (GH/IGF-1) axis (Bang et al., 2011). Several recent studies undertaken in both mice and humans highlight a novel role of Fibroblast growth factor 21 (FGF21) in the development of GH resistance and subsequent growth failure in chronic childhood

conditions (Guasti et al., 2014; Inagaki et al., 2008; Kubicky et al., 2012). However, the precise molecular mechanism of FGF21s' actions remains largely unknown.

This PhD thesis aims to clarify and discuss the mechanistic interplay of FGF21 on GH receptor (GHR) signalling and downstream events, as a potential candidate in childhood growth attenuation. Clarifying the molecular mechanisms of GH resistance causing growth failure in chronic childhood conditions could lead to direct clinical benefits for patients enhancing their therapeutic management and improving overall clinical outcomes. This has the potential to advance the quality of life of children with GH resistance both in the short and long-term.

1.1 An overview of skeletal development and growth plate physiology.

Skeletal bone is specialised and mineralised connective tissue formed of cartilage and bone. The development of skeletal bone in mammals proceeds through a series of complex processes, which ultimately results in the generation of the final adult skeleton. Three distinct embryonic committed lineages initiates the process of bone development; 1) somites develop the axial skeleton and the lateral plate, 2) mesoderm forms the limb skeleton and 3) the cranial neural crest gives rise to the branchial arch and craniofacial bones and cartilage (Olsen et al., 2000). Physiologically the skeletal frame work shares several important functions throughout development; serving as a mechanical and structural support of the body whilst also providing muscle attachment and protection of vital organs and bone marrow. Moreover, it helps maintaining mineral homeostasis and acid-base balance offering an environment enriched with growth factors and cytokines and a site for haematopoiesis within marrow spaces; essential for life (Baron, 2000; Clarke, 2008).

The skeletal structure is grouped into four general categories based on location and morphology. These include the flat bones, (skull, mandible, scapulae, sternum, ribs and ileum) long bones, (clavicles, humeri, radi, ulnae, metacarpals, fermurs, tibiae, fibulae, metatarsals and phalanges) short bones, (carpal and tarsal bones, patellae, and sesamoid bones) and irregular bones (vertebrae, sacrum, coccyx and hyoid bone) (Baron, 2000; Clarke, 2008). The skeletal

backbone is built from condensations of mesenchymal cells that adhere through the expression of adhesion molecules and selective regulatory genes that proceed to differentiate into two distinct processes during embryogenesis; 1) intramembranous ossification and 2) endochondral ossification (Hall and Miyake, 2000; Kronenberg, 2003). Intramembranous ossification is characteristic of the formation of most craniofacial skeletal bone and the medial clavicles. Neural crest-derived mesenchymal cells proliferate and condense into compact nodules through the expression of specific adhesion molecules. These condensations differentiate directly into bone-forming osteoblasts, which later become committed bone precursor cells, expressing a matrix rich in Collagen type I (Col1). Osteoblast differentiation is further driven via the expression of transcription factor Runt-related transcription factor 2 (RUNX2). Moreover, the Wnt/ β-Catenin signalling pathway has been shown to be essential in directing mesenchymal cells into the osteogenic program. Alternatively, endochondral ossification constitutes a greater degree of complexity. Mesenchymal cells can differentiate into chondrocytes (cartilaginous cells), providing a platform for bone morphogenesis. This developmental phase is responsible for the formation of most vertebrate appendicular and axial skeleton (Baron, 2000; Mellis et al., 2011; Ortega et al., 2004).

1.1.1 Longitudinal bone formation and structure.

During embryogenesis, independent ossification centres form the epiphysis, diaphysis and metaphysis at the early stages of embryogenesis. Longitudinal bones are composed of two wider extremities located at the ends of long bone (the epiphysis), a cylinder hollow shaft in the middle (the diaphysis) and a cone-shaped transition zone separating the epiphysis and diaphysis (**Figure 1.1 A**) The diaphysis is composed primarily of dense cortical bone, whilst the metaphysis and epiphysis are composed of a trabecular meshwork bone surrounded by a relatively thin shell of dense cortical bone. The metaphysis forms the wide portion of the long bone found between the epiphysis and the narrow diaphysis playing a key role in growth plate development during childhood (Baron, 2000; Clarke, 2008).

In the early stages of linear bone growth the diaphysis and epiphysis begins to separate, forming the epiphyseal line; commonly referred to as the growth plate (**Figure 1.1 B**). The growth plate is well known as a vital tissue, determining the future length and shape of the mature bone. Skeletal bone development undergoes longitudinal and radial growth and remodelling. This is demonstrated throughout childhood and adolescence (Clarke, 2008). Later in adolescent life at the point when the maximum height potential is achieved, the epiphysis and metaphysis fuse, resulting in linear growth cessation and ossification of the growth plate (Baron, 2000; Clarke, 2008). Fusion of the epiphyseal region is an active process accompanied by an environment of its own hormonal control, cellular mechanisms and structural features. Estrogen is considered a key component in the control of growth plate fusion (Weise et al., 2001). Distinct differences have been shown in humans and rodents comparing longitudinal bone development. Unlike the natural fusion of human growth plate at the stage of full adult height, rodents are shown to grow continuously throughout life and do not experience epiphyseal closure. Alternatively, it is shown that their linear growth rate is considerably reduced with age (Legato, 2004).

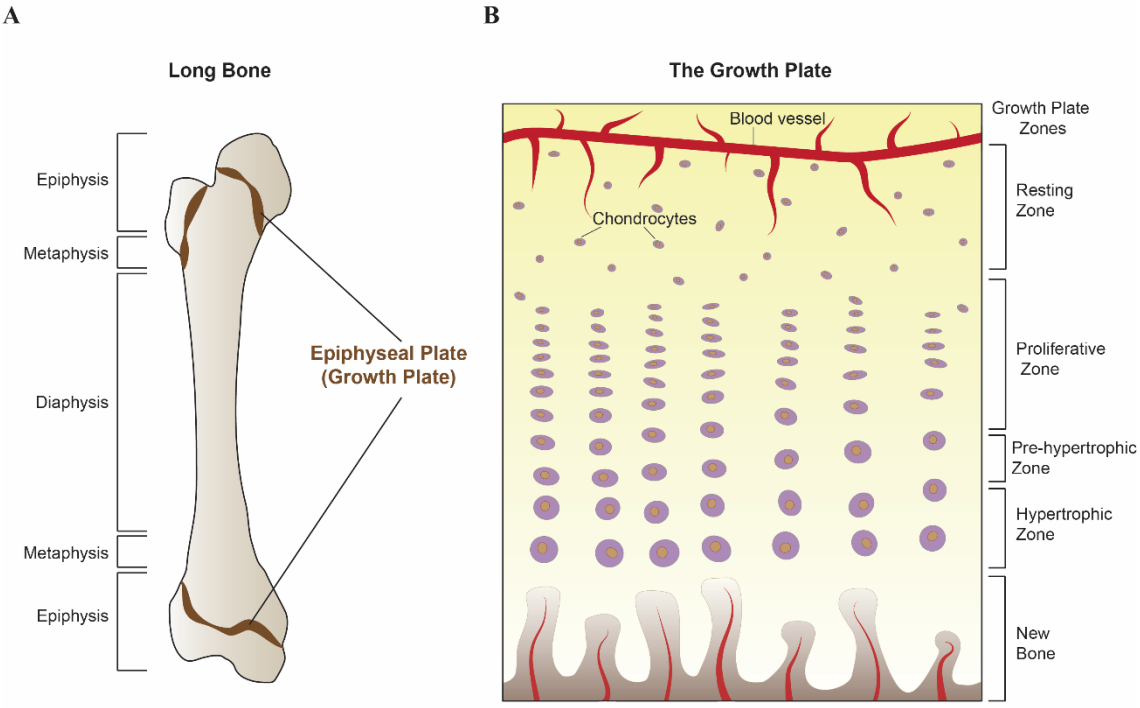

Figure 1.1 An illustration of growth plate development. (A) The long bone is formed of the diaphysis (shaft), epiphysis (end) and metaphysis (between the growth plate and diaphysis). **(B)** The growth plate is organised into a series of anatomic zones; resting, proliferative, pre-hypertrophic and hypertrophic zone. Chondrocytes in the resting zone mature as it passes through each zone, resulting in the formation of new bone. Adapted from (Wolpert, 2011).

1.1.1.1 Endochondral ossification and the growth plate.

Endochondral ossification begins during foetal life and continues until growth ceases in early adulthood. Bone development begins at two distinct sites in the long bones; the primary (diaphyseal) and the secondary (epiphyseal) sites of ossification. The first site of ossification proceeds within the primary centre of ossification at the diaphysis centre (**Figure 1.2 A**). Embryonic mesenchymal cells condense and differentiate into chondrocytes forming the '*cartilage model*'. Ossification of cartilage is followed by hypertrophy of the chondrocytes in the mid-shaft region of the bones. Deposition of a periosteal bone collar by recently differentiated osteoblasts surrounds the mid-shaft. Blood vessels, osteoclasts (cartilage and bone-resorbing cells), bone marrow and osteoblast precursors invade the model via the bone collar which proceeds to form the primary centre of ossification. The primary centre further expands towards the ends of the cartilage model, as the osteoblasts deposit bone on cartilage remnants. In long bones, a secondary ossification centre subsequently forms at each end of the '*cartilage model*', leaving a cartilaginous growth plate between the primary and secondary ossification centres by the segregation of chondrocytes at different stages of differentiation (Mackie et al., 2007; Mackie et al., 2011).

1.1.1.2 Organisation and regulation of growth plate zonation.

The growth plate is a highly organised and spatially polarised structure that is divided into a series of anatomic zones. This include; resting, proliferative, pre-hypertrophic and hypertrophic chondrocytes (Ballock and O'Keefe, 2003) . Each zone displays a unique morphological and biochemical characteristic during the process of chondrocyte differentiation (**Figure 1.1 B**) (Ballock and O'Keefe, 2003; Chagin and Savendahl, 2009). Chondrogenesis is an essential process for the synthesis of new chondrocytes both during embryogenesis and throughout linear development (Marino, 2011).

The initial stage of longitudinal growth begins with the aggregation and condensation of mesenchyme. Bone morphogenetic proteins (BMPs) play an important role in the early stages of

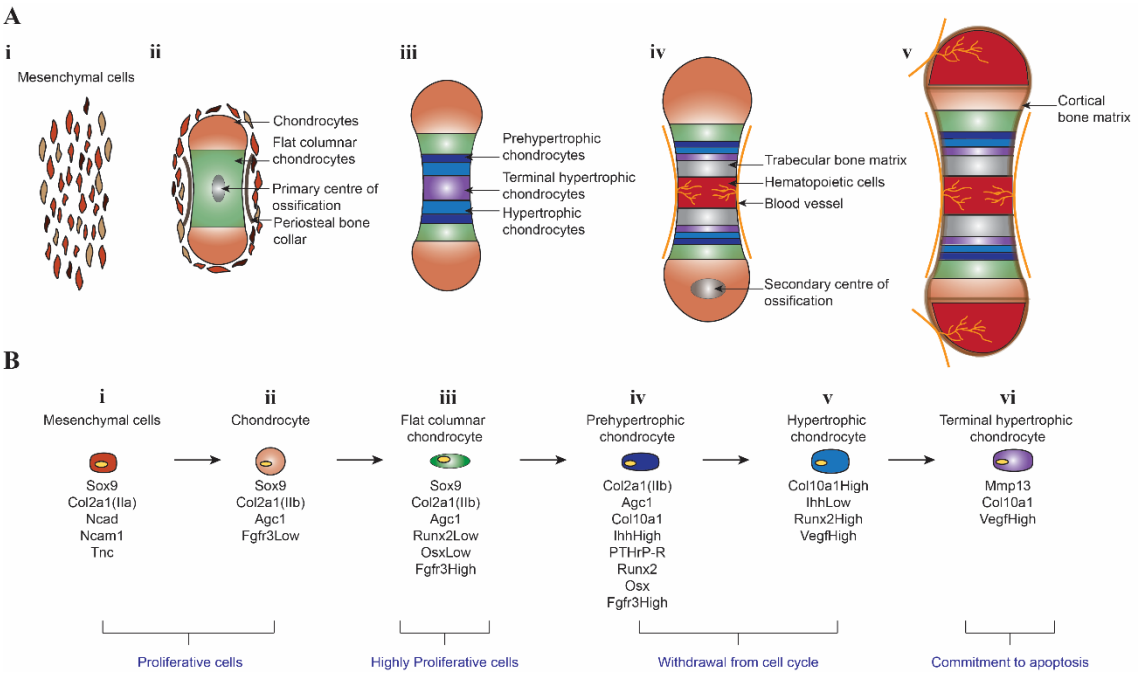

Figure 1.2 The cellular actions and molecular markers of chondrogenesis. (A) Model of endochondral bone development beginning with mesenchymal cell condensation. **(i)** Chondrocyte differentiation and development of cartilage template, **(ii)** chondrocyte maturation and hypertrophy, **(iii)** separation of cartilage growth regions, vascular invasion, and initiation of cortical and trabecular bone, **(iv)** generation of the secondary centre of ossification, separating articular cartilage and the growth plate. **(B)** Model outlining the process of chondrogenesis and chondrocyte differentiation. Markers expressed at each stage of chondrocyte differentiation. Adapted from (Zuscik et al., 2008).

mesenchymal cell condensation and shaping. At the primary phase of chondrogenesis the condensing mesenchyme begin to express an array of Extracellular matrix (ECM) markers and cell adhesion molecules, including; collagen type II (Col2), neural-cadherin (Ncad), neural-cell adhesion molecule 1 (Ncam1), and tenascin C, while also broadly expressing a vital transcription factor, SOX9 (**Figure 1.2 Bi**). The Sox family of transcription factors have an important role throughout chondrogenesis and chondrocyte differentiation. Condensed mesenchyme proceeds to differentiate into resting chondrocytes (the germinal or stem cell zone) and become abundantly expressed in the epiphyseal region of the growth plate. Chondrocytes in the resting zone are small, round, singly or distributed in pairs with a low proliferative rate. Here, they express early chondrocyte lineage markers such as; SOX9, Collagen type II alpa1 IIb (Col2a1 (IIb)), Aggrecan (AgC1), low levels of Fibroblast growth factor receptor 3 (FGFR3) and specific downstream targets of the Indian hedgehog (Ihh) signalling pathway (**Figure 1.2 Bii**).

Resting chondrocytes proceed to enter the matrix-rich proliferating zone, where flattened chondrocytes undergo a series of cell divisions in a longitudinal direction. Here, the chondrocytes become organised into a column orientation (Chagin and Savendahl, 2009; van der Eerden et al., 2003). Proliferative chondrocytes begin to express low levels of Runx2 and Osterix (Osx) and high levels of FGFR3 (**Figure 1.2 Biii**). The synthesis of these ECM proteins aids in the separation of recently divided cells and is considered essential for the structure and function of the growth plate matrix. (Ballock and O'Keefe, 2003; Chagin and Savendahl, 2009; Gat-Yablonski and Phillip, 2015; Mackie et al., 2011).

Subsequently, proliferating chondrocytes begin to lose their proliferative capacity and differentiate into pre-hypertrophic chondrocytes. Morphologically pre-hypertrophic chondrocytes start to enlarge and express Ihh, parathyroid hormone-related protein receptor (PTHrP-R), as well as increase the expression of alkaline phosphatase (AP), that widens the growth plate by increasing phosphate ions required for calcification of the ECM and regulatory transcription factors Runx2 and Osterix which encourages chondrocyte differentiation and assists during cartilage mineralisation (**Figure 1.2 Biv**).

Furthermore, differentiation of chondrocytic cells results in the transitioning of pre-hypertrophic chondrocytes into hypertrophic chondrocytes. Morphologically, hypertrophic chondrocytes increase more in size and roundness, reducing their DNA synthesis with a 10-fold increase in their intracellular volume. Rather than a passive swelling this is an active process, marked by an increase in organelles such as mitochondria and the endoplasmic reticulum. Hypertrophic chondrocytes display an elevated secretion of extracellular matrix proteins including; collagen type 10 (Col10), osteonectin and chondrocalcin displaying an increased intracellular calcium concentration (**Figure 1.2 Bv**). This is essential for the synthesis of matrix vesicles; small membrane-enclosed particles released by chondrocytes (Chagin and Savendahl, 2009). Matrix vesicles contain large amounts of annexins, which mediates calcium uptake. These vesicles secrete calcium-phosphates, hyproxyapatite and matrix metalloproteinases (MMPs), which causes mineralisation of vesicle and its surrounding matrix. The calcification of the matrix that surrounds chondrocytes, provides a platform for the formation of new bone tissue (Chagin

and Savendahl, 2009; Marino, 2011). In addition, the release of angiogenic factors such as; Vascular Endothelial Growth Factors (VEGFα) and Fibroblast growth factor 2 (FGF2) secreted by terminally differentiated hypertrophic chondrocytes stimulates the invasion of cartilage by blood vessels and bone cells (**Figure 1.2 Biv**). Only the most terminally differentiated hypertrophic chondrocytes express the matrix degrading enzyme Mmp13; an enzyme that regulates mineralisation of osteoblasts, required for the creation of bone marrow space that supports vascular invasion. Thus, the vascularisation and invasion of cartilage leads to the generation of new bone. Ultimately, hypertrophic chondrocytes stop dividing and undergo apoptosis (Ballock and O'Keefe, 2003; Chagin and Savendahl, 2009; Gat-Yablonski and Phillip, 2015; Zuscik et al., 2008).

Linear bone growth proceeds in parallel with the production of chondrocytes. The progression from proliferating to terminally differentiated hypertrophic cells is key for the growth of those skeletal elements, formed by endochondral ossification. Without chondrocyte proliferation and hypertrophy endochondral bones cannot grow in length, and without hypertrophic cell death and the concomitant vascular invasion the cartilage model cannot be replaced by bone.

1.1.2 Growth plate senescence.

Linear growth in humans proceeds rapidly during the prenatal and early postnatal stages of life, followed by a period of slow growth and eventual cessation at maximum adult height. The decline in growth rate however does not appear to be caused by a change in hormonal levels but rather by systemic mechanisms intrinsic to the growth plate. This postnatal program induces both a progressive loss of function and progressive structural involution, termed as '*programmed growth plate senescence*' (Nilsson and Baron, 2005).

The senescent decline in growth rate as observed with age is driven by a decline in the proliferative capacity of chondrocytes resulting in subsequent structural and functional change within the growth plate (Lui et al., 2011). Primarily, programmed senescence begins with a

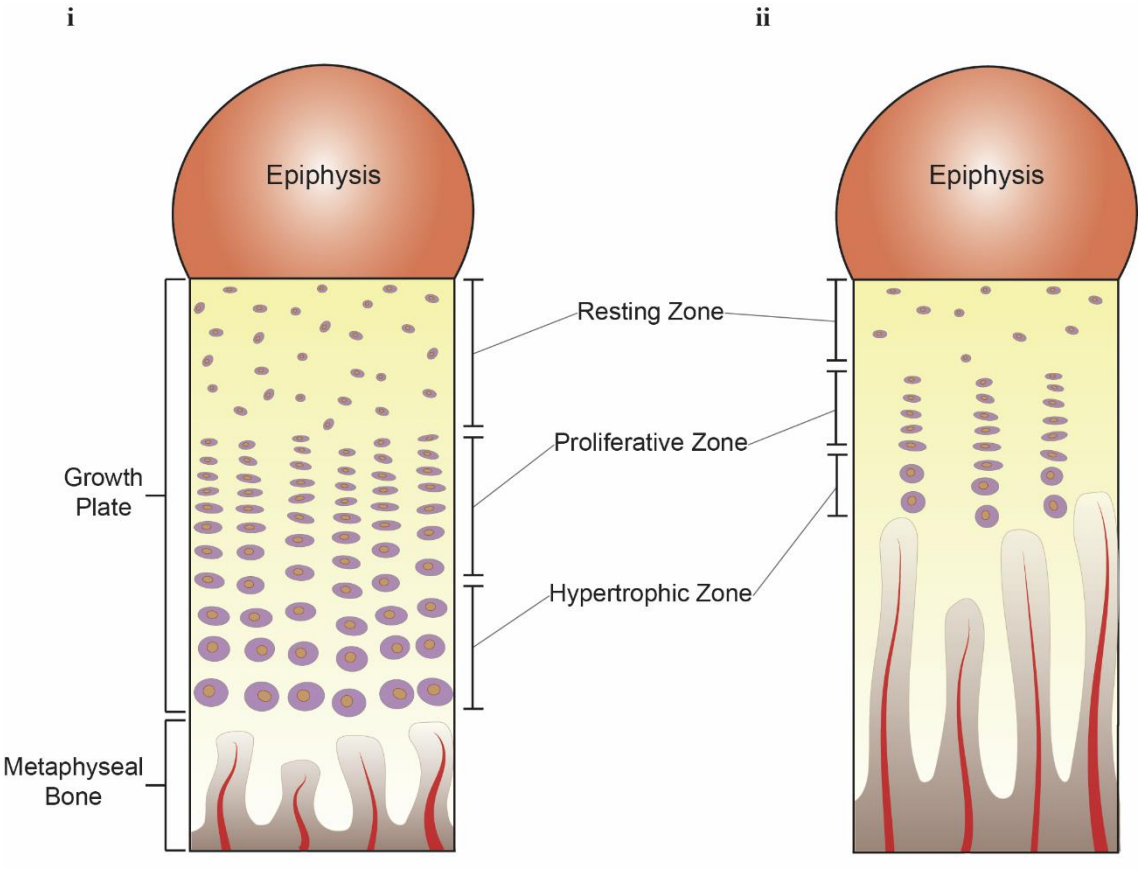

Figure 1.3 Structural changes during growth plate senescence. (i) The growth plate during prenatal and early postnatal stages of life. **(ii)** A senescent decline in growth rate, observed through a reduction in the overall height of the growth plate and of each growth plate zone. Adapted from (Nilsson and Baron, 2004).

reduction in the overall height of the growth plate and consequent reduction in the area of each zone within the growth plate. This phenomenon is accompanied by a decrease in the number of resting zone chondrocytes and the number of proliferative and hypertrophic chondrocytes per column. Columns become more widely spaced, whilst the size of hypertrophic cells become smaller (**Figure 1.3**). Moreover, an age dependent increase in the apoptosis of hypertrophic chondrocytes has been reported to contribute to the age-dependent decline in growth rate (Nilsson and Baron, 2004; Weise et al., 2001). In humans, estrogen accelerates this developmental process, particularly through the rapid depletion of resting chondrocytes, thus playing a key role in bone elongation at puberty and epiphyseal closure (Rochira et al., 2015).

These senescent changes have been widely studied in rodents and rabbits. An *in vivo* study undertaken by Stevens et al., 1999 involved the transplantation of growth plates between rabbits of different ages, which resulted in different growth rates in the recipient. The growth rate

of transplanted growth plates were highly dependent on the age of the donor animal, i.e. younger age donors led to a higher growth rate in both young and older recipients. Thus, this study further confirms that the age-dependent decline in growth rate is due to a mechanism that is intrinsic to the growth plate rather than to a systemic mechanism (Lui et al., 2011; Stevens et al., 1999).

1.1.2.1 Growth plate fusion and final height.

In humans and most mammals growth plate senescence is followed by epiphyseal fusion; an abrupt event in which the growth plate cartilage is completely replaced by bone. Epiphyseal fusion is an active process, carefully regulated by hormones as well as cellular mechanisms and structural features. Estrogen is pivotal for epiphyseal fusion in both young men and women. The key role of estrogen was recently confirmed in two genetic disorders, 1) estrogen deficiency, caused by mutations in the gene that encodes aromatase and 2) estrogen resistance, caused by mutations in the gene that encodes estrogen receptor α (ER-α). In both conditions it was found that the growth plate failed to fuse and longitudinal bone growth persisted, although more slowly into adulthood. Conversely, premature exposure to estrogen (e.g. precocious puberty) resulted in a premature epiphyseal fusion, confirming its fundamental role in the process of epiphyseal fusion (Nilsson and Baron, 2004; Nilsson and Baron, 2005).

1.2 Hormonal regulation of childhood linear growth.

A complex network of hormones carefully regulate normal linear growth and development throughout childhood and adolescence. These hormones are synthesised in adequate volumes to meet our body's needs and demand. Our essential systemic hormonal regulators utilised during developmental and childhood growth are controlled by; GH, thyroid hormones, glucocorticoids (GC) and sex hormones (estrogen and androgens) (Robson et al., 2002). I will be focusing my discussion on the actions of GH and activation of downstream signalling events.

GH is considered as the primary anabolic hormone during stress and fasting and is a key mediator in the control of several complex physiologic processes, involving linear growth and

metabolism. Alongside the direct effect of GH on the functional activation of target tissues, a large contribution of GHs' action occurs indirectly via means of Insulin-like growth factor 1 (IGF-1) synthesis and free fatty acids (FFA). GH induced IGF-1 and insulin in well-nourished subjects, promotes linear growth via direct actions on cartilage and bone, further demonstrating its importance in anabolic storage and growth of lean body mass (LBM), adipose tissue and glycogen reserves. In addition, GH is also considered as an important modulator of total body metabolism promoting tissue protein deposition, utilisation of body fat and reducing the use of sugars by inducing the resistance of body tissues to insulin to result in increased blood glucose levels. Conversely, during a fasting state, GH induces FFA oxidation leading to a reduction in glucose levels, protein oxidation and preservation of LBM and glycogen stores (Moller and Jorgensen, 2009).

1.3 Growth hormone receptor activation and signalling.

1.3.1 Growth hormone physiology.

The human GH gene family is localised on the q22-24 region of chromosome 17. It encodes for two distinct GH molecules of approximate molecular size 22 kilodatons (kDa) and 20kDa, of which 90% of GH found in circulation is known to constitute the 22kDa form (Gunawardane et al., 2000; Herrington and Carter-Su, 2001). Naturally, it is produced as a 217 amino acid (aa) precursor protein. The 26 N-terminal amino acids correspond to a signal peptide that is essential for hormone secretion. During the release of GH, the signal peptide becomes cleaved to yield mature GH. Mature GH is a four helical single-chain polypeptide hormone of 191 aa that is synthesised and released by somatotroph cells located primarily in the lateral wings of the anterior pituitary in a pulsatile manner. GH is secreted throughout an individual's lifetime and has a short half-life of 14 minutes (Rozario et al., 2000). Its release is often described as a cyclical pattern with peaks and troughs occurring every few hours and a typically elevated peak occurring early during sleep (Gunawardane et al., 2000). The level of GH varies with age displaying an increase throughout childhood, a peak during puberty and a slow decline during adolescence (Laron, 2001; Rozario et al., 2000).

The release of GH is tightly regulated by central and peripheral signals. It is promoted by the stimulatory effects of hypothalamic peptide Growth hormone-releasing hormone (GHRH) and inhibited by somatostatin (**Figure 1.4**) (Kato et al., 2002; van der Eerden et al., 2003). GHRH is a 44 aa polypeptide synthesised in the arcuate nucleus of the hypothalamus reaching the anterior pituitary somatotrophs via the portal venus system leading to GH transcription and secretion (Gunawardane et al., 2000). The secretion of GHRH is stimulated by several factors including, depolarisation, α2-arenergic stimulation, hypophysectomy, thyroidectomy and hypoglycaemia; acting via a seven transmembrane G protein coupled stimulatory cell-surface receptor on the somatotrophs and is inhibited by somatostatin, IGF-1 and the activation of GABAergic neurons. (Gunawardane et al., 2000).

Somatostatin is a cyclic peptide encoding a single gene in humans exerting inhibitory effects on endocrine and exocrine secretions. Specialised cells in the anterior pituitary (periventricular nucleus, arcuate nucleus) produce somatostatin, secreting the peptide into the adenohypophyseal portal venous system, via the median eminence to exert its effects on the anterior pituitary. Somatostatin has a short half-life of approximately 2 minutes due to a rapid inactivation by tissue peptidase in humans. The release of somatostatin is inhibited by high blood glucose and is induced by serum GH/IGF-1 levels, exercise and immobilisation (Giustina and Veldhuis, 1998; Gunawardane et al., 2000; Patel, 1999). Studies have also shown that GH is further regulated by other hypothalamic peptides, which act in synergism with GHRH; named *'Ghrelin'* (Laron, 2001). Ghrelin is a 28 aa peptide; a natural ligand for the GH secretagogue receptor (Hataya et al., 2001).

1.3.2 The Growth hormone / Insulin-like growth factor-1 axis.

GH can exert its metabolic actions via a 'direct' effect; a result of GH binding its receptor on target tissues (e.g. adipose tissue and chondrocytes) proceeding to the subsequent activation of a complex regulatory signalling cascade or alternatively via an 'indirect' effect by means of IGF-1 production. Ultimately GH stimulation promotes longitudinal growth primarily by regulating the expression of IGF-1 in both hepatic and non-hepatic tissues (e.g. growth plate) (**Figure 1.4**). In non-hepatic tissues, other growth factors and cytokines, in addition to GH, may

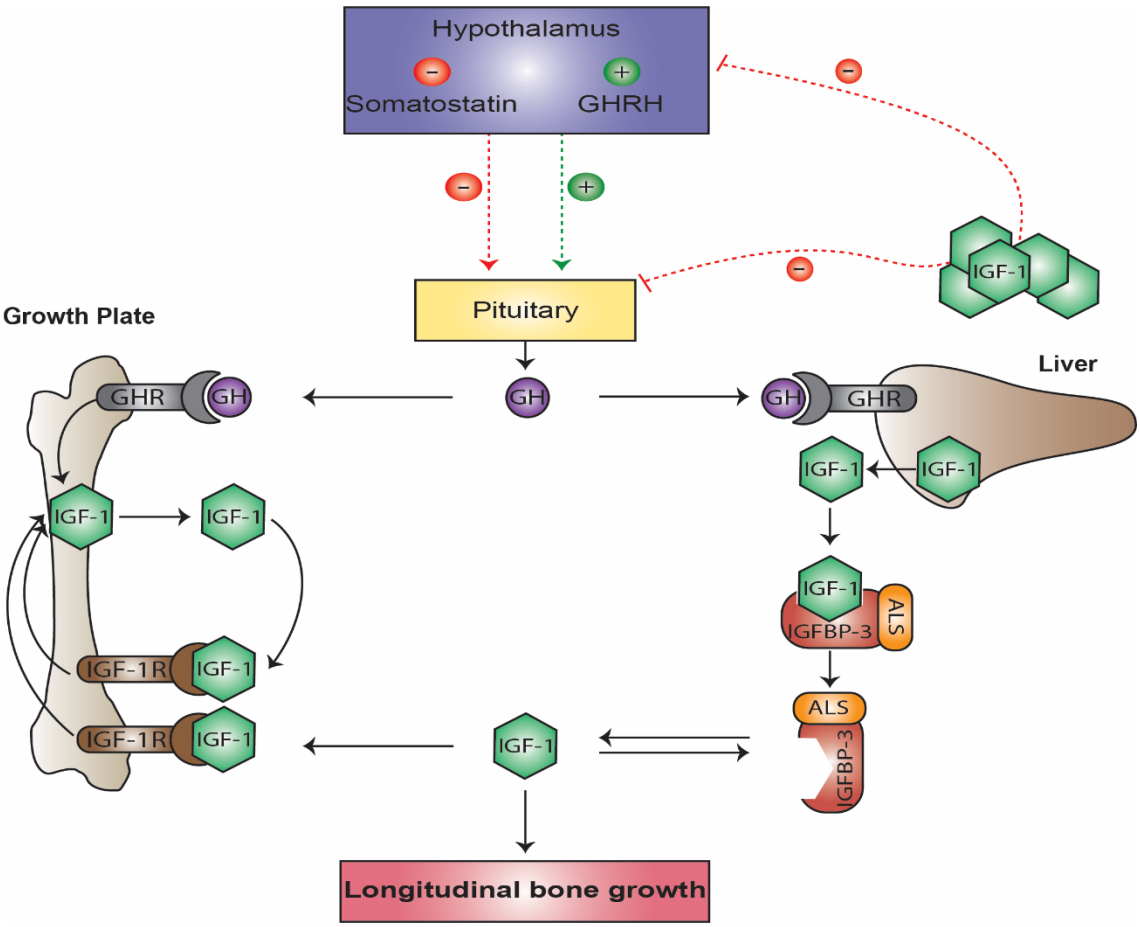

Figure 1.4 The Growth hormone/ Insulin-like growth factor axis. GH is synthesised and released by somatotrophs of the anterior pituitary. Its release is tightly regulated by central and peripheral signals; promoted by stimulatory effects of GHRH and inhibited by somatostatin. GH acts on hepatocytes to induce signal transduction to produce the release of IGF-1. IGF-1, IGF binding protein-3 (IGFBP-3) and acid labile subunit (ALS) are important components of IGF-1 activity. Alternatively GH can bind directly to GHR within chondrocytes of the growth plate to stimulate the production of IGF-1. Ultimately IGF-1 promotes longitudinal bone growth and muscle growth. Adapted from (Roelfsema and Clark, 2001).

induce local growth effects through IGF-1 production or via mechanisms independent of IGF-1 (David et al., 2011). Experimental studies of GH/IGF-1 knockout mice clearly demonstrate the importance of normal functioning GH/IGF-1 axis in bone growth, whereby knockout GH/IGF-1 mice were seen to develop severe growth failure (Bajpai and Menon, 2006; Lupu et al., 2001). *In vivo* studies for double gene disrupted mice for liver deficient IGF-1 (LID) and acid labile subunit (ALS) knockout demonstrated a reduction in serum IGF-1, a significant linear growth reduction and a 10% decrease in bone mineral density (Yakar et al., 2002). In addition, it was reported that *Igf1*$^{-/-}$ mice had a 24% reduction in cortical bone size and shortened femoral lengths (Bikle et al.,

2001). Other models of growth failure include; Laron syndrome, mutations in GH releasing hormone receptor and IGF-1 and IGF-1 receptor knockout mice (Walenkamp and Wit, 2007).

1.3.3 Growth hormone receptor physiology.

GH activity is mediated by the binding of GH to the transmembrane GHR which is present as a homodimer on the surface of most cells. GHR is considered a major player in human growth action. It is a member of the class 1 cytokine receptor superfamily of transmembrane proteins and is highly abundant in the liver, adipose tissue, heart, kidneys, intestine, lung, pancreas, cartilage and skeletal muscle where it induces the synthesis of IGF-1. There are two isoforms of GHR; 1) the full length membrane bound human receptor (620 aa) with a single transmembrane region and 2) the GH binding protein (GHBP) that occurs separately as a short soluble form corresponding to the extracellular domain of the full-length receptor involved in GH signalling (Kato et al., 2002; Zhu et al., 2001). GHR is encoded by a single gene located on the short arm of chromosome 5. This gene spanning 86 kilobase pairs includes 10 exons and 9 introns, (exons 2 encodes a secretion signal sequence, exon 3-7 encode the large extracellular GH binding domain, exon 8 the transmembrane domain and exon 9 and 10 encode the intracellular domain) (Rosenbloom, 2000). Its structural composition is composed of an extracellular domain (ECD) (246 aa) consisting of two fibronectin type III domain each with a seven stranded β sandwich connected by a short flexible linker which is the focus of ligand binding (Waters, 2016). These two domains are connected to a rigid single pass helical transmembrane domain (24 aa) via a flexible linker. The intracellular domain (ICD) (350 aa) comprises of a proline rich Box 1 motif, essential for the binding of their cognate tyrosine (Janus) kinase the main target of the receptor activation process for downstream signalling and a less conserved Box 2 motif consisting of aromatic and acidic residues (**Figure 1.5**) (Brooks et al., 2008; Goffin and Kelly, 1997; Pass et al., 2009; Rotwein, 2012; Waters, 2016). Newly synthesised GHR is formed as a precursor in the endoplasmic reticulum where the protein undergoes high N-linked mannose glycosylation and dimerisation. The transmembrane protein is transported to the Golgi apparatus where it becomes further glycosylated before appearing at the membrane surface of the cell. Throughout the

biosynthesis of GHR it is continuously modified as its maturity transforms from immature to mature GHR (Sedek et al., 2014).

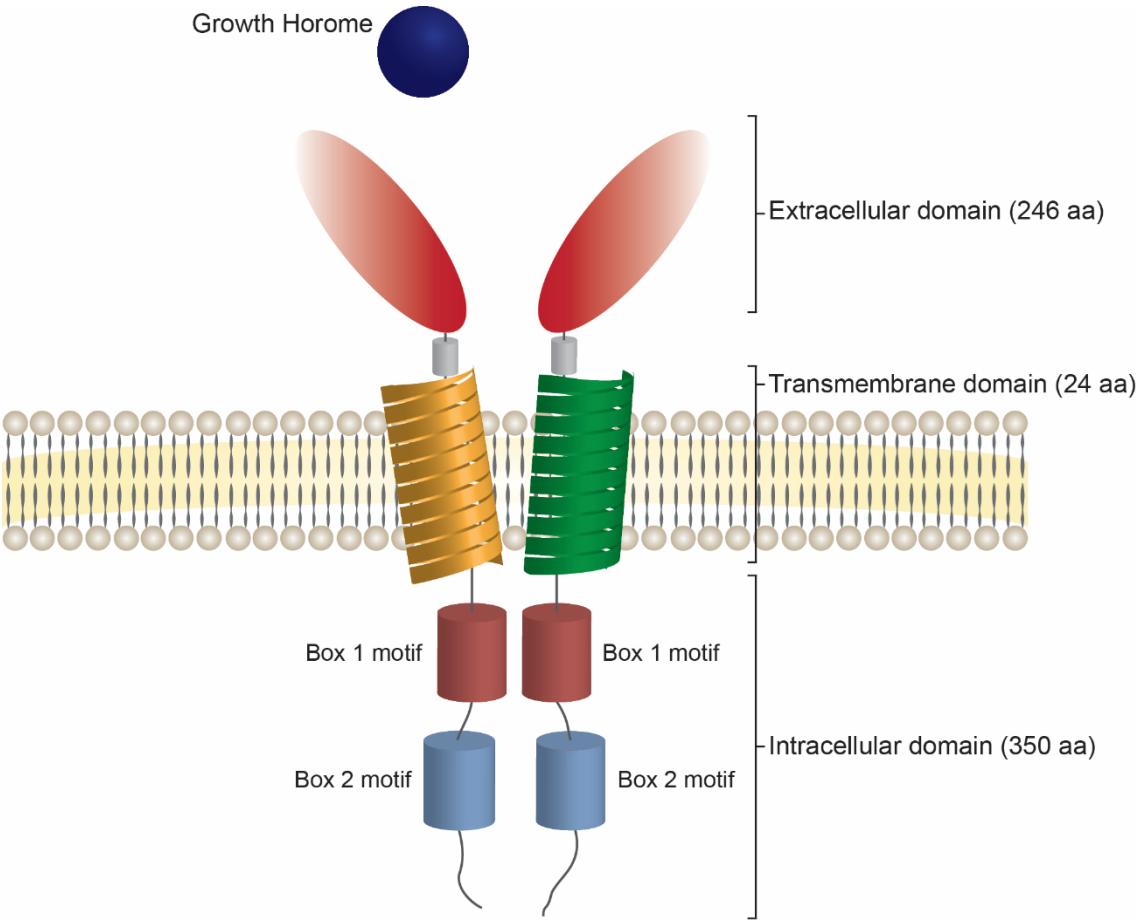

Figure 1.5 Growth hormone receptor structure. The extracellular domain (246 aa) is formed of two fibronectin type III domains, each with a seven stranded β sandwich domain connected by a short flexible linker. The ECD is connected to a rigid single pass helical transmembrane domain (24 aa) via a flexible linker. The intracellular domain (ICD) (350 aa) has a proline rich Box 1 motif, essential for the binding of their cognate tyrosine (Janus) kinase to activate downstream signalling a less conserved Box 2 motif. Adapted from (Rozario et al., 2000).

1.3.4 Growth hormone downstream signalling cascade.

GH/GHR binding triggers a multitude of signal transduction pathways that are essential in regulating the transcription of GH target genes involving growth and metabolism (Herrington and Carter-Su, 2001; Pass et al., 2012). The GHR system is known to utilise the Janus kinase (JAK) signalling cascade which in turn results in the recruitment and/ or activation of an array of downstream signalling molecules including; Mitogen-activated protein kinases (MAPKs),

Insulin Receptor Substrate-1 (IRS1), Phosphatidylinositol-3-Phosphate-Kinase (PI3K), Diacylglycerol (DAG), Protein Kinase-C (PKC), intracellular calcium ($Ca2^{+}$) and Signal transducers and activators of transcription (STAT) (**Figure 1.6**) (Ahmed and Farquharson, 2010; Gevers et al., 2009; Rotwein and Chia, 2010). Ultimately, GH induced JAK activation results in a change of the enzymatic activity, transport function and gene expression, that subsequently promotes growth, metabolic activity and cellular events e.g. haematopoiesis, immune development and others (Rawlings et al., 2004).

1.3.4.1 Janus kinase/ Signal transducers and activators of transcription signalling pathway.

The JAK/STAT pathway is predominately involved in longitudinal growth throughout childhood. A single GH molecule binds two molecules of the GHR proceeding in a sequential process. The initial binding of GH to a single molecule of GHR is of a high affinity binding step followed by a second contact with a new GHR molecule at a different face of the GH molecule forming a stabilised dimer (Herrington and Carter-Su, 2001). GH induced signalling via the activation and dimerisation of the ECD, subsequently leads to the phosphorylation of the ICD. This conformational orientation allows for the binding of two JAK2 proteins into close proximity of one another, such that each JAK2 is able to phosphorylate the activating tyrosine of the other JAK2 molecule, locking JAK2 in an active conformation. Following the phosphorylation of tyrosine (Tyr) residues at Box 1 in the ICD creates docking sites for Src homology 2 (SH2) domain proteins including; STAT1, STAT3 and STAT5 (isoforms STAT5a, STAT5b) (Ahmed and Farquharson, 2010). STAT5b has been identified as an important key mediator of GH-induced IGF-1 gene transcription and subsequent linear bone growth. STAT5b is phosphorylated by JAK2 at the specific Tyr and/or serine residues. The tyrosyl-phosphorlated-STAT5b forms a homodimer, subsequently leading to its translocation into the nucleus. Here, STAT5b binds to chromosomal GH-responsive elements (GHRE) and drives the transcriptional regulation and expression of GH-responsive genes including; IGF-1, IGF-Binding Protein 3 (IGFBP-3), ALS, FGF21 and suppressor of cytokine signalling 2 (SOCS2) (**Figure 1.6**) (Brito et al., 2012; David

et al., 2011; Deng et al., 2007; Gevers et al., 2009; Pfeifer et al., 2008; Xu et al., 2006; Zhu et al., 2001).

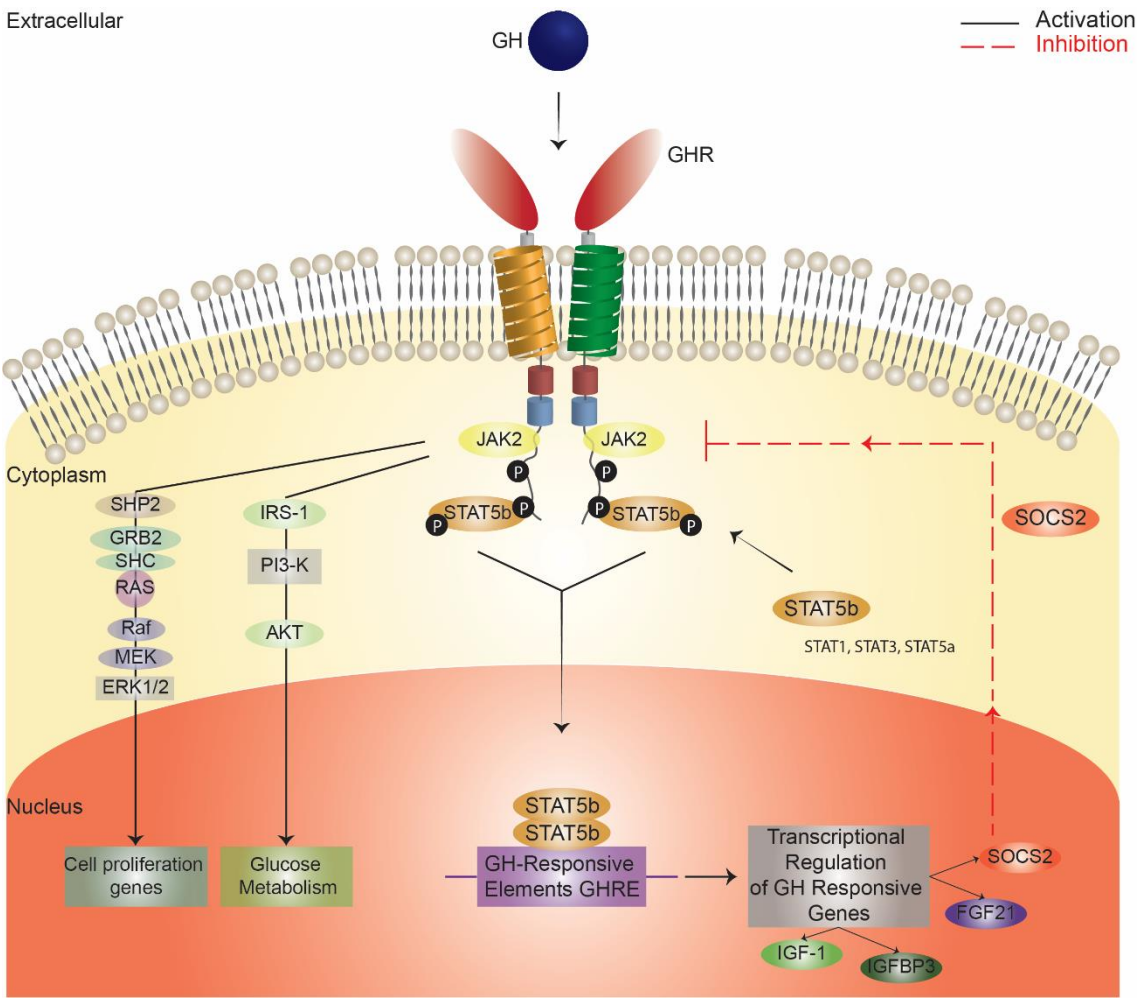

Figure 1.6 A schematic of Growth hormone signalling. GH/GHR interaction triggers the JAK-2 cascade and the activation of a series of pathways (STAT, ERK1-2 and PI3K). Dimerisation of the GHR ECD and phosphorylation of the ICD allows for JAK-2 binding and phosphorylation. STAT5b is recruited and phosphorylated, leading to its translocation into the nucleus where it is involved in the transcriptional regulation of GH-responsive genes (IGF-1, IGFBP-3, SOCS2, and FGF21). SOCS2 acts as an important negative regulator of GH signalling. Adapted from (Ahmed and Farquharson, 2010; Rotwein and Chia, 2010; Yu et al., 2012).

1.3.5 Insulin-like growth factor family and physiology.

The IGF family are members of the insulin related peptides that include; relaxin and several peptides isolated from lower invertebrates. It was Salmon and Daughaday that discovered IGF-1 and IGF-2 in 1957 (Laron, 2001). IGF-1 is known as a major mediator of GH stimulated somatic growth and independent anabolic responses in many cells and tissues. Thus the exploration of the IGF-1 axis has been widely studied for its function in skeletal growth. The *IGF-*

1 gene is present on the long arm of chromosome 12q23-23 consisting of six exons that include two leader exons with two promoters. This small peptide consists of 70 aa with a molecular weight of 7649 Da and a structural composition formed of an A and B chain bound by disulphide bonds and a C peptide region of 12 aa (Laron, 2001). Synthesis of IGF-1 mainly occurs in hepatocytes, however it has been seen that some IGF-1 synthesis also occurs in peripheral tissue including bone, cartilage and some solid organs. Studies have shown that approximately 75% of circulating IGF-1 derives from the liver of which 99% of circulating IGF-1 is bound to transport proteins. At birth IGF-1 plasma levels range between 20 to 60 ng/ml which is later seen to almost rise seven folds between birth and the peak at puberty (Rozario et al., 2000). The IGF-2 gene is a maternally imprinted gene located on chromosome 11p15. This polypeptide hormone is widely expressed, mainly secreted by the liver and also in utero by the placenta. In humans IGF-2 is known to be more abundantly expressed during foetal life than IGF-1 playing a pivotal role on foetal growth, also contributing to placental size and nutrient delivery (Kadakia and Josefson, 2016).

Over the past two decades there has been an additional identification of six IGF-BP's and nine IGFBP-related proteins (IGFBP-RPs). IGFBP-3 represents the predominant binding protein that is involved in IGF-1 activity. In circulation, IGF-1 exists as a ternary structure bound with one molecule IGFBP-3 and an 88 kDa ALS protein which is known to stabilise the IGF-1 – IGFBP3 complex, to further extend its half-life to approximately 16 hours (Brito et al., 2012; David et al., 2011; Laron, 2001; Locatelli and Bianchi, 2014; Roelfsema and Clark, 2001).

IGF-1 acts via the binding to type 1 IGF receptor (IGF-1R); a receptor tyrosine kinase with a tetrameric structure (Saegusa et al., 2009). IGF-1R is widely expressed in many tissues in the body, however the number of receptors expressed within a given tissue is highly dependent on several systemic and tissue factors including; circulating GH, thyroxine, platelet-derived growth factor (PDGF) and fibroblast growth factor (Gunawardane et al., 2000). The IGF-1R is formed of two extracellular spanning α subunits containing the ligand-binding domains and two transmembrane β subunits with tyrosine kinase activity. The alpha subunit is able to bind to IGF-1, IGF-2 and insulin, however it is known to have a greater affinity to IGF-1 linking to the receptor via a disulphide bond. The β subunit comprises of a short ECD, the transmembrane domain, and

an ICD; containing a tyrosine kinase domain, which constitutes the signal transduction mechanism. Following ligand binding, the IGF-1 receptor undergoes a conformational change resulting in the subsequent activation of tyrosine kinases that lead to the auto-phosphorylation of the opposite β-subunit on specific tyrosine residues. This activity results in the phosphotyrosines which are able to bind to adapter molecules including insulin receptor substrate-2 (IRS-2) and Shc which activates the RAS activating protein SOS. Ultimately this complex activates the mitogen activated protein kinase (MAP kinase) pathway to promote cell growth (Gunawardane et al., 2000).

1.3.6 Negative regulation of Growth hormone induced Suppressor of cytokine signalling.

SOCS proteins, discovered in 1999 are a family of negative regulatory proteins that are predominantly expressed in response to the activation of a wide range of cytokine and growth factor signal cascades, particularly the JAK/STAT signalling system, acting as a classical negative feedback loop (Letellier and Haan, 2016). There are 8 known members including SOCS1 – SOCS7 and the cytokine inducible SH2-containing protein (CIS) (Ahmed and Farquharson, 2010; Kile and Alexander, 2001; Krebs and Hilton, 2001; Turnley, 2005; Yoshimura and Yasukawa, 2012) . Structurally, SOCS proteins have a poorly conserved amino-terminal domain of variable length and sequence, a central SH2 domain, as well as a highly conserved 40 aa C-terminal domain, named the SOCS box (Letellier and Haan, 2016; Vesterlund et al., 2011). SOCS proteins can interact with a series of signalling intermediates through the binding of their SH2 domain to phosphorylate tyrosine residues, particularly those on cytokine receptors and JAK proteins, leading to the blockade of the downstream signals (Letellier and Haan, 2016). Elongins B and C proteins together with other molecules including Cullin5 and Rbx-I have been shown to bind to the SOCS-Box forming an E3 ubiquitin-ligase complex; this in turn induces poly-ubiquitination of associated proteins leading to the degradation of these molecules via the proteasome. SOCS-Box may thus act as a generic adaptor molecule that targets SOCS associated signalling pathways e.g. JAK molecules or receptors for destruction subsequently terminating signalling through specific interactions via SOCS and SH2 domains (Greenhalgh and Alexander, 2004).

During GH stimulation SOCS1-3 become activated, however SOCS2 has been identified to have a vital role in the negative regulation of GH signalling thereby involved in cell growth. STAT5b binds to the promoter of *SOCS2*. In turn, this induces the transcription of *SOCS2*, where the levels have been demonstrated to peak within 2h, *in vivo* (Tollet-Egnell et al., 1999). SOCS2 binds to at least two phosphorylated tyrosines on GHR to negatively regulate JAK2 and STAT5b activation (**Figure 1.6**). Although the molecular actions of SOCS2 are not entirely clear the main reported mechanisms are said to include; 1) SOCS2/GHR binding to block positive regulators and 2) proteosomal degradation via the ubiquitin ligase complex (Krebs and Hilton, 2001; Turnley, 2005; Vesterlund et al., 2011). This is supported by experimental studies on Socs2 knockout mice where these mice exhibited gigantism, characterised by increased body weight and bone length, alterations in major urinary protein levels, thickening of dermal layers and elevation of *Igf-1* mRNA in some tissues (Greenhalgh et al., 2005). Similarly other *in vivo* investigations on mice lacking the *Socs2* gene were seen to be indistinguishable from their littermates at birth, while at three weeks of age are found to show an accelerated growth often resulting in adult mice that are ~30-40% larger than their counter wild-type mice as a result of uncontrolled response to GH causing subsequent increased bone length (Letellier and Haan, 2016). In addition, a meta-analysis of 47 genome wide association studies (GWAS) involving 114,223 adults from six ethnic groups revealed the single nucleotide polymorphism (SNPs) rs3782415 (SOCS2) as one of several SNPs strongly associated with height (Fontenele et al., 2015). Thus, these observations clearly indicate the importance of SOCS2 in controlling linear growth via GH and/ or IGF-1. It is also evident that sex steroids such as estrogens can modulate GH actions on GHR expression and signalling. In particular E2 is seen to induce SOCS2 levels negatively regulating GHR activation and downstream events of the JAK/STAT cascade (Fernandez-Perez et al., 2013).

1.4 Normal linear growth patterns and growth disorders.

1.4.1 Normal growth during childhood development.

Physical growth relates to the attainment of adult height and appropriate weight and an increase in size of all organs (with the exception of the lymphatic tissue). Development on the other hand considers growth in function and capability. Together growth and development are driven by genetic, nutritional and environmental factors.

Typically, healthy infants and children grow in a predictable fashion, following a standard pattern of progression in weight, length and head circumference. It is described that normal human growth is a relatively smooth and orderly process with periods of rapid growth (growth spurt) and is separated by periods of no measurable growth. During growth, two distinct phases proceed from birth to adolescence. The initial phase during infancy (between birth and 1 year of age) is predominantly dependent on maternal nutrition and intrauterine environment reflecting the stages of rapid and continual growth, although it is seen that the rate of growth begins to decrease over the due course. The second phase during childhood (age 2 years to the onset of puberty) is a relatively constant growth period with a consistent annual growth increment that is dominated by GH. At puberty (the process of physical and biologic maturation from child to adult) a second growth spurt is observed (**Figure 1.7 A**). This growth period differs slightly between boys and girls. In this second growth phase endocrine factors including gonadotropins and sex steroids (along with GH itself) also play a role in the pubertal growth spurt (Doyle, 2012). Typically this consists of a phase of acceleration, followed by a phase of deceleration which leads to the eventual cessation of growth with the closure of the epiphyses (Abbassi, 1998). The initiation of accelerating growth velocity is approximately age 11 in boys and 9 in girls, however this varies widely between individuals. The peak height velocity occurs at a mean age of 13.5 years in boys and 11.5 years in girls and on average males are 12-13 cm taller than females primarily due to a 2 year delay in bone closure as compared to females and more pronounced growth spurt during puberty (**Figure 1.7 B**) (Stang, 2005).

1.4.2 Definition and assessment of short stature.

The longitudinal measure of a child's height and weight provides a dynamic statement of his or her general condition, health and well-being (Haymond et al., 2013). Normal (physiologic) height encompasses the 95% confidence interval (CI) for a specific population (Nichols, 2016; Rogol et al., 2000). The more an individual's height deviates from the 2.5 percentile the more likely it is that there is an existence of underlying disease in the apparently normal child (Nichols, 2016; Rogol et al., 2000). Growth velocities of an individual are highly variable in consecutive growth intervals. Hence, growth velocity is best assessed routinely using measurements taken every 3 to 4 months in infants and 6 months in children. Such growth charts provide essential information for the screening, surveillance and monitoring of children's growth. Identifying abnormal growth patterns in short stature has beneficial impact on minimising health conditions and optimising final adult height. Often, short stature in children is unrecognised at the early stages and is thus diagnosed at a late age resulting in a decrease in the opportune time to intervene to improve final height. Identifying the underlying cause(s) contributing to abnormal growth is critical for appropriate treatment (Haymond et al., 2013).

1.4.3 European Society for Paediatric Endocrinology: classification of short stature.

Identifying the root cause of short stature can be a highly complicated task due to the wide range and number of current clinical conditions. Many cases of monitored growth in children tend to be normal variants; displaying no pathology or psychosocial issues causing reduced height. Many children may have constitutional delay in growth and or puberty; a normal growth rate but a delayed bone age relative to their age. On the other hand many have a family history or poor/ abnormal growth patterns, and although many may eventually achieve a normal adult height, others remain short as adults. In other cases if the parental height of a child is diagnosed as short, then it is likely that it is due to genetic or familial short stature (Haymond et al., 2013).

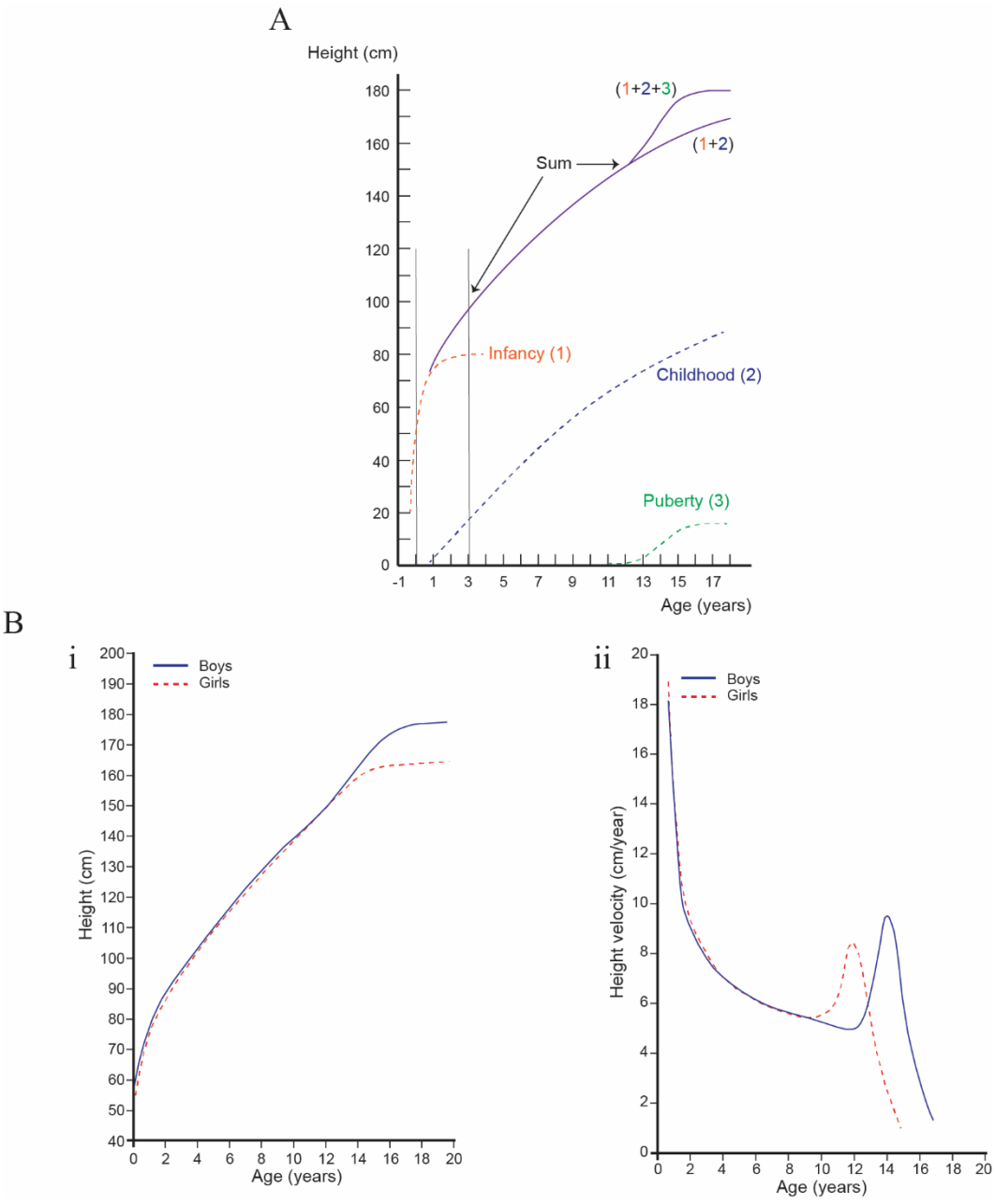

Figure 1.7 Growth patterns in healthy boys and girls. (A) The infancy-childhood-puberty (ICP) model describes an overview of the postnatal linear growth curve from the latter intrauterine life to maturity, mathematically divided into three additive and superimposed components; infancy, childhood and puberty. Each phase is controlled by biological mechanisms. The early stages of infancy (1) growth is highly dependent on nutrition. Childhood (2) growth is controlled by GH. Pubertal (3) growth is stimulated by a combination between sex steroids and GH. **(B) (i)** Representative growth chart of boys and girls between age 0 to 20 years. Boys have a maximum growth spurt ~2 years after puberty, showing a typically rapid growth pattern reaching full adult height by age 17 to 18 years. Girls display a rapid growth spurt during menstruation usually following the peak height velocity, reaching maximum height by age 14 to 15 years. **(ii)** Linear growth velocity (cm/year) is highest immediately after birth. With age (years) there is a gradual decline in growth velocity until the pubertal growth spurt. Pubertal linear growth spurt begins earlier in girls (age ~9 years) than boys (age ~11 years). Adapted from (Tse et al., 1989).

The European Society for Paediatric Endocrinology (ESPE) classifies short stature into three main categories. 1) Primary growth disorders (conditions intrinsic to the growth plate), 2) secondary growth disorders (chronic diseases or extrinsic factors that cause a change in growth plate physiology) and 3) non-recognisable causes (e.g. idiopathic short stature).

1.4.3.1 Primary conditions of short stature.

Primary conditions of short stature include GH insensitivity (GHI). GHI is a group of extremely rare genetic disorders in which the body is unable to utilise the growth hormone that it produces. Thus, typically it is characterised by normal or elevated levels of serum GH and subnormal circulating concentrations of IGF-I, IGF-II, and IGFBP-3. This can develop through mutations in the GHR gene or in the genes involved in the signalling cascade that is activated following the interaction between GH and GHR. GHI is commonly marked by short stature and delayed bone age. Other common symptoms that have been identified include; delayed onset of puberty, a prominent forehead, low blood sugar and obesity in adulthood (Rosenbloom, 1997). Some examples of known genetic causes of GHI include; 1) GH receptor deficiency - Laron syndrome, (>250 reported cases), 2) IGF-1 deficiency, 3) STAT5b deficiency and 4) ALS deficiency (Woods, 2007). In addition, skeletal dysplasia a large heterogeneous group (>400 recorded syndromes) of genetic disorders are widely known to contribute to the primary conditions of short stature. Typically individuals with skeletal dysplasia are characterised by disproportionate short stature, associated with traits including shorter and bowed long bones, shorter ribs, polydactyly, impaired bone density and bone modelling, disorganised development of growth cartilage and ossification defects (Cho and Jin, 2015).

1.4.3.2 Secondary conditions of short stature.

Many contributing factors of secondary short stature have been identified. GH deficiency (GHD) occurs relatively rarely after major structural lesions of the hypothalamus and pituitary gland, following surgery for their treatment, or as a result of deletions/ mutations within the

structural gene for GH or its receptor. This consequently leads to the inadequate secretion of GH from the anterior pituitary gland. The result of GHD develops growth retardation, short stature and maturation delays reflected by the delay of lengthening of the bones of the extremities relative to the chronological age of the child (Rosenbloom, 1997). Whilst some children are born with GHD (congenital), others develop GHD at some point during childhood or adolescence. Other endocrine associated conditions include; multiple pituitary deficiencies, Cushing syndrome and hypothyroidism. More so additional secondary contributors to GH related disorders include, insufficient nutritional intake (malnutrition) and chronic disorders in organ systems (e.g. Liver disorders, intestinal disorders; Crohn's disease, malabsorption) (Haymond et al., 2013)

Nutrition is a highly important determinant of statural growth; essential for the physical and psychosocial well-being of children and adults (Mericq et al., 2014). Good nutrition ensures the availability of essential 'building blocks' for normal growth. Thus, malnutrition, marked by various nutrient deficiencies, is considered a leading cause of failure to thrive and growth attenuation in children. Often, when food becomes replenished, sporadic catch-up growth usually occurs, bringing the child back to its original growth trajectory. Catch-up growth is defined as; height velocity above the normal statistical limits for age or maturity during a defined period of time following a transient period of growth inhibition. However, in some cases catch-up growth is insufficient and can lead to a permanent growth deficit (Gat-Yablonski and Phillip, 2015). Starvation has been shown to interfere with the actions of GH signalling, subsequently resulting in increased levels of GH and a reduction in IGF-1 activity, indicative of GH resistance (Inagaki et al., 2008; Kubicky et al., 2012).

Moreover, impaired linear growth during childhood has been recurrently associated with chronic inflammatory conditions such as inflammatory bowel disease (IBD), particularly with Crohn's Disease (Pass et al., 2009). It is suggested that inflammation and undernutrition play a key role in the development of short stature. Elevated inflammatory cytokine production is speculated to act directly on hepatic IGF-1 and on chondrocytes of the growth plate of long bones but the mechanism of action remain unclear (Sanderson, 2014). Thus, IGF-1 expression is decreased, whilst GH production remains normal in chronic inflammation (Gasparetto and

Guariso, 2014; Walters and Griffiths, 2009). In addition, paediatric IBD has also been described to increase the risk of vertebral fractures, as well as abnormalities in biochemical levels such as GH deficiency, highlighting the deleterious effect of chronic inflammation on skeletal health (Wong et al., 2014; Wong et al., 2010).

1.4.3.3 Idiopathic short stature.

The definition of Idiopathic short stature (ISS) is of an individual that is greater than 2.0 SD below the corresponding mean height for a given age, sex and population and a thorough history, physical examination and additional investigations present with no identifiable disorder. In addition children categorised with ISS are considered to be GH sufficient, having no history of low birth size, normal body proportions, well-nourished and no psychiatric disorder. The diagnosis of ISS is likely to be based on no identifiable positive findings, eliminating the known recognisable conditions associated with short stature (Wit et al., 2008). The ESPE further categorise ISS into two groups. 1) Familial (idiopathic) short stature; including children with normal pubertal onset, delayed pubertal onset or onset of puberty not yet known. 2) Non-familial (idiopathic short stature); including children with normal pubertal onset, delayed pubertal onset (constitutional delay in growth and puberty, or constitutional delay in growth and adolescence) or onset of puberty not yet known (Wit et al., 2007).

1.5 The Fibroblast growth factor family.

The discovery of fibroblast growth factor (FGF) in 1973 was first established by Armelin in pituitary extracts (Armelin, 1973). Since, the exploration of FGFs has widely expanded; today consisting of 22 members divided into seven subfamilies based on structural integrity and function. These members are further grouped into three main categories; 1) Intracellular FGFs (FGF11/12/13/14), 2) Endocrine FGFs (FGF19/21/23), and 3) Paracrine FGFs (the rest) (**Figure 1.8**) (Cuevas-Ramos et al., 2012; Iglesias et al., 2012; Murata et al., 2011). The heterogeneity of FGFs is observed through the size variation in molecular mass; ranging between 17 – 34kDa. In

contrast these members share a common conserved sequence of 120 aa, displaying 16 – 65% homology (Eswarakumar et al., 2005).

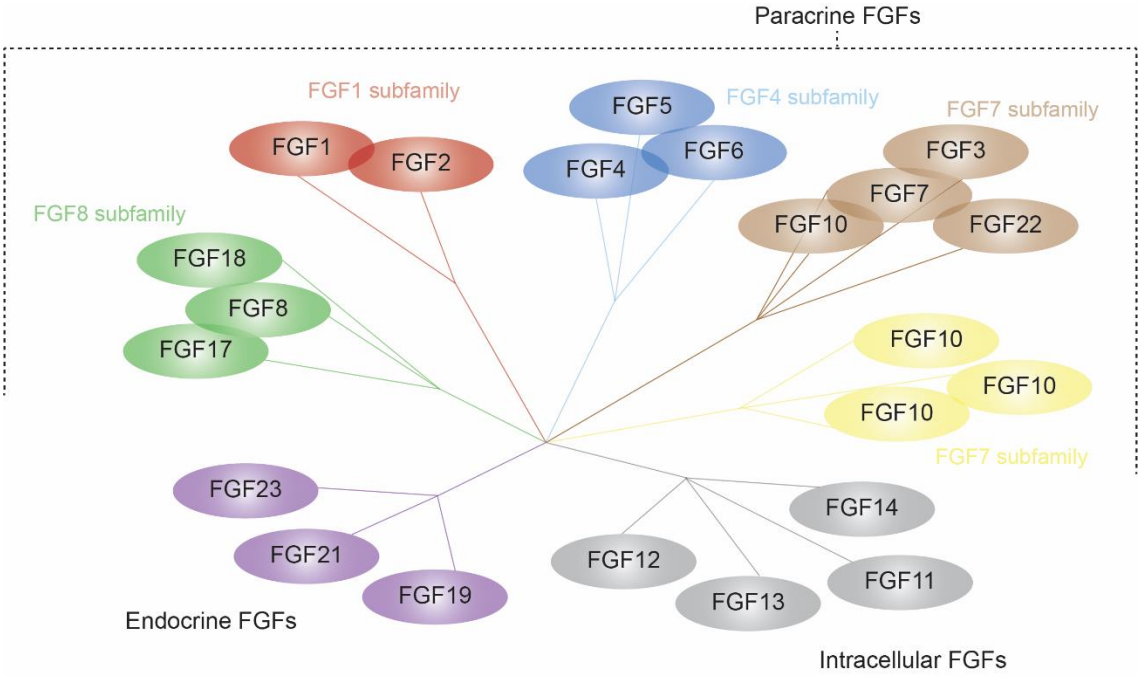

Figure 1.8 The Fibroblast growth factor family. The FGF family is formed of 22 members, divided into seven subfamilies, further grouped into three main categories; 1). Intracellular FGFs (FGF11/12/13/14), 2). Endocrine FGFs (FGF19/21/23), and 3). Paracrine FGFs (the rest). Adapted from (Laestander and Engstrom, 2014).

Structurally, FGFs are considered as a single-chain polypeptide, with a conserved domain that is flanked by non-conserved extensions. It is formed of a homologous core region of 120 – 130 aa that are arranged into 12 antiparallel β-strands (β1 – β2). This core is flanked by divergent N- (amino) and C-(carboxyl) terminals. The terminal tails show a high degree of variability in length and primary sequence that accounts for the wide range of ligand biology. The heparin binding site (HBS) located within the FGF core, is composed of a β1 – β2 loop and a portion of the region spanning β10 and β12. In the paracrine FGF subfamily, the HBS offers a positively charged surface to attract their binding to negatively charged heparin. This retains the ligand within the pericellular region to promote local receptor activation and signalling. In contrast, the HBS of the endocrine FGF family is composed of ridges by the β1 – β2 loop and the β10 – β12 region (lacking the β11 strand), subsequently altering the HBS structure displaying an atypical trefoil fold, reducing heparin binding to the core backbone to promote the endocrine nature of this

subfamily (Belov and Mohammadi, 2013). Although endocrine FGFs can interact with FGFR's, they display a low affinity for heparin sulfate proteoglycan (HSPG) and consequently requires additional cofactors e.g. the Klotho family to aid in binding and activation (**Figure 1.9**) (Mohammadi et al., 2005; Smith et al., 2013; Suzuki et al., 2008; Yang et al., 2012; Yie et al., 2012).

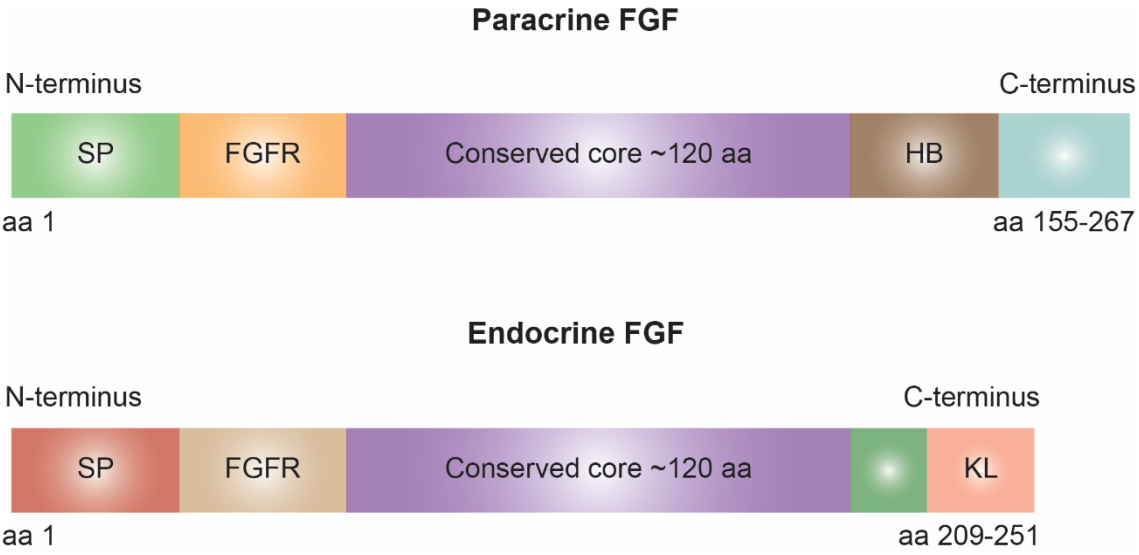

Figure 1.9 Paracrine and endocrine Fibroblast growth factor domains. The conserved core (~120 aa) is a shared sequence in both paracrine and endocrine FGF peptides, despite the variability in functional events. The common shared single peptide (SP) and FGFR binding domains (directs interaction with high-affinity FGFRs) are situated in the N-terminal region. The C-terminal region displays variability; paracrine FGFs are associated with low-affinity HSPGs (HB- paracrine ligands). Endocrine FGFs are associated with klotho co-receptors (KL – endocrine ligands). Adapted from (Kilkenny and Rocheleau, 2016).

The functional role of FGFs has been shown to mediate a wide variety of cellular responses throughout growth and development in multiple biological systems promoting cellular proliferation, differentiation and metabolism (Fukumoto, 2008; Ornitz and Itoh, 2015). The interlink between the role of FGFs during embryogenesis were shown to induce morphogenesis by regulating cell proliferation, differentiation and cell migration, whilst during adulthood they were identified to regulate the nervous system, tissue repair, would healing and tumor angiogenesis (Eswarakumar et al., 2005). Typically, most FGFs act as paracrine factors in i.e. stimulating spermatogenesis, mesoderm induction, somitogenesis, organogenesis and pattern formation. Endocrine FGFs on the other hand are shown to regulate major metabolic processes

including; glucose, lipid, cholesterol and bile acid metabolism and serum phosphate/ vitamin D homeostasis (Beenken and Mohammadi, 2012).

1.5.1 Endocrine Fibroblast growth factor 21.

FGF21 is part of the endocrine FGF19 subfamily consisting of FGF19, FGF21 and FGF23; differing in structural composition and functionality from the typical FGF members. Human FGF21 is a 181 aa peptide (~22.3 kDa molecular mass) that derives from a 209 aa mature protein (Fisher and Maratos-Flier, 2016; Iglesias et al., 2012; Kilkenny and Rocheleau, 2016; Murata et al., 2011). In humans, the *FGF21* gene is located on chromosome 19 at the 5' region of the a1-2-fucosyltranferase and is composed of three exons. In mice the *Fgf21* gene is located on chromosome 7 (Cuevas-Ramos et al., 2012). The mammalian *FGF21* gene is highly conserved, sharing ~80% homology between humans and rodents (Fisher and Maratos-Flier, 2016). The mature FGF21 protein is formed of 28 aa hydrophobic N-terminus peptide that directs constitutive secretion. FGF21 differs from the other members of FGFs in that it lacks the FGF heparin-binding domain posing the inability to bind to extracellular heparin (Kilkenny and Rocheleau, 2016; Wu et al., 2012). This is due to the modified β-trefoil structural motif present at the C-terminus. The ridged formation of the β1 – β2 domain and the β10 and β12 spanning region, reduces the heparin sulphate proteoglycan binding allowing for the FGF21 to escape the heparin rich ECM of secreting cells and diffuse through the matrix or alternatively into circulation to target tissues to function in an endocrine manner (Kilkenny and Rocheleau, 2016). FGF21 is abundantly expressed and secreted in the liver and accounts for the main source of circulating FGF21. However, it is also synthesised in the pancreas, white adipose tissue (WAT) and skeletal muscle, digestive tract and skin. It is found in detectable levels in the plasma, ranging approximately between 0.05 – 2ng/ml in healthy adults (Kilkenny and Rocheleau, 2016).

1.5.2 Fibroblast growth factor receptor family.

The majority of FGF signalling activation is initiated through a highly complex interaction of FGFs with a family of transmembrane tyrosine kinase FGF receptors (FGFR) sharing a high affinity (K_d 20-600 pM) for the FGF ligands. The FGFR family is a subfamily descending from the receptor tyrosine kinases (RTKs) comprising; FGFR1, FGFR2, FGFR3 and FGFR4. A new addition to the FGFR family includes a closely related receptor lacking the FGF signalling tyrosine kinase domain named FGFR5 or FGFRL (Tiong et al., 2013). The classification of FGFR's are based on the genes that encode them; FGFR1 *(flg)*, FGFR2 *(bek)*, FGFR3, FGFR4 *(flg2)*, and FGFR5. FGFRs share a high degree of sequence homology (~55 – 72%), particularly found within the amino acid level with a typical molecular size ranging between 55 to 150kDa (Kilkenny and Rocheleau, 2016; Ornitz and Itoh, 2015; Tiong et al., 2013).

The structural overview of FGFR's encompasses a hydrophobic rich N-terminal extracellular domain consisting of three immunoglobulin-like (Ig-like) subdomains (D1, D2 and D3); each separated by a short stretch of acidic residues, a single α-helix transmembrane domain with a long juxtamembrane sequence, and a split intracellular tyrosine kinase domain and a C terminal tail (Sarabipour and Hristova, 2016). A unique feature of FGFR's is the presence of a contiguous segment of (~30 serine residues) glutamic and aspartic acid connecting the D1-D2 linker, termed the acid box (Belov and Mohammadi, 2013; Tiong et al., 2013). The D3 subdomain of FGFR determines the specificity of binding of the vast array of ligand availability. The D1 domain and the acid box however are proposed to have a role in receptor auto-inhibition (**Figure 1.10 A**) (Beenken and Mohammadi, 2009; Beenken and Mohammadi, 2012; Belov and Mohammadi, 2013; Yie et al., 2012).

A number of FGFR isoforms exist due to alternative splicing at specific exons primarily within the second half of D3 domain of FGFR1 – 3. Exon splicing in the ligand-binding domain of exon 7 (exon IIIA) FGFR1-3 (N-terminal region of D3) and exon 8 (exon IIIB) and 9 (exon IIIC) (responsible for variability in the C-terminal sequence), generates the additional receptor isoforms with varying ligand affinities that are referred to as the IIIA, IIIB and IIIC isoforms. Variation in coding, is tissue and development specific. Exon IIIB isoform is generally restricted

to cells of epithelial lineage and the IIIC isoform is mainly found in cells of mesenchymal lineage (Ornitz and Itoh, 2015).

1.5.3 Fibroblast growth factor 21 receptor affinity.

It is well established that FGF21 has a high affinity for FGFR1 interaction. Recent studies have shown that isoform FGFR1-IIIC is the favoured receptor for FGF21. However, the interaction between FGF21 and FGFR1-IIIC requires the presence of co-factors or co-receptors such as β-Klotho (KLB) in order to signal efficiently (Angelin et al., 2012; Ding et al., 2012; Iglesias et al., 2012; Li et al., 2013). Unlike FGFRs that are ubiquitously expressed in a variety of tissues, the localisation of FGF21 and β-Klotho have been found to be predominately in the liver, pancreas and WAT (Wu et al., 2012). β-Klotho originates from the Klotho family also including; α-Klotho and γ-Klotho/ Klotho-LPH related protein (KLPH)/ also called Lactase-like Klotho (Lctl) (Ornitz and Itoh, 2015). β-Klotho is a type I single-pass transmembrane protein. It has a large extracellular sequence of 996 aa and a relatively short cytoplasmic sequence of 27 aa. The extracellular region contains two tandem repeats of β-glycosidase domain (D1: 77-508 aa and D2: 517-967 aa) (**Figure 1.10 B**). Moreover, β-Klotho has 11 putative extracellular N-glycosylation sites. The inactive β-glycosidase domains (due to an absence of glutamate residues at position 241 and 889) and a pattern of extensive glycosylation provide multiple mechanisms for β-Klotho to associate at the cell surface. The expression of β-Klotho primarily exists in tissue of enterohepatic origin (e.g. liver and pancreas); expression levels are also high in both brown and WAT and to a lesser degree in the hypothalamus and brainstem (Kilkenny and Rocheleau, 2016; Yang et al., 2012). An *in vivo* study on rodents, demonstrated the effects of FGF21 on the growth and metabolism of *β-Klotho*-/- knockout mice which were negligible, demonstrating the importance of β-Klotho for the activation and action of FGF21 (Ding et al., 2012).

1.5.4 Fibroblast growth factor 21 signalling and activation.

Several studies confirm that the activation of FGF21 is induced via the ternary formation of a two pre-complex structure with FGFR1-IIIC and β-Klotho. The presence of both the receptor and co-receptor is highly important for signal transduction and individually are considered

insufficient to support FGF21 signalling (Kharitonenkov and Larsen, 2011; Smith et al., 2013). Yie and colleagues revealed the investigation of the proposed mechanism of FGF21 activation (Yie et al., 2012). It is suggested that when FGF21 or β-Klotho is present alone, the inhibitory domain (D1/ linker region) of FGFR1-IIIC intervenes by inhibiting their interaction via the D2-D3 region of the receptor (**Figure 1.11 A**) (Cuevas-Ramos et al., 2012; Yie et al., 2012). As

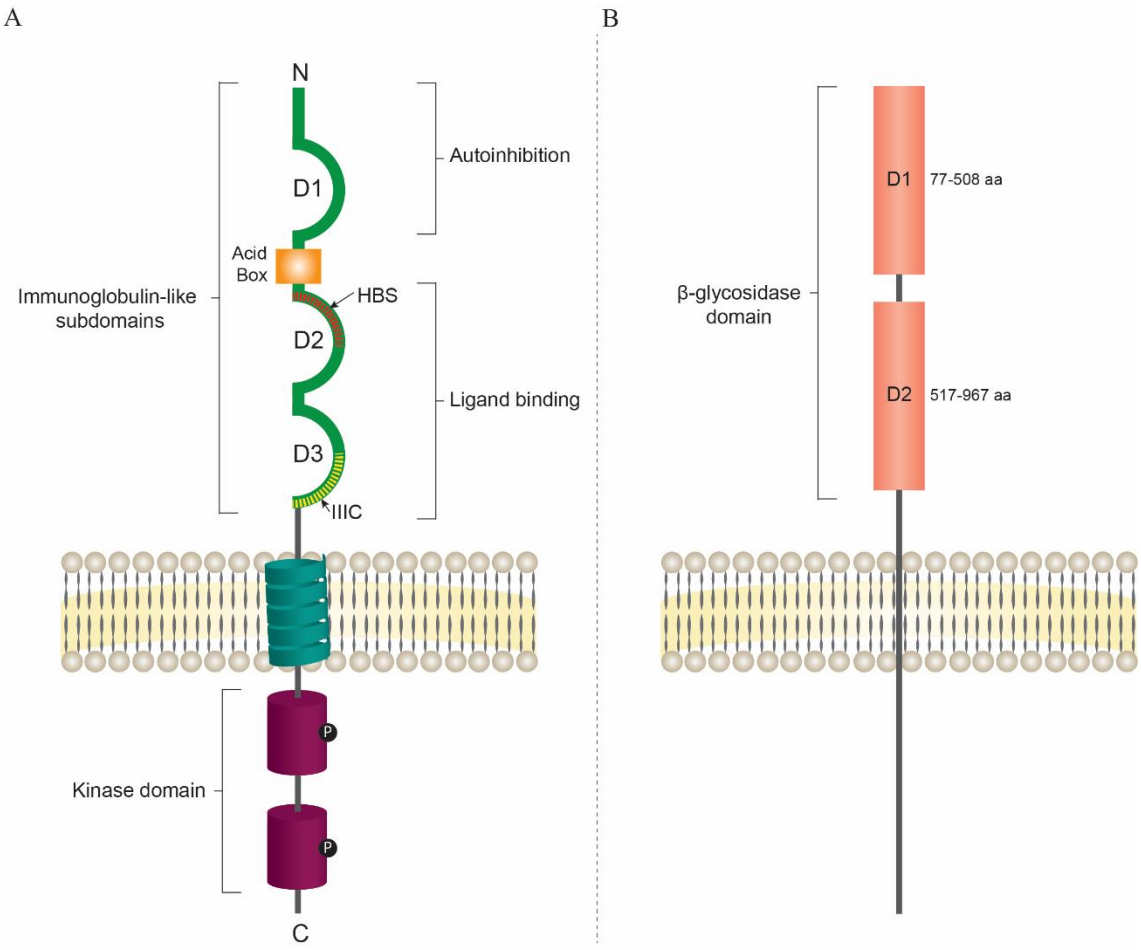

Figure 1.10 Schematic structure of Fibroblast growth factor 1-IIIC and β-Klotho. (A) FGFR; a N-terminal extracellular domain formed of three immunoglobulin-like (Ig-like) subdomains (D1, D2 and D3), separated by a short stretch of acidic residues, a single α-helix transmembrane domain with a long juxtamembrane sequence, and a split intracellular tyrosine kinase domain and a C terminal tail. Between the D1-D2 linker is a contiguous segment of (~30 serine residues), the acid box. Subdomain D3 determines the specificity of ligand binding and subdomain D1 has a role in receptor auto-inhibition. A number of FGFR isoforms exist due to alternative splicing at specific exons primarily within the second half of D3 domain generates FGFR isoforms (e.g. FGFR1-IIIC). **(B)** β-klotho (KLB), a type I single-pass transmembrane protein. It has a large extracellular sequence of 996 aa and a relatively short cytoplasmic sequence of 27 aa. The extracellular region contains two tandem repeats of β-glycosidase domain (D1: 77-508 aa and D2: 517-967 aa). Adapted from (Kilkenny and Rocheleau, 2016).

FGF21 comes into vicinity activation of the ligand proceeds in a two-step motion. Initially, FGF21 binds to β-Klotho via its C-terminus (Kharitonenkov and Larsen, 2011). This interaction over-rides the inhibitory effect of the D1/linker region of FGFR1-IIIC. This conformational alteration thus allows the binding of FGF21 to the D2-D3 region of FGFR1-IIIC via its N-terminal to form a FGF21/FGFR1-IIIC/β-Klotho complex (**Figure 1.11 B**) (Cuevas-Ramos et al., 2012; Kharitonenkov and Larsen, 2011; Yie et al., 2012). Subsequently, this triggers the dimerisation of FGFR1-IIIC bringing the two tyrosine kinase domains into close proximity allowing them to cross-phosphorylate neighbouring tyrosines in their activation loop (Cuevas-Ramos et al., 2012). The active tyrosines recruit adaptor proteins and phosphorylation of cytoplasmic substrates initiate downstream signalling cascades, such as RAS-MAPK, PI3K-AKT, PLCγ and STAT pathways (Ornitz and Itoh, 2015).

1.5.5 Metabolic actions of Fibroblast growth factor 21 in human physiology.

The role of FGF21 in glucose homeostasis and lipid metabolism has been highlighted in changes of nutritional status such as starvation and feeding involving a dual regulation via peroxisome proliferator-activated receptor alpha (PPARα) and peroxisome proliferator-activated receptor gamma (PPARγ) (**Figure 1.12**) (Cuevas-Ramos et al., 2012; Iglesias et al., 2012; Kim and Lee, 2015).

It was first discovered in 2007 that in a fasting state the increased expression of hepatic FGF21 was induced by PPARα activation in the liver acting in an endocrine mechanism by transducing an adaptive response to starvation. PPARα is highly abundant in the liver and binds directly to the peroxisome proliferator response elements (PPRE) on the *FGF21* gene promoter to induce its transcription (Bae et al., 2014). In turn this stimulates the oxidation of fatty acids and the production of ketone bodies (*β*-hydroxybutyrate, acetoacetate and acetone), acting as a major energy source for the brain (Ge et al., 2012). Thus, it is well known that fasting induced hepatic FGF21 expression plays a pivotal role in driving the process of fatty acid oxidation and ketogenesis (Kim and Lee, 2015). Glucose, a feeding signal also induces human *FGF21* gene

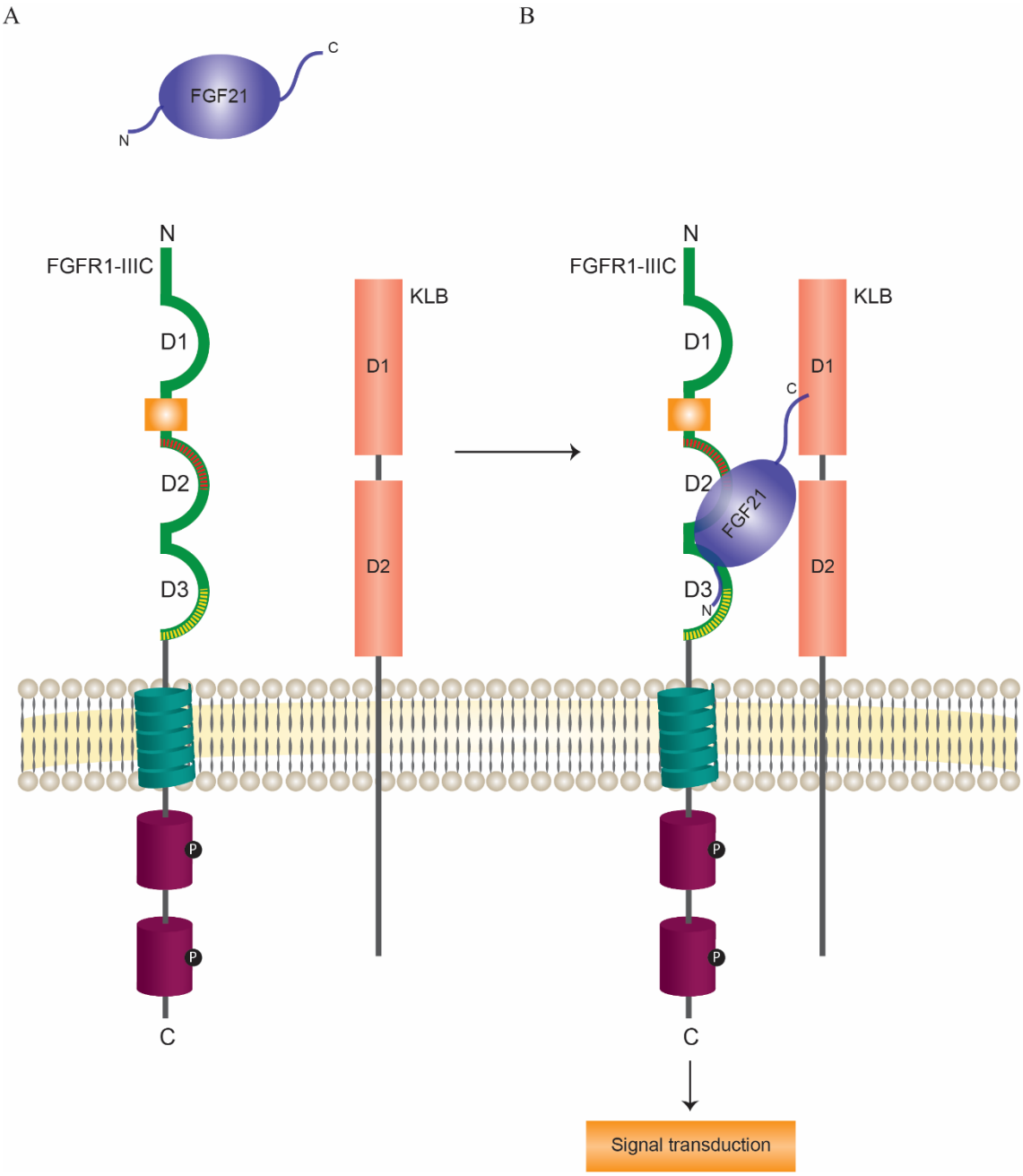

Figure 1.11 Fibroblast growth factor 21 signalling and activation. (A) D1/ linker region of FGFR1-IIIC inhibits ligand interaction via the D2-D3 region of the receptor when FGF21 or β-Klotho (KLB) are present alone. **(B)** In the presence of FGF21, activation of the ligand proceeds in a two-step motion. 1) FGF21 binds to β-Klotho via its C-terminus to overcome the inhibitory effect of the D1/linker region of FGFR1-IIIC. 2) A conformational alteration allows the binding of FGF21 to the D2-D3 region of FGFR1-IIIC via its N-terminal forming a FGF21/FGFR1-IIIC/β-Klotho complex. Adapted from (Cuevas-Ramos et al., 2012; Kilkenny and Rocheleau, 2016).

expression in the liver through carbohydrate response element binding protein (ChREBP) activation (Cuevas-Ramos et al., 2012). In addition, elevated levels of hepatic FGF21 also plays a key role in regulating fasting glucose levels by enhancing gluconeogenesis via the upregulation

of the hepatic PPARγ coactivator 1 alpha (PGC1α). Hepatic derived circulating FGF21 enters the brain activating hypothalamic-pituitary-adrenal axis, to enhance PGC1α and gluconeogenesis (Kim and Lee, 2015). Several other factors have been reported in the positive and negative regulation of FGF21 expression including; glucocorticoid receptor (GR) activating transcription factor 4 (ATF4) cAMP-responsive element binding protein (CREBH), farnesoid X receptor (FXR) and liver X receptor (LXR) under various conditions (Inagaki, 2015).

Conversely, it is shown that in a feeding state, PPARγ activation (and its agonists including some fatty acids and the insulin-sensitising drugs thiazolidinediones, rosiglitazone and pioglitazone) promotes FGF21 production in white adipocytes to enhance glucose uptake by increasing the expression of glucose transporter 1 (GLUT-1) and increasing triglyceride degradation. A combination of PPARγ and ChREBP are seen to co-ordinately regulate *FGF21* gene expression in adipocytes (Cuevas-Ramos et al., 2012). Adipocyte derived FGF21 is known to act in an autocrine fashion, amplifying the effects of PPARγ. This effectively establishes a closed loop, aimed at maintaining the circulating systemic levels of FGF21 (Bae et al., 2014; Cuevas-Ramos et al., 2012).

FGF21 has also been shown to provide defence against hypothermia by enhancing thermogenesis via increasing expression of uncoupling protein 1 in response to cold exposure. WAT is converted to a 'brown-like' state following prolonged cold exposure, which is driven by FGF21 expression. (Cuevas-Ramos et al., 2012; Kim and Lee, 2015). FGF21 co-receptor β-Klotho is also expressed in the central nervous system (CNS). FGF21 is able to cross the blood brain barrier which suggests a potential role in the regulation of both food intake and energy expenditure (Cuevas-Ramos et al., 2012).

1.5.6 Metabolic diseases associated with Fibroblast growth factor 21.

Although FGF21 is well known for its regulation during a fasting and feeding state, it has also been identified as a mediator for several pathological conditions and/or potential candidates for the therapeutic intervention for various disorders.

Studies have reported that increased circulating FGF21 levels in patients are associated with fasting, macronutrient diet composition, physiological/ environmental stress and several metabolic syndromes including; obesity, type 2 diabetes (T2D) (insulin resistant state), impaired glucose tolerance, fatty liver disease, muscle atrophy and coronary heart disease (CHD) (**Figure 1.12**) (Cuevas-Ramos et al., 2012; Erickson and Moreau, 2016; Iglesias et al., 2012; Kim and Lee, 2015; Woo et al., 2013). Obesity induced serum FGF21 levels were found in both children and

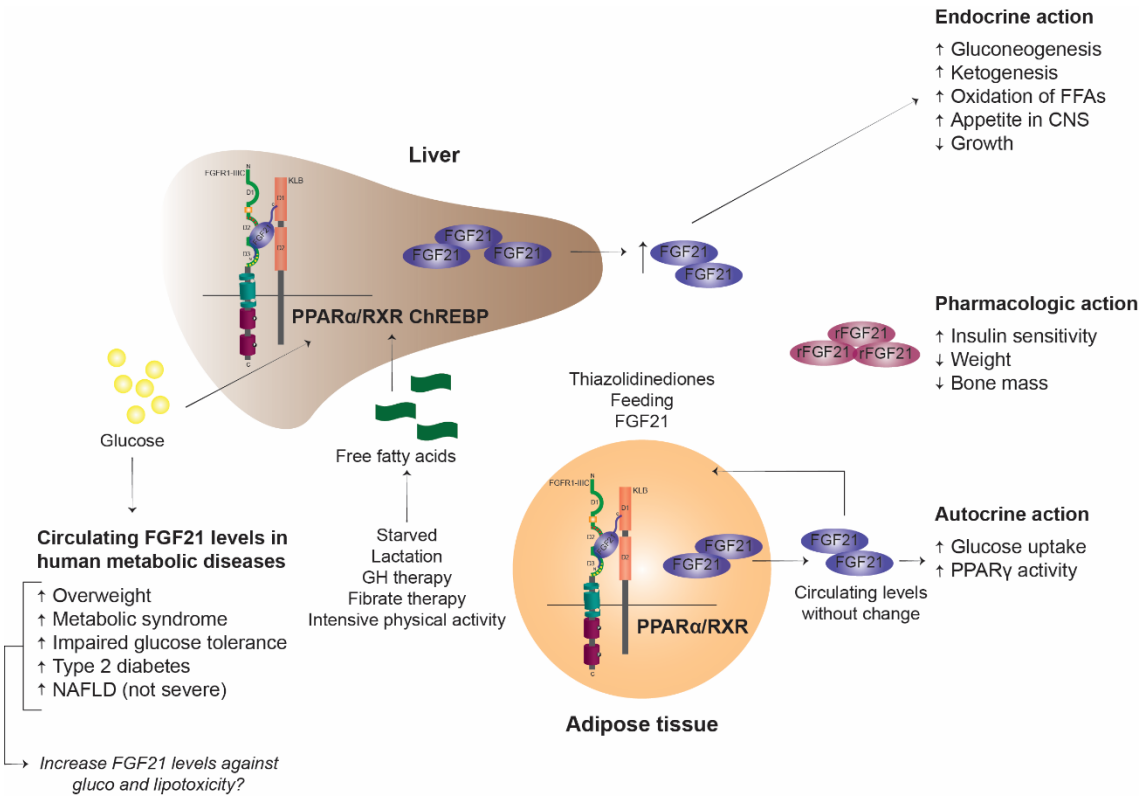

Figure 1.12 An overview of Fibroblast growth factor 21 regulation and function. Hepatic FGF21 expression is regulated by PPARα activation. Excessive FFA concentration (stimulated by i.e. starvation, lactation, GH therapy and intensive physical activity) induces the production of FGF21 and circulatory release. Elevated FGF21 levels aim to improve energy production (via gluconeogenesis) and utilisation (increased oxidation of FFA, ketogenesis and glucose uptake). FGF21 also stimulates appetite and induces growth failure during prolonged starvation as an adaptive response mechanism. Adipocyte-derived FGF21 induces an autocrine response to amplify PPARγ activation, excluding changes in systemic FGF21 levels. Pharmacologic PPARγ agonists; chronic administration of FGF21 (recombinant FGF21; rFGF21) may have beneficial (increased insulin sensitivity) and undesirable consequences (reduced bone mass). Carbohydrates also induce FGF21 expression mediated by ChREBP. Elevated FGF21 levels have also been associated with insulin resistance. Increasing FGF21 levels are known to be induced by hyperglycemia and high FFAs and usually present with increased FGF21 levels. This may be stimulated via a mechanical response against glucotoxicity and lipotoxicity. Adapted from (Cuevas-Ramos et al., 2012).

adults, illustrating a correlation between FGF21 and body fat mass. *In vivo* studies on obese rodents showed that they responded poorly to exogenous FGF21 suggesting that obesity could be a FGF21-resistant state. In addition, serum FGF21 levels were significantly higher in CHD patients than control groups, which was further seen to be exaggerated in CHD patients with diabetes and hypertension than without such comorbidities (Iglesias et al., 2012). As for renal failure circulating FGF21 levels were found to be independently associated with renal function than control patients with a progressive increase in FGF21 levels from early to the end stage of the disease and ~8 – 15 time higher in long term dialysis patients (Iglesias et al., 2012). Inversely, reduced FGF21 levels were observed in type 1 diabetes and latent autoimmune diabetes in adults (Ge et al., 2012; Iglesias et al., 2012). Metabolic benefits of FGF21 administration include improved insulin sensitivity, glucose homeostasis and also preservation of β-cell function in diabetic models. Moreover, FGF21 therapy was shown to significantly improve the lipid profile; decreasing triglyceride and low-density lipoproteins whilst increasing high-density lipoproteins (Bae et al., 2014; Iglesias et al., 2012).

Over-nutrition and refeeding also upregulate *FGF21* gene expression. This response may be induced by dietary carbohydrates as it was shown that carbohydrates induce FGF21 gene expression through the transcription factor Carbohydrate response element binding protein ChREBP (Erickson and Moreau, 2016).

1.5.7 Regulation of Fibroblast growth factor 21 expression by nutrition.

Nutritional signals can act directly or indirectly to play a pivotal role in regulating gene expression in mammals. Several studies demonstrate that a nutritional imbalance including; calorie deprivation, over/ under supply of macronutrients (carbohydrates, fatty acids, proteins), changes in amino acid composition or bioactive dietary compounds alters FGF21 levels (**Figure 1.13**) (Erickson and Moreau, 2016; Perez-Marti et al., 2016; Solon-Biet et al., 2016).

In humans prolonged fasting (after 7 days) induces the increased expression of hepatic FGF21, whilst FGF21 levels were found to be largely unchanged during short intervals of fast (2

days) (Erickson and Moreau, 2016). In addition, rats fed a high carbohydrate diet (HCD) (mixed sugar and starch) was found to influence increased hepatic mRNA and serum FGF21 levels and increase metabolic activity in the liver and WAT (Erickson and Moreau, 2016; Perez-Marti et al., 2016). HCD induced FGF21 expression promoted lipogenesis, glucose uptake and metabolism and a reduction of fatty acids and fatty acid oxidation in the liver and similarly lipogenesis, glucose uptake and metabolism and lipolysis in WAT (Perez-Marti et al., 2016). In rodents and humans, besides glucose, high hepatic FGF21 is also induced by fructose, sucrose and xylitol via ChREBP which binds to carbohydrate response element (ChoRE) localised on the FGF21 promoter (Erickson and Moreau, 2016; Perez-Marti et al., 2016).

It was suggested that in mice a sustained high fat diet (HFD) were associated with an increased expression of *FGF21* mRNA expression in the liver and WAT. However conflicting *in vivo* data reported no significant changes in hepatic FGF21 levels in mice fed a HFD compared to mice on a low-fat diet for 16 weeks (Erickson and Moreau, 2016). Such inconsistencies may be explained through the variation in fatty acid composition included in diets. Butyrate and α-lipoic acid have also been shown to modulate hepatic FGF21 expression. Butyrate produced by bacterial fermentation of dietary fibre in the large intestine is suggested to regulate FGF21 expression via its ability to inhibit histone deacetylase-3 (HDAC3). α-lipoic acid derived from leafy green vegetables and red meats induces hepatic and plasma FGF21 levels via CREBH dependent mechanisms (Perez-Marti et al., 2016).

Several studies have demonstrated that hepatic FGF21 levels are increased by low protein diets and more specifically by singly restricted amino acids including leucine or methionine (Erickson and Moreau, 2016; Perez-Marti et al., 2016; Solon-Biet et al., 2016). In wild-type mice, elevated FGF21 expression promoted by leucine deprivation resulted in a significant change in lipid metabolism in the liver, including; inhibition of fatty acid synthase activity, decrease in the expression of lipogenic genes and an increase in the mobilisation of lipid stores. Similarly, methionine deprivation in mice, shared a comparable phenotype including; a resistance to diet-induced obesity, improved glucose homeostasis, increase fatty acid activation and oxidation in the liver, increase lipolysis in WAT and increased Ucp1 expression in brown adipose tissue – all

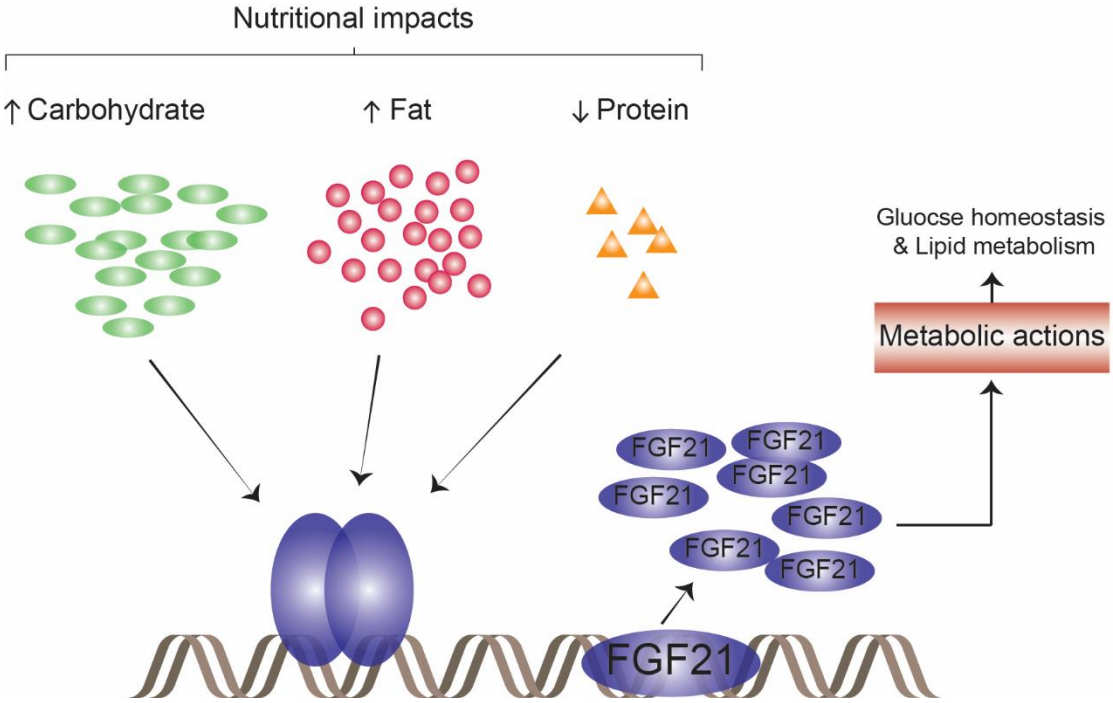

Figure 1.13 Nutrition induced Fibroblast growth factor 21 expression. Endogenous FGF21 levels are regulated by macronutrient availability (carbohydrates, fats and protein). High carbohydrate and fat, and low intake drives the transcription and upregulation of FGF21 to induces a wide profile of metabolic actions, primarily involved in glucose homeostasis and lipid metabolism. Adapted from (Perez-Marti et al., 2016).

associated with elevated FGF21 expression (Perez-Marti et al., 2016). In the same way serum FGF21 levels are shown to increase in both humans and rodents during a low-protein diet (LPD) independent of caloric intake. Protein restriction is known to influence increased food intake and energy expenditure. Ketogenic diets – rich in fat and low in carbohydrate and protein is widely

accepted to contribute to elevated FGF21 expression. Whilst the supplementation of proteins during ketogenic diets is seen to prevent elevated circulatory FGF21 levels (Perez-Marti et al., 2016). In addition, LPD increases general control non-derepressible 2 (GCN2); (a kinase sensor for amino acid supply) dependent phosphorylation of eIF2a which subsequently leads to increased ATF4 protein expression. The GCN2/eIF2a/ATF4 cascade induces elevated FGF21 expression via protein restriction. The 5' regulatory region of FGF21 containing two conserved functional ATF4 binding sequences binds to ATF4 promoting transcriptional activation in response to amino acid restriction. Lastly, hepatic mTORC1 activity has also been identified to promote FGF21 expression. mTOR signalling pathway regulates amino acid sufficiency, activating protein

translation, cell growth and other processes. It is suggested that mechanistically PGC1α induces increased FGF21 however other unidentified mechanisms may be involved (Perez-Marti et al., 2016; Solon-Biet et al., 2016).

1.5.8 Fibroblast growth factor 21 and Growth hormone resistance.

Good nutrition is fundamental for a child's overall health, growth and development. Thus, malnutrition during early infancy (particularly within 2 years of life) is well described to have severe negative outcomes, causing a significant reduction in linear growth and development (Gat-Yablonski et al., 2013; Prentice et al., 2006). Recent evidence suggests that an elevated expression of FGF21 during prolonged periods of chronic food restriction develops GH resistance leading to growth failure and the subsequent attenuation of skeletal growth and growth plate chondrogenesis (Guasti et al., 2014; Kubicky et al., 2012; Wu et al., 2012). The molecular mechanistic role of FGF21 is not yet fully elucidated and thus FGF21 actions on skeletal growth remain not entirely known.

An *in vivo* study undertaken by Kubicky et al., 2012 has demonstrated that *Fgf21* knockout mice that were restricted of food for 4 weeks showed increased body and tibial growth compared to their wild-type littermates. When daily injections of recombinant human FGF21 were administered to *Fgf21* knockout mice the differences in body and tibial growth compared to wildtype were prevented. In addition, a single injection of GH stimulated increased mRNA hepatic STAT5 and IGF-1 expression in food restricted *Fgf21* knockout mice than wildtype (Kubicky et al., 2012). Similarly, an *in vivo* study by Inagaki et al., 2008 using a *Fgf21* transgenic mouse model demonstrated complementary results. FGF21 was shown to inhibit the expression of STAT5 and downstream targets including IGF-1. Moreover, FGF21 was found to induce liver expression of IGF-1 binding protein 1 and SOCS2 which were collectively suggested to blunt GH signalling (Inagaki et al., 2008).

Coinciding with these *in vivo* findings a Finnish PreBaby clinical assessment on metabolism and growth in very pre-term (VPT) infants revealed a significant negative association

between the mean FGF21 level during the first 5 weeks of life and growth failure. Furthermore, in primary chondrocytes obtained from rib cartilage FGF21 upregulated GH-induced SOCS2 expression and inhibited GH-induced STAT5 phosphorylation and IGF-1 expression (Guasti et al., 2014). Mericq et al., 2014 demonstrated in preterm babies that at birth and 12 months, no differences were observed between preterm and term infants, whilst at 6 months serum FGF21 levels in term infants was significantly higher than that of pre-term infants (Mericq et al., 2014).

This evidence highlights a novel mechanistic role of FGF21 in the development of GH resistance secondary to prolonged chronic undernutrition. This may further unravel the cause of GH failure associated with chronic childhood conditions e.g. undernutrition, chronic conditions (Crohn's Disease), inflammation, metabolic alterations, premature birth and anorexia.

The role of FGF21 in GH resistance together with nutritional imbalance in patients associated with underlying chronic conditions has elicited a large interest in recent studies of childhood growth failure. It is envisaged that elevated expression of FGF21 has a vital role in GH resistance by a direct action on human chondrocytes. Here described are two proposed mechanisms of FGF21s' actions in the development of GH resistance (**Figure 1.14**). Firstly, activation of the FGF21/FGFR1-IIIC/β-Klotho complex may inhibit early GH/GHR signalling events e.g. JAK/ STAT5 phosphorylation. Secondly, FGF21/FGFR1-IIIC/β-Klotho complex activation may act independently to interact with SOCS2; a negative regulator of GH signalling to inhibit further downstream GHR signalling events.

This study aims to unravel the interplay of FGF21 in GHR signalling from early to late downstream events to determine a thorough understanding of the molecular mechanisms of FGF21 induced GH resistance and subsequent childhood growth failure. Elucidation of such mechanisms has the potential to open novel avenues for future beneficial therapeutic intervention, to ultimately overcome and improve the quality of life of children with GH resistance and subsequent growth failure.

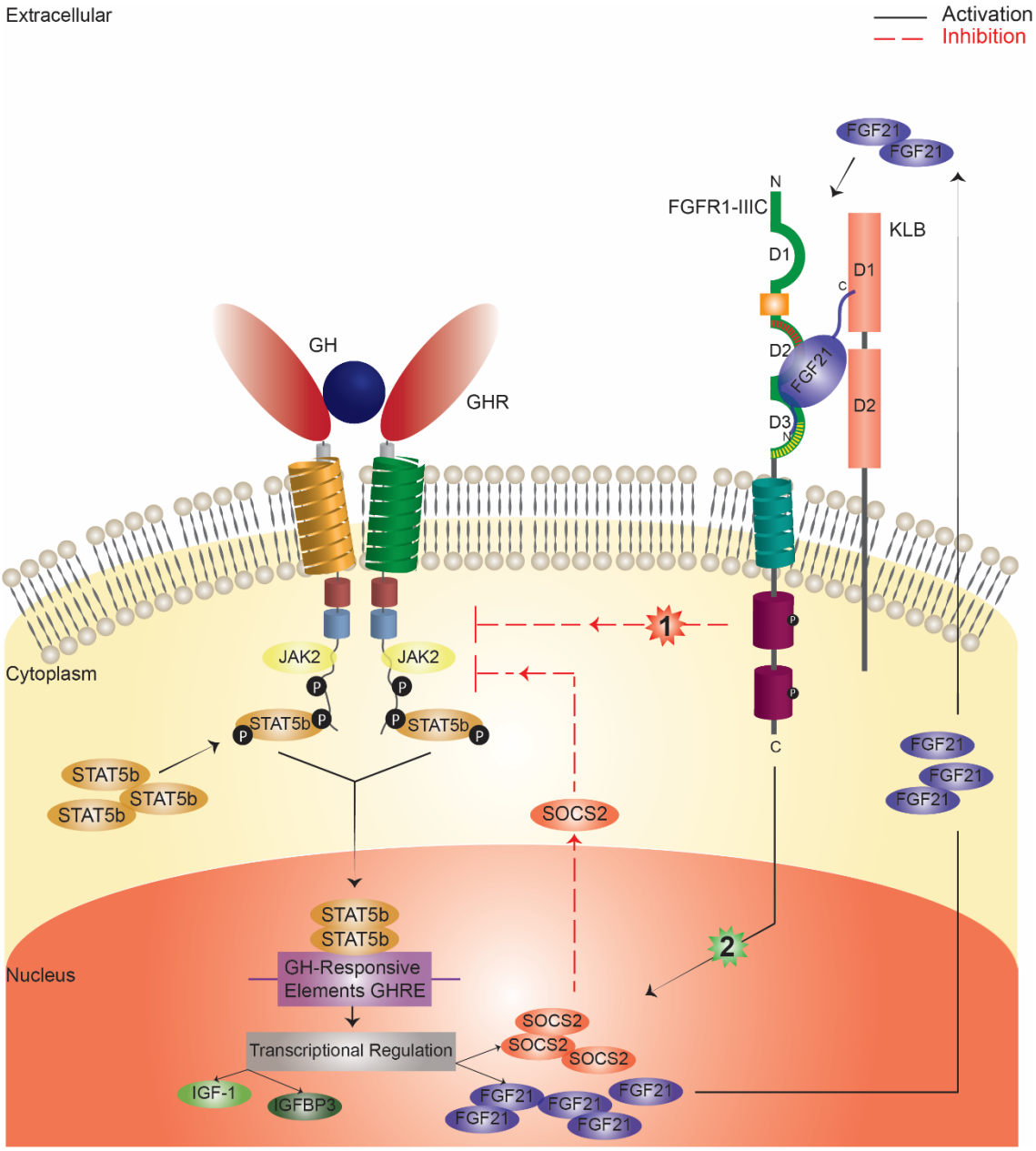

Figure 1.14 Postulated mechanisms of Fibroblast growth factor 21 in the development of GH resistance. Elevated expression of FGF21 during chronic conditions (e.g. prolonged undernutrition) is thought to develop GH resistance and growth failure. The precise mechanisms of FGF21s' actions in the development of GH resistance is unknown. Two proposed mechanisms of FGF21 induced GH resistance. **(1)** FGF21/FGFR1-IIIC/β-Klotho complex activation inhibits early GH/GHR signalling events, including JAK2/STAT5b phosphorylation. **(2)** FGF21/FGFR1-IIIC/β-Klotho complex activation directly interacts with SOCS2 (negative regulator of GH signalling) upregulating SOCS2 expression to inhibit further activation of downstream GHR signalling events.

1.6 Research hypothesis and project aims.

It is well described that hepatic IGF-1, a key mediator of linear growth is carefully regulated by GH secretion from the somatotroph cells of the anterior pituitary gland. However, not all actions of GH are mediated via IGF-1 expression. Several studies highlight IGF-1 secretion to be responsive to nutritional cues (Fazeli and Klibanski, 2014; Hawkes and Grimberg, 2015). Undernutrition is thought to affect GH signalling at multiple sites of the cascade, leading to the consequential development of a GH resistance state (Hawkes and Grimberg, 2015). Recently, a new mechanism for the undernutrition induced GH resistance and growth failure was proposed in mice. In an *in vivo* study by Kubicky et al., 2012, FGF21, the expression of which was seen to be induced by undernutrition was shown to cause GH resistance. More importantly, undernutrition induced growth failure was totally abolished in FGF21 knock-out mice.

It is hypothesised that FGF21 causes GH resistance by a direct action on human chondrocytes, primarily targeting GHR and downstream signalling events. In addition, it is further envisaged that the elevated circulating FGF21 concentration induced by severe chronic conditions (i.e. pre-term birth, malnutrition) are associated with the development of GH resistance and reduced growth rate. Thus, the aim of this PhD was to unravel *in vitro* the molecular mechanistic interplay of FGF21 on GHR and downstream signalling events involving the JAK/STAT signalling cascade, directly linked with linear growth. Furthermore, VPT infants were recruited from a Finnish population at the Kuopio University Hospital as part of a clinical investigation, to aim to address the link between macronutrient induced elevated FGF21 levels and growth attenuation.

It has been proven to be extremely difficult to detect endogenous GHR levels using commercially available antibodies. Thus to achieve these aims; **(i)** initially Human embryonic kidney (HEK-293) stably transfected cell lines expressing exogenous human or mouse GHR were generated *in vitro* to allow us to monitor GHR activity. **(ii)** HEK-293 human/ mouse GHR stable lines and chondrocytic cells (immortalised juvenile human costal chondrocytes C28/I2, mouse embryonic mesenchymal cells C3H 10T1/2) were validated for the expression of key mediators of the JAK/STAT pathway (GHR, JAK2, STAT5, pJAK2, pSTAT5, SOCS2) and FGF21 activity

(FGF21, FGFR1, FGFR1-IIIC, β-klotho) (**Chapter 3**). Following the establishment of a suitable model to investigate GHR and downstream signalling events, **(iii)** the direct effect of chronic FGF21 on GHR and individual mediators of the JAK/STAT pathway were evaluated to clarify the inhibitory effects of FGF21s' action in the development of GH resistance (**Chapter 4**).

To address the second aim of this investigation, **(i)** FGF21 and IGF-1 serum concentrations were measured in our cohort of VPT infants at varying time-points (weeks) after birth. **(ii)** Together hormonal levels and the patient database of our cohort of weekly documented growth and nutritional intake, were used to examine multi-comparison association studies to determine the link between elevated FGF21 levels triggered by macronutrient availability and its association in childhood growth failure (**Chapter 5**).

CHAPTER 2. Materials and methods

2.1 Origin of cell lines.

Human embryonic kidney cell line (HEK-293) was established by the transformation and culturing of embryonic kidney cells with sheared adenovirus 5 DNA. The transformation resulted in the incorporation of ~4.5kb from the viral genome into human chromosome 19. The line was established by Alex Van der Eb in early 1970s at the University of Leiden, Holland and the transformation was performed by Van der Eb's colleague, Frank Graham (Thomas and Smart, 2005).

C28/I2, human chondrocyte cell line was derived from primary cultures (day 5) isolated from juvenile human costal cartilage from a female aged 15 years. Chondrocytes were transfected using polybrene with vectors encoding simian virus 40 large T antigen inserted in the retroviral neomycin-resistant pZipNeosv(X) vector and selection in suspension culture over agarose. Stable lines were generated that exhibit chondrocyte morphology of continuous proliferative capacity (>80 passages) in monolayer cultures (Goldring et al., 1994). The C28/I2 human chondrocyte cell line is widely used as a model to study normal and pathological cartilage repair mechanism related to chondrocyte biology and physiology.

The C3H 10T1/2 cell line was established in 1973 and characterised by Catherine A Reznikoff. It is a mouse embryonic mesenchymal cell line that originates from the generation of primary cultures of 14 to 17 day old whole mouse embryos (inbred C3H Heston strain) disaggregated with 0.25% trypsin. The resulting cell line was sub-cloned for immortalisation and contact-inhibited growth. C3H10T1/2 cells maintain a stable morphology even after long periods in culture. When sub-confluent, they appear fibroblast-like with extended cytoplasmic processes. In confluent cultures the cells appear as a flat, regular, epithelioid-like sheet (Pinney and Emerson, 1989). Both C28/I2 and C3H 10T1/2 cell lines were a kind gift from Dr Mary B Goldring, Hospital for Special Surgery, New York, USA.

2.1.1 Routine tissue culture.

HEK-293 cells were grown in high glucose (4500mg/litre) Dulbecco's modified Eagle medium (DMEM) *(Sigma-Aldrich, Poole, UK)* supplemented with 10% Fetal Bovine serum (FBS) *(GIBCO, Paisley, UK)* and 1% Penicillin-Streptomycin (P/S) *(Sigma-Aldrich)*. C28/I2 and

C3H 10T1/2 cells were grown in Dulbecco's modified Eagle medium/ Nutrient Mixture F-12 Ham (DMEM- F12HAM) *(Sigma-Aldrich)* supplemented with 10% FBS and 1% (100x) Anti-biotic Anti-mycotic (AB/AM) *(Life technology limited, Paisley, UK).*

Cryovials of frozen stocks stored in liquid nitrogen vessels (approximately -196˚C) were thawed and transferred to a 15ml falcon tube containing 9ml of complete growth media. Cells were centrifuged *(Heraeus Labofuge 400 centrifuge, Thermo Scientific)* at 1500rpm for 5 minutes. The supernatant was carefully discarded without disturbing the pellet. The pellet was re-suspended in 10ml of complete growth media and the cells were cultured in T75cm^2 culture flasks *(Cellstar, Stonehouse, UK)* at 37˚C and 5% CO_2 *(Galaxy 170S, New Brunswick).*

Cells cultured in T75cm^2 culture flasks were used to expand cell lines. All cell lines were passaged twice a week to maintain a cell population at approximately 1.0 x 10^5 cells/ml. Cells were passaged when they reached ~80 to 90% confluency. Media was aspirated from the cell culture flask and cells were washed with Phosphate Buffered Saline (PBS) without calcium *(Sigma-Aldrich).* Cells were detached from the flask using 3ml 0.05% (1x) Tyrpsin-EDTA *(GIBCO)* and incubated at 37°C, 5% CO_2 for 5 minutes. Detachment of surface adherent cells was verified via microscopic examination, before the addition of 7ml of complete growth media to inactivate trypsin. The cell suspension was then transferred into a new T75cm^2 flask at a 1:10 dilution ratio of cells to complete growth media.

For experimental studies, cells were plated in either 96-well plates, 6-well plates (*Cellstar*) or T75cm^2 culture flasks. To determine the seeding density of cells to plate for experimental investigations, media was aspirated from T75cm^2 flasks and cells were washed with (1x) PBS. As described previously, cells were detached from the flask using 3ml 0.05% (1x) Tyrpsin-EDTA *(GIBCO)* and incubated at 37°C, 5% CO_2 for 5 minutes. Detachment of cells was verified via microscopic examination, before the addition of 7ml complete growth media to inactivate trypsin. The cell suspension was then transferred into a 15ml falcon tube and centrifuged at 1500rpm for 5 minutes to generate a cell pellet. The supernatant was discarded and the cell pellet was re-suspended in 1ml of media. The number of viable cells was determined using a glass haemocytometer by combining a 1:1 ratio of the cell suspension and Trypan-Blue *(Sigma-Aldrich).* The haemocytometer was viewed under a microscope and the number of cells

was determined within a given area and an average of the number of cells was calculated, expressed as (average cell number) x 10^4 cells/ml. Cells were seeded at 5.0 x 10^3 cells/well, 3.0 x 10^5 cells/well or 1.0 x 10^5 cells/ml in 96-well plates, 6-well plates or T75cm^2 culture flasks, respectively. The final volume of media was as follows; 96-well plates: 100µl, 6-well plates: 2ml and T75cm^2 culture flasks: 10ml. Cells were incubated at 37°C and 5% CO_2 until they reached the recommended confluency to perform functional studies.

2.2 Primary culture of human growth plate tissue biopsies.

Human growth plate tissue biopsies were obtained through our collaborative partners Professor Lars Sävendahl and Dr Farasat Zaman at Karolinska Institutet, Department of Women's and Children's health, Stockholm, Sweden. Primary chondrocytes retain at least partly their chondrogenic phenotype and signalling pathways involved in its regulation (Emons et al., 2011; Karimian et al., 2011; Zaman et al., 2014). Thus, primary cultures of human growth plate biopsies should offer an ideal model to investigate cellular interactions of GHR signalling and to further trace downstream cascade events.

Growth plate biopsies were obtained from children undergoing elected epiphyseal surgery at different stages of puberty in order to arrest further leg growth, due to constitutional tall stature or leg length difference (**Table 2.1**). A needle was inserted into the bone (visualised using real-time x-ray technology) to isolate growth plate biopsies from the right and left tibia and femur of each patient (*n*=3) (**Figure 2.1 i**). Extracted biopsies were placed immediately into collection media prepared using DMEM high glucose (4500mg/L), L-glutamine media *(Invitrogen, Paisely, UK)*, HEPES (4-(2-hydroxyethyl)-1-piperazineethanesulfonic acid) without sodium pyruvate and phenol red and Gentamicin (10µg/ml) *(Invitrogen)* kept on ice before processing of the biopsies in the lab. Growth plate biopsies were visualised using a dissection microscope under sterile conditions (**Figure 2.1 ii**). The growth plate biopsy was sectioned into thin slices of approximately 2mm thickness and individual slices were randomly distributed into 24-well plates *(Cellstar)* containing culture media (50 ml DMEM + gentamicin, 1ml 10% bovine serum albumin (BSA) *(Sigma-Aldrich)*, 50µl *β*-glycerophosphate (1M) *(Sigma-Aldrich)*, 50µl

ascorbic acid (50mg/ml) *(Sigma-Aldrich)*) for latter experimental investigation (**Figure 2.1 iii-iv**).

Table 2.1 Clinical background of patients recruited from Karolinska University Hospital, Stockholm, Sweden. A total of three patients were recruited for elected surgery of growth plate removal from the tibia and femur due to constitutional tall stature or leg length difference.

Patient (*n* = 3)	**Sex**	**Age (years, months)**	**Height (cm)**	**Diagnosis**
1	Female	13,8	180.0	Constitutional tall stature
2	Female	11,1	173.1	Constitutional tall stature
3	Female	12,0	177.1	Constitutional tall stature

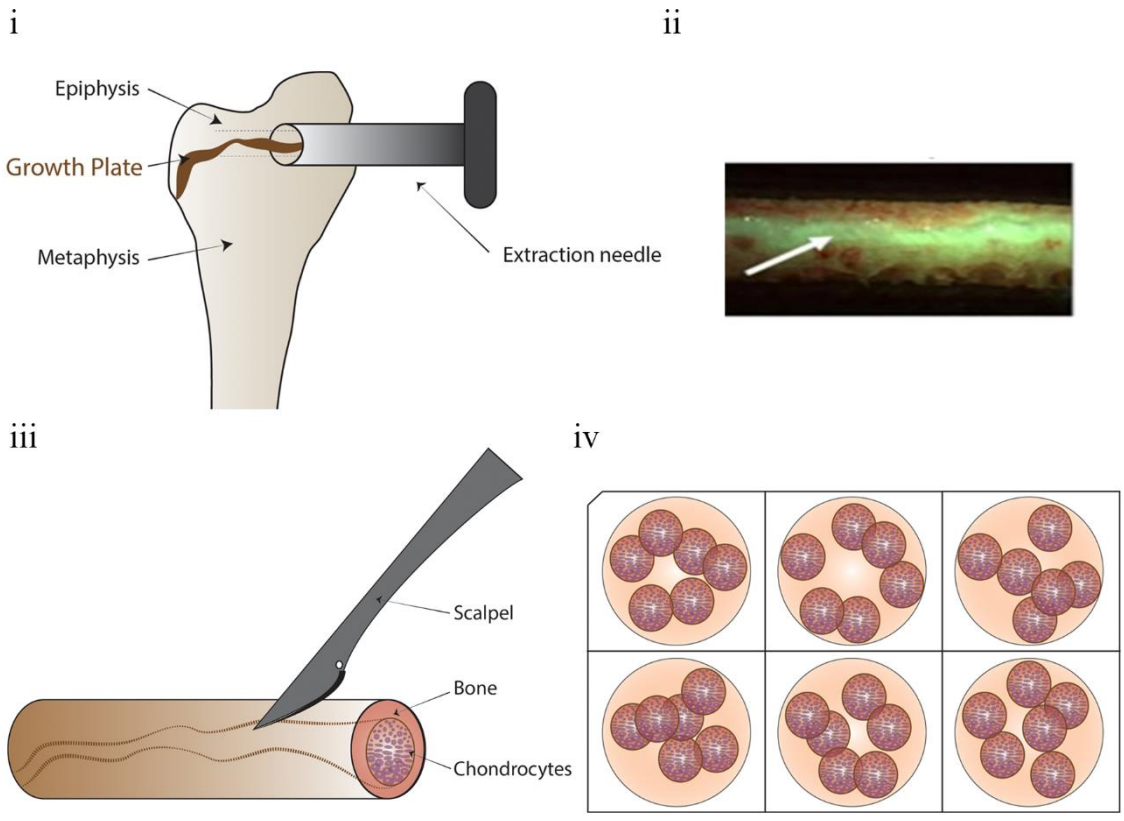

Figure 2.1 Methodology of human growth plate biopsy extraction and primary culture. (i) A needle was inserted into the growth plate region (visualised using real-time x-ray) to obtain the growth plate cartilage. **(ii)** Tibia growth plate cartilage biopsy as visualised in a dissection microscope following collection of the biopsy. **(iii)** Growth plate biopsies were sectioned into thin slices (2mm) using a scalpel. **(iv)** Growth plate slices were transferred at random into 24-well culture plates for proceeding experimental investigations. Adapted from (Zaman et al., 2014).

2.3 Collection of patient serum samples.

As part of a clinical investigation 64 very pre-term (VPT) infants (41 males, 64.1%) were recruited during the first week of life from a PreBaby study of a Finnish population at the Kuopio University Hospital neonatal intensive care unit. The clinical characteristics of VPT infants are reported in **Table 2.2**.

Table 2.2 Clinical characteristics of the 64 VPT infants (41 males, 64.1%). Median and range at birth, nadir (lowest point of weight/ length SDS) and total growth follow-up of postmenstrual age, weight (kg/ SD) and length (cm/ SD).

	Median	**Range**
At birth		
Gestational age, week	29.00	23.43 – 31.86
Weight, kg	1.14	0.50 – 1.88
Weight, SD[a]	-0.54	-3.76 – 2.36
Length, cm	37.00	29.00 – 44.00
Length, SD[a]	-0.25	-4.70 – 4.10
At nadir		
Postmenstrual age for weight, week	33.72	28.00 – 40.00
Weight, kg	1.57	0.66 – 2.63
Weight, SD[b]	-2.57	-4.88 – -0.49
Postmenstrual age for length, week	34.57	29.57 – 40.43
Length, cm	40.55	32.42 – 50.00
Length, SD[b]	-2.74	-6.05 – -0.43
Total growth follow-up		
Postmenstrual age for, week	115.86	36.85 – 184.57
Weight, kg	10.60	2.81 – 15.60
Weight, SD[b]	-0.74	-4.49 – 1.87
Length, cm	80.10	46.80 – 98.20
Length, SD[b]	-0.70	-4.51 – 1.40

[a] Birth weight and length were converted to SDS using the population-based birth size reference for singletons or twins (Sankilampi et al., 2013). [b] Weight and length at nadir and total growth follow-up were converted to SDS using the population-based birth size reference for singletons (Sankilampi et al., 2013).

The gestational age, weight and length was recorded at birth for each individual patient. Infants were monitored for their weight, recumbent length (transformed into SD scores (SDSs), using the contemporary population-based reference) and nutritional intake (total (kcal/kg), fat (kcal/kg), fat (%), protein (kcal/kg), carbohydrate (kcal/kg) and enteral (kcal/kg) energy) at weeks 1, 3, 5, 7 and 9 (in-patient) and weeks 1 and 2 (out-patient).

Mixed umbilical blood samples were obtained immediately after birth and peripheral venous or arterial samples in weeks 1, 3, 5, 7 and 9 (in-patient) and weeks 1 and 2 (out-patient). Serum samples were prepared by centrifugation after blood collection, separated into aliquots and stored at -80˚C. Serum FGF21 (pg/ml) and IGF-1 (ng/ml) concentration levels were determined using commercially purchased enzyme-linked immunosorbent assays (ELISA) (Chapter 2, section 2.18).

The growth pattern of VPT infants were evaluated during two distinct growth phases; 1) Growth deflection = (length/weight SDS at nadir – length/weight SDS at birth) and 2) Catch-up growth = (length/weight SDS at total growth follow-up – length/weight SDS at nadir), differentiated by the point of nadir (lowest point of weight/ length SDS) (**Figure 2.2**). The sampling of hormonal levels (FGF21 and IGF-1) and nutritional intake taken at weeks 1, 3, 5, 7 and 9 (in-patient) and weeks 1 and 2 (out-patient) were separated in individual patients to reflect mean hormonal and nutritional levels during growth deflection and catch-up growth (**Table 2.3**).

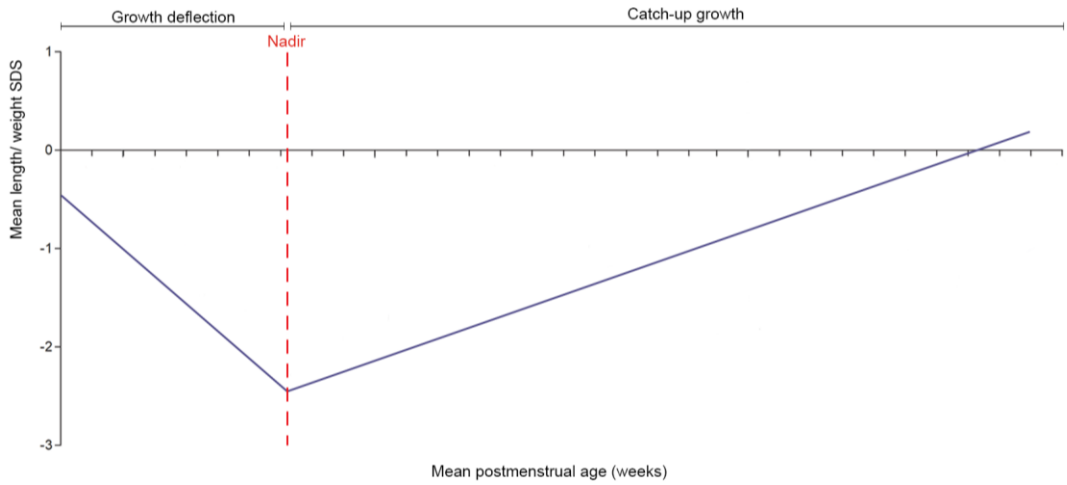

Figure 2.2 An evaluation of growth patterns in very pre-term infants. Growth in our cohort was assessed in two phases. 1) Growth deflection = (length/weight SDS at nadir – length/weight SDS at birth). 2) Catch-up growth = (length/weight SDS at total growth follow-up – length/weight SDS at nadir). The two growth phases were separated by the point of nadir = (lowest point of weight/ length SDS)

Table 2.3 Assessment of hormonal levels and nutritional energy intake during growth deflection and catch-up. Mean and (range) of hormonal levels and nutritional intake during growth deflection and catch-up growth of 64 VPT infants.

	Mean (range)	
	Growth deflection	**Catch-up growth**
Hormonal levels		
FGF21, pg/ml	483.35 (15.00 – 3232.57)	223.04 (24.66 – 1022.27)
IGF-1, ng/ml	5.63 (0.39 – 24.90)	7.82 (0.84 – 25.85)
Nutritional intake		
Total energy, kcal/kg	110.82 (53.47 – 147.13)	118.88 (28.26 – 179.45)
Fat energy, kcal/kg	51.98 (15.92 – 79.50)	60.48 (13.29 – 89.21)
Fat energy, %	44.88 (25.71 – 55.94)	50.85 (34.70 – 58.27)
Protein energy, kcal/kg	12.17 (8.10 – 15.05)	12.10 (2.11 – 19.37)
Carbohydrate energy, kcal/kg	47.52 (27.96 – 67.14)	46.52 (12.87 – 75.54)
Enteral energy, kcal/kg	96.65 (12.86 – 147.13)	116.25 (28.26 – 179.45)

2.4 Bacterial transformation.

Bacterial transformation describes a complex process in which foreign DNA is introduced into a cell. This is important not only for studies involving bacteria but also as bacteria are commonly used for both storing and replicating plasmids. Thus most commercial available plasmids are designed to carry both a bacterial origin of replication and an antibiotic resistance gene for use as a selectable marker in bacteria.

pCMV6-AC-Myc-DDK plasmid was engineered to express the complete human GHR ORF nucleotide sequence 1914 base pairs (bp) tagged at the C-terminal with Myc-DDK, ampicillin antibiotic resistant and Neomycin resistant (positive selection marker). This vector was purchased from *Origene/ Cambridge Bioscience, Cambridge, UK* (**Figure 2.3 i**).

pCMV6-Entry plasmid was engineered to express the complete Mouse GHR ORF nucleotide sequence 1950bp tagged at the C-terminal with Myc-DDK, kanamycin antibiotic resistant and Neomycin resistant (positive selection marker). This vector was purchased from *Origene/ Cambridge Bioscience, Cambridge, UK* (**Figure 2.3 ii**).

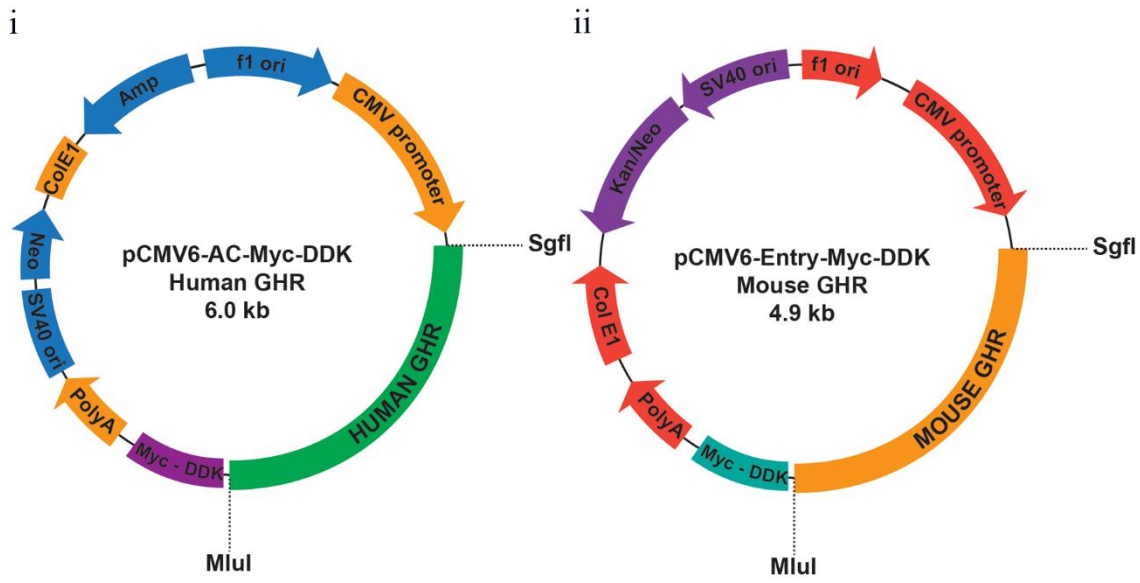

Figure 2.3 An illustration of human and mouse Growth hormone receptor expressing plasmid maps. (i) pCMV6-AC-Myc-DDK human GHR (1914bp). Total plasmid size 6.0 kilo-bases (kb). Ampicillin antibiotic resistant and Neomycin resistant. **(ii)** pCMV6-Entry-Myc-DDK mouse GHR (1950 base pairs). Total plasmid size 4.9kb. Kanamycin antibiotic resistant and Neomycin resistant.

50ng of pCMV6-AC-Myc-DDK Human GHR (100ng/µl) or pCMV6-Entry-Myc-DDK Mouse GHR (100ng/µl) and 100µl of competent cells (DH5α) was added to an eppendorf tube, vortexed and kept on ice for 30 minutes. Cells were heat shocked at 42°C using a heat block *(GrantBio PSC18, Thermo Shaker)* for 80 seconds and transferred immediately on ice. 400µl Luria Broth (LB) *(Sigma-Aldrich)* (25g/Litre, w/v) was added to the cells and the eppendorf tube was placed on a shaker block *(GrantBio PSC18, Thermo Shaker)* at 850rpm for 1 hour at 37°C. 200µl of the preparation was added directly to earlier prepared ampicillin (50ng/µl) or kanamycin (50ng/µl) agar plates (25g/Litre LB w/v, 12g/Litre Agar w/v) *(Sigma-Aldrich)*, under sterile conditions. Bacteria were carefully spread over the agar plate with a sterile glass rod and were incubated overnight at 37°C. After 24 hours the plates were visualised for the growth of colonies. Individual colonies were picked with a sterile pipette tip and placed in a falcon containing 4ml of LB and ampicillin (50ng/µl) or kanamycin (50ng/µl). Falcon tubes were placed on a shaker *(Innova 4300 incubator shaker, New Brunswick)* at 37°C for several hours until the LB appeared cloudy; indicating the bacterial growth. Following, the bacteria was transferred into a glass flask containing 200ml LB and ampicillin (50ng/µl) or kanamycin (50ng/µl) to further expand the growth of bacteria overnight at 37°C on a shaker *(Innova 4300 incubator shaker, New Brunswick)*

After 24 hours flasks were removed to perform plasmid DNA purification (Chapter 2, section 2.5).

2.5 Purification of DNA plasmid.

Plasmid DNA purification was undertaken using a plasmid midi kit (*Qiagen, Manchester, UK*) as described in the instruction manual. Briefly, bacteria grown in LB was centrifuged at 4500g *(Sorvail legend RT, Labcare)* for 15 minutes at 4°C to form a pellet. The supernatant was discarded and the pellet was re-suspended in resuspension P1 buffer (50mM Tris-Cl, pH 8.0, 10mM EDTA, 100µg/mL RNase A). Lysis Buffer P2 (200mM NaOH, 1% SDS) was added and the contents were mixed thoroughly by vigorous inversion several times. The falcon tubes were incubated on ice for 15 minutes and centrifuged at 4500g for 30 minutes at 4°C. Meanwhile the column was washed with buffer QBT (750mM NaCl, 50mM MOPS, pH7.0, 15% isopropanol, 0.15% Triton X-100) and the waste was discarded. The supernatant was added to the column and the contents were discarded. The column was further washed twice with buffer QC (1.0M NaCl, 50mM MOPS, pH 7.0, 15% isopropanol), and the flow through was discarded. DNA was eluted with buffer QF (1.25M NaCl, 50mM Tris-Cl, pH 8.5, 15% isopropanol) into a sterile falcon tube. The DNA was precipitated with the addition of 100% isopropanol and mixed thoroughly. The falcon was centrifuged at 4500g for 45 minutes. The supernatant was carefully discarded and the pellet was washed with 70% ethanol at room temperature (RT) and centrifuged at 4000g for 30 minutes. The supernatant was discarded and the cell pellet was allowed to air-dry for 5 – 10 minutes. The pellet was re-suspended in 200µl distilled H_2O (dH_2O). The concentration of purification DNA was quantified using a Nano-drop spectrophotometer *(ND-1000 spectrophotometer, LabTech).*

2.6 Sequencing.

10µl of purified DNA product (100ng/µl), original DNA plasmids and 10µl of primers 10pmol/µl (Forward: T7 promotor 5'-TAATACGACTCACTATAGGG-3', Reverse: pCMV6 plasmid 5'- CGTCATCCTTGTAATCCAGGA -3' were sent to the Genome Centre for

sequencing. The centre sequenced the samples by Sanger Sequencing using BigDye 3.1 chemistry with visualisation on the ABI 3730 capillary sequencer. The sequences were visualised using Chromas (Technelysium, DNA sequencing software). Purified product sequences were confirmed by comparing chromatograms to the original plasmid sequence available in public databases.

2.7 Transfection and generation of GHR expressing HEK-293 stable lines.

Transfection technology introduces genetic material into a cell via means other than viral transduction, such as via electroporation or lipsome-mediated fusion. It has been established as an exceptional strategy used for functional studies in cell lines or primary cells, in which we can modify the expression of a particular gene or miRNA through inhibition or overexpression and observe possible phenotypic effects on the cell, such as proliferation, cell death and pure morphological changes (Kim and Eberwine, 2010).

The HEK-293 cell line has been widely employed as an expression tool for recombinant proteins since it was originally generated over 40 years ago. It is well known that the HEK-293 cell line is an ideal choice for a transient expression system. Stable cell lines can also be obtained through antibiotic selection. The principle attributes of using HEK-293 cell line include; its quick and easy growth and maintenance, amenability to transfection using a wide variety of methods, high transfection efficiency to transfection and protein production, faithful translation and processing of proteins. Thus, this places them as a popular research tool in cell biology studies and an ideal cell line for therapeutic protein and virus production (Thomas and Smart, 2005).

HEK-293 cells were seeded at 3 x 10^5 cells/well density in a 6 well plate. 1 hour prior to transfection the cells were serum starved in serum free medium (DMEM without FBS and P/S). Transfection master-mix was prepared with 2µg of pCMV6-AC-Myc-DDK Human GHR, pCMV6-Entry-Myc-DDK Mouse GHR or pcDNA3-EGFP (empty plasmid GFP tagged to assess transfection efficiency) *(Addgene, Cambridge, USA)* plasmid with 10µl of transfection agent Polyethylenimine (PEI) (1mg/ml) and 500µl of serum free medium in separate eppendorf tubes. Transfection master-mix was vortexed for 5 seconds and left at RT for 10 minutes. Transfection master-mix was added directly to each well. After 3 hours the medium was removed and replaced with complete growth medium. After 24 hours cells were treated with Neomycin (G418)

(500µg/ml) *(Sigma-Aldrich)*; a positive selection marker. The concentration of G418 treatment for the generation of stable lines was determined using a dose responsive curve. Cells expressing human or mouse GHR were expanded in culture to generate stable cell lines; HEK-293 Human GHR (HEK-293 hGHR), HEK-293 Mouse GHR (HEK-293 mGHR).

2.8 Treatment of cell lines and primary culture.

2.8.1 Removal of glycosylated sugars via enzymatic glycosidase treatment.

HEK-293 hGHR/ mGHR cells were seeded in 6-well plates at 3 x 10^5 cells/well density. Once cells had reached ~90% confluency, media was discarded and washed with PBS without calcium, following the addition of 150µl of cell lysis N-glycosidase F (N-GF) buffer (20mM sodium phosphate *(Sigma-Aldrich)* (pH 7.5), 0.1% sodium dodecyl sulfate (SDS) *(Sigma-Aldrich)*, 0.75% Nonidet P-40 *(Sigma-Aldrich)*, 50mM β-mercaptoethanol *(Sigma-Aldrich)* and protease tablet inhibitor cocktail *(Sigma-Aldrich)*) or Endo-glycosidase H (Endo-H) buffer (50mM sodium acetate *(Sigma-Aldrich)*, 25mM EDTA *(Sigma-Aldrich)*, 1% SDS, 0.1% Nonidet P-40 and protease tablet inhibitor cocktail) to the well. Cells were carefully detached from the well and collected into eppendorf tubes. Cells were kept on ice for 20 minutes and centrifuged at 13,300rpm *(Heraeus Fresco17 centrifuge, Thermo Scientific)* for 10 minutes at 4°C. The supernatant was transferred into new eppendorf tubes. 20µl of cell lysates were treated with or without 2µl of N-GF *(New England Biolabs, Hitchen, UK)* or Endo-H *(New England Biolabs)* overnight at 37°C. After 24 hours the reactions were stopped with (2x) laemmli buffer *(Sigma-Aldrich)* and samples were processed for western blotting and stored at -20˚C.

2.8.2 GH and FGF21 responsiveness on GHR half-life.

hGHR and mGHR expressing HEK-293 stable cell lines were plated at 3 x 10^5 cells/well in 6-well plates. When cells reached ~80% confluency, cells were serum starved overnight before treatment with cycloheximide (CHX) (100 µg/ml) *(Sigma-Aldrich)* with or without recombinant human GH (0.5µg/ml) *(Life technology)*, recombinant human FGF21 (5µg/ml) *(VWR,*

Lutterworth, UK) or both for 1-8 hours. Cells were lysed at indicated time intervals (Chapter 2, section 2.14.1) and the protein concentration was quantified (Chapter 2, section 2.14.2). Samples were prepared for western blotting and stored at -20˚C.

2.8.3 GH and FGF21 responsiveness on GHR ubiquitination.

HEK-293 hGHR stable cells were prepared in T75cm^2 culture flasks at a density of 1.0 x 10^5 cells/ml. When cells reached ~70% confluency, media was removed and replaced with serum free media with or without recombinant human FGF21 (5µg/ml) overnight. The next day cells were challenged with or without recombinant human GH (0.5µg/ml) for 16 hours. After 16 hours, media was removed from the flasks and cells were washed with PBS without calcium. Cells were then lysed for protein extraction (Chapter 2, section 2.14.1) and the protein concentration was determined (Chapter 2, section 2.14.2). Cell lysates were then used for immunoprecipitation (Chapter 2, section 2.15).

2.8.4 GH and FGF21 responsiveness on GHR signalling.

Stable cell lines and chondrocytic cells were seeded at a cell density of 3 x 10^5 cells/well in 6-well plates. The next day cells were serum starved and treated with or without recombinant Human FGF21 or Mouse FGF21 (5µg/ml) *(VWR)* overnight. Cells were challenged in the absence or presence of recombinant human GH (0.5µg/ml) for 10 or 30 minutes. At each time-point cells were washed with PBS without calcium and were lysed (Chapter 2, section 2.14.1). The protein concentration was determined (Chapter 2, section 2.14.2) and cells were prepared for western blotting and stored at -20˚C.

In another experimental design cells were seeded at 3 x 10^5 cells/well in 6-well plates or human growth plate biopsies were randomly selected and transferred into 24-well plate culture dishes (Chapter 2, section 2.2). The following day cells were serum starved and treated with or without recombinant human FGF21 or mouse FGF21 (5µg/ml) overnight. The next day cells were treated with or without recombinant human GH (0.5µg/ml), for 8, 16 or 24 hours. Cells and human growth plate biopsies were processed for RNA extraction (Chapter 2, section 2.9) and stored at -

80˚C. Alternatively, cells were lysed (Chapter 2, section 2.14.1) and/or protein concentration was quantified (Chapter 2, section 2.14.2) and prepared for western blotting, stored at -20˚C.

2.8.5 GH and FGF21 responsiveness on cell proliferation.

HEK-293 hGHR/ mGHR stable cell lines and chondrocytic cells were seeded in 96 well plates at a cell density of 5.0 x 10^3 cells/well. When cells reached ~50% confluency media was removed from each well and replaced with serum free media with or without recombinant human/ mouse FGF21 (5µg/ml) overnight. The next day cells were treated with or without recombinant human GH (0.5µg/ml), for 72 or 96 hours. Following indicated time intervals, cells were assessed for cell proliferation (Chapter 2, section 2.16).

2.9 RNA extraction of cell lines and primary culture.

RNA extracted from cultured cell lines were purified using the RNeasy Mini kit *(Qiagen)*. Primary cultures of human growth plate tissue biopsies were processed for RNA extraction using TRIzol *(Sigma-Aldrich)*.

2.9.1 RNA extraction of cell lines.

At the end each of time interval following the treatment of cells, media was removed from the well and cells were washed several times with PBS without calcium. 350µl of buffer RLT was added and cells were collected into an eppendorf tube and centrifuged at 13,300rpm *(Heraeus Fresco17 centrifuge, Thermo scientific)* for 3 minutes. The supernatant was transferred into new eppendorf tubes. One volume of 70% ethanol was added and 700µl were transferred to an RNeasy mini column placed in a 2ml collection tube and centrifuged for 15 seconds at 13,300rpm speed. The flow through was discarded. 700µl of wash Buffer RW1 was added to the column and centrifuged at 13,300rpm speed for 15 seconds and the flow through discarded. An additional step using RNase free DNase set *(Qiagen)* was incorporated into the protocol to ensure the removal of DNA. A master-mix of 10µl DNaseI and 70µl RDD buffer was prepared and 80µl

was added to each sample and incubated at RT for 15 minutes. Preparations were washed again with 700µl wash buffer RW1 and centrifuged at top speed for 15 seconds. 500µl Buffer RPE was added to the RNeasy spin column and centrifuged for 2 minutes at 13,300rpm speed. 30µl of RNase-free water was directly added to the spin column membrane and centrifuged for 1 minute at maximum speed to elute RNA into new eppendorf tubes. RNA concentrations (ng/µl) were quantified using a Nano-drop spectrophotometer. RNA was stored at -80˚C.

2.9.2 RNA extraction of primary culture.

Human growth plate biopsies taken from one well were transferred into a sterile eppendorf tube and dissolved in 0.5ml of Trizol reagent. The biopsies were homogenised using ultrasound technology at amplitude 37% *(sonics and materials Inc., CV26, VibraCell TM probe)* for 15 seconds and placed on ice. This was repeated three times per each tube to ensure the breakdown of the biopsy. An additional 0.5ml of Trizol was added to each tube to make a total volume of 1ml and were incubated for 20 minutes at RT. 0.2ml of Chloroform *(Sigma-Aldrich)* was added to each tube and were mixed vigorously by hand for 15 seconds followed by a further incubation for 3 minutes at RT. Samples were centrifuged at 12,000g for 15 minutes at 4˚C. The upper aqueous phase containing the RNA (approximately 0.5ml) was transferred into a new eppendorf tube. 0.5ml of 100% isopropanol *(Sigma-Aldrich)* was added per tube and incubated for 10 minutes at RT. Samples were centrifuged at 12,000g for 10 minutes at 4˚C. The supernatant was removed to leave the gelatinous pellet. The pellet was washed with 1ml 75% ethanol. The samples were vortexed for 3 seconds and centrifuged at 7,500g for 5 minutes at 4˚C. The supernatant was discarded and the sample was allowed to air dry for 10 minutes. The pellet was re-suspended with 50µl nuclease-free water by pipetting up and down several times. The tubes were heated in a heat block for 10 minutes at 60˚C. The RNA concentration was measured using a Nanodrop device. RNA was stored at -80˚C.

2.10 Retrotranscription (cDNA synthesis).

2.10.1 Retrotranscription of RNA obtained from cell lines.

1µg of RNA was used to generate cDNA. 1µg of random hexamers *(New England Biolabs)* was added to individual RNA samples to make a total volume of 15µl with Rnase/Dnase free water. The preparation was incubated at 70°C for 5 minutes for RNA denaturation *(Veriti 96 well thermos cycler, Applied Biosystems)*. Meanwhile a master-mix made of 2µl of (10x) Moloney Murine Leukemia virus (M-MLV) reaction buffer *(New England Biolabs)*, 1µl (10mM) deoxyribonucleotide triphosphate (dNTPs) *(New England Biolabs)*, 1µl M-MLV RT *(New England Biolabs)* and 1µl Ribonuclease inhibitor (RNAsin) *(New England Biolabs)* was prepared per reaction sample, vortexed and 5µl was added to the earlier prepared RNA following the initial incubation stage. Samples were further incubated at 25°C for 10 minutes, 42°C for 90 minutes (cDNA synthesis) and 70°C for 15 minutes (M-MLV inactivation) for 1 cycle. cDNA was stored at -20°C.

2.10.2 Retrotranscription of RNA obtained from primary cultures.

cDNA was generated using BioRad iScript cDNA synthesis kit. A reaction mix was made up of 15µl of RNA sample, 4µl 5x iScript reaction mix and 1µl iScript Reverse Transcriptase. Samples were incubated at 25˚C for 5 minutes, 42˚C for 30 minutes and 85˚C for 5 minutes for 1 cycle *(Thermocycler, BioRad)*. cDNA was stored at -20°C.

2.11 Polymerase Chain Reaction.

Polymerase Chain Reaction (PCR) was originally developed by Kary Mullis in the 1980s. This technology is based on the synthesis of new complementary DNA strands using DNA polymerase that can add nucleotides only onto pre-existing 3'-OH group. Thus, in this reaction it requires a primer to which it can add the first nucleotide, allowing for the possibility to delineate a specific region of template sequence to be amplified. As a result the specific sequence amplifies

and accumulates in billions. Several components are required to initiate a PCR reaction. The DNA template contains the target sequence. To begin a high temperature is applied to cause the double-stranded DNA molecule to separate as single strands. The addition of DNA polymerase enzyme encourages the synthesis of new DNA complementary to the target sequence. The assistance of primers; heat resistant short pieces of single stranded DNA are complementary to the target sequence. The polymerase actions the synthesis of new DNA from the end of the primer using single units of A, T, G and C nucleotides that act as essential building blocks for the synthesis of new DNA strands (Kubista et al., 2006).

PCR reactions to detect *GHR (Human), Ghr (Mouse), FGF21 (Human), FGFR1 (Human),* isoform *FGFR1-IIIC (Human), β-KLOTHO (Human), SOCS1 (Human), SOCS2 (Human), SOCS3 (Human)* and *GAPDH (Human)* was performed in a GS1 thermocycler (G-storm). PCR reactions were prepared using 0.15µl (5U/µl) *Taq* polymerase *(New England Biolabs),* 2.5µl (10x) Standard *Taq* buffer *(New England Biolabs),* 0.5µl (200µM) of each dNTP, 1µl cDNA, 0.5µl (0.5µM) of specific forward and reverse primers and 20.35µl RNase/DNase free water per each reaction. A full list of gene sequences and PCR reaction cycle conditions are detailed in **Appendix**, **Table 7.1**. cDNA obtained from human rib cartilage was used as a positive control. PCR products were electrophoresed and visualised on an agarose gel (Chapter 2, section 2.12).

2.12 Agarose Gel Electrophoresis.

1% agarose gel was prepared by dissolving 1g agarose (w/v) *(Sigma-Aldrich)* in 100ml of (1x) Tris-Acetate-EDTA buffer (TAE) *(Fisher Scientific, Loughborough, UK).* The solution was heated in a microwave for approximately 1 – 2 minutes, whilst gently swirling every 30 seconds to ensure all of the agarose had dissolved. After the solution had cooled for 2 – 4 minutes, 1:20,000 gel red stain *(Biotium, Cambridge, UK)* was added to the gel mixture and the gel was swirled to disperse the dye evenly. The agarose gel was then poured into a gel tray, a comb was inserted to form the wells and the gel was allowed to set for 30 minutes until it had completely solidified. Once the gel was set, 25µl of PCR product were mixed with 5µl of (5x) DNA loading

buffer blue *(Bioline, London, UK)* and loaded on the gel alongside an appropriate DNA ladder according to the size of interest; 5µl GeneRuler 100bp DNA ladder *(Thermo Scientific)* or Hyperladder 1kb *(Bioline)*. The gel was electrophoresed at 110 V for 30 – 45 minutes and DNA bands were visualised under ultra violet light using Kodak Electrophoresis and Documentation analysis system UV transilluminator *(Uvitec)*.

2.13 Real-time quantitative PCR.

Real-time quantitative PCR (RT-qPCR) is a highly sensitive and reliable method for the detection of gene expression levels via a logarithmic amplification PCR and quantification of specific cDNA sequences. RT-qPCR assesses the amount of synthesised amplification product in every amplification cycle and relative abundance of each transcript can be assessed during the logarithmic phase of amplification. Thus, the basis of this technology demonstrates that the more abundant a particular mRNA is, the earlier it will reach a threshold during repeated cycles of amplification. Data collection is based on a fluorescence reading (Arya et al., 2005). SYBR green will be used as the method of detection for RT-qPCR assays in this thesis. SYBR green directly binds to double-stranded DNA (amplification product) and emits light.

As our sample collection is likely to differ in the rate of overall gene transcription and the amount of cell contents, normalisation against a constantly expressed housekeeping gene is commonly performed and the relative mRNA quantification is analysed. In this study, the relative expression from all samples were quantified against the housekeeping gene Glyceraldehyde 3-phosphate dehydrogenase (*GAPDH*) which has been widely shown as a marker expressed in all tissue (Barber et al., 2005).

RT-qPCR reactions were prepared using 1µl of cDNA (~25ng), 0.5µl of each specific forward and reverse primers (0.5µM), 3µl dH_2O and 5µl of SYBR green *(Qiagen)*. A full list of gene sequences and PCR reaction cycle conditions are detailed in **Appendix**, **Table 7.2**.

The amount of the assayed transcript in each test sample was calculated using the obtained cycle threshold (CT) values. These are defined as the number of cycles required for the fluorescent signal to cross the threshold. A comparative CT calculation was used to determine the

relative values of target RNA levels in our samples. The CT values obtained during the exponential increase of the products were normalised, as described above to housekeeping gene, *GAPDH* which is expressed as a ΔCT value (e.g. CT IGF-1 - CT GAPDH). ΔCT values can be used to compare differences in relative transcript levels in different samples by calculating ΔΔCT value (e.g. ΔCT Treated - ΔCT Untreated). Due to the exponential nature of PCR, all calculations are in logarithm base 2, and therefore fold change is calculated by 2-ΔΔCT formulae (Livak and Schmittgen, 2001).

2.14 Quantitative Western Blotting.

2.14.1 Protein extraction.

Lysis buffer was prepared prior to protein extraction. 7ml of Radio-Immunoprecipitation Assay (RIPA) buffer *(Sigma-Aldrich)* was supplemented with 1 tablet of protease inhibitor cocktail *(Sigma-Aldrich)* or 10ml of RIPA buffer was supplemented with 1 tablet of protease and phosphatase inhibitor cocktail *(Thermo Scientific)* depending on the protein of interest evaluated. Each preparation was vortexed until the tablet was completely dissolved.

During protein extraction culture media was aspirated from each well or culture flasks. Cells were washed with PBS without calcium. 150µl (6-well plates) or 1ml (T75cm^2 flasks) of prepared lysis buffer was added to the well or flask. A cell scraper *(Cellstar)* was used to detach the cells from the surface of the well or flask. Lysed cells were collected into 1.5ml eppendorf tubes, kept on ice for 20 minutes and centrifuged at 13,300rpm *(Heraeus Fresco17 centrifuge, Thermo scientific)* at 4°C for 10 minutes. The supernatant was collected into a new 1.5ml eppendorf tube and was used to quantify the protein concentration (Chapter 2, section 2.14.2) and stored at -20°C.

2.14.2 Quantification of protein concentration.

The BCA protein assay is a detergent-compatible formulation based on bicinchoninic acid (BCA) for the colorimetric detection and quantification of total protein to allow for equal

protein load during western blot analysis for the purpose of quantitative comparisons between samples. This method combines the reduction of Cu^{+2} to Cu^{+1} by protein in an alkaline medium with a highly sensitive and selective colorimetric detection of the curprous cation (Cu^{+1}) using a unique reagent containing bicinchoninic acid. The purple-coloured reaction product, formed by the chelation of two molecules of BCA with one cuprous ion exhibits a strong absorbance at 590nm that is linear with increasing protein concentrations over a broad working range (0-2000µg/ml).

Protein concentration of cell lysates were determined using Pierce BCA Protein Assay Kit *(Thermo Scientific)* as described in the instruction manual. Briefly, BCA serial dilution standards were made in the range of 0 - 2000µg/ml with RIPA buffer. Cell lysates were diluted 1:1 with RIPA buffer to ensure absorbance values were within the standard range. 25µl of BCA standard or sample was added to a flat bottomed 96 well plate *(Cellstar)*. Protein working dye reagent was prepared by mixing 50:1 (v/v) BCA Reagent A with BCA Reagent B. 200µl of working dye reagent was added to each well and mixed thoroughly by placing the plate on a shaker for 30 seconds. The plate was incubated at 37°C for 30 minutes. The plate was cooled at RT and the absorbance was measured using a Vmax kinetic plate reader *(Molecular Devices)* at 590nm. A standard curve was generated by plotting optical density readings at 590nm against the concentration of BSA standard. The protein concentration of each sample was determined by extrapolating from the standard linear curve.

2.14.3 SDS polyacrylamide gel electrophoresis.

The following solutions were prepared to make western gels for SDS polyacrylamide gel electrophoresis (PAGE). 10% resolving gel and 12% stacking gels for western blotting were made using the solutions listed in (**Table 2.4**). Acrylamide, resolving buffer and stacking buffer was purchased from *Fisher Scientific*. Tetramethylethylenediamine (TEMED) and ammonium persulfate (APS) (10mg/ml) were purchased from *Sigma-Aldrich*. The resolving gel and stacking gel were prepared using 1.5mm thickness glass plates *(BioRad)*. The resolving gel was left to set

for 30 minutes. Once the resolving gel was set the prepared stacking gel was poured on top of the set resolving gel and a 10 well comb was inserted, which was further allowed to set for 30 minutes. The comb was removed from the gel and the plates were placed into a gel tank *(BioRad),* which was filled with (1x) running buffer (1g SDS, 3.03g Tris-Base *(Sigma-Aldrich),* 1.44g Glycine *(Sigma-Aldrich)* in 1L dH_2O). Cell lysate samples were prepared between 20 to 40µg in (2x) Laemmli Buffer *(Sigma-Aldrich),* boiled at 95°C for 5 minutes and centrifuged at 13,000rpm *(Heraeus Fresco17 centrifuge, Thermo scientific)* for 1 minute. Samples were then loaded alongside PageRuler, Plus Prestained protein ladder 10 – 250kDa *(Thermo Scientific)* using gel-loading tips *(StarLab).* The gels were electrophoresed at 150 – 175 V for 50 minutes using a power-pack *(BioRad),* until the samples ran through the gel and the laemmli dye was visible at the bottom of the gel.

Table 2.4 Preparation of resolving and stacking gels for western blotting.

Resolving gel (10%)		**Stacking gel (12%)**	
Solution	**Volume**	**Solution**	**Volume**
Acrylamide	6.7ml	Acrylamide	800µl
Water	8.3ml	Water	3.8ml
Running (resolving) buffer	5ml	Stacking buffer	325µl
SDS	0	SDS	0
APS	150µl	APS	50µl
TEMED	30µl	TEMED	5µl

2.14.4 Immunoblotting.

Size-separated proteins were blotted onto a 0.45µm nitrocellulose membrane *(GE Health care Life sciences, USA)* using a semi-dry transfer system *(BioRad).* A sandwich formed of multiple layers including; (1) filter paper, (2) nitrocellulose membrane, (3) gel and (4) filter paper were all initially soaked in (1x) transfer buffer (20mM Trisbase, 120mM Glycine and 20% methanol) before being placed in the semi-transfer machine in the order described. The sandwich was pressed gently with a roller to remove air bubbles and excess buffer to avoid interference during the transfer stage. Blotting was performed at 15V for 1 hour using a power-pack (*BioRad).* Transfer of samples from the gel to the membrane was verified by immersing the membrane into 0.1% Ponceau Red Stain *(Sigma-Aldrich)* for 3 minutes and then washed with dH_2O to remove

excess stain and visualise the presence of all protein products in a sample. The membrane was then transferred to a 50ml falcon tube and blocked with 10ml of 5% non-fat milk powder *(ASDA)* in PBS-0.1% Tween-20 for 1 hour at RT on a roller *(Stuart, SRT9)* to reduce unspecific binding.

Primary antibodies specific to the protein of interest and housekeeping antibodies were prepared in falcon tube containing 5% non-fat milk powder in PBS-0.1% Tween-20. A detailed list of primary antibodies used for western blot analysis can be found in **Appendix**, **Table 7.3**. The membrane was incubated overnight with the prepared primary antibody at 4°C on the roller. The next day, the primary antibody solution was removed and the membrane was washed three times with PBS-0.1% Tween-20 for 15 minute intervals. Secondary antibodies, goat anti-mouse or goat anti-rabbit (conjugated with IR fluorophores that emit light at either 680 nm or 800 nm, from *LI-COR*) were used at a dilution of 1:10,000 prepared in 5% non-fat milk powder in PBS-0.1% Tween-20 and incubated for 1 hour at RT on the roller in the dark using foil to cover the falcon. After, the secondary antibody solution was removed and the membrane was washed three times with PBS-0.1% Tween-20 for 15-minute intervals.

Immuno-reactive products were detected and quantified using a LI-COR Odyssey Scanner 2.2 *(Licor)*. All membranes were scanned at intensity 5 unless otherwise stated. LI-COR Odyssey software V3.0 was later used to quantify protein expression.

2.15 Immunoprecipitation.

For immunoprecipitation studies to assess ubiquitination of GHR, HEK-293 hGHR cells were grown in T75cm^2 flasks. Treatment conditions have been described in Chapter 2, section 2.8.3. After the indicated time interval, media was removed from the flask and discarded. 5ml of PBS without calcium was used to wash the cells and discarded. An additional 5ml of PBS without calcium was added to the flask to detach the adherent cells from the surface of the flask and cells were transferred to 15ml falcon tubes and centrifuged at 1500rpm *(Heraeus Labofuge 400 centrifuge, Thermo scientific)* for 5 minutes to generate a cell pellet. The supernatant was removed and the cell pellet was re-suspended in 1ml of RIPA buffer with protease inhibitors. Samples were kept on ice for 20 minutes and centrifuged at 13,300rpm *(Heraeus Fresco17 centrifuge, Thermo*

scientific) for 10 minutes. Without disturbing the pellet the supernatant was transferred to a clean eppendorf tube. From each sample 150µl of the cell lysate was transferred into new eppendorf tubes to determine the protein concentration at a later stage and stored at -20˚C (Chapter 2, section 2.14.2). To the existing cell lysate collection 30µl of agarose beads (Protein A/G plus agarose, sc-2003, *(Santa Cruz Biotechnology, USA)* was added and samples were placed on a rotor *(SB2, Stuart)* at 4˚C for 1 hour. This 'preclearing' stage is designed to allow for the removal of potentially reactive components from the lysate, which might bind non-specifically to the beads. Next samples were centrifuged at 2500rpm for 5 minutes. Without disturbing the pellet, the samples were transferred to a new eppendorf tube. RIPA buffer was added to each sample collection to make a total volume of 1ml. 15µl of antibody IgG (normal rabbit IgG sc-2027, control IgG, *(Santa Cruz Biotechnology)* or GHR B-10 *(Santa Cruz Biotechnology)*, sc-137185, mouse monoclonal IgG) was added to the sample and placed in the rotor at 4˚C overnight to enable the antibody to bind to the specific protein of interest in solution. The next day samples were removed from the rotor at 4˚C and 30µl of agarose beads was added to each sample and further placed on the rotor at 4˚C for 2 hours for the formation of the antibody-antigen complex with the agarose beads. The samples were removed and centrifuged at 2500rpm for 5 minutes. The supernatant was discarded. The pellet was washed one time with 500µl of RIPA buffer and two times with PBS each time centrifuging at 2500rpm for 5 minutes between washes and discarding the supernatant each time. 80µl of (2x) laemmli buffer was added to re-suspend the pellet and boiled at 95˚C *(GrantBio PSC18, Thermo shaker)* for 5 minutes. Samples were centrifuged at 13,300rpm for 1 minute and the sample was transferred to a new eppendorf tube without disturbing the pellet and stored at -20˚C for latter western analysis (Chapter 2, section 2.14.3).

2.16 Cell proliferation.

For cell proliferation studies, stable cell lines and chondrocytic cells were seeded in 96 well plates. To allow for a more stable adherence of cells to the culture plate surface, the plate was coated with collagen I, Rat tail *(GIBCO)*. A solution of 50ml dH_2O, 67µl acetic acid *(Fisher*

Scientific) and 1ml collagen was prepared. 100µl of the prepared collagen was added to each well and was left at RT for 1 hour. After, the solution was aspirated from each well and the wells were washed twice with 100µl of PBS without calcium and allowed to air dry for approximately 1 – 2 hours. As previously described cells were seeded at 5.0 x 10^3 cells/well. Treatment conditions have been described in Chapter 2, section 2.8.5. At the end of the time-point, media was removed from each well and treated with 100µl of cell-counting reagent kit -8 *(Sigma-Aldrich)* (1:100, cell counting reagent: serum free media) and incubated at 37˚C for 1 hour. The cell-counting kit-8 assay uses a highly water-soluble tetrazolium salt which is reduced by dehydrogenases in cells to give a yellow coloured product – formazan, which is soluble in tissue culture medium. The amount of the formazan dye generated is directly proportional to the number of metabolically active and living cells, thus giving an indirect indication of cell proliferation. The absorbance was measured at 450nm using a plate reader *(Multiscan FC, Thermo scientific)*.

2.17 Immunohistochemistry of human growth plate tissue.

Human growth plate tissue samples were obtained from children undergoing epiphyseal surgery at different stages of puberty in order to arrest further linear leg growth, due to constitutional tall stature or leg length difference.

Human growth plate tissue sections (prepared using an outsourced company) were incubated at 60°C for 40 minutes to allow for a stronger fixation of the tissue onto the slide before proceeding to deparaffinisation. Slides were next deparaffinised using xylene (two times for 10 minutes), and then placed in graded alcohol (Ethanol) baths; 99% ethanol (two times for 5 minutes), 95% ethanol (10 minutes), 70% ethanol (5 minutes) and dH_2O (10 minutes). Antigen retrieval was performed in 0.01M citric acid and 0.1M sodium citrate in dH_2O at 80°C for 20 minutes. Sections were further washed three times with dH_2O. Endogenous peroxidase activity was reduced by incubating in 3% hydrogen peroxide in methanol for 10 minutes at RT. Sections were washed two times with PBS and once with 0.01% PBS-tween. To decrease non-specific binding, slides were incubated with 3% goat serum in PBS at RT for 1 hour. Primary antibodies

were diluted in PBS and were incubated overnight at 4°C. A detailed list of primary antibodies used for immunohistochemistry can be found in **Appendix**, **Table 7.4**.

The next day sections were washed five times in 0.01% PBS-tween and incubated with secondary antibodies; Goat anti-rabbit IgG *(Vector Laboratories)* or Goat anti-mouse IgG *(Santa Cruz Biotechnology)* at a dilution of 1:200 prepared in 1% BSA in PBS for 1 hour at RT. Sections were washed five times in 0.01% PBS-tween and incubated with Avidin-conjugated peroxidase (1.5ml PBS, 15µl solution A and 15µl Solution B) *(Vector Laboratories)* for 1 hour at RT. Thereafter sections were washed with 0.01% PBS-tween for a total of 20 minutes. Peroxidase activity was detected under the microscope using a DAB-kit *(Vector Laboratories)*. Following detection of protein expression slides were rinsed in dH_2O and counterstained with Alcian Blue to stain the matrix of the tissue. Sections were dehydrated in graded alcohol baths containing distilled H_20, 70% ethanol, 95% ethanol, 99% ethanol and xylene each for 5 minutes. Sections were mounted with pertex.

2.18 Enzyme-linked immunosorbent assay.

An enzyme-linked immunosorbent assay (ELISA) is typically performed in 96 well plates; a conventional method used for the detection of antibodies, antigens, proteins and glycoproteins in biological samples or culture media. The vital step in the ELISA assay is the immobilisation of the antigen of interest. This can be achieved via the direct adsorption to the assay plate or indirectly via a capture antibody that has been attached to the plate.

The direct detection method comprises a labelled primary antibody which reacts directly with the antigen (usually directly immobilised on the assay plate). Alternatively, the indirect detection assay uses a secondary antibody that has a high specificity for the detection of primary antibody only; achieved by using primary antibodies from different host species (e.g. mouse IgG and rabbit IgG). The most sensitive and robust ELISA platform is a capture-based assay termed 'sandwich' assay (**Figure 2.4**). In this design the analyte to be measured is bound between two primary antibodies; the capture antibody and the detection antibody. The detection antibody in this setting is usually labelled with an enzyme e.g. horse radish peroxidase or alkaline phosphatase. This binds to any target antigen already bound to the capture antibody on the plate.

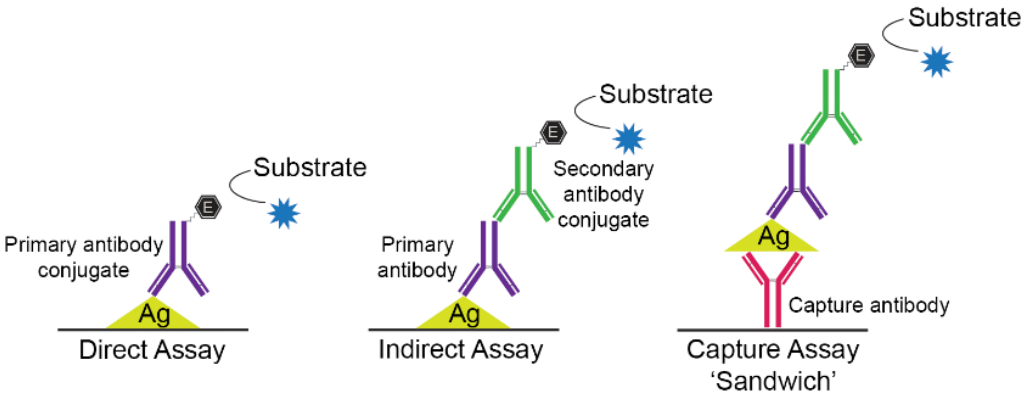

Figure 2.4 An illustration of direct vs indirect ELISA platforms. The antigen of interest is immobilised by a direct adsorption to the plate or alternatively the attachment of a capture antibody to the plate surface. The detection of the antigen can be achieved by using an enzyme-conjugated primary antibody (direct assay) or via matched unlabelled primary and conjugated secondary antibodies (indirect assay).

Lastly the substrate is added to the plate. Usually, ELISA assays are chromogenic using a reaction that converts the substrate (e.g. TMB 3,3',5,5'-Tetramethylbenzidine, ABTS 2,2'-azino-bis(3-ethlybenzothiazoline-6-sulphonic acid)) into a coloured product that is then used to measure the absorbance on a plate reader (Aydin, 2015; Voller et al., 1978).

Biological serum samples collected from 64 VPT infants (Chapter 2, section 2.3) were tested for FGF21 (pg/ml) and IGF-1 (ng/ml) concentration levels using purchased ELISA assay kits.

2.18.1 Human FGF21 enzyme-linked immunosorbent assay.

Serum FGF21 concentrations were measured by human FGF21 ELISA kit (BioVendor) according to the manufacturer's instructions. Serum samples were diluted 1:3. The measuring range was 30 to 1920 pg/ml. Briefly, 100µl of standard, reconstituted quality controls or diluted samples were added in duplicate to wells. The plate was incubated at RT for 1 hour and placed on an orbital microplate shaker at 300rpm. The wells were washed three times with 350µl wash solution. In the final wash, the plate was inverted onto a paper towel and tapped several times to remove access solution. 100µl of biotin labelled antibody was added to each well. The plate was incubated at RT for 1 hour and placed on a shaker at 300rpm. As before, the wells were washed as described above. 100µl of streptavidin-HRP conjugate was added to each well and the plate

was incubated at RT for 30 minutes, placed on at shaker at 300rpm. Wells were washed again three times as described. 100µl of substrate solution was added to each well. The plate was incubated for 15 minutes at RT. The colour development reaction was stopped with 100µl of stop solution. The absorbance was measured using a plate reader at 450nm and reference wavelength at 630nm.

2.18.2 Human IGF-1 enzyme-linked immunosorbent assay.

Serum IGF-1 concentrations were measured by human IGF-1 ELISA kit (Mediagnost GmbH) according to the manufacturer's instructions. The measuring range was 2 to 50 ng/ml. Briefly, 80µl of conjugate AK (containing the biotinylated anti-IGF-1 antibody) was added to all wells. 20µl of sample buffer PP, standard or sample was added to the well. The plate was covered with sealing tape and incubated at RT for 1 hour on a shaker at 350rpm. The wells were washed five times with 300µl of wash buffer. 100µl of enzyme conjugate EK was added into each well. The plate was covered with tape and incubated for 30 minutes at RT on a shaker at 350rpm. The wells were washed five times as described above. 100µl of substrate solution S was added to each well and incubated in the dark for 15 minutes at RT. The colour development reaction was stopped by adding 100µl of stopping solution SL to each well. The absorbance was measured within 30 minutes at 450nm (reference filter ≥ 590nm).

2.19 Statistical analysis.

All *in vitro* data have been evaluated using Excel (2013), LI-COR Odyssey Scanner Software (version 2.2) or GraphPad Prism (version 5). Data are expressed as means ± standard error mean (SEM) calculated from at least three experimental replicates, where indicated each with two or three biological replicates. GraphPad Prism version 5 was used to perform multiple statistical analyses including; One-way Analysis of Variance (ANOVA), Dunnett's post hoc test, Two-way ANOVA, Bonferroni post *t*-tests and Non-linear regression one phase decay. Statistical significance was defined as $*p<0.05$, $**p<0.01$, $***p<0.001$.

Clinical data evaluation was performed in SPSS software (version 24.0). FGF21 and IGF-1 serum concentrations were not normally distributed when tested using the kolmogorov-Smirnov test, therefore hormonal values were transformed logarithmically to achieve normality of residuals in the statistical analyses. Growth trends in VPT infants were evaluated in two phases. Growth deflection = ΔSDS for length/ weight from birth to nadir. Catch-up growth = ΔSDS for length/ weight from nadir to total growth follow-up. Log transformed FGF21/ IGF-1 levels and nutritional intake at weeks 1, 3, 5, 7 and 9 (in-patient) and weeks 1 and 2 (out-patient) were separated individually for each patient and averaged to reflect mean levels during growth deflection and catch-up growth. Statistical tests to evaluate hormonal and nutritional levels during deflection and catch-up growth included; Bivariate correlation and Paried *t*-test analysis. To assess factors associated with growth deflection and catch-up growth, linear regression analysis was carried out. The outcome measures were; ΔSDS for length/ weight from birth to nadir, ΔSDS for length/ weight from nadir to total growth follow-up. As explanatory factors, mean hormonal levels (log transformed IGF-1, FGF21) and nutritional intake (total kcal/kg, fat kcal/kg or %, protein kcal/kg, carbohydrate kcal/kg and enteral kcal/kg energy) during deflection and catch-up growth were included. Additional covariates, gestational age at birth, birth length SD, birth weight SD and sex were selected. p values <0.05 were considered significant.

CHAPTER 3. Results

Validation of the Growth hormone receptor model

3.1 Introduction.

The role of GH is well established as a major growth promoting anabolic mediator, playing a pivotal role in childhood skeletal growth and development (Carter-Su et al., 2016; David et al., 2011; Rotwein and Chia, 2010). The direct binding of GH to GHR, triggers an array of metabolic actions on multiple target tissues including; liver, adipose, skeletal muscle and pancreas (Brooks et al., 2008; Waters, 2016). Alternatively, a large proportion of GH can act indirectly through the production of IGF-1 (David et al., 2011; Gevers et al., 2009). Ultimately, both the '*direct*' and '*indirect*' effect of GH has an important function predominately involved in regulating somatic growth (Vijayakumar et al., 2011). The wide exploration of studies on the mechanistic function of GH, GHR and IGF-1 are demonstrated through the vast documented list of human genetic disorders associated with growth failure and the development of transgenic/ knockout animal models (i.e. mutations in the genes encoding GHRH (little mouse), Pit1 (Snell dwarf), GH insensitivity (Laron mouse), IGF-1 and IGF-1R knockout (growth retardation at birth) highlighting their critical role in the mediation of longitudinal growth (Frank, 2001; Walenkamp and Wit, 2007).

Somatotrophs of the anterior pituitary gland are the primary source for the synthesis of GH; released as a 22kDa circulatory protein (Frank, 2001; Kato et al., 2002). Structurally, it is formed of four antiparallel helical clusters with loops of varying length between helices (Frank, 2001; Rozario et al., 2000). Typically, the daily serum GH profile is characteristic of intermittent peaks, followed by prolonged inter-pulse troughs, caused by the pulsatile release of GH in the pituitary (Frank, 2001; Gunawardane et al., 2000; Roelfsema and Clark, 2001). The activity of GH is initiated through a direct interaction with GHR; a single membrane-spanning type I glycoprotein (~110kDa) that originates from the class 1 cytokine receptor superfamily of transmembrane proteins (Carter-Su et al., 2016; David et al., 2011; Waters, 2016). This ubiquitously expressed receptor plays a vital role in signal transduction, receptor internalisation and downregulation (Frank, 2001). The organisation of GHR is formed of three essential components; 1) the ECD (two fibronectin type III domains each of a seven stranded β sandwich), 2) the transmembrane domain, (a rigid single pass helical domain) and 3) the ICD (containing a

proline rich Box 1 motif) vital for downstream GHR signalling (Brooks et al., 2008; Kato et al., 2002).

GH/GHR binding mediates the actions of downstream signalling events via the tyrosine Janus kinase cascade, initiating the activity of several associated pathways including MAP kinase, PI3 kinase and STAT to induce proliferation, differentiation, cell migration and apoptosis (David et al., 2011; Rawlings et al., 2004; Rotwein and Chia, 2010). This chapter will be focusing in-depth on the exploration of the JAK2/STAT5 pathway; which of the signalling pathways is predominately associated with postnatal skeletal growth (David et al., 2011; Martinez et al., 2015).

An overview of the mechanical system of GHR activity and downstream signalling are often described as a relatively complex multi-step process (Rawlings et al., 2004). GH interaction with the GHR dimer leads to the recruitment and cross-activation of the receptor associated tyrosine kinase, JAK2. The phosphorylation of JAK2 molecules and the subsequent phosphorylation of multiple GHR intracellular tyrosine residues, creates anchoring sites for several SH2 domain mediators, among which STAT5b has been demonstrated to have a pivotal role in linear growth. The phosphorylation and translocation of STAT5b to the nucleus in the form of a homodimer, activates GHRE, inducing the transcription of GH-responsive genes including hepatic IGF-1 to promote linear growth (David et al., 2011; Martinez et al., 2015).

This system is carefully regulated by SOCS 1 – 3. These proteins act to stimulate a negative feedback mechanism in which the interaction of its SH2 domain to signalling intermediates of the cascade cause a subsequent phosphorylation of tyrosine residues leading to the inhibition of downstream signalling events. Several studies show the importance of GH-induced SOCS2 activation, primarily associated with the regulation of childhood linear growth as highlighted through the interaction of SOCS2 with phosphorylated tyrosines on GHR to negatively regulate JAK2 and STAT5 activity (Ahmed and Farquharson, 2010; Greenhalgh et al., 2005). In addition, the significance of SOCS2 was further elucidated in $SOCS2^{-/-}$ knockout mice models which displayed enlarged body growth, from an increase in the size of most organs and bones (Turnley, 2005; Vesterlund et al., 2011). Moreover, it is also suggested that SOCS2 is part

of an E3 ubiquitin ligase complex that targets interacting proteins (i.e. GHR) for proteasomal degradation, via the SOCS-box and the Elongin B/C adapter protein (Vesterlund et al., 2011).

The biology and physiology of FGF21 are well characterised, as described in Chapter 1, section 1.5. FGF21 (highly expressed in the liver) belongs to the FGF19 subfamily (FGF19, FGF21, and FGF23) of FGFs that are known to lack the FGF heparin-binding domain which allow it to circulate and function as an endocrine factor (Cuevas-Ramos et al., 2012; Kilkenny and Rocheleau, 2016). It is well described that FGF21 activity is highly dependent on the presence of FGFR1 (in particular isoform FGFR1- IIIC) with the assistance of co-receptor β-Klotho. Thus, FGF21 activity is subject to the formation of a ternary structure including, FGF21/FGFR1-IIIC/β-Klotho complex to induce signal transduction and the activation of several signalling pathways (i.e. RAS-MAPK, STAT, PI3-AKT and others) to ultimately activate multiple metabolic actions, predominately involved in glucose homeostasis and lipid metabolism (Cuevas-Ramos et al., 2012; Kharitonenkov and Larsen, 2011; Ornitz and Itoh, 2015). The novel role of elevated FGF21 as seen under chronic childhood conditions (i.e. severe undernutrition, IBD) in the development of GH resistance and subsequent growth attenuation has elicited recent research interests (Guasti et al., 2014; Kubicky et al., 2012). However, the mechanical role of chronic FGF21 on GHR signalling and downstream events are not fully clear and warrant further experimental investigation.

3.2 Aim and study design.

The aim of this chapter was to generate a model system to study in-depth the activation of GHR signalling and key downstream signalling mediators including; JAK2/STAT5, SOCS2 and IGF-1. This offers a platform to undertake thorough analyses to investigate the fundamental question of this PhD; '*To unravel the mechanistic role of FGF21 in the pathogenesis of GH resistance and subsequent growth failure in chronic childhood conditions*'.

A major drawback in studying GHR is the lack of high quality commercially available antibodies for the detection of endogenous GHR. Thus, *in vitro*, human embryonic kidney cells (HEK-293) that are considered to have a high transfection efficiency were employed to generate stable cell line models to overexpress exogenous human and mouse GHR to more easily follow the activity and fate of the GHR protein. In addition, alongside the generation of stable cell line models, chrondocytic human C28/I2 (isolated from rib cartilage transduced with simian virus 40 (SV40) containing the large T-antigen) and mouse C3H 10T1/2 (generated from primary cultures of 14-17 day whole mouse embryos) cells were also cultured. Both chondrocytic cell lines have been well characterised for their use in studying normal and pathological chondrocyte biology and physiology (Emons et al., 2011; Karimian et al., 2011; Zaman et al., 2014).

The generated HEK-293 hGHR and HEK-293 mGHR stable cell lines and chondrocytic cells, were verified for their suitability for the latter investigations outlined in this PhD (Chapter 4), to study the effects of chronic FGF21 on GHR signalling. Initially, the expression of exogenous GHR in both HEK-293 hGHR and HEK-293 mGHR stable cell line models was assessed at the mRNA and protein level. In addition, the molecular integrity of GHR signalling involving key mediators of the JAK/STAT pathway was examined, including; JAK2, STAT5 and SOCS2 using PCR and western blot analysis. The stable cell line model was further validated for the endogenous expression of *FGF21* and co-receptors (*FGFR1*, *FGFR1-IIIC* and *β-KLOTHO*) using PCR and RT-qPCR. Immunohistochemistry of human growth plate biopsies were additional used to examine the co-expression and co-localisation of FGF21, FGFR1 and β-Klotho.

3.3 Results.

3.3.1 Establishment of HEK-293 GHR expressing stable lines and confirmation of pattern levels.

A suitable human and mouse stable cell line model to study GH/GHR activation and downstream signalling was generated through the application of transfection technology in a HEK-293 cell line, combining polyethylenimine (PEI), a universal transfection agent with commercially available human and mouse GHR plasmids (obtained from *Origene, USA*); 1) pCMV6-AC-Myc-DDK Human GHR, 6.0kb (**Figure 3.1 Ai**) and 2) pCMV6-Entry-Myc-DDK Mouse GHR, 4.9kb (**Figure 3.1 Aii**). Once HEK-293 cells reached ~90% confluency, cells were treated with the prepared transfection master-mix using 2µg of pCMV6-AC-Myc-DDK Human GHR or pCMV6-Entry-Myc-DDK Mouse GHR for 24 hours to achieve overexpression of full length GHR (**Figure 3.1 B**). Empty plasmid with GFP tag, pcDNA3-EGFP (obtained from *Addgene, USA*) was used as a control to determine transfection efficiency. Optimised transfection conditions achieved ~70% transfection efficiency (**Figure 3.1 C**). Following, transfection of the HEK-293 cell line, GHR expressing stable lines were established via antibiotic selection using neomycin/G418 (500µg/ml). Cells were then expanded and used for experiments or banked.

HEK-293 hGHR and mGHR stable lines were validated for the expression of GHR at the protein and mRNA level to determine the suitability of this model to trace key signalling mediators of GHR activation and downstream events. Western blot analysis revealed full-length protein expression of GHR represented by multiple protein products in both stable lines, HEK-293 hGHR (**Figure 3.2 Ai**) and HEK-293 mGHR (**Figure 3.2 Aii**) of approximate molecular size ranging between ~110 –140 kDa. The expression of GHR as multiple protein products has been shown in several previous studies (Deng et al., 2007; Gent et al., 2002; van den Eijnden et al., 2006; van Kerkhof et al., 2001). The expression of GHR was also confirmed at the mRNA level using PCR (**Figure 3.2 Bi-ii**). Immuno-fluorescent staining of GHR in HEK-293 mGHR stable line cells further verified the expression of GHR (**Appendix**, **Figure 7.1**).

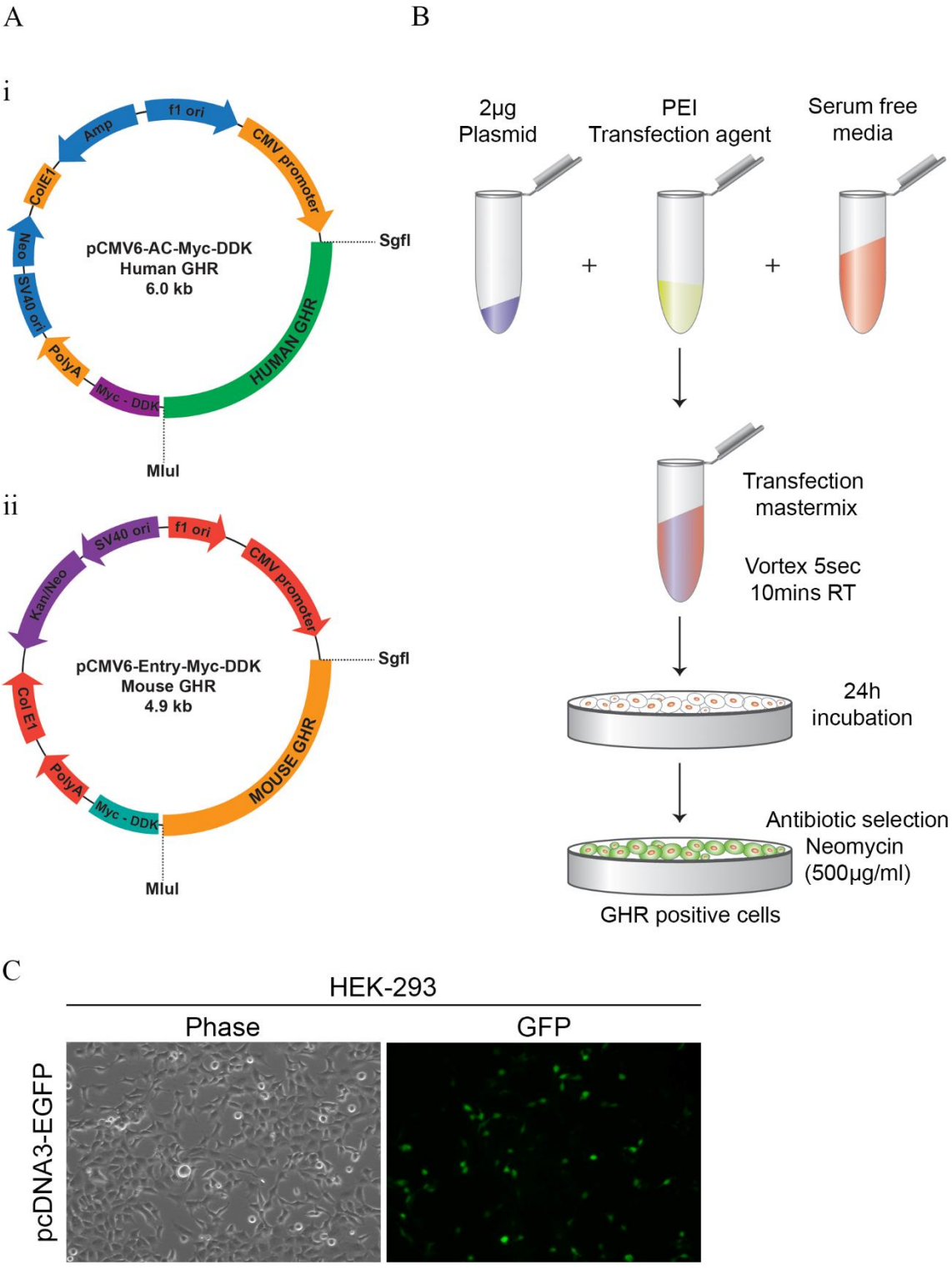

Figure 3.1 Generation of GHR expressing stable cell lines. (A) Illustration of plasmid maps, **(i)** pCMV6-AC-Myc-DDK (Human GHR), **(ii)** pCMV6-Entry-Myc-DDK (mouse GHR). **(B)** Schematic of transfection protocol. HEK-293 cells were non-transfected (control) or transfected with 2µg of pCMV6-AC-Myc-DDK (Human GHR), pCMV6-Entry-Myc-DDK (mouse GHR) *(Origene, USA)* or 2µg pcDNA3-EGFP (GFP tagged, *Addgene, USA*) for 24 hours. GHR expressing positive cells were selected through antibiotic treatment with neomycin/G418 (500µg/ml) and cultured to expand the generation of stable cell line. **(C)** Representative images of transfected HEK-293 cells with pcDNA3-EGFP at 24 hours. Images taken in phase contrast and GFP (x10 magnification).

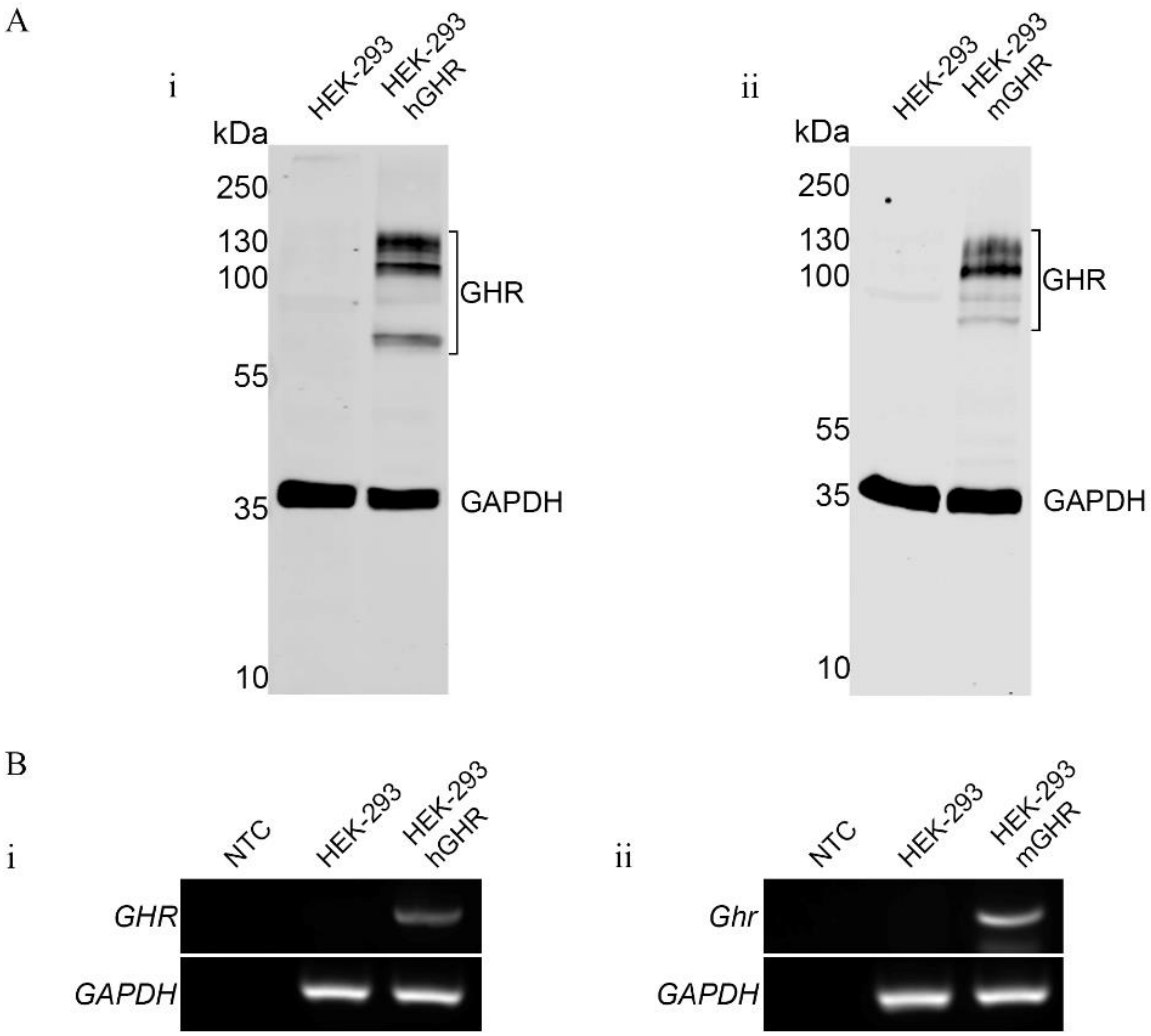

Figure 3.2 Confirmation of the expression of GHR in HEK-293 stable line models. (A) Western blot analysis of anti-GHR (glycosylated mature GHR ~140 kDa, precursor GHR ~110 kDa) in stable lines, *left to right*: **(i)** HEK-293 (control), HEK-293 human GHR (HEK-293 hGHR), **(ii)** HEK-293 (control), HEK-293 mouse GHR (HEK-293 mGHR). The molecular weight (kDa) of protein standard is reported on the *left*. Representative images of an independent experiment (n=1). **(B)** PCR analysis, *left to right*: **(i)** NTC: Non-template control (PCR sample where cDNA was omitted), HEK-293 (control), HEK-293 hGHR mRNA expression of human *GHR* (468bp) **(ii)** NTC, HEK-293 (control), HEK-293 mGHR mRNA expression of mouse *Ghr* (122bp). Housekeeping GAPDH was used as a loading control in both western blot and PCR analysis.

In order to distinguish between mature and immature GHR protein, detected as multiple protein products on western blot imaging (**Figure 3.2 A**), whole cell lysates extracted from human and mouse GHR HEK-293 stable lines were treated with specific enzymes; N-glycosidase F (N.GF) and Endo-glycosidase H (Endo H) to activate the removal of glycosylated sugars. Glycosylation describes the process of the attachment of sugar moieties during post-translational

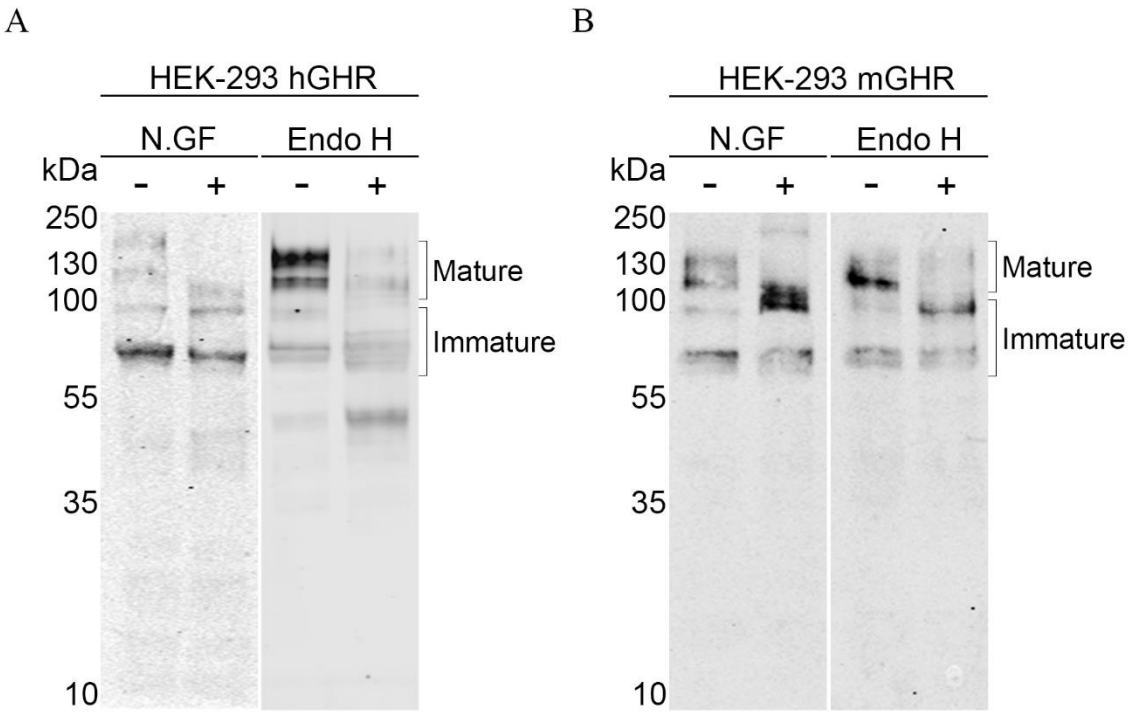

Figure 3.3 Enzymatic treatment with glycosidase revealed mature glycosylated GHR and immature GHR precursor in stable cell lines. Total protein was extracted and lysates were incubated with or without enzymes N-glycosidase F (N.GF) or Endoglycosidase H (Endo H) overnight at 37˚C and separated on a 10% SDS-PAGE, immunoblotted with anti-GHR antibody. ~140 kDa glycosylated mature GHR (Cell surface), ~110 kDa immature precursor GHR (Endoplasmic reticulum and Golgi apparatus). *Left to right*: **(A)** HEK-293 hGHR untreated or treated with N.GF and Endo H, respectively. **(B)** HEK-293 mGHR untreated or treated with N.GF and Endo H, respectively. The molecular weight (kDa) of protein standard is reported on the *left*. Representative images of three independent experiments (*n*=3).

modification (PTM). Thus, treatment with specific enzymes offers an insight into the critical function of the biosynthetic-secretory pathway, allowing us to monitor protein folding before its release and later trafficking to the Golgi apparatus. PTM is characterised by the addition of various glycosidic linkages including; N-, O-, and C-linked glycosylation, glypiation (GPI anchor attachment) and phosphoglycosylation. Glycosidase enzymes catalyse the hydrolysis of glycosidic bonds, removing sugars from proteins. Such enzymes are critical for glycan processing in the endoplasmic reticulum (ER) and Golgi. Each enzyme is highly specific for the removal of a particular sugar (i.e. mannosidase; hydrolyses mannose) (Breitling and Aebi, 2013). Commercially available enzymes to remove sugars added during PTM are used to reveal protein products processed in the Golgi and ER. N.GF (an amidase) is used to remove almost all N-linked oligosaccharides from glycoproteins by cleaving between the innermost N-acetylgucosamine and

asparagine residues of high mannose, hybrid and complex oligosaccharides. In contrast, recombinant glycosidase Endo-H differs slightly by cleaving within the chitobiose core of high mannose and some hybrid oligosaccharides from N-linked glycoproteins.

Enzymatic treatment of whole cell lysates with N-GF and Endo-H in HEK-293 hGHR (**Figure 3.3 A**) and HEK-293 mGHR (**Figure 3.3 B**) stable lines displayed a shift in higher molecular weight GHR protein products (~140 kDa), indicative of the removal of sugars that are usually added in the Golgi. Thus, in keeping with previous experimental studies our findings show that GHR protein products at ~140kDa are representative of the glycosylated mature GHR protein present on the cell surface membrane, whilst GHR protein product at ~110kDa are representative of immature precursor GHR found within the ER and Golgi.

3.3.2 Growth hormone induces the activation of the JAK/STAT pathway.

It is well known that GH/GHR binding leads to the subsequent activation of the Janus kinase signalling cascade, in turn stimulating key downstream signalling mediators involving the phosphorylation of JAK2 and STAT5 to ultimately promote longitudinal bone growth during childhood development via the production of IGF-1 (Ahmed and Farquharson, 2010).

Initially, the protein expression of early downstream mediators, JAK2 and STAT5 were investigated, optimising the dose of recombinant human GH treatment to identify the appropriate concentration for future experimental set-ups (**Appendix**, **Figure 7.2**). For subsequent studies cells were treated with 0.5µg/ml recombinant human GH. HEK-293 hGHR/ mGHR stable lines and chondrocytic cells were serum starved overnight. The next day cells were challenged with recombinant human GH (0.5µg/ml) for 10 and 30 minutes before collection of whole cell lysates at indicated time intervals. Housekeeping GAPDH was not detectable in the chondrocytic cell lines, thus β-actin was instead used as a loading control. The endogenous protein expression of STAT5 (92kDa) in the absence and presence of GH was confirmed in HEK-293 hGHR (**Figure 3.4 A**), HEK-293 mGHR (**Figure 3.4 B)** stable lines and chondrocytic cells, C28/I2 (**Figure 3.4 C**) and C3H 10T1/2 (**Figure 3.4 D)**. HEK-293 hGHR and mGHR stable lines were responsive to GH treatment, as shown through the activation and expression of pSTAT5(Tyr694) at 10 and 30

minutes (**Figure 3.4 A-B**), as can similarly be seen in the chondrocytic cell lines C28/I2 and C3H 10T1/2 (**Figure 3.4 C-D**). Thus, this model confirms that GH exposure induces the elevated expression of pSTAT5 suggesting the activation of the latter downstream signalling events of the JAK/STAT cascade.

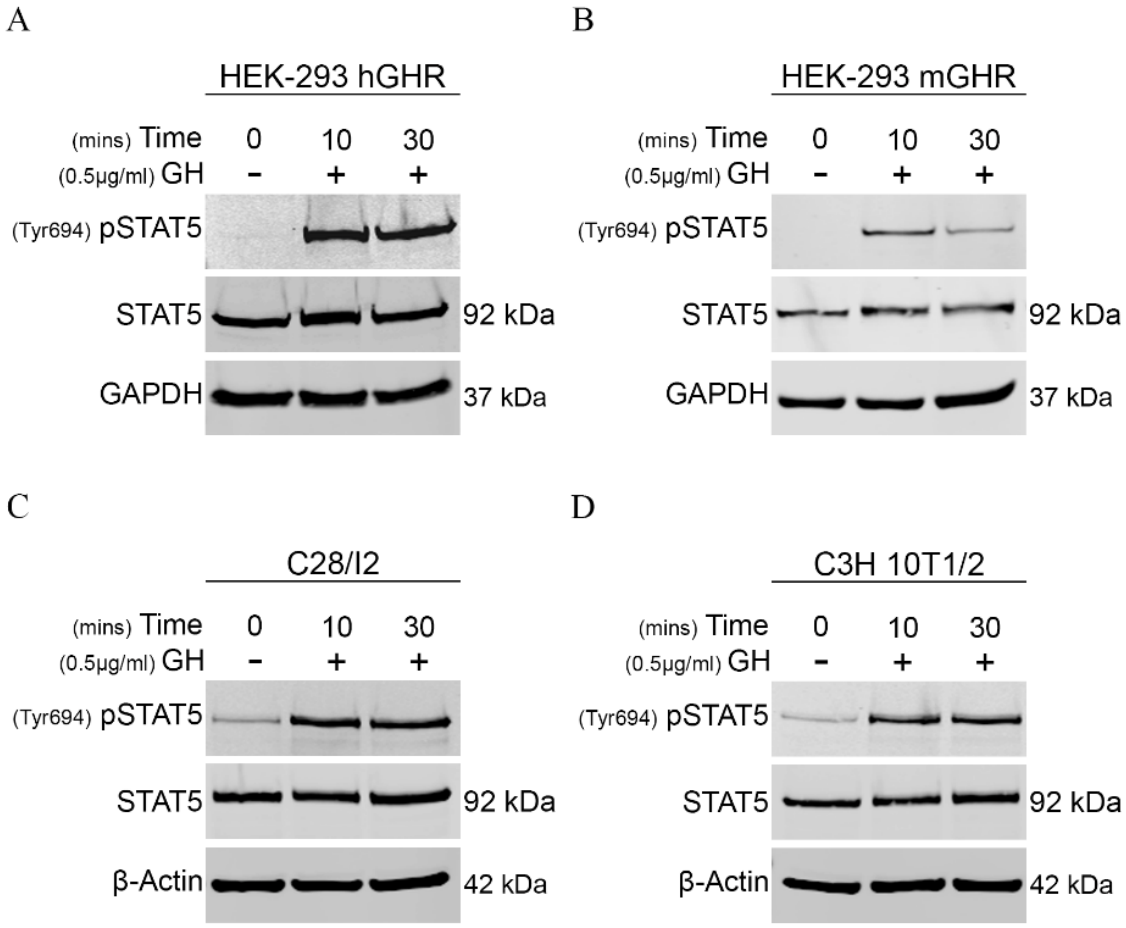

Figure 3.4 GH activates downstream signalling mediators of the JAK/STAT cascade. (A) HEK-293 hGHR, **(B)** HEK-293 mGHR, **(C)** C28/I2 and **(D)** C3H 10T1/2 cells were serum starved overnight and incubated with or without recombinant human GH (0.5µg/ml) for 10 or 30 minutes. Whole cell lysates were extracted and size-separated onto a 10% SDS-PAGE before western blot analysis of STAT5 (92kDa) and pSTAT5(Tyr694) protein expression. Housekeeping GAPDH (37kDa) and β-Actin (42kDa) were used as loading controls. Representative images of three independent experiments (*n*=3).

As previously described SOCS proteins are known as essential negative regulators of a variety of cytokine and growth factor signals (Letellier and Haan, 2016). Several studies highlight the important role of SOCS2 in the activation of a negative feedback loop in the JAK/STAT signalling cascade. SOCS2 expression is mediated via the stimulation of GH activity. GH-induced STAT5b binds to the promoter of SOCS2 to activate SOCS2 expression. In turn, SOCS2 binds to

at least two phosphorylated tyrosines on the GHR to inhibit further activation of the JAK/STAT cascade, thus playing a fundamental role in the regulation of linear growth and development during infancy (Turnley, 2005; Vesterlund et al., 2011).

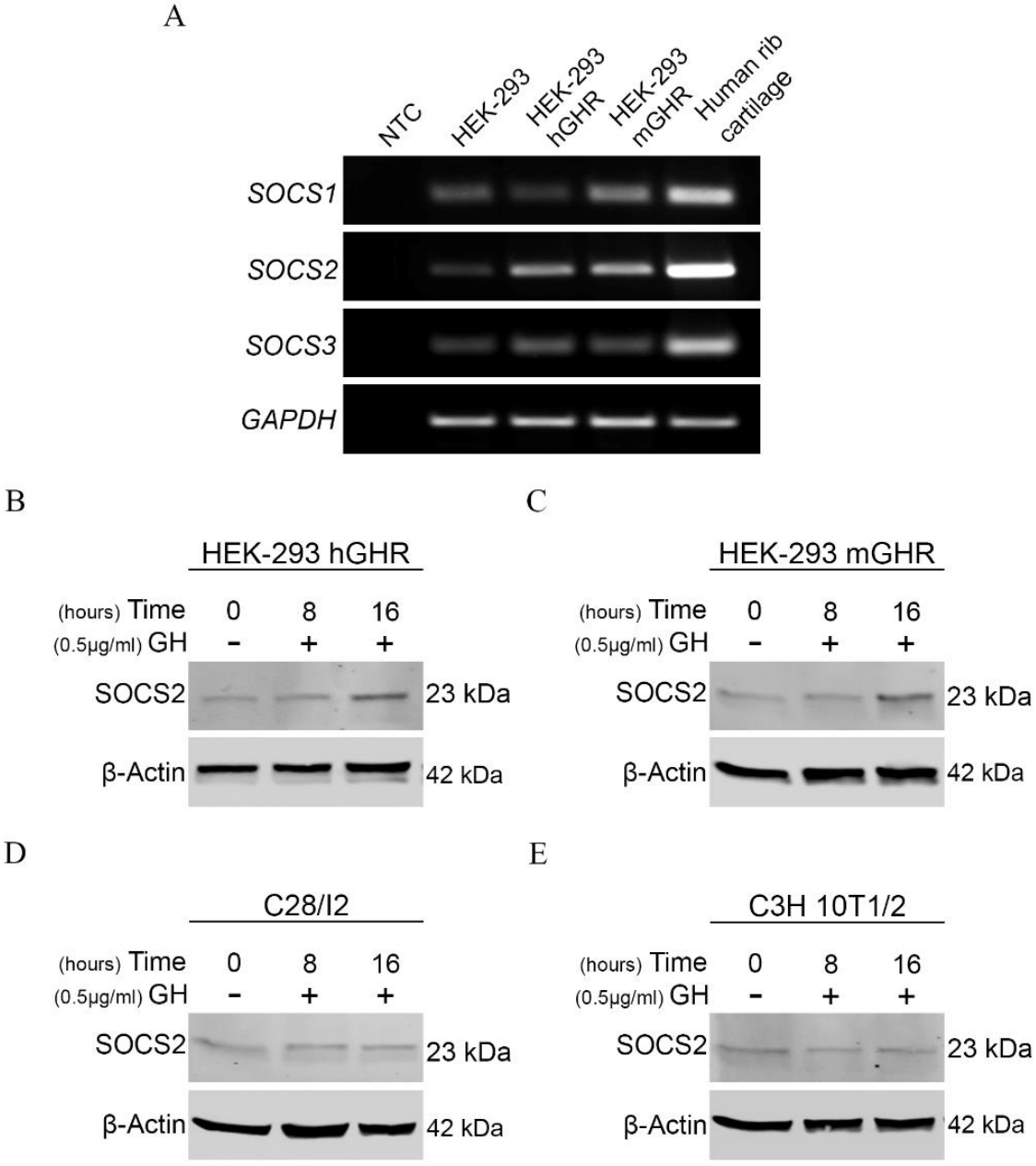

Figure 3.5 Confirmation of SOCS expression. (A) HEK-293 hGHR and mGHR stable lines were assessed for the mRNA expression of *SOCS1* (124bp), *SOCS2* (290bp) and *SOCS3* (120bp) using PCR. Human rib cartilage was used as a positive control. Human *GAPDH* (housekeeping gene) expression was used as a loading control. NTC: non-template control (PCR sample where cDNA was omitted). **(B)** HEK-293 hGHR **(C)** HEK-293 mGHR **(D)** C28/I2 and **(E)** C3H 10T1/2 cells were serum starved overnight and challenged with recombinant human GH (0.5µg/ml) for 8 and 16 hours. Whole cell lysates were extracted and run onto a 10% SDS-PAGE and assessed using western blot analysis for the expression of SOCS2 (23kDa) protein. Housekeeping β-Actin (42kDa) was used as a loading control. Representative images of three independent experiments (n = 3).

PCR analysis revealed the mRNA expression of *SOCS1*, *SOCS2* and *SOCS3* in the stable cell lines HEK-293 hGHR and HEK-293 mGHR using human rib cartilage as a positive control (**Figure 3.5 A**). Furthermore, HEK-293 hGHR/ mGHR stable lines and chondrocytic cells were serum starved overnight and treated with recombinant human GH (0.5µg/ml) for 8 and 16 hours before collection of whole cell lysates at indicated time-points. Western blot analysis showed the expression of SOCS2 protein (23kDa) in the absence and presence of GH at 8 and 16 hours in both stable cell lines and chondrocytic cells (**Figure 3.5 B-E**). Treatment with GH induced an increase in the expression of SOCS2 protein levels at 16 hours compared to untreated cells in HEK-293 GHR stable lines (**Figure 3.5 B-C**). However, our data on GH-induced SOCS2 levels in chondrocytic cells were inconclusive in our western blot setting (**Figure 3.5 D-E**).

3.3.3 Expression of the FGF21 receptor complex repertoire in stable lines.

To explore our interest in studying the effects of chronic FGF21 on GH/GHR signalling, HEK-293 hGHR and mGHR stable cell line models were initially investigated to examine the expression of *FGF21* and the receptor complex; *β-KLOTHO*, *FGFR1* and isoform *FGFR1-IIIC*

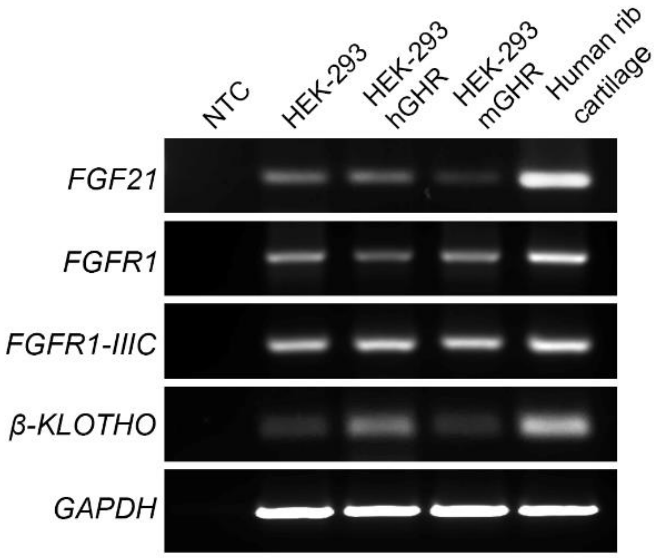

Figure 3.6 HEK-293 GHR stable lines express *FGF21* and receptor complex *FGFR1* and *β-KLOTHO*. Assessment of the mRNA expression of human *FGF21* (168bp) and receptor complex; *FGFR1* (215bp), *FGFR1-IIIC* (110bp) and *β-KLOTHO* (124bp) using PCR. *left to* right: NTC: non-template control (PCR sample where cDNA was omitted), HEK-293 (control), HEK-293 hGHR, HEK-293 mGHR, human rib cartilage (positive control). Human *GAPDH* (housekeeping gene) was used as a loading control.

at the mRNA level. Human rib cartilage was used as a positive control. The expression of human *FGF21*, *FGFR1*, isoform *FGFR1-IIIC* and *β-KLOTHO* was confirmed in both HEK-293 hGHR and HEK-293 mGHR stable lines using PCR (**Figure 3.6**). The stable cell line model, thus demonstrates its potential responsiveness to recombinant FGF21.

3.3.4 FGF21 receptor expression in human growth plate zones.

To further verify the role of FGF21 directly at the growth plate, the expression and localisation of the FGF21 and the receptor complex; FGFR1 and β-Klotho was investigated in male pubertal (average age 12.3 years) human growth plate tissue isolated from the tibia of patients undergoing elected epiphyseal surgery using immunohistochemistry. GHR, FGF21, FGFR1 and β-Klotho were expressed within the human growth plate tissue and were seen to be highly localised in the proliferative and pre-hypertrophic zones (**Figure 3.7 ii-v**). It is well known that the proliferative and maturation process of chondrocytes are induced by various endocrine factors including GH (Brito et al., 2012). This confirms the possibility of a functional cross-talk between intracellular pathways initiated by GH, FGF21 and co-receptors (FGFR1/β-Klotho) as postulated by our group (Guasti et al., 2014) and others (Kubicky et al., 2012).

3.3.5 The effect of GH on the endogenous expression of FGF21.

To determine the effect of GH on the endogenous expression of FGF21, HEK-293 hGHR and mGHR stable lines and C3H 10T1/2 cells were serum starved overnight and challenged with recombinant human GH (0.5µg/ml) for 8, 16 and 24 hours. RNA was extracted at indicated time intervals and cDNA was used to assess the endogenous expression of human *FGF21* or mouse *Fgf21* expression using RT-qPCR analysis. **Figure 3.8 Ai-iv** illustrates the representative dissociation curve of human *FGF21,* mouse *Fgf21,* human *GAPDH* and mouse *Gapdh* (standard reference housekeeping gene, used for normalisation). A single PCR-product was produced in each assay run, demonstrated by the single peak dissociation curve. This highlights the specificity of amplicons generated. RT-qPCR revealed no significant differences in the endogenous human

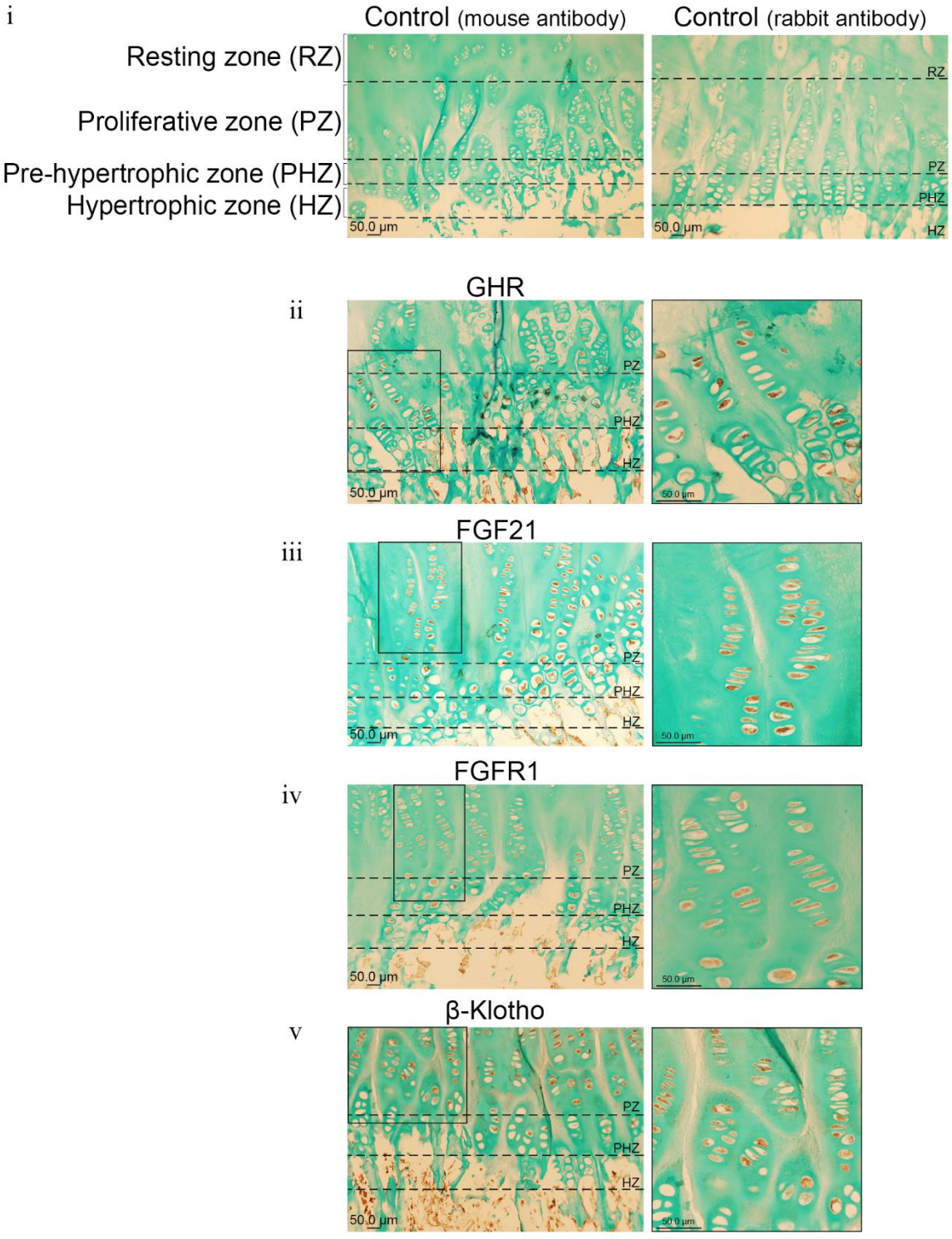

Figure 3.7 FGF21 and receptors FGFR1/ β-Klotho are localised in the proliferative and pre-hypertrophic zones of the human growth plate. Human growth plate tissue biopsies isolated from children undergoing epiphyseal surgery to arrest further leg growth. **(i)** Negative control: sections incubated with secondary antibody only; goat anti-mouse (*Left panel*), goat anti-rabbit (*right panel*). Immunohistochemical localisation of **(ii)** GHR, **(iii)** FGF21, **(iv)** FGFR1 and **(v)** β-Klotho in male human growth plate tissue (tibia) in late puberty, average age 12.3 years, Representative images of six patients (*n*=6). Images counterstained with Alcian Blue. Magnification: x40. Scale bar: 50µm.

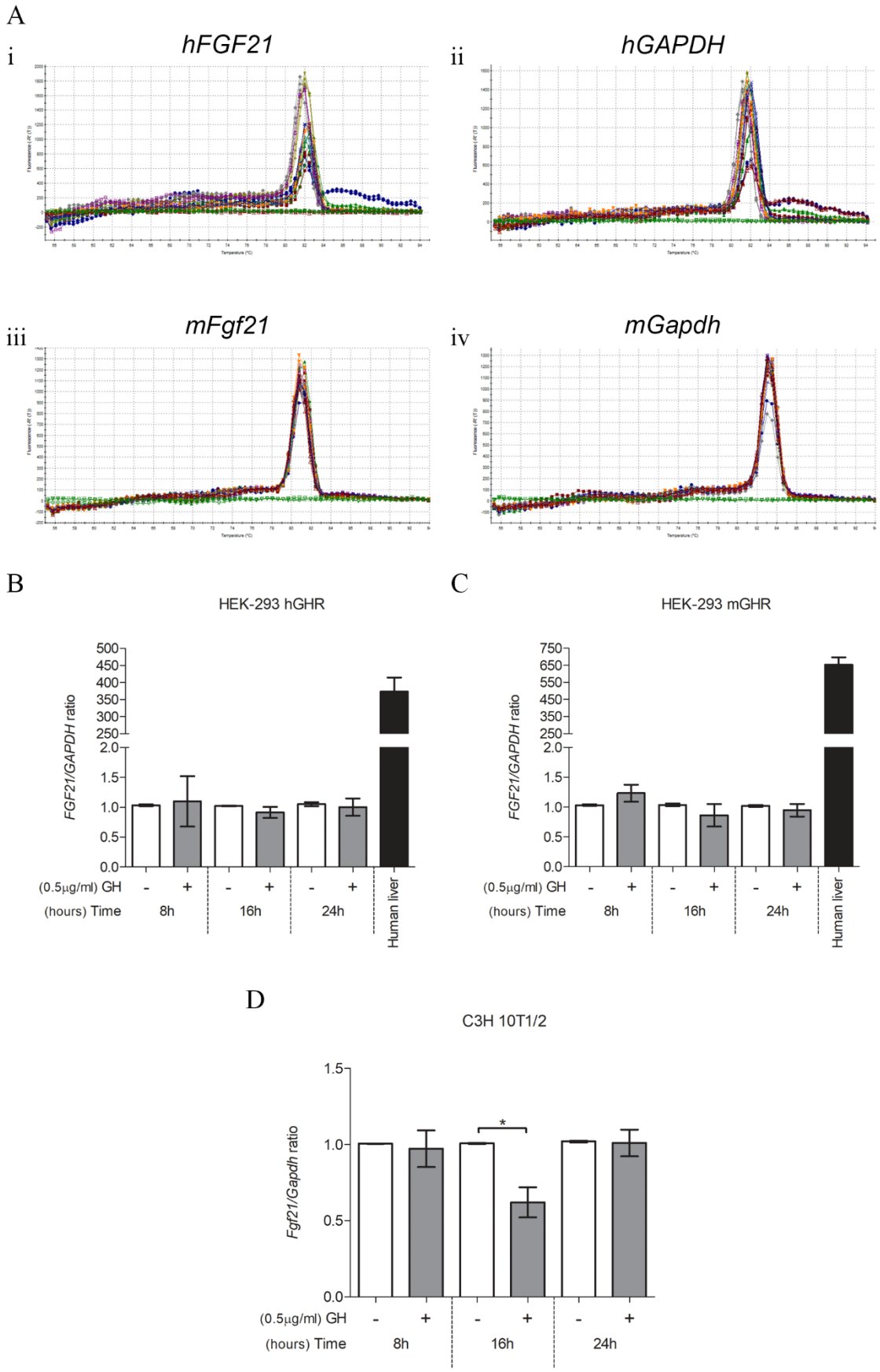

Figure 3.8 Endogenous FGF21 levels are unaffected by GH. HEK-293 hGHR, HEK-293 mGHR stable cell lines and C3H 10T1/2 cells were serum starved overnight and challenged with recombinant human GH (0.5µg/ml) for 8, 16 and 24 hours before RNA extraction and analysis of endogenous human *FGF21* or mouse *Fgf21* expression by RT-qPCR. **(A)** Representative

dissociation curves from RT-qPCR. X-axes: temperature ˚C, Y-axes: first negative derivative of the change in fluorescence. **(B)** HEK-293 hGHR **(C)** HEK-293 mGHR analysis of endogenous human *FGF21* expression. Human liver was used as a positive control for HEK-293 GHR stable line cells. **(D)** C3H 10T1/2 analysis of endogenous mouse *Fgf21* expression. Data are expressed as relative to untreated (control) and normalised using human G*APDH* or mouse *Gapdh* (housekeeping gene). Error bars represent the mean ± SEM from three independent experiments (n=3), each with three replicates. *p<0.05 was considered significant. One-way ANOVA, Dunnett's multiple comparison test.

FGF21 expression in the presence of GH at 8, 16 and 24 hours in HEK-293 hGHR and HEK-293 mGHR stable lines. Human liver was used as a positive control (**Figure 3.8 B-C**). The endogenous *FGF21* expression in HEK-293 GHR stable cell lines were significantly lower compared to human liver (positive control). Similarly, GH treatment at 8 and 24 hours had no effect on the endogenous expression of mouse *Fgf21* in C3H 10T1/2 cells. However, GH treatment at 16 hours displayed a significant reduction (0.39 fold decrease) in the endogenous mouse *Fgf21* expression (p=0.0109) compared to untreated (control) (**Figure 3.8 D**).

3.4 Discussion.

GH/GHR interaction and the activation of a multitude of downstream signalling events together play an essential role in promoting growth during infancy (Robson et al., 2002). It is well known that the JAK/STAT signalling cascade is predominantly involved in longitudinal skeletal growth, primarily via the actions of IGF-1 synthesis. This system is carefully regulated by GH-induced SOCS2 expression, acting as a key negative feedback mediator to inhibit downstream events of GHR signalling (Ahmed and Farquharson, 2010; David et al., 2011; Turnley, 2005; Vesterlund et al., 2011). The main aim of this chapter was to develop a cell system in which to monitor in-depth the signalling events of the JAK/STAT cascade.

Employing transfection technology using HEK-293 cells and commercially available human/ mouse GHR expressing plasmids, stable cell line models; HEK-293 hGHR and HEK-293 mGHR were successfully established, verifying the exogenous expression of human and mouse GHR at the mRNA and protein level (**Figure 3.2** and **Appendix**, **Figure 7.1**). Moreover, coinciding with previous experimental studies by van den Eijnden and Strous, 2007, our findings confirm the identification of glycosylated mature GHR protein (~140 kDa) and GHR immature precursor (~110 kDa) protein products (**Figure 3.3**) (van den Eijnden and Strous, 2007). It is well known that GHR is initially synthesised as a non-glycosylated nascent precursor with 5-high mannose oligosaccharides that is trafficked from the ER to the Golgi apparatus (Sedek et al., 2014). Several studies reveal the dimerisation of GHR in the ER during the early biogenesis process. Thus, GHR is expressed in the form of a dimer at the cell surface membrane, even in the absence of GH interaction (Frank and Fuchs, 2008; Gent et al., 2002). As the GHR precursor transports through Golgi complex, it acquires carbohydrates where it becomes complex glycosylated (removal of high-mannose sugars) to yield mature GHR presenting at the membrane cell surface (Frank and Fuchs, 2008; Sedek et al., 2014; van den Eijnden and Strous, 2007). Thus, treatment of HEK-293 hGHR and mGHR stable lines with glycosidase enzymes facilitated the removal of sugar moieties (high-mannose GHR precursor) that are known to be added during post-translational modifications of GHR, unveiling glycosylated mature (cell surface) GHR and precursor immature GHR (ER and Golgi) protein.

Validation of the HEK-293 hGHR and HEK-293 mGHR stable cell line models and chondrocytic cell lines confirmed the expression of key signalling mediators of the JAK/STAT pathway including; JAK2, STAT5 and negative feedback regulator SOCS2 (**Appendix**, **Figure 7.2**, **Figure 3.4** and **Figure 3.5**). As previously described by Deng et al., 2012 and Han et al., 1996, the actions of GH-induced activation on downstream signalling mediators of the JAK/STAT cascade was highlighted through the rapid response and expression of pJAK2 and pSTAT5 (**Appendix**, **Figure 7.2** and **Figure 3.4**). In addition, coinciding with several experimental studies, the upregulation of GH-induced SOCS2 expression was confirmed in the HEK-293 hGHR/ mGHR stable cell line models (Guasti et al., 2014; Pass et al., 2012). However, it was difficult to conclude the effect of GH-induced SOCS2 expression in the chondrocytic cell lines (**Figure 3.5**).

Furthermore, the endogenous expression of *FGF21* and receptor complex repertoire; *FGFR1*, *FGFR1-IIIC* and *β-KLOTHO* was verified in HEK-293 hGHR/ mGHR stable cell lines (**Figure 3.6**), highlighting the ability of this model to potentially respond to exogenous FGF21 treatment. Moreover, our findings reveal for the first time the localisation of FGF21 and receptor complex (FGFR1 and β-Klotho) to be predominately expressed within the proliferative and pre-hypertrophic zones in the human growth plate tissue (**Figure 3.7**). It is well known that the proliferative, pre-hypertrophic and hypertrophic growth plate zones play an essential role in chondrocyte proliferation and maturation where GHR signalling occurs to promote longitudinal bone growth (Abad et al., 2002; Brito et al., 2012; van der Eerden et al., 2003). Thus, as demonstrated in recent findings it was expected that FGF21 and the receptor complex (FGFR1 and β-Klotho) expression was likely to be highly localised in the growth plate zones, which have elevated proliferative chondrocyte activity. Experimental studies using double immuno-fluorescent staining will further aid to unravel the co-localisation of the expression of FGF21 and its co-receptors (FGFR1 and β-Klotho) in single cells to clarify FGF21s' dependent activity on the presences of FGFR1 and β-Klotho (Angelin et al., 2012; Ding et al., 2012). Lastly, it was shown that GH had no effect on the endogenous expression of FGF21 in HEK-293 stable lines. However, C3H 10T1/2 cells displayed a reduction in the *Fgf21* expression at 16 hours when

treated with GH (**Figure 3.8**). More experimental research is required to better understand the cause of reduced *Fgf21* expression in this setting. It is unlikely that GH acts as a co-factor by inducing the increased FGF21 expression as seen in several chronic childhood conditions, e.g. poor nutrition, Crohn's disease (Cuevas-Ramos et al., 2012; Erickson and Moreau, 2016).

Overall, this chapter describes the generation and thorough validation of the stable cell line models, HEK-293 hGHR, HEK-293 mGHR and chondrocytic cells, as successful tools to carefully trace downstream GHR signalling events of the JAK/STAT cascade. Coupled with the verification of the expression of FGF21 and co-receptor complex (*FGFR1*, *FGFR1-IIIC* and *β-KLOTHO*), further highlights the suitability of these models as a strong platform to investigate and understand the mechanistic role of chronic FGF21 in the development of GH resistance and subsequent growth failure.

Generating stable cell lines to overexpress a given protein may be criticised as a non-physiological representative model. Although commercial antibodies to detect GHR are available on the market, they have been highly problematic in the application for their use to detect the endogenous expression of GHR protein levels. Thus, by overexpressing GHR in the HEK-293 model opens an opportunity to allow us to perform key experimental studies to assess GHR stability (i.e. via treatment with cycloheximide to inhibit the synthesis of new proteins and study the fate of existing GHR proteins) and to furthermore assess the effects of chronic FGF21 on GHR stability, degradation and ubiquitination. Moreover, to address and evaluate the effect of chronic FGF21 on the activation of the JAK2/STAT5 cascade, the study design in this thesis will encompass observing the interaction of recombinant human/ mouse FGF21 treatment on early (GHR, JAK2, STAT5) and late (SOCS2, IGF-1) multi-step processes of GHR downstream signalling events. Together this will offer a deeper understanding of the inhibitory effects of FGF21 in the development of GH resistance and its role in subsequent growth attenuation.

CHAPTER 4. Results

The role of chronic Fibroblast growth factor 21 levels in the development of Growth hormone resistance: Cell models to gain mechanistic insights

4.1 Introduction.

FGF21 is considered an endocrine factor belonging to the FGF19 subfamily (including; FGF19, FGF21 ad FGF23) that has been shown to be predominately expressed in the liver, acting as the primary source of circulatory FGF21 levels (Beenken and Mohammadi, 2012; Iglesias et al., 2012; Murata et al., 2011). It is well known that FGF21 has a high affinity for FGFR1 (in particular isoform FGFR1-IIIC), however its activity is highly dependent on the presence of membrane bound co-receptor β-Klotho (Smith et al., 2013; Yie et al., 2009). Thus, the complex formation of a ternary FGF21/ FGFR1-IIIC/β-Klotho structure triggers the signal transduction and intracellular activation of several downstream signalling pathways, including; RAS-MAPK, PI3K-AKT, PLCγ and STAT (Cuevas-Ramos et al., 2012; Kharitonenkov and Larsen, 2011; Ornitz and Itoh, 2015).

The metabolic actions of FGF21 are well revised. It is known that FGF21 plays a fundamental role in glucose homeostasis and lipid metabolism via the expression of regulatory mediators, PPARα and PPARγ. During a fasting state, elevated hepatic FGF21 levels are induced by PPARα to promote fatty acid oxidation and ketogenesis. Glucose (a feeding signal) is also seen to activate hepatic FGF21 expression via ChREBP, whilst in contrast, glucose fasting increases hepatic FGF21 levels stimulated by PGC1α to enhance gluconeogenesis. In adipocytes, PPARγ and ChREBP also regulate FGF21 levels, driven by feeding signals to enhance glucose uptake, while circulatory FGF21 levels remain unchanged (Chapter 1, Figure 1.12) (Cuevas-Ramos et al., 2012; Iglesias et al., 2012; Kim and Lee, 2015). However, it is shown that excessive elevated levels of FGF21 are seen to be undesirable having severe negative outcomes. It is reported that chronic FGF21 plays a central role in the contribution of several pathological conditions including; obesity, T2D, impaired glucose tolerance, fatty liver disease, muscle atrophy and CHD (Cuevas-Ramos et al., 2012; Erickson and Moreau, 2016; Iglesias et al., 2012; Kim and Lee, 2015). A thorough review of FGF21 biology and physiology are described in Chapter 1, section 1.5.

Several recent *in vivo* and *in vitro* studies and clinical cases have identified a clear correlation between elevated FGF21 expression secondary to severe chronic conditions (e.g. long-

term undernutrition) and the development of GH resistance and subsequent growth failure. A previous investigation performed in our lab by Guasti et al., 2014 highlighted a significant inverse association between mean FGF21 levels (during the first 5 weeks of life) and the change in SD score for length in a Finnish PreBaby population of VPT infants. In addition, the use of primary chondrocytes (obtained from rib cartilage) revealed that recombinant FGF21 was able to inhibit GH induced pSTAT5 activity and IGF-1 expression whilst stimulate SOCS2 levels (Guasti et al., 2014). Similarly, Mericq et al., 2014 showed elevated serum FGF21 levels in term infants compared to pre-term infants at 6 months; further emphasising an inverse correlation with growth rates in infancy (Mericq et al., 2014).

Several *in vivo* investigations coincide with these findings. A $FGF21^{-/-}$ knockout mouse model placed on a restricted diet showed a partial increase in both body and tibial growth compared to their wildtype littermates, whilst when given daily injections of recombinant FGF21 to $FGF21^{-/-}$ mice these differences in length were no longer identifiable (Kubicky et al., 2012). Furthermore, a FGF21 knock-in transgenic mouse model developed by Inagaki et al., 2008 showed a reduction in STAT5 expression and growth promoting mediator, IGF-1. In addition, FGF21 was seen to stimulate hepatic IGF-BP1 and negative regulator SOCS2 (Inagaki et al., 2008). Thus, these recent findings clearly highlight the link between elevated FGF21 levels and poor growth outcomes associated with a failure in downstream GHR signalling. The precise mechanistic interplay of FGF21s' action on GHR signalling warrants further investigation to support current research findings.

4.2 Aim and study design.

In Chapter 3, the essential tools were generated to study in-depth GHR signalling using molecular techniques to establish suitable human and mouse GHR expressing stable lines. The models were further validated for the expression of key mediators involved in downstream GHR signalling including; JAK2, STAT5 (and its phosphorylated form) and SOCS2. In addition, the endogenous expression of *FGF21* and its receptor complex (*β-KLOTHO*, *FGFR1* and isoform *FGFR1-IIIC*) were highlighted in both stable line models confirming their responsiveness to recombinant FGF21 treatment.

Having developed an appropriate model to explore the molecular mechanics of early and late downstream GHR signalling events, the aim of this chapter was to address the fundamental role of chronic FGF21 levels in the development of GH resistance and subsequent growth failure, focusing on cellular events triggered by GHR activation. Initially, the study design explored the effect of chronic FGF21 exposure directly on GHR expression and turnover in HEK-293 hGHR/ mGHR stable lines. Blocking of protein translation by drug cycloheximide (CHX) was used to determine GHR half-life and the rate of degradation. Investigating the stability of a given cellular protein is one of the first stages towards understanding whether its cellular abundance and activity are subjected to proteolytic regulation or internalisation/ recycling. CHX is an inhibitor of protein synthesis (interfering with protein translocation) and the decay of a target protein over time can be determined by SDS-PAGE and western blot analysis. Once GHR half-life was established using CHX, further experimental studies were performed involving treatment with recombinant human GH, FGF21 or a combination of the two, to identify the effect of chronic FGF21 exposure on modifications in GHR internalisation and proteolytic degradation.

Recent findings indicate that SOCS2 is part of a multimeric complex posing ubiquitin ligase activity, directly regulating GHR levels on the plasma membrane through ubiquitination and subsequent degradation in a proteasomal dependent manner (Vesterlund et al., 2011). It is proposed that elevated FGF21 levels may enhance GH-mediated GHR depletion from the plasma membrane on target cells through SOCS2 activity. Thus, the experimental design was optimised

to study the effect of chronic FGF21 on the ubiquitination (degradation of proteins via the proteasome) of GHR protein using immunoprecipitation.

In addition, using both the GHR expressing stable line models, chondrocytic cell lines and/ or primary cultures of human growth plate biopsies, the effect of chronic FGF21 exposure was assessed on early downstream events (GH binding to GHR, STAT5 and SOCS2 activation etc.) through to late downstream events (IGF-1 expression). The study design incorporated treatment of HEK-293 hGHR/ mGHR stable lines, chondrocytic cells (C28/I2 and C3H 10T1/2) or primary cultures of human growth plate biopsies with human/ mouse recombinant FGF21 which were further challenged with human recombinant GH; both dose and time dependently. Collection of RNA and whole cell protein lysates were examined using RT-qPCR and western blot analysis, respectively. The aim of these experiments were to offer a deeper insight into the chronic effects of FGF21 on GH-induced modifications in GHR signalling, revealing the mechanical interplay of FGF21 in the progression of GH resistance and poor growth outcomes.

4.3 Results.

4.3.1 Chronic FGF21 reduced GH-induced GHR half-life.

GHR is internalised via the ubiquitin conjugation system. A specific 10aa sequence between 323 and 332 found within the GHR cytosolic tail (termed the UbE motif) targets GHR for ubiquitination (Alves dos Santos et al., 2001; van Kerkhof et al., 2000). Several studies reveal that GHR has a relatively short half-life of approximately 2 – 5 hours (dependent on the experimental set-up), where degradation of the receptor is said to occur within the lysosome (Baxter, 1985; van Kerkhof et al., 2000). It is suggested that GHR undergoes proteolytic cleavage within the extracellular domain resulting in the formation of soluble GHBP. Down-regulation of signal transducing GHR leads to the eventual extinction of the signalling pathway(s) and a rapid degradation of primary messengers, the receptor and its ligand (van Kerkhof et al., 2000).

It is well known that GH is a potent regulator of growth and metabolism. It has a very short plasma half-life of approximately 20 minutes, due to the fast renal clearance and its small molecular mass (22 kDa) (Deng et al., 2007; van Kerkhof et al., 2000). Following GH binding to GHR, the GH/GHR complex becomes internalised via clathrin-coated pits leading to its subsequent degradation in lysosomes (Alves dos Santos et al., 2001). A study by Deng et al., 2007 revealed that GH treatment reduced the half-life of GHR from more than 4 hours to approximately 1 hour, thus GH binding further stimulates GHR ubiquitination, internalisation and degradation (Deng et al., 2007). Hence, when GH is present, two GHR polypeptides dimerise resulting in the activation of GHR downstream signalling and the subsequent phosphorylation by tyrosine kinase JAK2. This is then targeted for ubiquitination and the complex is endocytosed (van Kerkhof et al., 2000).

As described in Chapter 1, section 1.6, it is hypothesised that chronic FGF21 levels cause GH resistance via a direct interaction/action on chondrocytes, as demonstrated in several recent experimental studies whereby elevated FGF21 levels in mice and humans led to a reduction in longitudinal growth and subsequent growth attenuation (Guasti et al., 2014; Kubicky et al., 2012).

Thus, the effect of chronic FGF21 exposure on GHR signalling was explored, initially investigating GHR half-life and ubiquitination.

The rate of GHR degradation was assessed using treatment with CHX (100µg/ml) to inhibit the synthesis of new proteins and to allow us to monitor the fate of previously existing or synthesised mature GHR protein. Initially, the time interval of GHR degradation was optimised using a wide spread treatment exposure (0 – 30 hours) to identify the appropriate conditions resulting in complete turn-over of mature GHR protein expression using western blot analysis (**Appendix**, **Figure 7.3**). For subsequent experimental investigations to assess GHR half-life, cells were treated with CHX between 0 and 8 hours.

HEK-293 hGHR and HEK-293 mGHR stable cell lines were cultured for 0 – 8 hours in the absence or presence of CHX. Mature GHR protein degradation over time (untreated 0 hours to 8 hours) was observed as the expression of the protein became less apparent in both HEK-293 hGHR (**Figure 4.1 Ai**) and HEK-293 mGHR (**Figure 4.1 Bi**) stable lines. The presence of recombinant human GH (0.5µg/ml) in CHX treated cells resulted in a significant reduction in GHR half-life in both HEK-293 hGHR and HEK-293 mGHR cells at 1 hour (p<0.0001 and p<0.0001, respectively), 2 hours (p<0.0001 and p=0.0009, respectively) and 3 hours (p=0136 and p=0.0033, respectively) compared to CHX treated cells only (**Figure 4.1 A-Bii**). In keeping with previous studies, the overall rate of mature GHR degradation was significantly reduced in the presence of recombinant human GH compared to CHX treated only from 1.355 to 0.7741 hours (p=0.0007) in HEK-293 hGHR (**Figure 4.1 Aiii**) and 1.566 to 0.6390 hours (p=0.0002) in HEK-293 mGHR (**Figure 4.1 Biii**) stable lines (Deng et al., 2007). No significant differences were detected in mature GHR expression and degradation rate in the presence of recombinant human FGF21 (5µg/ml) alone in CHX treated cells compared to CHX treated only, in both stable lines (**Figure 4.1 A-Bii** and **A-Biii**). Interestingly, chronic exposure to recombinant FGF21 in the presence of recombinant human GH in CHX treated cells resulted in a greater shift and rapid reduction of mature GHR half-life compared to CHX GH treated cells, where western blot imaging revealed the expression of mature GHR to be almost abolished by 5 to 8 hours (**Figure 4.1 A-Bi**). This difference in expression of mature GHR was significant at the 1 hour time-point

in both HEK-293 hGHR and mGHR stable lines (p=0.0003 and p<0.01, respectively) (**Figure 4.1 A-Bii**). In addition the overall rate of mature GHR degradation was also significantly reduced in FGF21/-GH treated cells compared to GH alone from 0.7741 to 0.4518 hours (p=0.0015) in HEK-293 hGHR (**Figure 4.1 Aiii**) and 0.6390 to 0.4931 hours (p=0.0225) in HEK-293 mGHR (**Figure 4.1 Biii**) stable lines. These findings thus confirm that chronic FGF21 expedites GH-induced GHR turn-over.

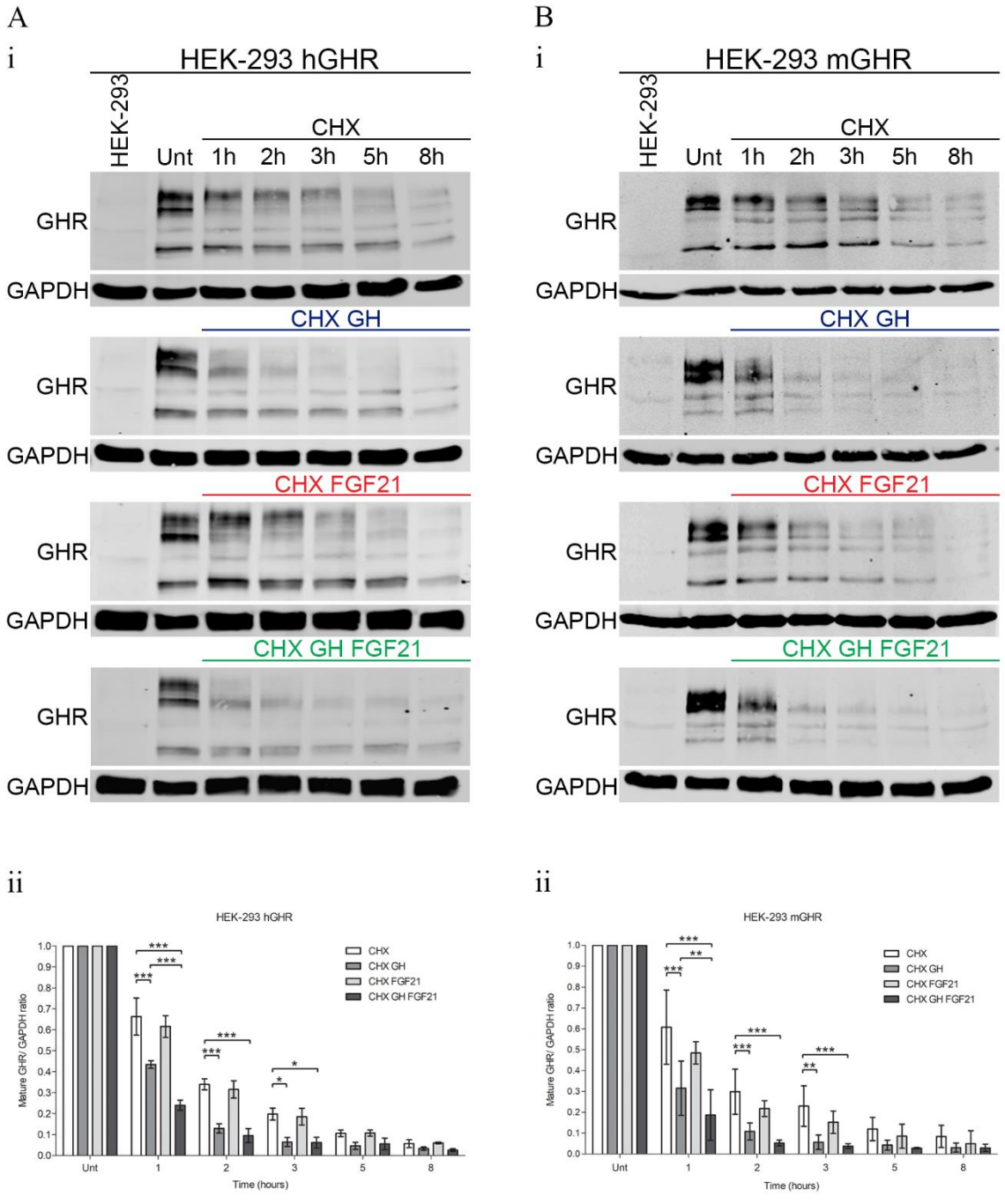

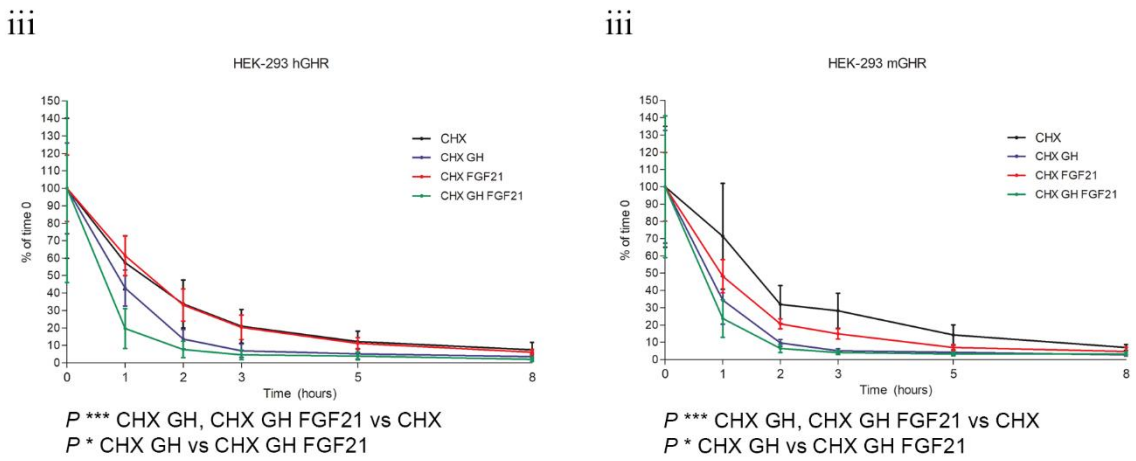

Figure 4.1 Chronic FGF21 exposure reduced GH-induced mature GHR half-life. HEK-293 hGHR and HEK-293 mGHR stable lines were serum starved overnight and treated with or without cycloheximide (CHX) (100µg/ml), recombinant human GH (0.5µg/ml) and/or recombinant human FGF21 (5µg/ml) for 0 (untreated) to 8 hours before the collection of cell lysates at indicated time intervals. Lysates were size separated onto a 10% SDS-PAGE before the analysis of GHR (~110 – 140 kDa) expression by western blotting. **(Ai)** HEK-293 hGHR **(Bi)** HEK-293 mGHR representative western blot images. Unt: untreated at 0 hours, HEK-293: negative control, non-transfected cells. **(A-Bii)** Quantification of mature GHR protein expression. Data indicate the ratio of treated (CHX, CHX + GH, CHX + FGF21, CHX + GH + FGF21) vs untreated 0 hours, normalised to housekeeping GAPDH. Error bars represent the mean ± SEM, from (n=4) independent experimental replicates. Two-way ANOVA, Bonferroni post t-tests. **(A-Biii)** Quantification of the rate (hours) of mature GHR half-life, expressed as % of time at 0 hours. Non-linear Regression, One phase decay. *p<0.05, **p<0.01, ***p<0.001 was considered significant.

4.3.2 Chronic FGF21 did not enhance GH-induced ubiquitination of GHR.

A further investigation was undertaken to assess the effect of chronic FGF21 exposure on the proteosomal degradation of GHR via the ubiquitin pathway. As previously described GHR is tagged for ubiquitination by the presence of a specific 10aa motif within its cytosolic tail (UbE-motif; DSWVEFIELD) (van Kerkhof et al., 2001). Ubiquitin is a 76 aa protein (8.5kDa) and is highly conserved throughout eukaryotes; well known for targeting proteins for degradation in a two-step motion: 1) Firstly, multiple ubiquitin molecules covalently attach to the target protein. 2) Secondly, the protein is tagged for degradation by a multi-subunit, ATP-dependent protease termed proteasome. Three enzymes are involved in the conjugation of ubiquitin to the substrate. The C-terminal Gly residue of ubiquitin is activated by enzyme E1 (ATP dependent manner). This step involves an intermediate formation of ubiquitin-adenylate, followed by the binding of

ubiquitin to a Cys residue of E1 in a thiolester linkage, with the release of AMP. Next, activated ubiquitin is transferred to an active Cys residue of one of several ubiquitin-carrier proteins (E2, ubiquitin conjugating enzyme, Ubc). Lastly, the conjugation process is catalysed by E3; ubiquitin protein ligase, which initiates the link between the ubiquitin (via its C-terminus in an amide isopeptide linkage) to the protein substrate (to an ε -amino group of an internal Lys residue) (Xu and Jaffrey, 2013).

To assess the effect of chronic FGF21 on the degradation of GHR via the ubiquitin-proteasome pathway, HEK-293 hGHR stable line cells were serum starved and treated overnight with or without recombinant human FGF21 (5µg/ml) before being challenged with recombinant human GH (0.5µg/ml) for 16 hours. Cell extracts were immunoprecipitated with anti-IgG rabbit (negative control) or anti-GHR antibody and size-seperated onto a 10% SDS-PAGE before analysis of ubiquitination via western blot analysis.

Initially, the methodology used for immunoprecipitation was verified by assessing the expression of GHR in both whole cell lysates (CL) and immunoprecipitated samples (IP) in HEK-293 hGHR cells. The expression of GHR was confirmed in both whole CL and IP samples (lanes 1, 3-8), whilst no detected GHR expression as expected in the negative control IP IgG sample (lane 2) (**Figure 4.2 i**). Furthermore, the quality of the ubiquitin antibody was assessed on whole CL (**Figure 4.2 ii**) which highlighted a classical pattern of degradation of all proteins (represented by multiple bands at different sizes) in each sample. Examination of ubiquitination of GHR in IP samples revealed no obvious visual difference between FGF21 GH or GH treated cells compared to control (untreated) (**Figure 4.2 iii**). Due to the technical limitations of the ubiquitin antibody used in this setting, quantification of blots were unable to be performed. Thus, conclusions from these blots must be further verified. In order to assess differences in ubiquitination, future experiments aimed at better detection of ubiquitinated proteins are needed e.g. denaturing the membrane before blocking has been shown to enhance the detection of ubiquitination. Furthermore, based on the recent findings in **Figure 4.1** where it was shown that chronic FGF21/-GH treatment significantly increases the degradation rate of GHR, suggests that FGF21 may induce degradation of GHR via other mechanisms other than the ubiquitin-proteosomal pathway.

Further consideration is required to understand the mechanical interplay of FGF21 GH-induced GHR degradation e.g. via proteasome independent mechanisms of GHR turnover or shedding.

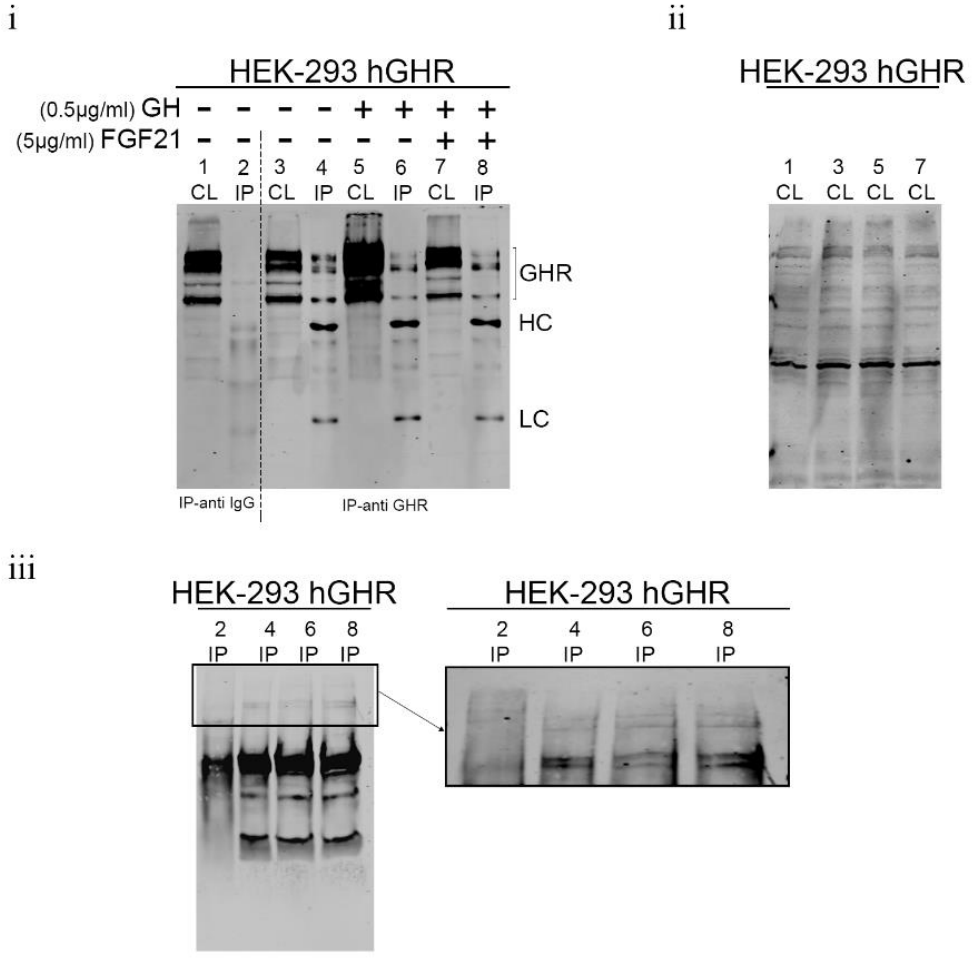

Figure 4.2 Assessment of chronic FGF21 on GH-induced GHR ubiquitination via immunoprecipitation. HEK-293 hGHR stable line cells were serum starved overnight with or without recombinant human FGF21 (5µg/ml) before being challenged with recombinant human GH (0.5µg/ml) for 16 hours. Whole cell lysates were collected and treated with protein A/G plus agarose beads before immunoprecipitation with anti-IgG (negative control) or anti-GHR. Samples were size-separated onto a 10% SDS-PAGE before analysis of ubiquitin via western blot. **(i)** Western blot image assessing GHR expression in whole cell lysates and immunoprecipitated sample. CL: cell lysate, IP: immunoprecipitated sample, HC: heavy chain IgG, LC: light chain IgG. **(ii)** Western blot image of ubiquitination of total protein in whole cell lysate. **(iii)** Western blot image showing ubiquitination of GHR expression in immunoprecipitated samples. (*n*=3) independent experimental replicates.

4.3.3 Chronic FGF21 inhibits GH-induced phosphorylation of STAT5.

Having revealed the direct effect of chronic FGF21 in the presence of GH on the reduction of mature GHR half-life, the effect of chronic FGF21 exposure was next investigated on early

and late downstream mediators of the JAK-STAT signalling cascade. In Chapter 3, Figure 3.4 it was demonstrated that the HEK-293 hGHR/ mGHR stable line model and chondrocytic cell lines were responsive to treatment of exogenous human recombinant GH, as shown through the rapid induction of pSTAT5(Tyr694) protein expression.

In order to test the effect of chronic FGF21 on the phosphorylation of STAT5, HEK-293 hGHR/ mGHR stable lines and chondrocytic cells were serum starved overnight with the treatment of human/ mouse recombinant FGF21 (5µg/ml). The next day cells were challenged with human recombinant human GH (0.5µg/ml). As can be seen in **Figure 4.3 A-Di**, western blot imagining illustrates the endogenous expression of STAT5 protein (92kDa) in the presence and absence of recombinant FGF21 and GH treatment. Quantitative western blotting analysis revealed a significant increase in GH-induced pSTAT5(Tyr694) protein expression at 10 and 30 minutes in both stable lines and chondrocytic cells (C28/I2; p=0.0001 and p=0.0001, respectively) (C3H 10T1/2; p=0.0045 and p=0.0012, respectively) compared to control (untreated) (**Figure 4.3 A-Dii**). FGF21 treatment alone had no effect on the phosphorylation of STAT5 vs control (untreated). Inversely, stable cell lines show a significant inhibition in pSTAT5(Tyr694) protein expression in chronic FGF21 and GH treated cells compared to GH treated cells at 10 and 30 minutes, both in HEK-293 hGHR (p=0.0002 and p<0.05, respectively) and HEK-293 mGHR (p=0.0084 and p=0.0493, respectively) (**Figure 4.3 A-Bii**). This demonstrates that FGF21 inhibits GH-induced STAT5 phosphorylation and which may cause a further reduction in downstream signalling events of the JAK/STAT cascade. Similarly in human chondrocytes (C28/I2) a chronic exposure to FGF21 was also seen to significantly inhibit GH-induced STAT5 phosphorylation at 10 and 30 minutes (p=0.0001 and p=0.0181, respectively) compared to GH treated cells (**Figure 4.3 Cii)**. In C3H 10T1/2 cells, a similar trend was observed. FGF21 and GH treatment induced a reduction in pSTAT5(Tyr694) at 10 and 30 minutes, without reaching statistical significance (all p values were >0.05) (**Figure 4.3 Dii**).

A

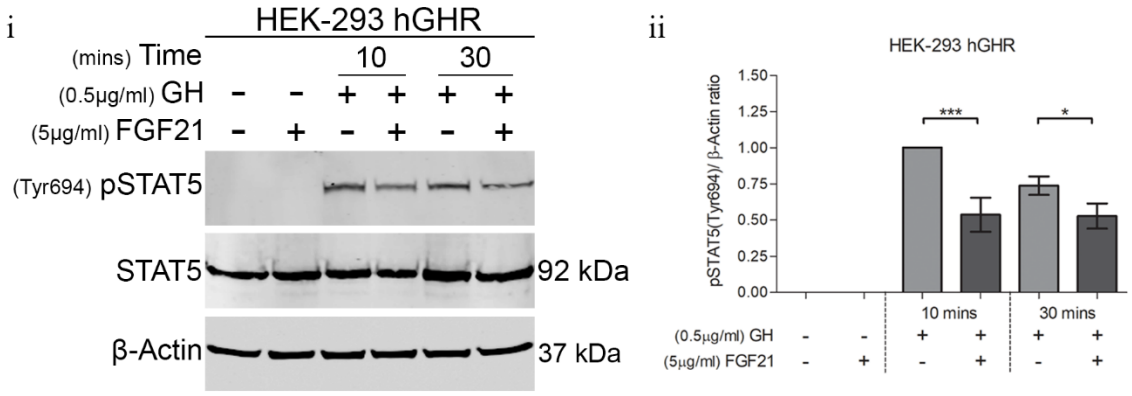
i
HEK-293 hGHR
(mins) Time
10
30
(0.5µg/ml) GH
(5µg/ml) FGF21
(Tyr694) pSTAT5
STAT5
92 kDa
β-Actin
37 kDa
ii
HEK-293 hGHR
pSTAT5(Tyr694)/ β-Actin ratio
1.50
1.25
1.00
0.75
0.50
0.25
0.00
***
*
10 mins
30 mins
(0.5µg/ml) GH
(5µg/ml) FGF21

B

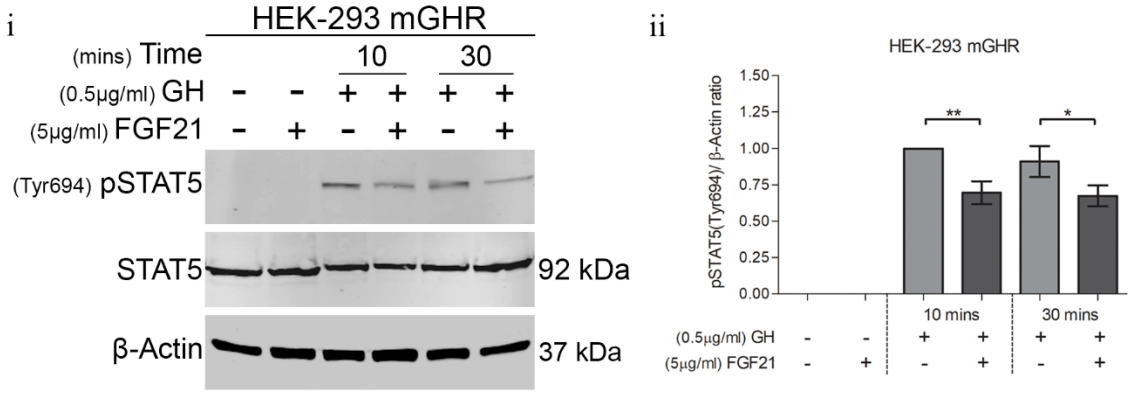
i
HEK-293 mGHR
(mins) Time
10
30
(0.5µg/ml) GH
(5µg/ml) FGF21
(Tyr694) pSTAT5
STAT5
92 kDa
β-Actin
37 kDa
ii
HEK-293 mGHR
pSTAT5(Tyr694)/ β-Actin ratio
1.50
1.25
1.00
0.75
0.50
0.25
0.00
**
*
10 mins
30 mins
(0.5µg/ml) GH
(5µg/ml) FGF21

C

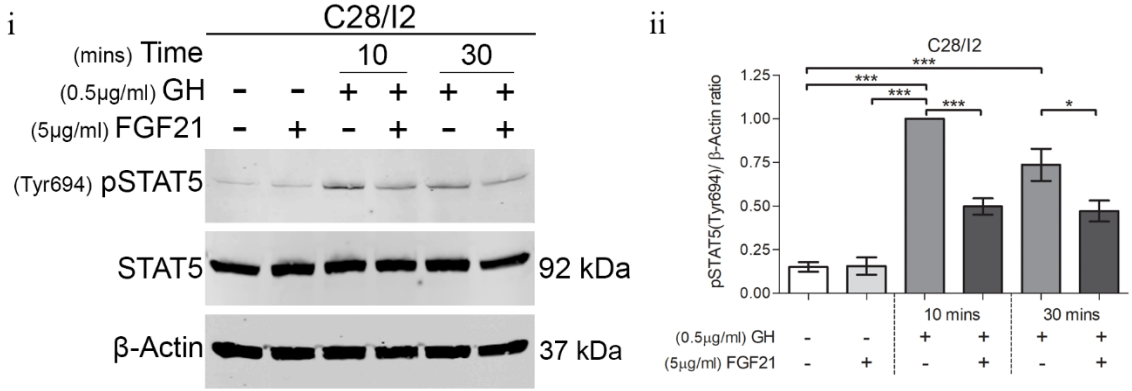
i
C28/I2
(mins) Time
10
30
(0.5µg/ml) GH
(5µg/ml) FGF21
(Tyr694) pSTAT5
STAT5
92 kDa
β-Actin
37 kDa
ii
C28/I2
pSTAT5(Tyr694)/ β-Actin ratio
1.25
1.00
0.75
0.50
0.25
0.00
***
*
10 mins
30 mins
(0.5µg/ml) GH
(5µg/ml) FGF21

D

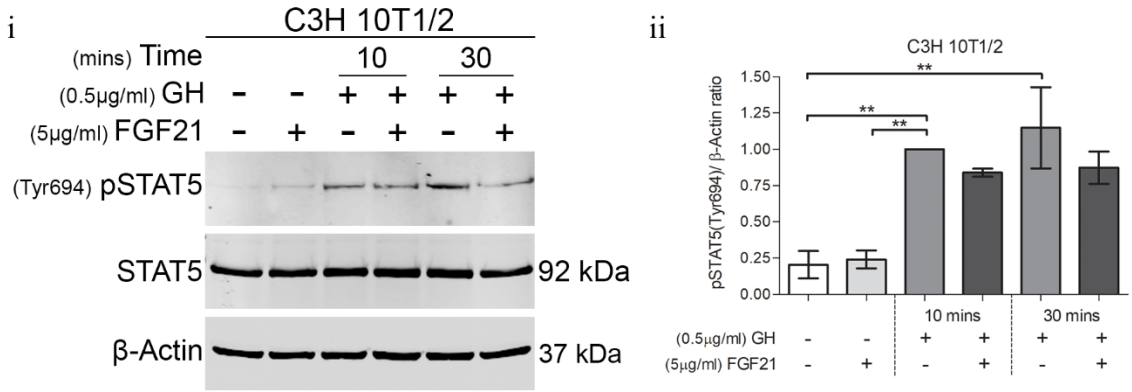
i
C3H 10T1/2
(mins) Time
10
30
(0.5µg/ml) GH
(5µg/ml) FGF21
(Tyr694) pSTAT5
STAT5
92 kDa
β-Actin
37 kDa
ii
C3H 10T1/2
pSTAT5(Tyr694)/ β-Actin ratio
1.50
1.25
1.00
0.75
0.50
0.25
0.00
**
**
**
10 mins
30 mins
(0.5µg/ml) GH
(5µg/ml) FGF21

Figure 4.3 Chronic FGF21 exposure in the presence of GH reduced pSTAT5 activity. Stable lines and chondrocytic cells were serum starved and treated overnight in the presence or absence of recombinant human/ mouse FGF21 (5µg/ml). Cells were further challenged with recombinant human GH (0.5µg/ml) for 10 or 30 minutes. Whole cell lysates were harvested at the indicated time-points and samples were size-separated onto a 10% SDS-PAGE gel before assessment of STAT5 (92kDa) and pSTAT5(Tyr694) by western blotting. **(Ai)** HEK-293 hGHR, **(Bi)** HEK-293 mGHR, **(Ci)** C28/I2 and **(Di)** C3H 10T1/2, representative western blot images. β-actin (37kDa) was used as a loading control. Quantification of pSTAT5(Tyr694) protein expression **(Aii)** HEK-293 hGHR (*n*=5), **(Bii)** HEK-293 mGHR (*n*=5), **(Cii)** C28/I2 (*n*=3), **(Dii)** C3H 10T1/2 (*n*=3), independent experiments. Error bars represent the mean ± SEM. Data indicate the ratio of pSTAT5(Tyr694) protein vs total protein, normalised to GH treatment alone at 10 minutes. *****p<0.05, ******p<0.01 and *******p<0.001. One-way ANOVA, Dunnett's multiple comparison test.

4.3.4 Chronic FGF21 increased GH-induced SOCS2 expression.

To further dissect the molecular events elicited by chronic FGF21, the effect of FGF21 exposure was assessed on the expression of SOCS2; a key negative regulator of the GHR signalling cascade. It is well known that SOCS2 expression is stimulated by high levels of GH and regulated by GH-dependent STAT5 activity (Vesterlund et al., 2011).

Initially the mRNA expression of *SOCS2* was examined. HEK-293 hGHR/ mGHR cells were serum starved and placed in an elevated FGF21 environment (5µg/ml) overnight before being challenged with recombinant human GH (0.5µg/ml) for 8 or 16 hours. RNA was extracted at the indicated time points and the cDNA was used to assess *SOCS2* levels by RT-qPCR. The dissociation curves shown in **Figure 4.4 Ai-ii** are representative of human *SOCS2* and housekeeping gene human *GAPDH*. The single peak curve demonstrates the specificity and amplification of a single PCR-product. As shown **Figure 4.4 B-C**, GH treatment significantly induced an increased expression of *SOCS2* compared to control (untreated) at 8 and 16 hours in HEK-293 hGHR (p=0.002 and p=0.0086, respectively) and HEK-293 mGHR (p=0.0158 and p=0.0148, respectively). FGF21 treatment alone was found not to stimulate an upregulation in *SOCS2* mRNA expression in both stable lines vs control (untreated). Chronic FGF21 treatment in the presence of GH resulted in a further increase in *SOCS2* mRNA expression vs GH treatment alone at 8 and 16 hours in both stable lines. This difference in elevated *SOCS2* mRNA expression was significant only at 16 hours in HEK-293 hGHR (p=0.0201) and HEK-293 mGHR (p=0.0224).

In addition, the effect of elevated FGF21 on GH-induced SOCS2 protein expression was investigated to understand if these findings mimicked those seen at the mRNA level. Western blot imaging in the HEK-293 hGHR/ mGHR stable cell line models and chondrocytic cells confirmed a similar trend/pattern as seen in RT-qPCR analysis. Western blot revealed GH treatment to stimulate the expression of SOCS2 protein (23kDa) compared to control (untreated). Whilst, a combined FGF21 and GH treatment was seen to further induce an increased SOCS2 protein expression compared to GH treatment alone in all cell lines (**Figure 4.4 D-G**). Due to technical experimental difficulties in high background interference of western blot imaging, the quantitative analysis of SOCS2 protein expression has not been undertaken and thus single representative western blot images have been illustrated.

The effect of chronic FGF21 treatment was further tested in primary cultures of human growth plate biopsies. Biopsies were extracted from the tibia and femur of three individual patients undergoing, elected epiphyseal surgery at different stages of puberty in order to arrest further leg growth, due to constitutional tall stature or leg length difference. Primary cultures derived from growth plate biopsies were treated by applying the same dose and time conditions as described above for the cell lines, with an additional observation taken at the 24 hour time-point. Assessment of mRNA *SOCS2* expression using RT-qPCR revealed an unexpected variation in *SOCS2* levels between times-points (8, 16 or 24 hours) taken from each individual patient and also across comparisons analysed between all three patients (**Appendix**, **Figure 7.4**). To understand these difference observed, human growth plate control (untreated) biopsies taken at 8, 16 or 24 hours were further examined for their endogenous mRNA expression of receptors human *β-KLOTHO, FGFR1*, isoform *FGFR1-IIIC* and *GHR* (**Appendix**, **Figure 7.6**). Interestingly, intra-variation of FGF21 receptor (*β-KLOTHO, FGFR1, FGFR1-IIIC*) and *GHR* mRNA expression was also observed between time-points (8, 16 or 24 hours) taken from each individual patient and also cross patient variation. Thus, this evidence might offer an explanation of the heterogeneity seen in *SOCS2* levels in the human growth plate biopsies. Due to the vast variability in *SOCS2* levels in the human growth plate data, **Appendix**, **Figure 7.4** cannot be taken as a true representative.

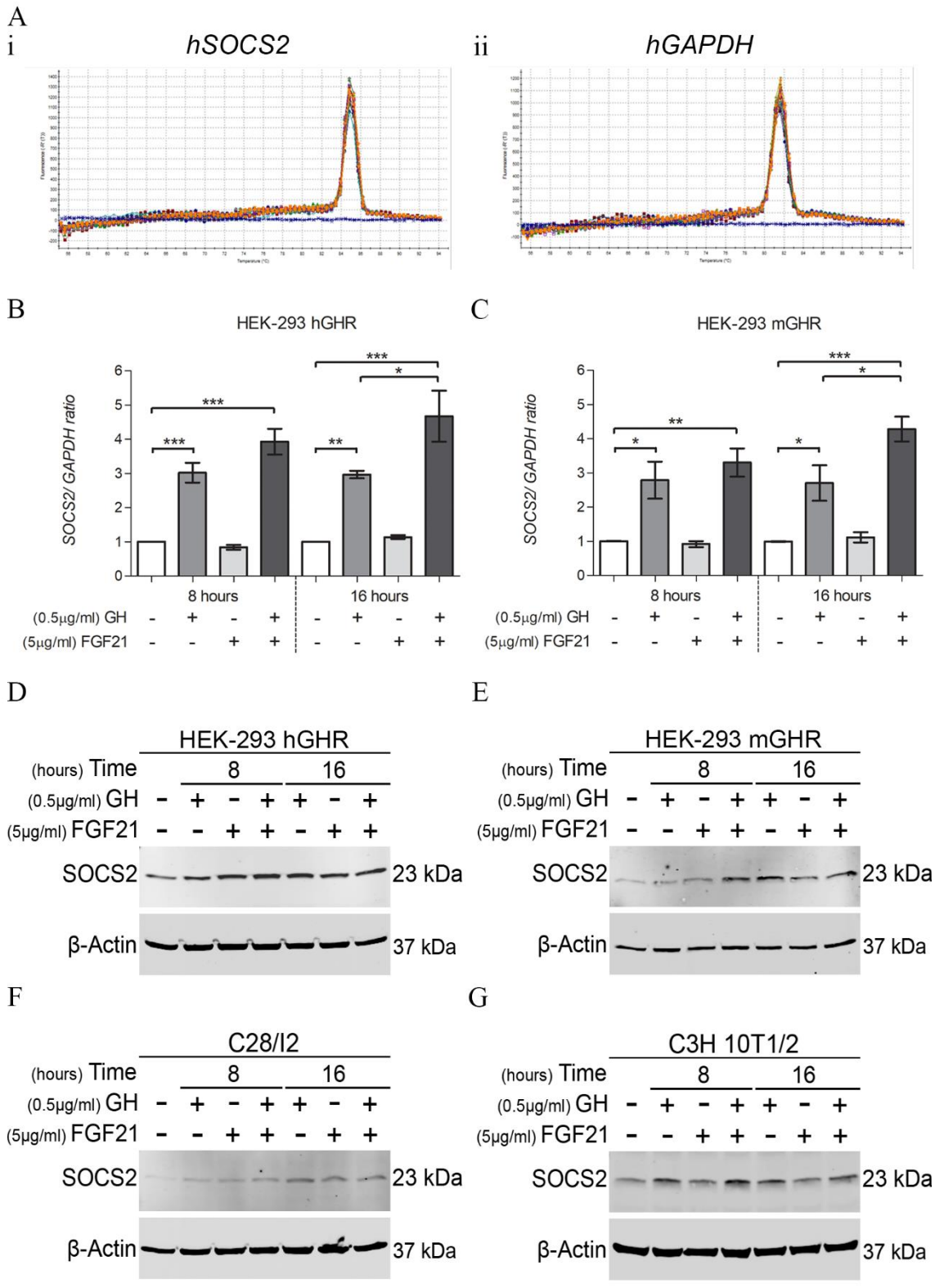

Figure 4.4 Chronic FGF21 exposure in the presence of GH increased SOCS2 expression. HEK-293 hGHR/mGHR stable lines and chondrocytic cells were serum starved and treated with or without recombinant human/ mouse FGF21 (5µg/ml) overnight. The next day cells were challenged with recombinant human GH (0.5µg/ml) for 8 or 16 hours before collection of RNA extracts or whole cell lysates. **(A)** Representative dissociation curve from RT-qPCR **(i)** human *SOCS2* **(ii)** human *GAPDH* (housekeeping). X-axes: temperature ˚C, Y-axes: first negative derivative of the change in fluorescence. **(B)** HEK-293 hGHR **(C)** HEK-293 mGHR, RT-qPCR analysis of human *SOCS2* expression. Data are expressed relative to control (untreated) and

normalised using human *GAPDH* (housekeeping gene). Error bars represent the mean ± standard error from HEK-293 hGHR (*n*=4) and HEK-293 mGHR (*n*=3) independent experiment, each with two biological replicates. *p<0.05, **p<0.01, ***p<0.001 was considered significant. One-way ANOVA, Dunnett's multiple comparison test. Whole cell lysates were assessed for their expression of SOCS2 (23kDa) by western blot. β-actin (37kDa) was used as a loading control. Representative western blot images, **(D)** HEK-293 hGHR (*n*=3) **(E)** HEK-293 mGHR (*n*=3) **(F)** C28/I2 (*n*=3) and **(G)** C3H 10T1/2 (*n*=3).

4.3.5 Chronic FGF21 reduced GH-induced IGF-1 expression.

To further elucidate the role of chronic FGF21 in GH resistance, the effect of elevated FGF21 was explored on the essential growth promoting factor IGF-1; a late downstream mediator of GHR signalling. **Figure 4.3** showed that chronic FGF21 levels in the presence of GH significantly inhibited pSTAT5 protein expression. Thus, it was hypothesised that as a result of the inhibition of early downstream targets of the GHR signalling cascade, a reduction in the expression of late GHR signalling mediators including IGF-1 could be observed.

The same experimental conditions including dosage (recombinant human FGF21, GH) and time (8, 16 hours) were applied as previously described. **Figure 4.5 Ai-ii** shows representative dissociation curves of human *IGF-1* and human *GAPDH* (housekeeping), confirming the specificity of the single amplicons generated. GH significantly stimulated the mRNA expression of *IGF-1* in treated cells vs control (untreated) at 8 and 16 hours in both stable lines; HEK-293 hGHR (p=0.0001 and p=0.0001, respectively) and HEK-293 mGHR (p<0.0001 and p<0.0001, respectively) (**Figure 4.5 B-C**). FGF21 treatment alone did not stimulate an increase in *IGF-1* mRNA expression vs control (untreated). Exposure of cells to a chronic FGF21 environment in the presence of GH resulted in a significant inhibition of *IGF-1* mRNA expression compared to GH treatment alone at 8 and 16 hours; HEK-293 hGHR (p=0.0271 and p=0.0333, respectively) and HEK-293 mGHR (p=0.0224 and p=0.0444, respectively) (**Figure 4.5 B-C**).

In addition, primary cultures of human growth plate biopsies were also assessed for the mRNA expression of *IGF-1* when stimulated with chronic FGF21 levels. Human growth plate biopsies were isolated from three individual patients as previously described. Primary cultures were prepared and treated with the same dosage of recombinant human FGF21 (5µg/ml) and GH (0.5µg/ml) and time (8 and 16 hours) with an additional observation at 24 hours. Similarly, as

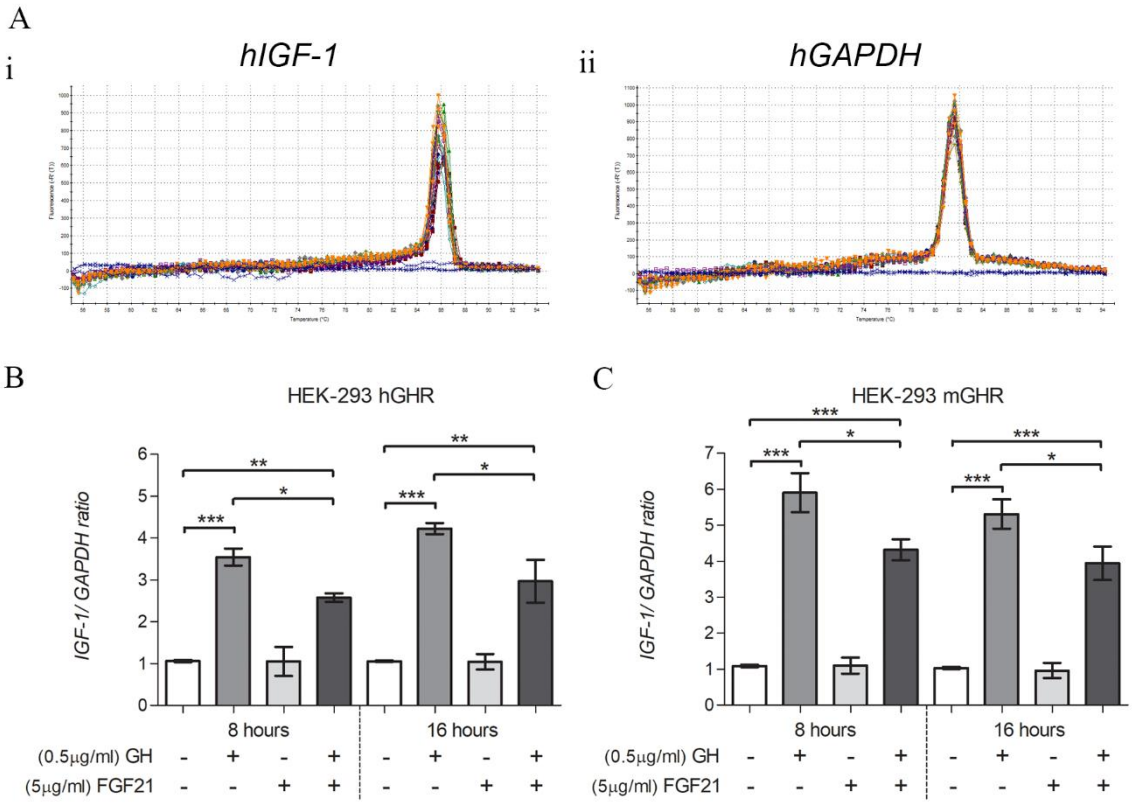

Figure 4.5 Chronic FGF21 exposure in the presence of GH inhibited IGF-1. HEK-293 hGHR/ mGHR stable lines were serum starved and treated with or without recombinant human FGF21 (5µg/ml) overnight. Cells were further challenged with human recombinant GH (0.5µg/ml) for 8, or 16 hours before collection of RNA extracts. **(A)** Representative dissociation curve from RT-qPCR **(i)** human *IGF-1* **(ii)** human *GAPDH*. X-axes: temperature ˚C, Y-axes: first negative derivative of the change in fluorescence. RT-qPCR analysis of human *IGF-1* expression of **(B)** HEK-293 hGHR **(C)** HEK-293 mGHR. Data are expressed relative to control (untreated) and normalised using human *GAPDH* (housekeeping). Error bars represent the mean ± standard error from three independent experiment (n=3), each with two biological replicates.* p<0.05, **p<0.01, ***p<0.001 was considered significant. One-way ANOVA, Dunnett's multiple comparison test.

described during the analysis of mRNA *SOCS2* levels, an unexpected variation in *IGF-1* mRNA expression was also observed in the human growth plate biopsies between varying point-times (8, 16 or 24 hours) in the same patient and across comparisons made between all three patients using RT-qPCR analysis (**Appendix**, **Figure 7.5**). As discussed in Chapter 4, section 4.3.4, this variation in *IGF-1* mRNA expression found between growth plate biopsies, may be as a consequence of the heterogeneity observed in the endogenous mRNA expression of FGF21 receptor (*β-KLOTHO*, *FGFR1*, *FGFR1-IIIC*) and *GHR* in control (untreated) growth plate biopsies as seen between varying time points of individual patients and cross patient comparisons (**Appendix**, **Figure 7.6**). Thus, the *IGF-1* expression data represented in **Appendix**, **Figure 7.5**

cannot be taken as a true representative of the human growth plate findings due to the variability seen in our results.

4.3.6 Chronic FGF21 inhibits GH-induced cell proliferation.

The effect of chronic FGF21 exposure was examined on the proliferative capacity of HEK-293 hGHR/ mGHR stable cell lines and chondrocytic cells (**Figure 4.6**). Cells were grown in 96 well culture plates until they reached ~50% confluency before being serum starved and treated with or without to recombinant human/ mouse FGF21 (5µg/ml) overnight. The following day cells were treated in the presence or absence of recombinant human GH (0.5µg/ml) for 72 or 96 hours before the assessment of cell proliferation.

In the presence of GH a significant increase in cell proliferation was observed compared to control (untreated) in HEK-293 hGHR at 72 hours (p=0.0191) (**Figure 4.6 Ai**) and 96 hours (p=0.0025) (**Figure 4.6 Aii**) and in HEK-293 mGHR at 96 hours (p=0.0080) (**Figure 4.6 Bii**). FGF21 treatment alone did not cause a significant change in cell proliferation vs control (untreated). Chronic FGF21 exposure in the presence of GH was seen to significantly inhibit cell proliferation vs GH treatment alone in HEK-293 hGHR at 96 hours (p=0.0027) (**Figure 4.6 Aii**) and in HEK-293 mGHR at 72 hours (p=0.0105) (**Figure 4.6 Bi**) and 96 hours (p=0.0220) (**Figure 4.6 Bii**).

A similar trend was also observed in the chondrocytic cell lines (**Figure 4.6 C-D**). GH induced a significant increase in cell proliferation vs control (untreated) in C28/I2 cells at 72 hours (p=0.0024) (**Figure 4.6 Ci**) and 96 hours (p=0.0021) (**Figure 4.6 Cii**). GH-induced cell proliferation in C3H 10T1/2 cells, however this difference was not significant (p>0.05) (**Figure 4.6 D**). FGF21 treatment alone had no effect on the proliferative capacity of chondrocytic cells vs control (untreated). As evident in the stable cell lines, chronic FGF21 exposure in the presence of GH caused a significant decrease in cell proliferation vs GH treatment alone in C28/I2 cells at 72 hours (p=0.0023) (**Figure 4.6 Ci**) and 96 hours (p=0.0018) (**Figure 4.6 Cii**) and C3H10 T1/2 at 96 hours (p=0.0044) (**Figure 4.6 Dii**).

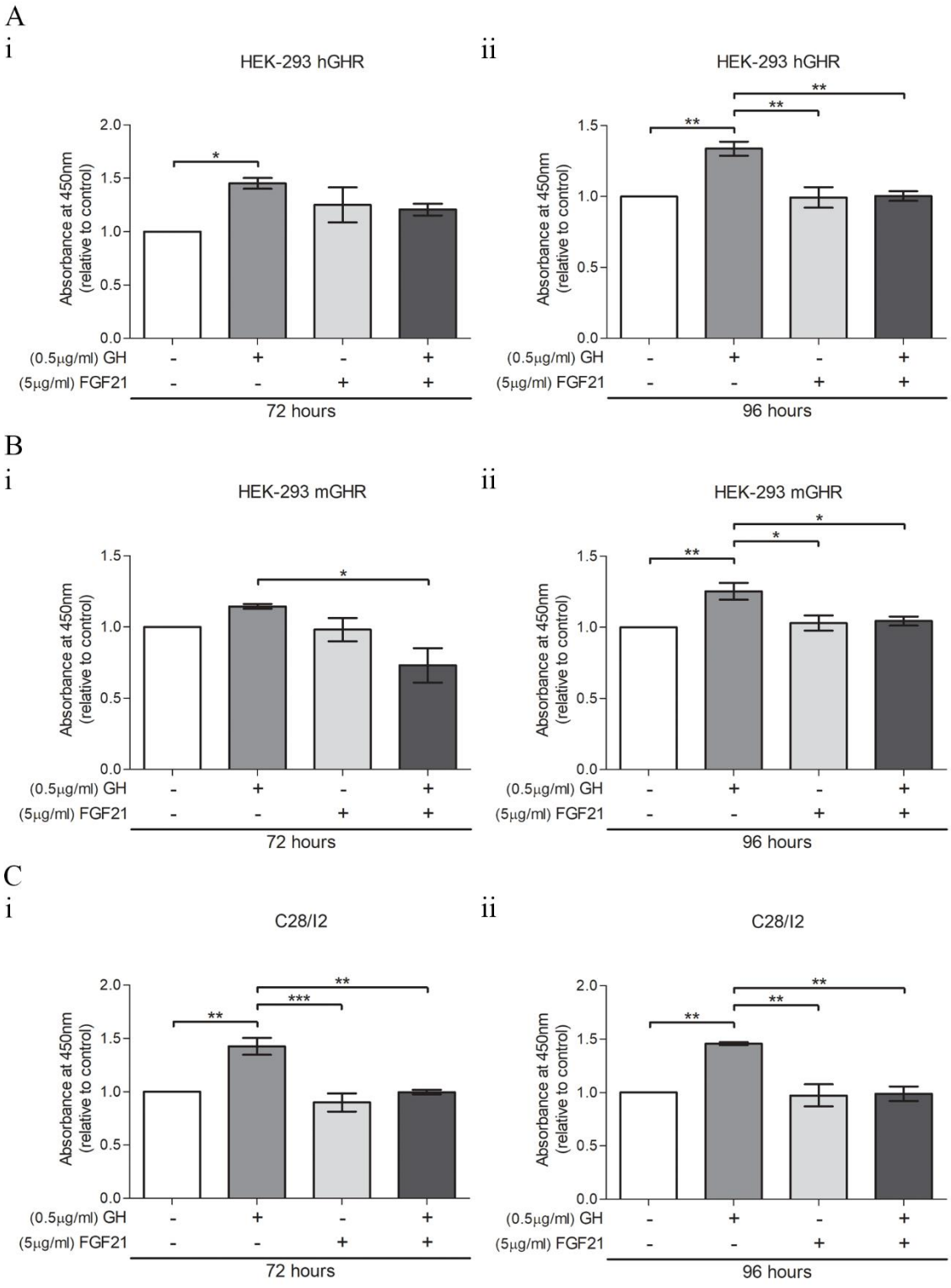
A
i
HEK-293 hGHR
Absorbance at 450nm (relative to control)
2.0
1.5
1.0
0.5
0.0
*
(0.5µg/ml) GH - + - +
(5µg/ml) FGF21 - - + +
72 hours
ii
HEK-293 hGHR
Absorbance at 450nm (relative to control)
1.5
1.0
0.5
0.0
**
**
**
(0.5µg/ml) GH - + - +
(5µg/ml) FGF21 - - + +
96 hours
B
i
HEK-293 mGHR
Absorbance at 450nm (relative to control)
1.5
1.0
0.5
0.0
*
(0.5µg/ml) GH - + - +
(5µg/ml) FGF21 - - + +
72 hours
ii
HEK-293 mGHR
Absorbance at 450nm (relative to control)
1.5
1.0
0.5
0.0
**
*
*
(0.5µg/ml) GH - + - +
(5µg/ml) FGF21 - - + +
96 hours
C
i
C28/I2
Absorbance at 450nm (relative to control)
2.0
1.5
1.0
0.5
0.0
**
***
**
(0.5µg/ml) GH - + - +
(5µg/ml) FGF21 - - + +
72 hours
ii
C28/I2
Absorbance at 450nm (relative to control)
2.0
1.5
1.0
0.5
0.0
**
**
**
(0.5µg/ml) GH - + - +
(5µg/ml) FGF21 - - + +
96 hours

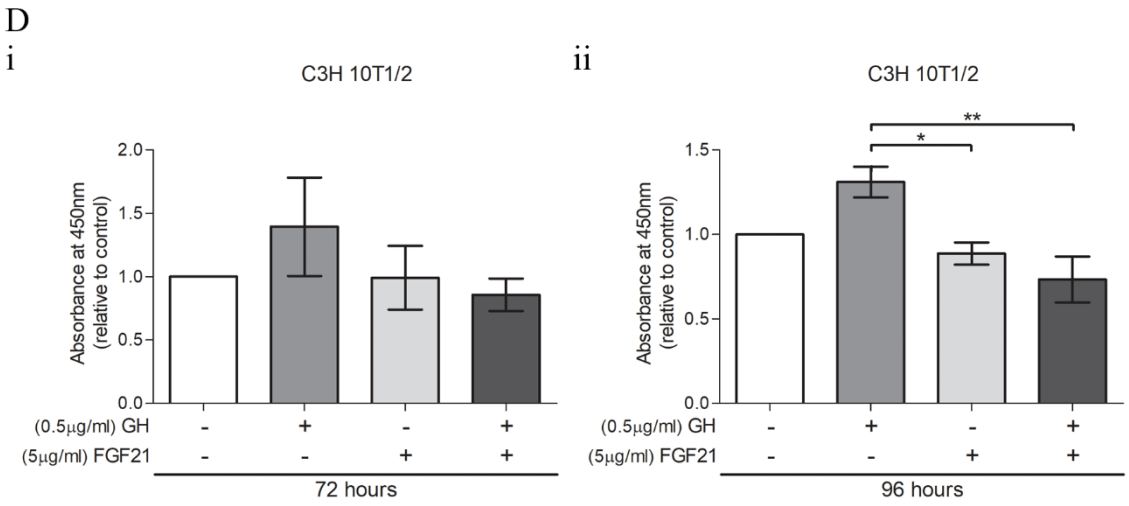

Figure 4.6 Chronic FGF21 exposure reduced GH-induced cell proliferation in HEK-293 stable lines and chondrocytic cells. Stable lines and chondrocytic cells seeded in 96 well plates were serum starved and treated overnight in the presence or absence of recombinant human/ mouse FGF21 (5µg/ml). The next day cells were challenged with recombinant human GH (0.5µg/ml) for 72 or 96 hours before assessment of cell proliferation using Cell-counting kit-8. **(A)** HEK-293 hGHR **(i)** 76 hours **(ii)** 96 hours. **(B)** HEK-293 mGHR **(i)** 76 hours **(ii)** 96 hours. **(C)** C28/I2 **(i)** 76 hours **(ii)** 96 hours. **(D)** C3H10T1/2 **(i)** 76 hours **(ii)** 96 hours. The absorbance was measured at 490nm. All comparisons were normalised to control (untreated). Error bars represent ± SEM of three independent experiments (n=3), each with 3 biological replicates. *****p<0.05, ******p<0.01, *******p<0.001 was considered significant. One-way ANOVA, Dunnett's multiple comparison test.

4.4 Discussion.

The importance of the GH-IGF-1 axis is highlighted through its linear growth promoting impact, driven essentially via the expression of IGF-1 in hepatic and non-hepatic tissues. Circulating GH can act directly at the growth plate to induce chondrocyte expansion, activating the JAK/STAT signalling cascade to stimulate local IGF-1 synthesis and regulate longitudinal growth (David et al., 2011; van der Eerden et al., 2003). Abnormalities of the GH-IGF-1 axis are one of the major determinants of growth retardation (Brito et al., 2012). A functional imparity in the GH-IGF-1 axis is well reported to be associated with the development of GH resistance; typically characterised by excessively high serum GH levels and low IGF-1 (Rosenbloom, 2000; Woods, 2007). Experimental and clinical evidence demonstrates the impact of severe chronic conditions including; prolonged poor nutritional intake, IBD (e.g. Crohn's disease), renal failure etc., as a contributing factor to the secondary cause of childhood short stature and growth failure. However, the precise molecular mechanisms for GH resistance remain unclear (Brito et al., 2012; Haymond et al., 2013). Several recent studies by Kubicky et al., 2012 and Guasti et al., 2014 have identified a novel role of chronic elevated circulating FGF21 levels, in the early progression of GH resistance and subsequent attenuation of skeletal growth and growth plate chondrogenesis in both mice and humans. This chapter unveils an in-depth exploration into the molecular mechanisms and interplay of FGF21 interaction on GHR signalling events from early targets to late downstream mediators of the cascade, highlighting its role in the development of GH resistance.

The generation of GH-responding HEK-293 cells expressing exogenous human and mouse GHR offered a strong platform to investigate the direct interaction of FGF21/GHR, revealing the *de novo* role of chronic FGF21 levels on GHR half-life and degradation. It is well known, that GHR abundance and cell surface availability is a key determinant of GH sensitivity and thus, receptor biogenesis, trafficking, degradation and stability is critical in understanding the actions of GH and GHR biology (Deng et al., 2007). The half-life and degradation rate of GHR protein overtime was shown in the HEK-293 stable lines, where its availability was seen to be abolished by 8 hours (**Figure 4.1**). The clearance of mature cell surface GHR in the absence of a

ligand is known to proceed by two mechanisms. 1) GHR is subjected to metalloprotease-mediated cleavage within the proximal extracellular domain causing the release of the extracellular domain of GHR; GHBP. Consequently this cleavage lessens the abundance of GHR, reducing its sensitivity to GH stimulation. 2) Alternatively, surface GHR can undergo ligand-independent down-regulation via a process that is inhibited by the disruption of proteasomal and lysosmal function (Deng et al., 2007; van den Eijnden et al., 2006; Wang et al., 2002).

In the presence of GH, a rapid shift in mature GHR half-life was observed, reducing the rate taken for GHR degradation by 43% in HEK-293 hGHR and 59% in HEK-293 mGHR stable lines compared to the absence of GH treatment (**Figure 4.1 A-Biii**). The findings on increased GH-induced mature GHR degradation coincide with past experimental studies by Deng et al., 2007. The path for GHR degradation in the presence of a ligand is thought to proceed via clathrin-coated pit-mediated endocytosis and lysosomal degradation, which was first reported in rabbit liver (Deng et al., 2007; van den Eijnden et al., 2006; van Kerkhof et al., 2000; van Kerkhof et al., 2001). Strous et al., 1996 and others show that in the presence of GH, the two GHR polypeptides dimerise, which are subsequently phosphorylated by JAK2 and are then targeted for ubiquitination (Strous et al., 1996). It is shown that both endocytosis and transport to lysosomes require an active ubiquitin-conjugation system. The presence of a 10aa motif (ubiquitin-dependent endocytosis (UbE motif), DSWVEFIELD) in the cytoplasmic tail of GHR, downstream of the Box-1 element is essential for GHR ubiquitination, internalisation and degradation (Deng et al., 2007; Gent et al., 2002; Govers et al., 1999; van den Eijnden et al., 2006; van Kerkhof et al., 2000; van Kerkhof et al., 2001). A study by Kerkhof et al., 2001 showed that GHR is ubiquitinated at the plasma membrane, before the process of endocytosis occurs, indicating that the resident time of the GHR at the cell surface is regulated by the ubiquitin conjugation system together with the endocytic machinery**.**

Intriguingly, for the first time, it was identified that chronic FGF21 levels in the presence of GH further decreased mature GHR half-life, reducing the rate taken for GHR degradation by 42% in HEK-293 hGHR and 23% in HEK-293 mGHR stable lines compared to GH treatment alone (**Figure 4.1 A-Biii**). Thus, this confirms a direct action of FGF21 on cell surface GHR

availability and degradation; implicating the consequential negative effects on the abrogation of downstream GHR signalling. This might be due to a functional interaction between the transduction machinery initiated by FGF21 and that initiated by GH, although the molecular events linking the two remain unknown. Although these findings highlight the action of chronic FGF21 on GH-induced GHR half-life and degradation, there was no evidence to suggest an increase in the ubiquitination of cell surface GHR (**Figure 4.2**). This was surprising, considering the findings on chronic FGF21 GH-induced elevated expression of negative feedback regulator, SOCS2 shown in HEK-293 hGHR/mGHR stable lines, chondrocytic cells and human growth plate biopsies (**Figure 4.4**). It is reported that SOCS2 exerts its action through two main mechanisms; 1) GH-induced STAT5b is thought to bind to the SOCS2 promoter, in-turn inducing SOCS2 expression which binds to phosphorylated tyrosines on GHR to negatively regulate the activation of downstream GHR signalling (Greenhalgh et al., 2005; Vesterlund et al., 2011), 2) alternatively, SOCS2 has been shown to regulate cellular GHR levels via direct ubiquitination in a proteasomal dependent manner. The C-terminal of SOCS2 contains a SOCS box, which is seen to interact with Elongin B and C, highlighting its ubiquitin ligase activity (Bullock et al., 2006; Vesterlund et al., 2011). Hence, it was expected that chronic FGF21 may upregulate GH-induced GHR ubiquitination. This suggests that FGF21 GH-induced GHR degradation may proceed through alternative mechanisms other than ubiquitination, or that subtle albeit biologically relevant changes in ubiquitination are not detectable in western blot settings. An alternative mechanism of degradation to evaluate is 'shedding', especially due to the rapid clearance of GHR observed in the HEK-293 stable lines at 1 hour when treated with FGF21 and GH (**Figure 4.1**). It is known that the endocytic machinery can select proteins for endocytosis via clathrin-coated pits or proteolysis, which is seen to result in shedding of the extracellular domain of GHR. These internalised proteins found within the endosome are either recycled back to the plasma membrane or targeted to the lysosome for degradation (Strous and van Kerkhof, 2002). It is also reported that a significant proportion of proteins turnover is independent of ubiquitin conjugation, proceeding via alternative mechanisms. Some examples have been shown in the evaluation of thymidylate synthase (an enzyme required for the synthesis of DNA precursors), Rpn4 (transcriptional regulator of proteasome homeostasis) and ornithine decarboxylase (an enzyme

committed to polyamine biosynthesis). Further investigation is required to explore the possibility of FGF21 induced mechanisms of GHR degradation.

Thus, it is proposed that the elevated SOCS2 expression seen through the concomitant chronic FGF21 levels and GH is an additive effect seen on the rapid GHR half-life and degradation/ internalisation, and overall resulting in an inhibition in downstream GHR signalling, inducing a state of GH resistance. Furthermore, the GH resistant state promoted through FGF21 GH-induced down regulation of GHR signalling was as expected seen to further inhibit cell proliferation in Hek-293 hGHR/ mGHR stable lines and chondrocytic cells (**Figure 4.6**).

Importantly, these inhibitory events were seen in HEK-293 hGHR/ mGHR stable cell line model and chondrocytic cell lines (**Figure 4.3**). These findings complemented previous experimental studies whereby elevated FGF21 levels were seen to reduce concentrations of pSTAT5 in both an *in vivo* FGF21-transgenic mouse model (Inagaki et al., 2008) and primary cultures of chondrocytes (obtained from rib cartilage) (Guasti et al., 2014). A subsequent reduction in late downstream mediators of GHR signalling including IGF-1 expression, was also detected in the HEK-293 model and primary cultures of human growth plate biopsies (**Figure 4.5**). It is well established that IGF-1 plays an essential role in stimulating longitudinal growth during infancy, as demonstrated through various IGF-$1^{-/-}$ knockout mouse models (e.g. LID-ALSKO mice) which display considerable reduction in linear growth (Yakar et al., 2002). Thus, the inhibitory effect of chronic FGF21 levels on early (pSTAT5) and late (IGF-1) mediators of the GHR signalling cascade further emphasises the interplay of FGF21 in developing GH resistance through direct actions on cell surface GHR.

Conclusively, this chapter highlights for the first time an in-depth exploration of the novel mechanisms of chronic FGF21 induced GH-resistance. The direct actions of chronic FGF21 were seen to increase GH-induced GHR turnover and elevate SOCS2 expression to inhibit GHR signalling. Downregulation in the GHR signalling cascade were evident through a reduction in key pathway mediators; pSTAT5 and IGF-1. Thus, these findings confirm the negative effects of chronic FGF21 in the development of GH resistance and subsequent growth failure. This opens a new avenue towards the development of potential treatment modalities to overcome FGF21

induced GH resistance. One possibility could be localised treatment strategies to inhibit the upregulation of FGF21 levels, dampening the effect of GH resistance. Alternatively, IGF-1 treatment may also offer a novel therapeutic approach to increase growth in patients with growth failure associated with elevated FGF21 levels.

Data on human growth plate biopsies showed vast heterogeneity in the endogenous expression of *GHR* and FGF21 receptors (*β-KLOTHO, FGFR1* and *FGFR1-IIIC*) between primary cultures established from different patient biopsies (**Appendix**, **Figure 7.6**). This offers explanation towards the inconsistencies observed in *SOCS2* and *IGF-1* expression between time-points and cross patient comparatives (**Appendix**, **Figure 7.4** and **7.6**). Although, initially thought as an ideal model and true representative of the biological system to study the effects of FGF21 on GHR signalling, several drawbacks have been identified in using human growth plate biopsies. Despite random distribution of individual growth plate slices between culture dishes in the experimental set-up, it is difficult to ensure that the individual growth plate slices retain the same number of chondrocytes and equal or identical gene expression levels. Moreover, there is an uncertainty of possible alterations in gene expression levels during the process of establishing cultures. Individual human growth plate biopsies may react differently when placed in plastic culture dishes. Furthermore, although it is considered that the survival of human growth plate biopsies post-surgery can remain in culture for 72 hours, it is challenging to determine early shut-down of biological systems within biopsies. Moreover, inherent differences between patients could be highly problematic in data interpretation, especially when performing cross patient comparative analyses.

In addition, non-physiological concentrations of recombinant FGF21 and GH were used in order to investigate the role of FGF21 in GHR signalling. This may be criticised as a drawback in this study. Although the dosage of recombinant FGF21 and GH used were higher than seen physiologically, it is known that *in vitro* cellular model systems can respond differently to trigger biological responses. Thus, the concentration of recombinant treatment used in the experimental design were based on previous investigations, which were further optimised in the model using varying dosages in preliminary experiments. Furthermore, it is shown that biologically active

FGF21 exists as a dimer (~50kDa), while recombinant FGF21 is predominantly in the monomeric (~25kDa) form, which is thought to have a lower bioactivity (Guasti et al., 2014). Moreover it is reported that the extracellular matrix itself can create a 3D environment recruiting local growth factors and cytokines. The use of recombinant FGF21 *in vitro* lacks the ability to be concentrated near/ around its receptor complex in a 2-dimensional environment with low expression of extracellular matrix components. Hence, a considerably higher concentration of recombinant FGF21 is required to elicit a biological response in an *in vitro* system.

To support these *in vitro* findings, future investigations on loss-of function studies will help to further validate and understand the mechanistic framework of FGF21s' action on target cells of GHR signalling. This can be achieved using lenti-viral vector mediated RNA silencing technology of FGFR1 and β-Klotho and by depletion of FGF21 from serum by applying techniques such as the use of dye-ligands, protein precipitation, depletion columns and others. Furthermore, generating transgenic FGF21 expressing mice models can be used to investigate and verify the role of chronic FGF21 on the development of GH resistance. It is well known that chronic conditions such malnutrition plays a vital role in the development of GH resistance and childhood growth failure. Using an *in vitro* experimental set-up, cells can be treated with various macronutrients to assess its effect on the activity of GHR signalling and further determine FGF21 levels. This will reveal the role of specific macronutrients on elevated FGF21 GH-induced GH resistance. In addition, identifying potential drug targets for the localised inhibition of chronic FGF21 levels may be investigated using the *in vitro* Hek-293 hGHR/ mGHR stable cell models and/ or the use of a transgenic FGF21 mouse model. This would encompass the initial identification of potential targets and optimising the dosage conditions. Finding a suitable drug for localised reduction in chronic FGF21 levels has the potential to enhance therapeutic management of childhood GH resistance; improving their quality of life.

CHAPTER 5. Results

The role of circulating Fibroblast growth factor 21 concentrations in the regulation of growth in pre-term and very pre-term infants

5.1 Introduction.

5.1.1 Pre-term birth and poor growth outcomes.

An evaluation of growth during early childhood is considered essential in the routine paediatric clinical practice (Cole et al., 2014; Doyle, 2015). In the UK the assessment of a child's length and weight gain are monitored against centile charts (set by UK World Health Organisation (WHO), 0-4 year's growth charts); providing a visual depiction of an individual's growth progress (Cole et al., 2014). Thus, too little or too much growth can indicate signs of current or past ill health conditions (Doyle, 2015). Pre-term birth, defined by the estimated gestational age as a proxy of maturity, is known as the leading cause of neonatal mortality worldwide (Euser et al., 2008; Villar et al., 2015). The WHO categorises pre-term birth into three main subgroups; pre-term (<37 weeks' gestation), very pre-term (VPT) (<32 weeks) and extremely pre-term (<28 weeks). Additionally, low birth-weight infants are grouped as those with a birth weight of ≤ 2,500g, which may be associated with premature birth and/or small for gestational age. The cut-off limits for weight describing more severe cases, include; very low birth weight (<1,500g) and extremely low birth weight (<1,000g) (Euser et al., 2008). It is well reported that surviving premature infants are more susceptible to physical and/or metabolic risks later in adult life i.e. poor linear growth/ weight gain, cardiovascular disease, metabolic syndrome and impaired neurodevelopment (Niklasson et al., 2003; Villar et al., 2015). Several studies highlight a clear association between the severity of pre-term birth and poor linear growth outcomes and/or weight gain during early infancy (Cole et al., 2014; Hollanders et al., 2017). A clinical investigation by Hollanders et al., 2017 showed that a subgroup of VPT infants with very low birth weights or normal birth weight had stable or decreased SD score for length, weight and head circumference SD compared to a subgroup of infants with only very low birth weights. Thus, the typical growth pattern of VPT infants is characterised by an initial postnatal growth loss, followed by an early neonatal peak in growth velocity. Most pre-term infants (~80%) show catch-up growth (defined as reaching an SD score of >-2.0 SDS of the reference population) in weight, length and head circumference following an initial postnatal growth failure, often achieved by 2 years of life.

However, for some cases of VPT infants catch-up growth is not completed causing a long-term growth deficit, which is associated with co-morbidities (Euser et al., 2008).

5.1.2 The importance of nutrition in growth during early infancy.

Nutrition is the key source for good health and development during the early years of life, playing a fundamental role in linear growth (Prentice et al., 2006). Human breast milk contains all the nutritional nourishments that an infant requires in the initial first 6 months of life, including; fat, carbohydrates, proteins, vitamins, minerals and water (Bartolo, 2014). An inefficient supply of macronutrients including; protein, fat and carbohydrates and micronutrients including; vitamin A, iodine, iron and zinc can have detrimental long-term side-effects on growth and metabolism (Prentice et al., 2006). This has been demonstrated in several clinical investigations, whereby malnutrition during the first 2 years of life caused significant stunting and a consequential reduction in linear growth later in childhood and adolescence. A correction in nutritional deficiencies at an earlier stage in life (within <2 years from birth) are seen to redeem such discrepancies, however at a later stage can pose to be more difficult to recover (WHO, 2009). In addition, it is well reported that extrauterine growth restriction is common in VPT infants (Su, 2014). Studies reveal that low birth weight and/or small for gestational age are risk factors for both linear growth stunting and undernutrition among infancy (Blake et al., 2016). An inadequate availability of postnatal nutrition is a vital contributing factor towards growth failure, as most VPT infants experience major protein and energy intake deficits during neonatal intensive care/ hospitalisation. Early aggressive nutrition, e.g. parenteral and enteral feeding is considered effective in improving growth where catch-up is observed. However, a continued provision of nutritional intake is vital throughout growth monitoring and hospitalisation (Su, 2014).

5.1.3 Undernutrition induced elevated FGF21 and growth failure.

An exploration of the novel role of FGF21 in growth failure and nutrition has elicited a large interest over the past recent years. As described in Chapter 1, section 1.5, FGF21 is one of

several members of the FGF19 subfamily including; FGF19/21 and 23. FGF21 lacks the FGF heparin-binding domain, thus allowing its release from the site of synthesis and function as an endocrine mediator (Kilkenny and Rocheleau, 2016; Wu et al., 2012). The preferential binding of FGF21 to isoform FGFR1-IIIC and β-Klotho stimulates its actions in the regulation of multiple metabolic pathways (Ding et al., 2012; Ornitz and Itoh, 2015). The role of FGF21 has predominantly been described in glucose homeostasis and lipid metabolism. A combination of mediators PPARα and PPARγ induce the expression of FGF21 to regulate and adjust to alterations in nutritional status. It is well known that during a fasting state, increased hepatic FGF21 secretion is seen to induce gluconeogenesis, fatty acid oxidation and ketogenesis, hence FGF21 is considered as an essential regulator to metabolic adaptations to fasting (Cuevas-Ramos et al., 2012; Iglesias et al., 2012; Kim and Lee, 2015).

Macronutrients (carbohydrates, fatty acids, and proteins), micronutrients (minerals and vitamins) and some bioactive dietary compounds play an essential role in controlling gene expression and thus metabolic homeostasis (Erickson and Moreau, 2016; Perez-Marti et al., 2016). Several recent investigations reveal the interplay of macronutrient availability on the endogenous expression of hepatic and circulating FGF21 levels (Perez-Marti et al., 2016). A high carbohydrate diet including; glucose, fructose and sucrose are seen to induce FGF21 expression in both rodents and humans via the activation of transcription factor ChREBP which binds to ChoRE, present on the *FGF21* promoter. In addition it is suggested that a high fat diet including; fatty acids and retinoic acid, further upregulates PPARα to induce *FGF21* mRNA expression in both the liver and WAT (Erickson and Moreau, 2016; Perez-Marti et al., 2016). Inversely a low dietary protein intake, in particular methionine and leucine are shown to increase hepatic and circulating FGF21 levels (Erickson and Moreau, 2016; Perez-Marti et al., 2016; Solon-Biet et al., 2016). Low protein diets stimulate the upregulation of general control non-derepressible 2 (GCN2; a kinase sensor for amino acid supply) dependent phosphorylation of eIF2a. Ultimately this leads to an increase in the expression of protein ATF4. The GCN2/eIF2a/ATF4 cascade in turn induces the elevated expression of FGF21 (Perez-Marti et al., 2016). Thus, an imbalance in macronutrient availability including; high dietary carbohydrate and fat and low protein intake,

drives the increased chronic hepatic and circulatory FGF21 expression. However, the effect of macronutrient supply on FGF21 induced expression in pre-term infants is not well described and warrants further research.

Separate investigations highlighted a clear negative association of the novel role of elevated FGF21 levels in childhood growth failure. A clinical case study undertaken by Mericq et al., 2014 illustrated an inverse relationship between FGF21 levels and growth rates in infancy. Additionally, an investigation on VPT infants by Guasti et al., 2014 revealed a significant negative correlation between mean FGF21 levels during the first weeks of life and postnatal growth failure. Here described separately are the effects of chronic elevated FGF21 levels associated with macronutrient intake and growth failure. It is envisaged that an imbalance in macronutrient availability during early infancy, may induce the elevated expression of FGF21 which acts as an additive effect on the interplay of FGF21 in linear growth reduction and subsequent growth failure.

5.2 Aim and study design.

This chapter aims to clarify the association between macronutrient availability (protein, fat and carbohydrate) on FGF21 expression and growth failure in VPT infants. As part of a clinical investigation 64 VPT infants (41 males, 64.1%) were recruited during the first week of life from a Finnish population at the Kuopio University Hospital intensive care unit. Infants were monitored weekly for their weight, recumbent length (transformed into SD scores (SDSs), using the contemporary population-based reference) and nutritional intake in the form of energy supply of total (kcal/kg), fat (kcal/kg and %), protein (kcal/kg) and carbohydrate (kcal/kg) energy, as well as enteral energy (kcal/kg).

Initially, FGF21 (pg/ml) and IGF-1 (ng/ml) serum concentrations were measured at in-patient weeks 1, 3, 5, 7 and 9 and out-patient weeks 1 and 2 after birth using commercially purchased ELISA kits (FGF21: *BioVendor*, IGF-1: *Mediagnost GmbH*). Next using measured hormonal levels and a documented patient database including; gestational age, postmenstrual age, weight SDS, length SDS, nutritional intake etc., multi-comparison correlation and linear regression association analyses were performed to ultimately understand the link between macronutrient induced chronic FGF21 levels and its role in the development of GH resistance and growth failure in VPT infants.

Growth patterns in our cohort were firstly evaluated immediately after birth including; length and weight SDS. The next interest was to assess the association of hormonal levels (FGF21 and IGF-1) relating to the observed linear growth (length SDS) patterns in individual patients. Following, the link between macronutrient availability (total energy (kcal/kg), fat energy (kcal/kg and %), protein energy (kcal/kg), carbohydrate energy (kcal/kg) including; enteral energy (kcal/kg) feeding) and growth patterns was examined in our cohort. Lastly, analyses were undertaken to study the association between macronutrient energy availability in the form of total energy, fat, protein and carbohydrate on hormonal levels (FGF21 and IGF-1) and its association with linear growth (length SDS) outcomes. A full description of the clinical cohort and statistics used in the growth evaluation of VPT infants can be found in Chapter 2, section 2.3 and 2.19.

5.3 Results.

5.3.1 An evaluation of growth patterns in very pre-term infants.

It is well characterised that children born VPT/ with small gestational age (<32 weeks) and very low birth weight (<1,500g) are associated with poor growth outcomes, including persistent stunting and limited/ no catch-up growth (Hollanders et al., 2017; Knops et al., 2005). Our clinical cohort of 64 VPT infants (41 males, 64.1%) were examined for their initial growth patterns assessing length and weight SDS from birth to 115.86 (range: 36.85 – 184.57) postmenstrual (PM) age (weeks). The clinical characteristics of our cohort are reported in **Chapter 2**, **Table 2.2**. A relatively uniform growth pattern was observed, consisting of a poor linear growth rate immediately after birth, evident by a rapid decrease in the mean length SDS (i.e. growth deflection). This was followed by a period of catch-up growth, observed by an increase in the mean length SDS after nadir (lowest point of length/ weight SDS) (**Figure 5.1 Ai**). At nadir the average length SDS was -2.74 SDS, which was seen at an average of 34.27 PM age (weeks). Further assessment of the mean weight SDS was seen to share a similar trend in the growth pattern of VPT infants. A period of growth deflection/ poor weight gain (decrease in mean weight SDS) after birth was followed by an immediate catch-up in growth after the point of nadir, shown by an increase in the mean weight SDS (**Figure 5.1 Aii**). At nadir the average weight SDS was -2.60 SDS, which was seen at an average of 33.64 PM age (weeks). Individual patient assessment of growth patterns for length and weight SDS are described in **Appendix**, **Figure 7.7 A-B**. The magnitude of deflection (ΔSDS for length from birth to nadir) was significantly negatively correlated with total catch-up growth (ΔSDS for length from nadir to PM age 115.86 weeks) (r = -0.25, p=0.045) (**Figure 5.1 B**) and with catch-up growth to 1 year (r = -0.27, p=0.035) (**Appendix**, **Figure 7.7 C**). The short-term (weekly) decrease in length SDS was fastest right after birth, whilst the fastest short-term catch-up was observed right after nadir (r = 0.35, p<0.001) (**Figure 5.1 C**).

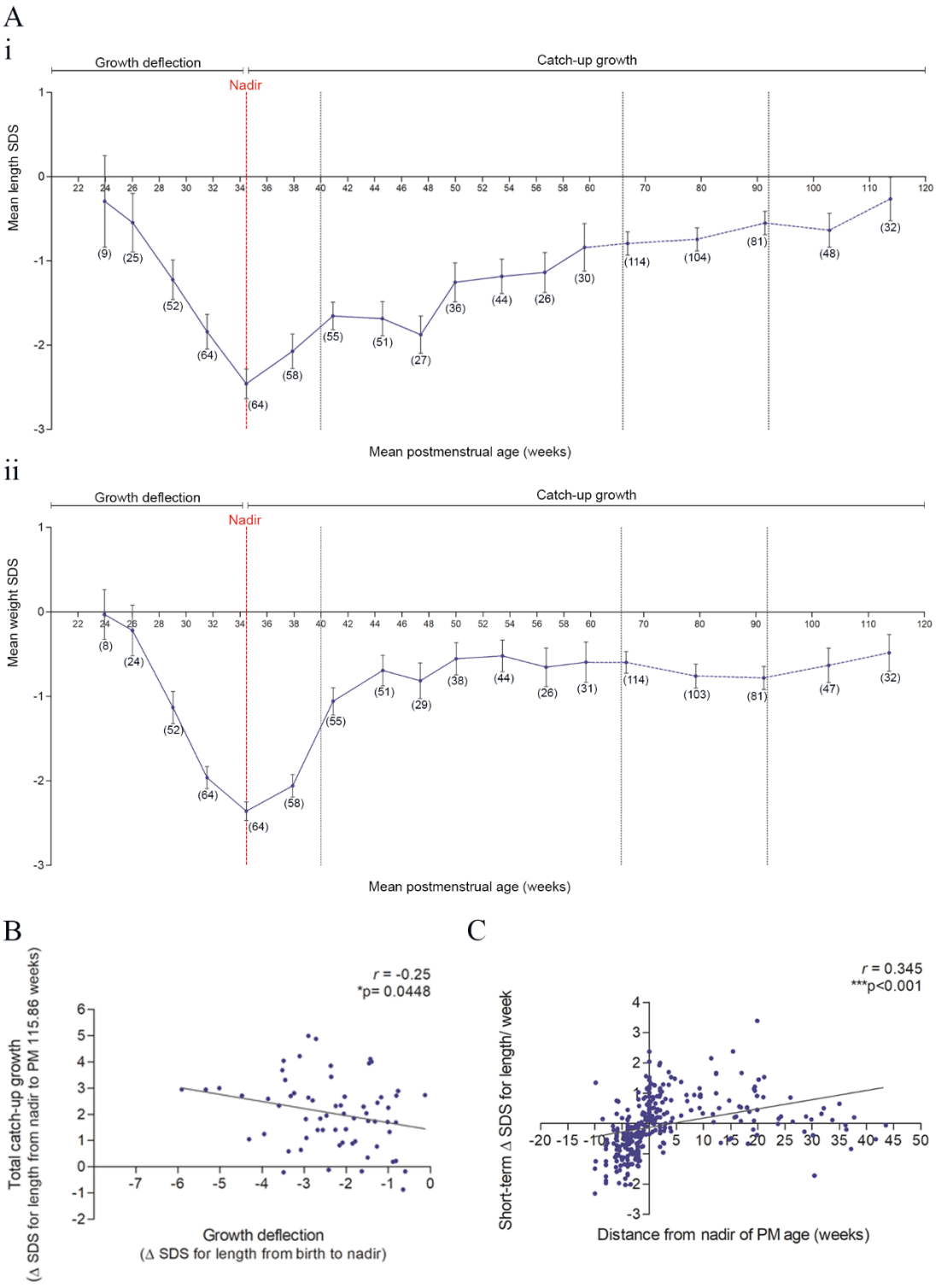

Figure 5.1 Very pre-term infants display a typical growth pattern of initial growth deflection followed by catch-up growth after nadir. (A) (i) mean length SDS **(ii)** mean weight SDS vs mean PM age 22 – 141.99 (weeks). Between (22 – 60.99) PM age the mean length/ weight SDS was assessed every 2.99 weeks. Between (61 – 141.99) PM age the mean length/ weight SDS was assessed every 11.99 weeks. Observations per a sub-group (PM age weeks) are recorded *n*=(x) on charts. (A table of the number of observations per sub-group of PM age (weeks) for length and weight SDS are described in **Appendix**, **Table 7.5**). Error bars represent the mean ± SEM. Nadir: lowest point of length/ weight SDS. **(B)** Magnitude of growth deflection (ΔSDS for length from birth to nadir) vs total catch-up growth (ΔSDS for length from nadir to PM 115.86 weeks). **(C)**

Assessment of short-term ΔSDS for length/ week vs distance from nadir of PM age (weeks). Pearson's R correlation (*r*) and *p* values were obtained from Bivariate correlation analyses.

5.3.2 Hormonal levels associated with growth patterns.

Several recent clinical studies demonstrate the negative effect of elevated FGF21 levels and a clear association with poor linear growth outcomes during infancy (Guasti et al., 2014; Mericq et al., 2014). Individual serum FGF21 and IGF-1 levels were evaluated in our cohort of VTP infants during in-patient weeks 1, 3, 5, 7 and 9 and out-patient weeks 1 and 2 after birth. Initially, the correlation was tested between individual patient serum FGF21 and IGF-1 levels with distance from nadir of PM age (weeks). A significant negative correlation was observed between FGF21 levels and distance from nadir of PM age (weeks) (r = -0.17, p=0.002) (**Figure 5.2 Ai**). Thus, FGF21 levels were significantly higher at a smaller PM age (weeks). Inversely, a significant positive correlation was observed between IGF-1 levels and distance from nadir of PM age (weeks) (r = 0.15, p=0.009), indicating that IGF-1 levels were lower at a smaller PM age (weeks) (**Figure 5.2 Bi**).

Next mean serum FGF21 and IGF-1 levels were evaluated separately during periods of growth deflection and catch-up growth in our VPT cohort. The mean values of hormonal levels evaluated during deflection and catch-up growth are reported in **Chapter 2**, **Table 2.3**. A paired *t*-test analysis revealed that FGF21 levels were significantly higher during growth deflection (Mean (M) = 483.35, Standard deviation (SD) = 581.32) compared to catch-up growth (M = 223.04, SD = 211.50) (t (56) = 3.74, p<0.001) (**Figure 5.2 Aii**). Inversely, paired *t*-test evaluation confirmed IGF-1 levels to be significantly lower during growth deflection (M = 5.63, SD = 5.46) compared to catch-up growth (M = 7.82, SD = 7.13) (t (42) = -2.07, p=0.044) (**Figure 5.2 Bii**).

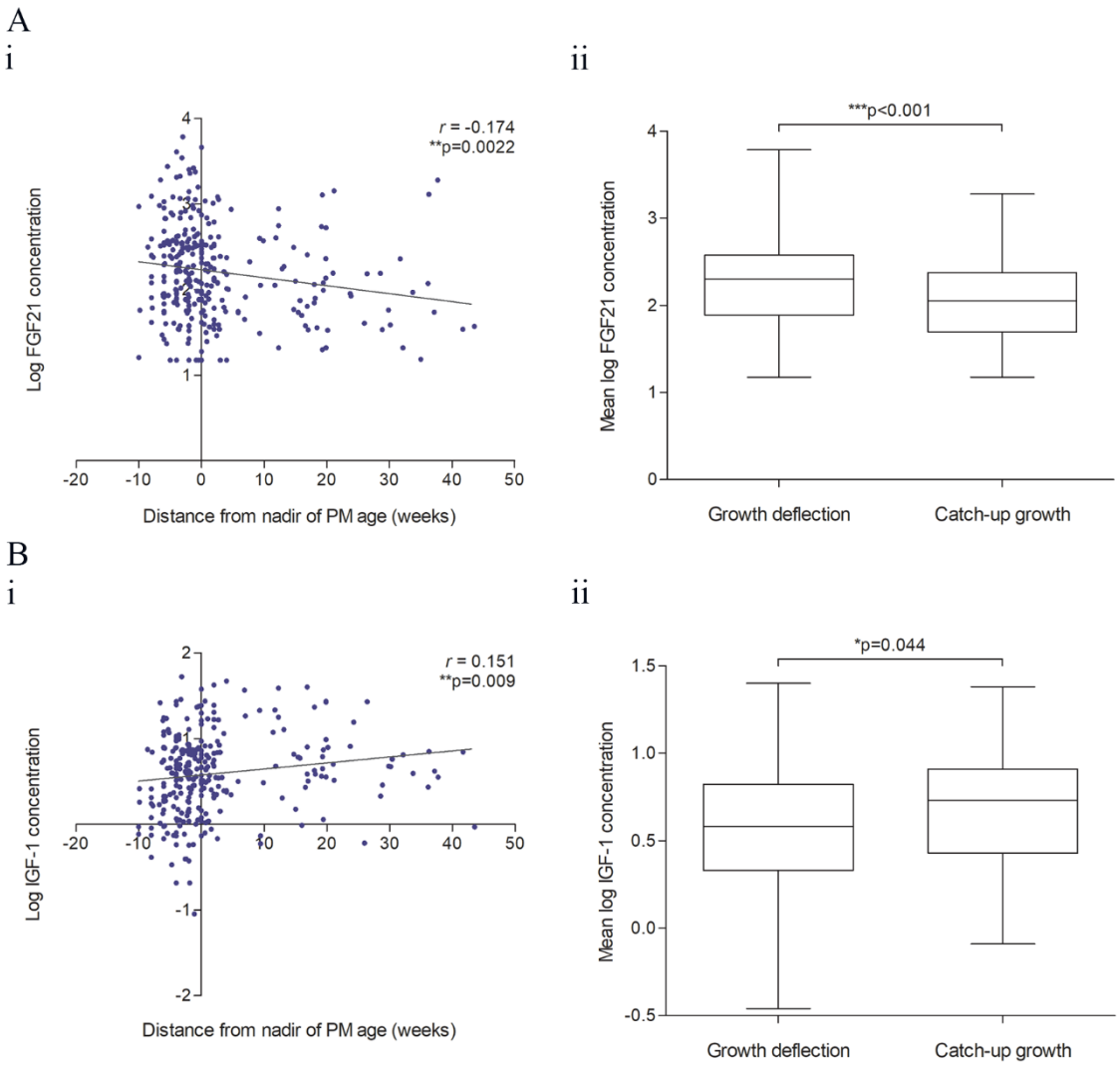

Figure 5.2 Growth deflection in very pre-term infants was associcated with evelated FGF21 and low IGF-1 levels. Correlation between individual log transformed **(Ai)** FGF21 and **(Bi)** IGF-1 concentration and distance from nadir of PM age (weeks). Pearson's R correlation (*r*) and *p* values were obtained from Bivariate correlation analyses. Assessment of **(i)** mean log FGF21 and **(ii)** IGF-1 concentrartion during deflection and catch-up growth phase. *p* values were obtained from Paried *t*-test analysis.

5.3.2.1 Linear regression model: The association between hormonal levels on the magnitude of growth deflection.

Linear regression models were used to determine the potential contributing effect of hormonal levels on the overall growth outcome when deflection and catch-up growth were evaluated seperately, while adjusting for other contributing clinical factors. Interestingly, a negative association was observed between mean IGF-1 levels during deflection and the magnitude of length deflection (standardised cofficients beta (β)= -0.17, *p*=0.038), but no

association with the magnitude for weight deflection (p=0.601). This suggests that higher IGF-1 levels during growth deflection are associated with a greater ΔSDS for length deflection (**Table 5.1**). Mean FGF21 during deflection was not signifcantly associated with the magnitude of length or weight growth deflection (p=0.339, p=0.526, respectively). Higher gestational age at birth was associated with a smaller magnitude in ΔSDS for length deflection (β= 0.62, p<0.001) and weight deflection (β= 0.30, p<0.001). A significant negative association was seen between birth length SD (β= -0.36, p<0.001) and birth weight SD (β= -0.71, p<0.001) with the magnitude of length and weight deflection. Thus, higher birth length/ weight SD was associated with a greater ΔSDS for length/ weight deflection.

Table 5.1 Linear regression analysis to test the association between mean hormonal levels during deflection on the magnitude of length/ weight growth deflection in 64 VPT infants. Additional covariates included in this model are gestational age at birth, birth length SD, birth weight SD and sex.

	Growth Deflection Δ SDS for length from birth to nadir		**Growth Deflection Δ SDS for weight from birth to nadir**	
	Standardised Coefficients Beta	*p* Value	Standardised Coefficients Beta	*p* Value
Gestational age at birth	0.62	**<0.001**	0.30	**<0.001**
Birth length, SD	-0.36	**<0.001**	-	-
Birth weight, SD	-	-	-0.71	**<0.001**
Sex	-0.07	0.386	-0.04	0.528
FGF21[a]	-0.78	0.339	0.04	0.526
IGF-1 [a]	-0.17	**0.038**	-0.04	0.601

[a] Mean log transformed FGF21 and IGF-1 levels during deflection. Growth deflection = (length/ weight SDS at nadir – length/ weight SDS at birth).

5.3.2.2 Linear regression model: The association between hormonal levels on the magnitude of catch-up growth.

Mean hormonal levels during catch-up growth were not associated with the magnitude of length or weight catch-up (FGF21: p=0.774, p=0.546, respectively) (IGF-1: p=0.395, p=0.266, respectively) (**Table 5.2**). Gestational age at birth was negatively associated with ΔSDS for length catch-up growth (β= -0.38, p=0.017). Hence, higher gestational age at birth was associated with

a smaller magnitude of length catch-up growth. Birth length SD, was negatively associated with ΔSDS for length catch-up growth (β= -0.48, *p*=0.008). This shows that a higher birth length SD was associated with a smaller magnitude in length catch-up. A further consideration of the effect of mean hormonal levels during growth deflection on the magnitude of catch-up growth showed no significant association with growth outcomes (all *p* values >0.05).

Table 5.2 Linear regression model evaluating the association between mean hormonal levels during catch-up growth on the magnitude of length/ weight catch-up growth in 64 VPT infants. Additional covariates included in this model are gestational age at birth, birth length SD, birth weight SD and sex.

	Growth Catch-up Δ SDS for length from nadir to total growth follow-up		**Growth Catch-up Δ SDS for weight from nadir to total growth follow-up**	
	Standardised Coefficients Beta	*p* Value	Standardised Coefficients Beta	*p* Value
Gestational age at birth	-0.38	**0.017**	0.32	0.071
Birth length, SD	-0.45	**0.008**	-	-
Birth weight, SD	-	-	-0.03	0.859
Sex	0.12	0.429	0.22	0.191
FGF21[b]	0.04	0.774	0.10	0.546
IGF-1[b]	0.13	0.395	0.19	0.266

[b] Mean log transformed FGF21 and IGF-1 levels during catch-up growth. Growth catch-up = (length/ weight SDS at total growth follow-up – length/ weight SDS at nadir).

5.3.3 Macronutrient availability and linear growth patterns.

The supply of nutrients during infancy and early childhood are essential for the long-term growth, health and development of a child. The availability of macronutrients including; protein, lipids and carbohydrates act as essential 'building blocks' for longitudinal growth, as demonstrated in several *in vivo* studies of the deleterious effects of protein restriction on linear growth. Thus, malnutrition in the early stages of childhood (the most influential cause of childhood growth failure) often leads to stunting of growth. When food is replenished back into a childs diet in order to recover a growth deficit, a period of spontaneous catch-up growth is

observed. However, in some cases catch-up growth is not completed and the child remains below their genetic height potential (Gat-Yablonski and Phillip, 2015).

The macronutrient availability, including; total energy, fat, protein and carbohydrate as well as enteral energy supply (weekly) was evaluated in our cohort of VPT infants during periods of deflection and catch-up growth. The mean values of nutritional energy intake evaluated during deflection and catch-up growth are reported in **Chapter 2**, **Table 2.3**. A significant positive correlation was observed between total energy (kcal/kg) supply and distance from nadir of PM age (r = 0.16, p=0.0002) (**Figure 5.3 Ai**). In addition, paired t-test analysis showed a significant lower mean total energy (kcal/kg) level during growth deflection (M = 110.82, SD = 19.25) compared to catch-up growth (M = 118.88, SD = 23.17) (t (53) = -2.31, p=0.025) (**Figure 5.3 Aii)**. Likewise, fat energy (kcal/kg) and fat energy (%) also showed a significant positive correlation with distance from nadir of PM age (r = 0.24, p<0.001; r = 0.33, p<0.001, respectively) (**Figure 5.3 B-Ci**). Mean fat (kcal/kg) energy was significantly lower during growth deflection (M = 51.99, SD = 14.05) than catch-up growth (M = 60.48, SD = 12.29) (t (53) = -4.18, p<0.001) (**Figure 5.3 Bii**). In addition mean fat (%) energy was also significantly lower during growth deflection (M = 44.88, SD = 7.10) compared to catch-up growth (M = 50.85, SD = 3.87) (t (53) = -7.22, p<0.001) (**Figure 5.3 Cii**). Similarly, enteral energy (kcal/kg) showed a significant positive correlation with distance from nadir of PM age (r = 0.24, p<0.001) (**Figure 5.3 Di**). A significantly lower mean enteral energy (kcal/kg) intake was observed during deflection (M = 96.65, SD = 31.70) than catch-up growth (M = 116.25, SD = 25.59) (t (53) = -4.36, p<0.001) (**Figure 5.3 Dii**). No difference were detected in protein and carbohydrate energy (kcal/kg) availability between distance from nadir of PM age and an evaluation of deflection and catch-up growth when assessed seperately (**Appendix**, **Figure 7.8**).

A

i

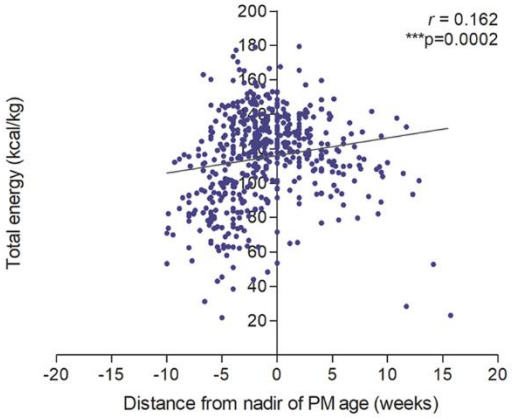

ii

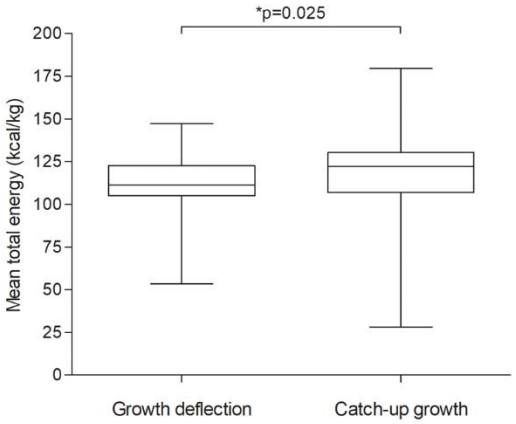

B

i

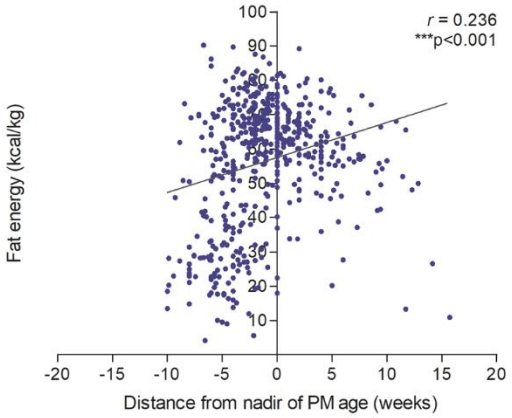

ii

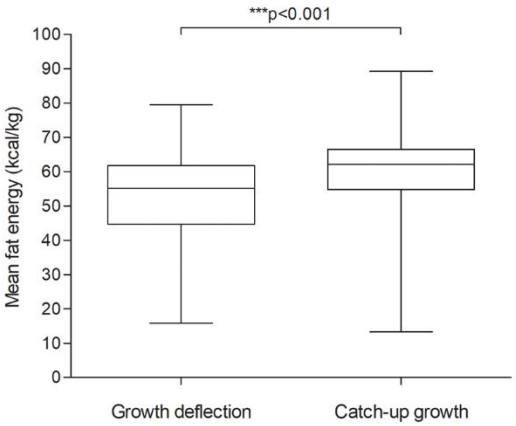

C

i

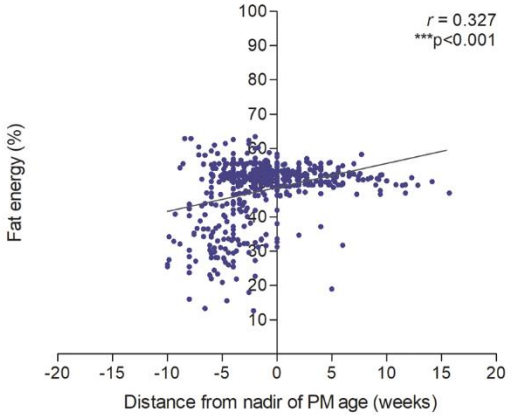

ii

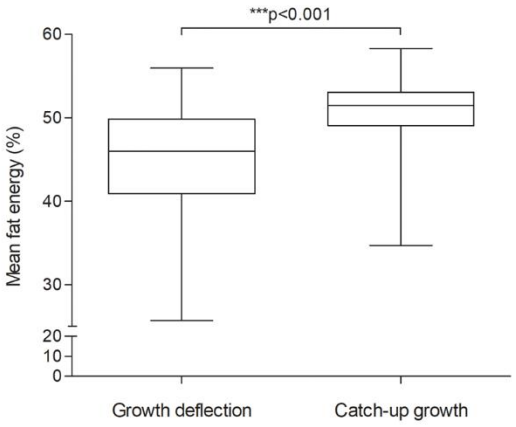

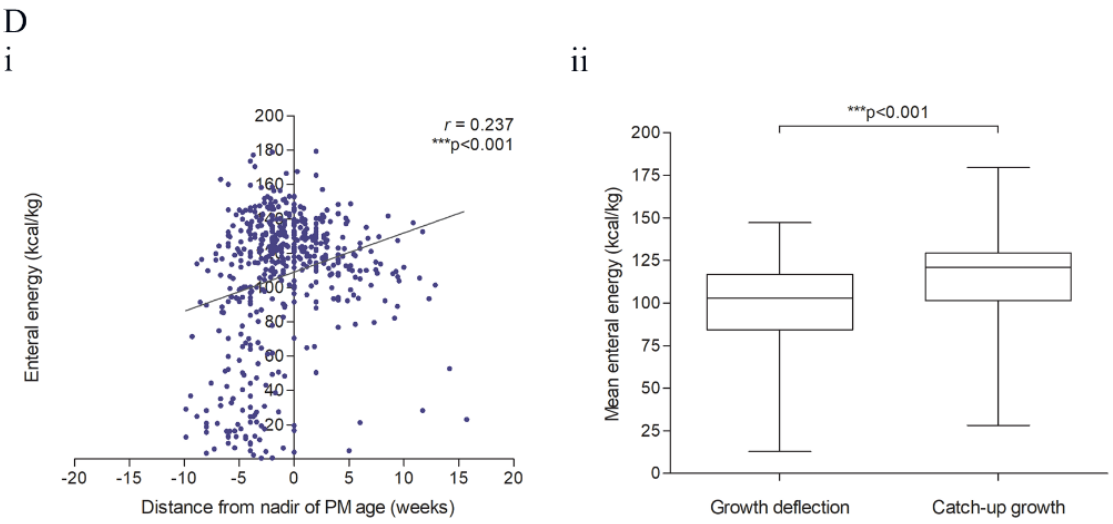

Figure 5.3 Total, fat and enteral energy was lower during growth deflection than catch-up. Assesment of macronutritent energy availability during growth deflection vs catch-up growth. **(Ai)** Total (kcal/kg), **(Bi)** Fat (kcal/kg), **(Ci)** Fat (%), **(Di)** Enteral (kcal/kg) energy vs distance from nadir of PM age (weeks). Pearson's R correlation (*r*) and p values were obtained from Bivariate correlation analyses. Mean **(Aii)** Total (kcal/kg), **(Bii)** Fat (kcal/kg), **(Cii)** Fat (%), **(Dii)** Enteral (kcal/kg) energy were evaluated seperately during deflection and catch-up growth. *p* values were obtained from Paried *t*-test analysis.

5.3.3.1 Linear regression model: The association between macronutrient energy intake on the magnitude of growth deflection.

Linear regression models were used to evaluate the potential contributing factors of macronutrient availability on growth failure during the deflection phase in our cohort, while adjusting for other contributing clinical factors (**Table 5.3**). There was a significant postive association between mean fat (%) intake during deflection and the magnitude of weight deflection (β= 0.60, *p*=0.024). Higher fat (%) availablity resulted in a smaller ΔSDS for weight deflection. No other nutritional factors were associated with growth failure during deflection. Other clinical covariates included in the regression model were associated with the magnitude of growth deflection. Gestational age at birth was postively associated with the magnitude of length and weight growth deflection (β= 0.589, *p*<0.001; β= 0.245, *p*=0.006, respectively). This indicates that higher gestestational age is associated with a smaller ΔSDS for length/ weight deflection. In addition a negative association was detected in birth length SD and birth weight SD and the

magnitude of growth deflection (β= -0.37, p<0.001; β= -0.76, p<0.001, respectively). Thus, a greater birth length/ weight SD resulted in a larger ΔSDS for length/ weight growth deflection.

Table 5.3 Assessment of mean macronutrient energy intake during growth deflection and the magnitude of length/ weight growth deflection in 64 VPT infants using linear regression analysis. Additional covariates included in this model are gestational age at birth, birth length SD, birth weight SD and sex.

	Growth Deflection Δ SDS for length from birth to nadir		**Growth Deflection Δ SDS for weight from birth to nadir**	
	Standardised Coefficients Beta	*p* Value	Standardised Coefficients Beta	*p* Value
Gestational age at birth	0.59	**<0.001**	0.26	**0.006**
Birth length, SD	-0.37	**<0.001**	-	-
Birth weight, SD	-	-	-0.76	**<0.001**
Sex	-0.05	0.514	-0.03	0.593
Total energy, kcal/kg [a]	0.13	0.967	3.38	0.146
Fat energy, kcal/kg [a]	-0.57	0.809	-3.07	0.079
Fat energy, % [a]	0.50	0.161	0.60	**0.024**
Protein energy, kcal/kg [a]	-0.003	0.992	-0.26	0.234
Carbohydrate energy, kcal/kg [a]	0.04	0.972	-1.15	0.175

[a] Mean of nutritional energy intake levels during growth deflection. Growth deflection = (length/ weight SDS at nadir – length/ weight SDS at birth).

5.3.3.2 Linear regression model: The association between macronutrient energy intake on the magnitude of catch-up growth.

Further evaluation was undertaken to assess the role of macronutrient availability during catch-up on the potential for catch-up growth. Assessment of mean macronutrient energy intake during catch-up growth was not associated with the magnitude of length or weight catch-up growth (**Table 5.4**). Birth length SD was negatively associated with the magnitude of length catch-up growth (β= -0.42, p=0.004). Thus a higher birth length SD resulted in a smaller magnitude for length catch-up growth.

Table 5.4 The role of mean macronutrient energy intake during catch-up growth and the magnitude of length/ weight catch-up growth in 64 VPT infants using linear regression analysis. Additional covariates included in this model are gestational age at birth, birth length SD, birth weight SD and sex.

	Growth Catch-up Δ SDS for length from nadir to total growth follow-up		**Growth Catch-up Δ SDS for weight from nadir to total growth follow-up**	
	Standardised Coefficients Beta	*p* Value	Standardised Coefficients Beta	*p* Value
Gestational age at birth	-0.29	0.070	0.19	0.311
Birth length, SD	-0.42	**0.004**	-	-
Birth weight, SD	-	-	-0.06	0.723
Sex	0.04	0.750	-0.03	0.873
Total energy, kcal/kg [b]	-6.63	0.176	-4.74	0.425
Fat energy, kcal/kg [b]	3.61	0.254	1.12	0.774
Fat energy, % [b]	1.00	0.907	1.26	0.197
Protein energy, kcal/kg [b]	0.74	0.240	1.17	0.116
Carbohydrate energy, kcal/kg [b]	2.86	0.153	2.96	0.204

[b] Mean of nutritional energy intake levels during catch-up growth. Growth catch-up = (length/ weight SDS at total growth follow-up – length/ weight SDS at nadir).

It was next questioned whether nutritional energy intake during growth deflection in VPT infants had an effect on the magnitude of catch-up growth (**Table 5.5**) . Interestingly, a negative association was observed between mean total energy intake during deflection and ΔSDS for length catch-up (β= -11.30, *p*=0.005). Therefore an increase in total energy availability during deflection caused a smaller magnitude of length catch-up growth. Whilst, mean fat and carbohydrate energy intake during deflection was positively associated with ΔSDS for length catch-up (β= 9.13, *p*=0.002; β= 4.14, *p*=0.005, respectively). This suggest that higher fat and carbohydrate supply in the deflection phase resulted in a greater magnitude of length growth catch-up. Gestational age at birth and birth length SD during deflection was negatively associated with ΔSDS for length catch-up (β= -0.466, *p*=0.001; β= -0.472, *p*<0.001, respectively, but not for weight catch-up growth. Thus, a higher gestational age at birth and birth length SD caused a smaller growth catch-up in VPT infants.

Table 5.5 Linear regression analysis to assess if mean macronutrient energy intake during deflection effects the magnitude of length/ weight catch-up growth in 64 VPT infants using linear regression analysis. Additional covariates included in this model are gestational age at birth, birth length SD, birth weight SD and sex.

	Growth Catch-up Δ SDS for length from nadir to total growth follow-up		**Growth Catch-up Δ SDS for weight from nadir to total growth follow-up**	
	Standardised Coefficients Beta	*p* Value	Standardised Coefficients Beta	*p* Value
Gestational age at birth	-0.47	**0.001**	0.09	0.611
Birth length, SD	-0.47	**<0.001**	-	-
Birth weight, SD	-	-	-0.09	0.499
Sex	0.15	0.156	0.11	0.406
Total energy, kcal/kg [a]	-11.30	**0.005**	-7.80	0.104
Fat energy, kcal/kg [a]	9.13	**0.002**	6.17	0.085
Fat energy, % [a]	-0.74	0.092	-0.42	0.428
Protein energy, kcal/kg [a]	0.53	0.145	0.41	0.350
Carbohydrate energy, kcal/kg [a]	4.14	**0.005**	3.11	0.076

[a] Mean of nutritional energy intake levels during growth deflection. Growth catch-up = (length/ weight SDS at total growth follow-up – length/ weight SDS at nadir).

5.3.4 Macronutrient availability and hormonal levels during deflection and catch-up growth.

Further assessment was performed to evaluate macronutrient availability and the associated effects on linear growth outcomes, potentially induced by hormonal levels. Initailly, the correlation between mean serum FGF21 and IGF-1 levels with mean macronutrient availability including; total energy, fat, protein, carbohydrate and enteral energy (kcal/kg) was evaluated seperately during periods of deflection and catch-up growth. A significant positive correlation was observed between mean fat (%) energy with the magnitude of linear growth deflection (ΔSDS for length from birth to nadir) (r = 0.31, p=0.031) (**Figure 5.4 Ai**). In addition, mean enteral energy (kcal/kg) was also seen to have a significant positive correlation with the magnitude of linear growth deflection (r = 0.21, p=0.025) (**Figure 5.4 Di**). Thus, higher fat (%) and enteral (kcal/kg) energy intake during deflection was associated with a smaller magnitude in length deflection. However, no significant differences were detected with mean fat (%) and

A

i

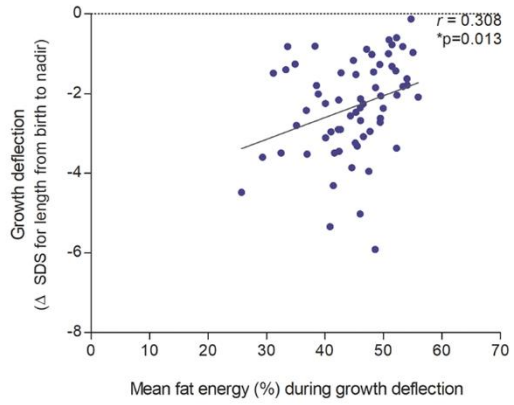

ii

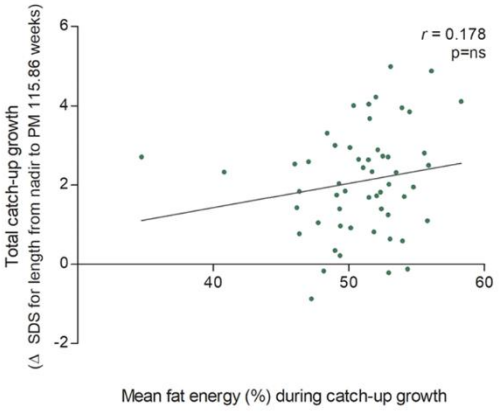

B

i

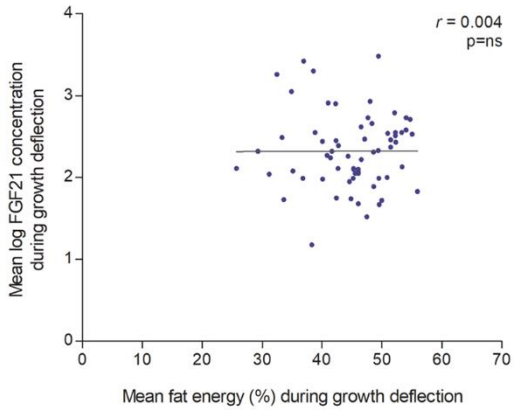

ii

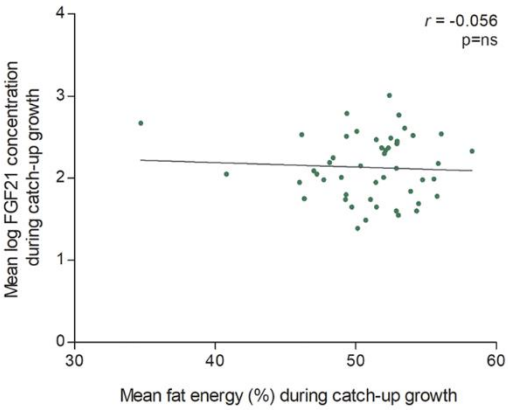

C

i

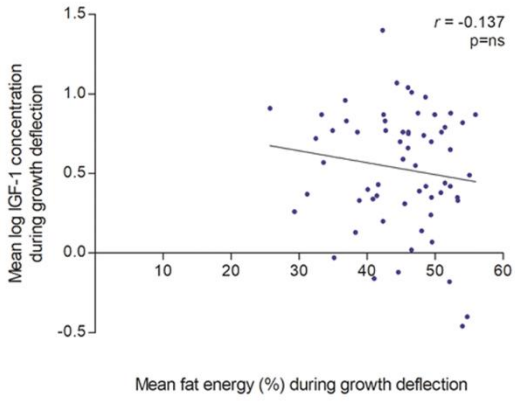

ii

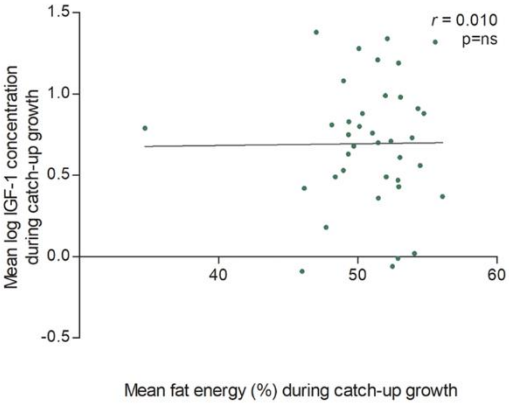

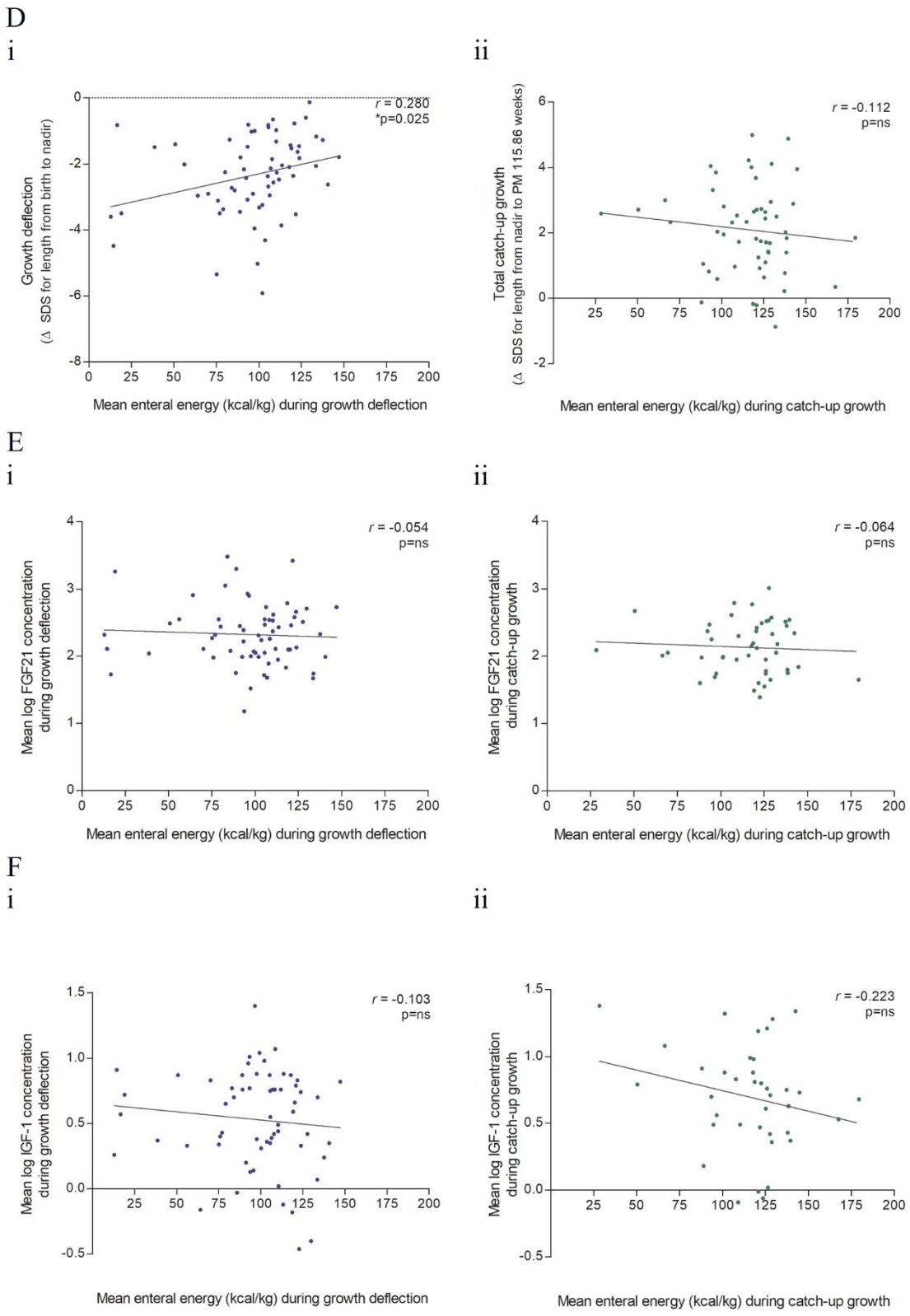

Figure 5.4 The magnitude of linear growth deflection is associated with the availability of fat and enteral energy supply. (A) Magnitude of **(i)** Growth deflection (Δ SDS for length from birth to nadir), **(ii)** Total catch-up (Δ SDS for length from nadir to PM 115.86 weeks) with mean fat energy (%) availability. **(B)** Mean log FGF21 concentration, **(C)** Mean log IGF-1 conentration vs mean fat energy (%) during **(i)** deflection and **(ii)** catch-up growth. **(D)** Magnitude of **(i)** Growth deflection (Δ SDS for length from birth to nadir), **(ii)** Total catch-up (Δ SDS for length from nadir to PM 115.86 weeks) with mean enteral energy (kcal/kg) availability. **(E)** Mean log FGF21 concentration, **(F)** Mean log IGF-1 conentration vs mean enteral energy (kcal/kg) during **(i)**

deflection and **(ii)** catch-up growth. Pearson's R correlation (*r*) and *p* values were obtained from Bivariate correlation analyses.

enteral (kcal/kg) energy availability and the magnitude of catch-up growth (ΔSDS for length from nadir to PM 115.86 weeks) (**Figure 5.4 A and Dii**), nor with mean FGF21 and IGF-1 concentration during the deflection and catch-up growth phase (**Figure 5.4 B-C** and **E-F**). This suggests that fat (%) and enteral (kcal/kg) energy availability is essential in linear growth outcomes during the initial growth phase immediately after birth in our cohort. Mean total energy (kcal/kg), fat energy (kcal/kg), protein energy (kcal/kg) and carbohydrate energy (kcal/kg) did not correlate with the magnitude of linear growth, as well as with mean hormonal levels when deflection and catch-up were assessed separately (**Appendix**, **Figure 7.9 A-L**).

5.3.4.1 Linear regression model: The association between hormonal levels and macronutrient energy intake on the magnitude of growth deflection.

Having separately evaluated hormonal levels and nutritional energy intake on the magnitude of length/ weight deflection and catch-up growth, the effect of both co-factors in combination was next assessed on the overall growth outcome using linear regression models to test if macronutrient availability regulated hormonal levels. Fat energy (%) during deflection was positively associated with the magnitude for weight deflection (β= 0.59, p=0.032). Thus higher fat energy (%) in deflection growth resulted in a smaller weight deflection (**Table 5.6**). All other mean macronutrient energy intake and hormonal levels during growth deflection had no association with the magnitude of length/ weight growth deflection when included in the same regression model. Gestational age at birth was positively associated with ΔSDS for length and weight catch-up growth (β= 0.59, p<0.001; β= 0.25, p=0.006, respectively). Birth length and weight SD was negatively associated with the magnitude of growth deflection (β= 0.386, p<0.001; β= -0.738, p<0.001, respectively). Thus, a higher gestational age resulted in a smaller magnitude of length/weight deflection, whereas a higher birth length and birth weight caused a greater magnitude of growth deflection.

Table 5.6 Assessment of mean macronutrient energy intake and hormonal levels during deflection on the magnitude of length/ weight growth deflection in 64 VPT infants using linear regression analysis. Additional covariates included in this model are gestational age at birth, birth length SD, birth weight SD and sex.

	Growth Deflection Δ SDS for length from birth to nadir		**Growth Deflection Δ SDS for weight from birth to nadir**	
	Standardised Coefficients Beta	*p* Value	Standardised Coefficients Beta	*p* Value
Gestational age at birth	0.59	**<0.001**	0.25	**0.006**
Birth length, SD	-0.39	**<0.001**	-	-
Birth weight, SD	-	-	-0.74	**<0.001**
Sex	-0.07	0.427	-0.04	0.562
Total energy, kcal/kg [a]	-0.85	0.786	3.75	0.123
Fat energy, kcal/kg [a]	0.24	0.918	-3.33	0.069
Fat energy, % [a]	0.41	0.249	0.59	**0.032**
Protein energy, kcal/kg [a]	0.05	0.866	-0.27	0.221
Carbohydrate energy, kcal/kg [a]	0.40	0.729	-1.32	0.141
FGF21[a]	-0.08	0.362	0.07	0.313
IGF-1 [a]	-0.15	0.074	0.01	0.862

[a] Mean nutritional energy inatke and log transformed FGF21 and IGF-1 levels during deflection. Growth deflection = (length/ weight SDS at nadir – length/ weight SDS at birth).

5.3.4.2 Linear regression model: The association between hormonal levels and macronutrient energy intake on the magnitude of catch-up growth.

Assessment of mean macronutrient energy and hormonal levels during catch-up growth were not associated with the magnitude of length/ weight catch-up growth (**Table 5.7**). Birth length SD, was negatively associated with ΔSDS for length catch-up growth (β= -0.52, *p*=0.011). Thus, a higher birth length SD, was associated with a smaller magnitude of length catch-up.

Mean macronutrient energy intake and hormonal levels during growth deflection were evaluated to test its impact on the magnitude of catch-up growth. The linear regression model showed that the mean macronutrient energy intake during deflection had a significant contribution on the magnitude of length catch-up growth (**Table 5.8**). Mean total energy during deflection was negatively associated with ΔSDS for length catch-up (β= -11.07, *p*=0.011), implicating that a higher total energy supply immediately after birth caused a smaller magnitude in catch-up growth after nadir. Mean fat (kcal/kg) and carbohydrate (kcal/kg) energy during deflection was postively

Table 5.7 Linear regression model to evaluate mean macronutrient energy intake and hormonal levels during catch-up growth on the magnitude of length/ weight catch-up growth in 64 VPT infants using linear regression analysis. Additional covariates included in this model are gestational age at birth, birth length SD, birth weight SD and sex.

	Growth Catch-up Δ SDS for length from nadir to total growth follow-up		**Growth Catch-up Δ SDS for weight from nadir to total growth follow-up**	
	Standardised Coefficients Beta	*p* Value	Standardised Coefficients Beta	*p* Value
Gestational age at birth	-0.33	0.120	0.38	0.115
Birth length, SD	-0.52	**0.011**	-	-
Birth weight, SD	-	-	-0.04	0.862
Sex	-0.08	0.704	0.07	0.739
Total energy, kcal/kg [b]	-12.07	0.144	-6.49	0.446
Fat energy, kcal/kg [b]	6.79	0.190	1.95	0.720
Fat energy, % [b]	-0.15	0.881	1.29	0.235
Protein energy, kcal/kg [b]	1.51	0.149	1.41	0.191
Carbohydrate energy, kcal/kg [b]	4.80	0.130	3.66	0.255
FGF21 [b]	0.07	0.697	0.21	0.283
IGF-1 [b]	0.18	0.328	0.15	0.430

b Mean nutritional energy inatke and log transformed FGF21 and IGF-1 levels during catch-up. Growth catch-up = (length/ weight SDS at total growth follow-up – length/ weight SDS at nadir).

associated with ΔSDS for length catch-up growth (β= 8.83, *p*=0.004; β= 4.11, *p*=0.006, respectively). This suggests that an increase in fat and carbohydrate intake during deflection resulted in a greater magnitude of catch-up growth. Macronutrient availability during deflection had no effect on the magnitude of weight catch-up growth. In addition, mean hormonal levels during deflection were also not associated with the magnitude for length/ weight catch-up growth. Gestational age at birth was negatively associated with length catch-up growth (β= -0.45, *p*=0.002), but not for weight catch-up growth. Birth length SD, was also negatively associated with ΔSDS for length catch-up growth (β= -0.52, *p*<0.001). Hence, a higher gestational age and birth length SD resulted in a smaller magnitude of length catch-up growth.

Table 5.8 Linear regression to test the effect of mean macronutrient energy intake and hormonal levels during growth deflection on the magnitude of length/ weight catch-up growth in 64 VPT infants using linear regression analysis. Additional covariates included in this model are gestational age at birth, birth length SD, birth weight SD and sex.

	Growth Catch-up Δ SDS for length from nadir to total growth follow-up		**Growth Catch-up Δ SDS for weight from nadir to total growth follow-up**	
	Standardised Coefficients Beta	*p* Value	Standardised Coefficients Beta	*p* Value
Gestational age at birth	-0.45	**0.002**	0.10	0.579
Birth length, SD	-0.52	**<0.001**	-	-
Birth weight, SD	-	-	-0.16	0.263
Sex	0.19	0.077	0.15	0.259
Total energy, kcal/kg [a]	-11.07	**0.007**	-7.70	0.117
Fat energy, kcal/kg [a]	8.83	**0.004**	6.01	0.102
Fat energy, % [a]	-0.63	0.160	-0.33	0.543
Protein energy, kcal/kg [a]	0.53	0.142	0.42	0.347
Carbohydrate energy, kcal/kg [a]	4.11	**0.006**	3.13	0.084
FGF21 [a]	-0.13	0.226	-0.17	0.197
IGF-1 [a]	0.12	0.273	0.08	0.560

[a] Mean nutritional energy inatke and log transformed FGF21 and IGF-1 levels during deflection. Growth catch-up = (length/ weight SDS at total growth follow-up – length/ weight SDS at nadir).

5.4 Discussion.

Childhood growth evaluation is a fundamental process in routine clinical paediatric practice, offering an informative insight into the early detection of linear growth abnormalities (Cole et al., 2014; Doyle, 2015). It is well characterised that pre-term birth (<37 weeks' gestation) carries severe long-term health risks, including; poor growth, metabolic diseases, impaired neurodevelopment and others (Niklasson et al., 2003; Villar et al., 2015). Growth failure and undernutrition after birth, are notably considered as common risk factors observed in pre-term infants (Blake et al., 2016; Hiltunen et al., 2018). Thus, the availability of an adequate nutrient supply (fat, protein and carbohydrates) in pre-term infants are essential for catch-up growth and childhood development, having a fundamental impact on overall linear growth outcomes (Hiltunen et al., 2018).

Monitoring growth patterns (length and weight SDS) in our cohort of 64 VPT infants showed a uniform trend typically displaying an initial growth deficit immediately after birth which was followed by a period of catch-up growth after the point of nadir. The magnitude of growth deflection was reflected by the scale of catch-up growth (**Figure 5.1**). The observations seen in our cohort coincided with several studies highlighting similar growth trends in pre-term born infants. A review by Euser et al., 2008, described the period of early postnatal growth in VPT and/or very low for birth weight infants to be invariable, showing a substantial growth failure after birth. For most pre-term infants, a growth deficit is described to be followed by a catch-up growth phase which begins during early infancy and seizes by an age of ~2 to 3 years, however it has also been seen to continue until adolescence. The catch-up phase is generally incomplete, thus pre-term infants often remain shorter showing persistent stunting and are lighter than term-born infants (Euser et al., 2008; Knops et al., 2005). Thus, a thorough evaluation of growth trends in pre-term infants suggests a long-term relationship between intrauterine growth retardation and growth attainment in adolescence.

It is thought that the severity of growth failure observed in pre-term infants after birth is partially induced by an imbalance in hormonal mediators. This imbalance or imparity in hormones associated with linear growth including; GH and IGF-1 have a fundamental impact on the overall

growth outcomes of infants, especially in the cases of GH resistance (Guasti et al., 2014). However, the precise molecular mechanism in which underlying chronic conditions causing GH resistance has yet to be elucidated.

This chapter explores a potential novel role of chronic FGF21 associated with growth attenuation and poor linear growth outcomes in our cohort of VPT infants. Elevated FGF21 and low IGF-1 levels were found to correlate with the prematurity of birth in VPT infants (i.e. infants of a smaller PM age in weeks, had higher FGF21 and reduced IGF-1 levels) (**Figure 5.2 A-Bi**). High FGF21 and low IGF-1 levels were also seen during the period of growth deflection. Inversely, low FGF21 and high IGF-1 levels were detected during growth catch-up (**Figure 5.2 A-Bii**). Thus, these findings clearly highlight a strong relationship between elevated FGF21 levels (seen during the growth deficit immediately after birth) and the severity of underlying chronic conditions associated with pre-term infants which may potentiate poor growth outcomes. This evidence is supported by recent clinical investigations undertaken by Guasti., et al 2014. This study identified elevated FGF21 serum levels during the first weeks of life in VPT infants to be independently associated with postnatal growth failure (Guasti et al., 2014). Surprisingly, despite a significant correlation between elevated FGF21 levels seen during growth deflection compared to catch-up growth (**Figure 5.2 Aii**), no significant association was observed in the linear regression model between FGF21 levels and the magnitude of length/ weight growth deflection (**Table 5.1**) or catch-up growth (**Table 5.2**), suggesting the potential interplay of other co-founding factors that may be more detrimental to the overall growth outcomes in our cohort. Unexpectedly, linear regression analyses reflected a significant negative association between IGF-1 levels and ΔSDS for length growth deflection (**Table 5.1**). Thus, higher IGF-1 levels during deflection was associated with a greater magnitude for length growth deflection. This finding was highly unpredicted, due to the numerous studies that confirm the importance of IGF-1 in fetal and postnatal growth and development. Several studies have shown that IGF-1 levels during the first postnatal weeks are positively related to early postnatal growth in pre-term infants. Thus, IGF-1 is key to aid in the prevention of postnatal growth restriction by instead promoting linear growth (de Jong et al., 2017). Our conflicting finding, hence requires further investigation to gain a better

understanding of the role of IGF-1 during the deflection growth phase in our VPT cohort. One suggestion may be that some individuals develop a partial IGF-1 resistant state or that IGF-1 levels reach saturation, hence having a restriction on linear growth outcomes.

Independently, the sufficient intake of macronutrients early on in pre-term infants has proven to be fundamental in linear growth outcomes, in addition to the importance of hormonal mediators associated with linear growth (GH/IGF-1 axis) (Hiltunen et al., 2018). In our cohort, the availability of total energy, fat and enteral energy levels were lower during deflection compared to catch-up growth (**Figure 5.3**), implicating that such factors could be important for length/ weight catch-up growth in VPT infants. It was further shown that higher fat energy levels during growth deflection influenced a smaller magnitude in ΔSDS for weight growth deflection (**Table 5.3**) Lipids are considered as an important energy source in normal diet, essential for normal growth and physical activity. Approximately, 45-55% of energy in the form of lipids are found in human milk, highlighting its importance in early development during infancy (Uauy et al., 2000).

Moreover, an overall higher total energy supply during deflection impacted a smaller magnitude of length catch-up growth (**Table 5.5**). Thus, it is speculated that a higher total energy intake after birth must help to correct the immediate growth failure seen in VPT infants, reducing the scale of catch-up growth required later in infancy. A clinical investigation on 78 extremely pre-term infants (<28 weeks' gestation) assessed the impact of nutritional management in the first 7 days of life on overall growth patterns until the corrected age of 2 years. This study showed that total energy intake during the first 7 days of life was significantly associated with weight, length and head circumference until the corrected age of 2 years (Hiltunen et al., 2018). This further reinforces the importance of an adequate nutritional supply immediately after birth on the long-term growth benefits in pre-term infants

Previous studies show the value of early nutritional intake on diminishing the cumulative nutritional deficit thereby preventing growth retardation (Christmann et al., 2018). It was revealed in the linear regression model that a higher fat and carbohydrate energy supply during growth

deflection caused a greater magnitude in length catch-up growth (**Table 5.5**). This therefore highlights the significance of energy intake in the form of fat and carbohydrate after birth, on the long-term linear growth benefits. A better understanding of the specific composition of carbohydrates, lipids, amino acids, vitamins and minerals supplied to pre-term infants immediately after birth would provide a clearer picture of those nutritional factors that are vital in promoting long-term catch-up growth in pre-term infants. Although there is a large awareness of the importance of a sufficient nutritional supply to support rates of long-term growth, it is thought that most pre-term infants do not tolerate feeding immediately therefore are seen to experience a significant deficit prior to achieving sufficient intake to support growth. Several strategies are suggested to help in the early pre-term growth deficit. These approaches include; a more aggressive early parenteral nutrition to aid in the reduction of the magnitude of early losses, a greater enteral intake of protein as well as the intake of other nutrients after enteral feeding and better attention to nutrition post discharge (Heird, 2001).

For the first time the effect of nutrition induced FGF21 levels associated with poor linear growth outcomes was explored in VPT infants. The linear regression model showed that high fat energy intake after birth resulted in a lower magnitude of weight deflection in VPT infants (**Table 5.6**). In addition, elevated total energy intake during deflection was associated with a smaller magnitude of length catch-up. This was unexpected considering our observation that higher fat and carbohydrate energy availability during deflection was associated with a greater magnitude in length catch-up (**Table 5.8**). Surprisingly, the linear regression model in which macronutrients and hormonal factors were assessed together, confirmed that FGF21 and IGF-1 levels were not associated with the magnitude of growth deflection or catch-up. Thus, in our cohort nutritional intake was found not to induce the expression of hormonal levels, but instead act independently with a direct effect on growth pattern outcomes. This suggests that an upregulation in FGF21 levels as seen during growth deflection maybe induced by other unknown underlying chronic conditions in VPT infants. The mechanistic actions that drive an upregulation in FGF21 in this setting requires further exploration to determine its association with GH resistance and growth failure.

Although there was no significant association between macronutrient induced hormonal levels in the linear regression models (**Table 5.6-5.8**), FGF21 concentration as previously mentioned was highly upregulated during growth deflection in VPT infants (**Figure 5.2 Aii**). In addition, a positive trend was observed between mean fat and carbohydrate energy intake and mean FGF21 levels during deflection, however this data was not significant (**Appendix**, **Figure 7.9 Di and Ji**). Several recent studies, have shown that an increase in carbohydrate diet increases hepatic FGF21 levels to promote lipogenesis, glucose uptake and metabolism and reduce fatty acid oxidation in the liver (Erickson and Moreau, 2016; Perez-Marti et al., 2016). Furthermore, a prolonged high fat diet has also been seen to upregulate FGF21 mRNA expression in both the liver and WAT (Perez-Marti et al., 2016). It is speculated that high fat and carbohydrate diet after birth may induce an upregulation in FGF21 levels seen during growth deflection. Thus, elevated FGF21 may cause a partial development in a GH resistant state, potentially contributing towards the immediate growth failure observed in VPT infants after birth. Additionally, it was shown that a high fat and carbohydrate intake during deflection resulted in a greater magnitude for length catch-up growth (**Table 5.8**). This further offers evidence to suggest that infants develop a GH resistant state during growth deflection caused by elevated FGF21 levels initially induced by high fat and carbohydrate energy, which is later corrected during catch-up growth. Moreover, this theory is supported by the detection of low FGF21 and high IGF-1 levels during catch-up growth (**Figure A-Bii**), indicating that elevated IGF-1 levels during catch-up stimulate linear growth.

The clinical evaluation of growth patterns in VPT infants has thus offered an insight into the potential actions of nutrition induced chronic FGF21 levels in the development of GH resistance and subsequent growth failure. Conclusively, it is proposed that higher fat and carbohydrate energy intake after birth may induce an upregulation in FGF21 levels, developing GH resistance and subsequent growth failure as seen during growth deflection, which is later corrected during the catch-up growth phase, evidently seen by a greater magnitude in length catch-up growth. However to gain a greater understanding of this potential proposed mechanism warrants further exploration.

A limitation to this study is the unavailability of the specific nutritional composition of amino acids, lipids and sugars as well as other potential factors (i.e. vitamins and minerals, inflammatory status) that may contribute to growth failure in VPT infants. This in-depth nutritional information and breakdown in macronutrient composition would allow for a greater understanding and identification of specific nutritional factors that may potentially induce an upregulation in FGF21 levels and confirm its role in GH resistance and growth failure. In addition, it is important to further evaluate any other underlying conditions and/ or co-morbidities in our cohort, i.e. liver dysfunction, elevated inflammatory cytokines, abnormalities in circulating proteins, irregular physiological signals etc. which may potentially influence the level of circulating IGF-1 and FGF21, having a greater detrimental effect on overall growth outcomes. Thus widening our evaluation of potential co-factors and chronic conditions in our cohort after birth is essential to provide a thorough assessment of individual patient status and its effect on hormonal levels. Lastly, it is also important to consider the role of IGF-2 in this setting. As previously described, IGF-2 is well known to play a pivotal role in early foetal life and growth (Kadakia and Josefson, 2016). Evaluating the expression of IGF-2 levels would provide a greater understanding of its bearing effect on FGF21 expression and linear growth outcomes.

Recruitment of VPT infants to form an increased cohort size may help to further identify any underlying factors, contributing towards poor growth outcomes by assessing a larger population. This also allows for a greater evaluation of a wider range of growth-regulating factors and more specific markers of GH and IGF-1 sensitivity. It is well known that elevated circulating FGF21 expression in patients are associated with numerous underlying chronic conditions i.e. prolonged undernutrition, T2D, impaired glucose tolerance etc. (Cuevas-Ramos et al., 2012). Thus, evaluating inflammatory markers, including; Tumor necrosis factor α (TNF-α), Interleukin 6 (IL-6), IL-1 and others, immediately after birth and at regular intervals throughout growth and development of VPT infants would further aid to provide a more clearer outlook, confirming the association between underlying chronic conditions and elevated FGF21 expression linked to growth failure.

CHAPTER 6. Discussion

FGF21, a member of the FGF19 subfamily of FGFs is well known for its ability to diffuse away from its tissue of synthesis and function as an endocrine factor. The importance of FGF21 has been highlighted in numerous studies where it was found to act as a key regulator in the metabolic adaptations to fasting, inducing, gluconeogenesis, fatty acid oxidation and ketogenesis (Guasti et al., 2014; Kubicky et al., 2012; Wu et al., 2012). However, chronic FGF21 levels have been widely associated with numerous undesirable outcomes in the cases of severe pathological conditions including; prolonged undernutrition, physical/ environmental stress, fatty liver disease, T2D and others (Cuevas-Ramos et al., 2012; Erickson and Moreau, 2016; Kim and Lee, 2015). A novel role of chronic FGF21 in the development of GH resistance has elicited a large interest over recent years. Several clinical studies demonstrate a clear association between elevated FGF21 levels and growth failure in infancy, induced by underlying chronic conditions i.e. undernutrition, premature born (Guasti et al., 2014; Mericq et al., 2014). However, the precise molecular mechanistic actions of FGF21 in the development of GH insensitivity and subsequent growth attenuation remains largely unknown.

This PhD thesis explores the molecular mechanistic interplay of chronic FGF21 levels on GHR signalling and key downstream mediators of the JAK/STAT cascade as a possible cause of GH resistance. Generating the appropriate tools via the establishment of stably transfected GHR expressing cell line models; HEK-293 hGHR and HEK-293 mGHR, has created a successful platform to trace GHR signalling and downstream mediators (**Figure 3.1**). An evaluation of the suitability of the stably transfected GHR expressing cells for its use in this investigation was confirmed through the exogenous expression of human and mouse GHR at the mRNA and protein level (**Figure 3.2**). In addition, further validation of the HEK-293 hGHR/ mGHR stable line models and chondrocytic cell lines highlighted the expression of essential signalling mediators associated with linear growth (JAK2, STAT5 and negative feedback regulator SOCS2) (**Appendix**, **Figure 7.2**, **Figure 3.4**, **Figure 3.5**). A vital component in the selection of cell models for subsequent experimental studies was to verify its responsiveness to recombinant GH and FGF21 treatment. The findings in this study also showed that HEK-293 GHR stable lines and chondrocytic cells were responsive to GH treatment, as seen through the rapid expression of

pSTAT5 (**Figure 3.4**). Furthermore, the endogenous expression of FGF21 and the receptor complex repertoire; FGFR1, isoform FGFR1-IIIC and co-receptor β-Klotho was confirmed in stable lines and human growth plate tissue (**Figure 3.6**, **Figure 3.7**). Thus, a strong cell model system was constructed to evaluate the unknown molecular mechanistic actions of elevated FGF21 on GHR signalling and its potential in growth failure.

This thesis further summarises the novel mechanisms of chronic FGF21 induced GH resistance, by unravelling its direct interaction in GHR signalling from early to late events of the JAK2/STAT5 cascade. The *de novo* role of chronic FGF21 was seen to increase GH-induced GHR turnover in HEK-293 GHR stably transfected cells (**Figure 4.1**), potentially activated by a functional interaction between the transduction machinery independently initiated by FGF21 and GH. Consequently the direct action of FGF21 on GHR degradation led to the abrogation of GHR signalling events. This was shown through the rapid reduction in linear growth signalling components including, STAT5 phosphorylation and IGF-1 expression (**Figure 4.3**, **Figure 4.5**). Thus, the inhibitory effect of chronic FGF21 levels on early (pSTAT5) and late (IGF-1) downstream events of the GHR signalling cascade, reveals FGF21s' ability to develop GH resistance, highlighting its role in linear growth attenuation.

Furthermore, a second independent action of chronic FGF21 was confirmed on GH-induced SOCS2 upregulation (**Figure 4.4**). It is speculated that an increase in the negative feedback regulator SOCS2, acts as an additive effect on the role of FGF21 in GH-induced GHR degradation by further prohibiting the activation of GHR signalling to induce a state of GH resistance. It is well described that SOCS2 exerts its actions via two main mechanisms. 1) SOCS2 binding to phosphorylated tyrosines on GHR blocks the association of positive signalling regulators (JAK2 and STAT5b activation), 2) SOCS2 regulates cellular GHR levels by direct ubiquitination in a proteasomal dependent manner (Greenhalgh et al., 2005; Vesterlund et al., 2011). Interestingly, in the HEK-293 hGHR stable cell line model, FGF21 did not increase GH-induced ubiquitination of cell surface GHR (**Figure 4.2**), despite our observations of FGF21s' actions on increased GHR turnover/ degradation and SOCS2 expression. An inability to detect subtle albeit biologically relevant changes in ubiquitination in the western blot setting may explain

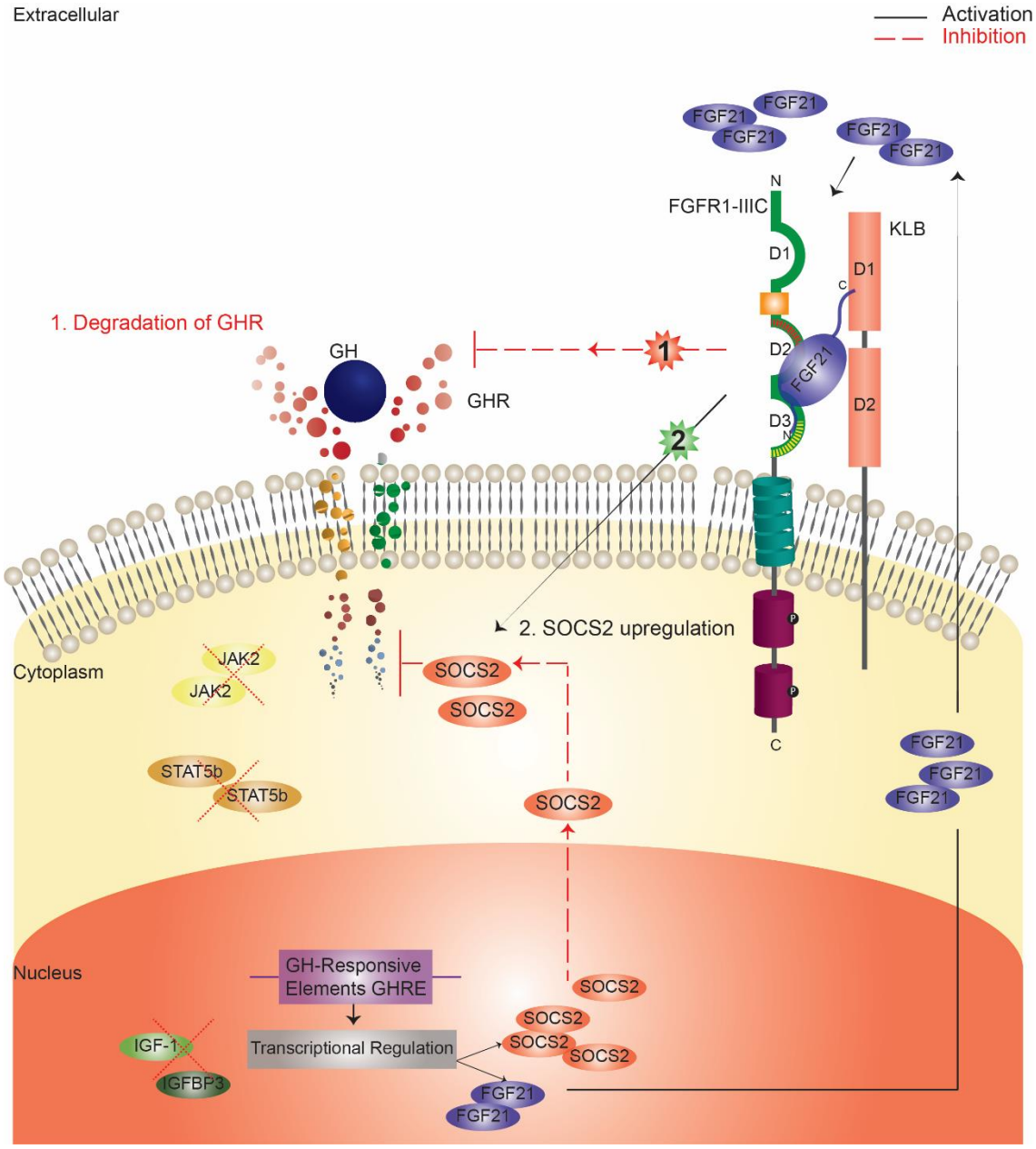

Figure 6.1 The mechanistic action of chronic FGF21 on GHR signalling in the development of GH resistance. Chronic FGF21 develops GH insensitivity via two mechanisms. 1) Chronic FGF21 increases GHR turnover/degradation leading to an inhibition of GH-induced downstream GHR signalling mediators; STAT5 phosphorylation and IGF-1 activity. 2) Chronic FGF21 increases the expression of GH-induced SOCS2 levels, further inhibiting the activation GHR and downstream signalling in the subsequent events of linear growth attenuation.

why FGF21 was not seen to induce GHR ubiquitination. Hence, further investigation is required to explore alternative mechanisms of GHR ubiquitination potentiated by chronic FGF21 e.g. via ubiquitin independent proteasomal degradation or shedding. Overall, a thorough evaluation of the mechanistic role of chronic FGF21 on GHR signalling has provided an insight into the direct actions of FGF21 in the development of GH resistance. These findings thus confirm two main

mechanisms of FGF21 in GH insensitivity and subsequent growth failure. 1) Chronic FGF21 increases GHR turnover, reducing the activation of GH-induced STAT5 phosphorylation and IGF-1 expression. 2) Chronic FGF21 upregulates GH-induced SOCS2 expression, suppressing GHR activation and downstream signalling events (**Figure 6.1**).

The combined clinical investigation on VPT infants has further broadened our understanding of the importance of postnatal nutrition in regulating circulatory FGF21 levels in the development of GH resistance and subsequent poor linear growth outcomes. It is well described that premature birth poses long-term health risks, particularly associated with growth failure which is further magnified by poor postnatal nutrition (Blake et al., 2016; Cole et al., 2014; Hiltunen et al., 2018; Hollanders et al., 2017; Niklasson et al., 2003; Villar et al., 2015). The molecular signals leading to GH insensitivity are however ill-defined. Thus, recruitment of VPT infants as part of a clinical evaluation has offered an applicable model to further investigate the unknown mechanisms associated with childhood growth failure. Our cohort of VPT infants showed a uniform growth trend that was demonstrated by an immediate growth deficit after birth, followed by catch-up growth after the point of nadir (**Figure 5.1**). This unique linear growth pattern in pre-term infants has been widely described across several clinical studies (Euser et al., 2008; Knops et al., 2005). Interestingly, an evaluation of deflection and catch-up growth independently, revealed an upregulation in FGF21 levels during the deflection phase as compared to catch-up growth (**Figure 5.2 Aii**), which was inversely correlated with IGF-1 levels (**Figure 5.2 Bii**, **Figure 6.2**). These findings offer evidence to suggest that elevated FGF21 levels as seen during a growth deficit may lead to growth failure in VPT infants via mechanisms of GH resistance defined in the *in vitro* observations. Surprisingly, an assessment of growth outcomes using linear regression models showed no association between FGF21 levels and the magnitude of length deflection or catch-up growth (**Table 5.1**,**Table 5.2**), confirming that other potential co-founding factors maybe more important in determining growth patterns in our cohort.

An evaluation of macronutrient and hormonal levels on growth outcomes highlighted the importance of total energy intake after birth which corrected the immediate growth failure seen in VPT infants, reducing the magnitude for catch-up growth required later in infancy. In addition,

high fat and carbohydrate energy intake after birth, caused a greater length catch-up growth in VPT infants (**Table 5.8**, **Figure 6.2**). However, in our cohort nutritional intake was found not to induce the expression of hormonal levels (**Table 5.6**, **Table 5.7**, **Table 5.8**). Thus, these findings confirm that the macronutrient availability in our cohort acts independently to rescue the immediate growth failure observed after birth.

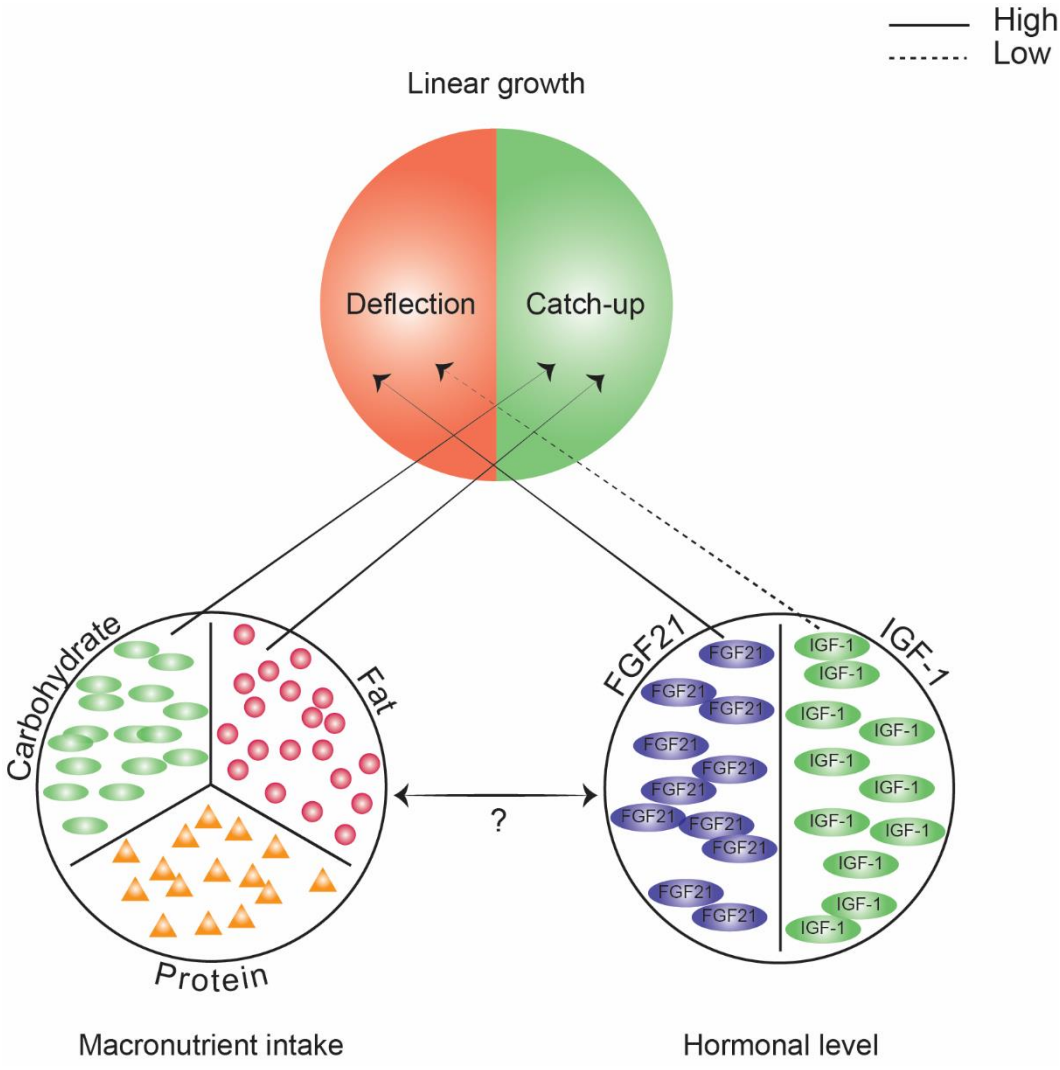

Figure 6.2 The role of hormonal levels and nutritional intake on linear growth patterns. VPT infants displayed a uniform growth trend; an initial growth deflection after birth and catch-up growth following nadir. High FGF21 and low IGF-1 levels were associated with growth deflection. High fat and carbohydrate energy intake after birth was associated with greater length catch-up growth in infants. Nutrition had a direct effect on linear growth outcomes without regulating hormonal levels.

Several studies offer data to suggest that high fat and carbohydrate consumption may induce elevated FGF21 levels (Erickson and Moreau, 2016; Perez-Marti et al., 2016). Here

described is a proposed novel potential mechanism of nutrition induced systemic FGF21 levels associated with poor linear growth outcomes. Despite no significant association between macronutrient induced hormonal levels, an elevated FGF21 level was found during deflection compared to catch-up growth (**Figure 5.2 Aii**). Furthermore, a positive correlation between mean FGF21 levels and fat or carbohydrate energy intake was observed during growth deflection (data not significant) (**Appendix**, **Figure 7.9 Di and Ji**). Hence, together with these findings it is postulated that an increase in fat and carbohydrate energy intake after birth in VPT infants, activates the upregulation of FGF21 expression to induce a partial GH resistant state during growth deflection, which is corrected later in infancy, demonstrated as seen by a greater catch-up growth (**Table 5.8**).

Conclusively, this PhD thesis unravels the *in vitro* molecular mechanistic actions of FGF21, highlighting its ability to develop GH resistance and subsequent growth failure. The clinical evaluation of growth trends in VPT infants further provides evidence to suggest that an imbalance in macronutrient availability, in particular fat and carbohydrate energy, may induce chronic FGF21 levels, consequently leading to GH insensitivity and stunted growth. Further investigation in humans is required to fully elucidate the effects of FGF21 on growth at the systemic level and in the growth plate, potentially induced by nutrition.

The successfulness of this PhD thesis originates from the *in vitro* establishment of the GHR expressing model systems which offered a strong foundation to evaluate in-depth the molecular mechanistic actions of chronic FGF21 on GHR signalling. Although creating a GHR over-expressing HEK-293 system may be criticised as non-representative of human physiological conditions, commercially available antibodies to detect endogenous GHR levels have been shown to be highly problematic. Thus, the taken approach to transfect HEK-293 cells to over-express GHR formed the essential tools to directly evaluate GHR biology. This platform alongside the use of chondrocytic cell lines further led to the successful capability to trace downstream GHR signalling events of the JAK/STAT cascade, validating the suitability for its use in this study. Ultimately this formed the strong foundation to perform key experimental studies in this thesis, unravelling for the first time the direct role of chronic FGF21 on GHR and downstream signalling

events in the development of GH resistance. The advantage of a combined clinical evaluation of IGF-1 and FGF21 levels and linear growth outcomes in VPT infants has further supported the *in vitro* findings in this thesis, strengthening our understanding of the interplay of chronic FGF21 on childhood growth outcomes.

In addition to the investigational success of this PhD, there has also been several drawbacks/ weaknesses to this study. A major obstacle was found in the use of human growth plate biopsies for *in vitro* experiments. Data obtained from these studies showed vast heterogeneity between various expression markers when comparing time-points and cross patient comparatives. Thus, selecting human growth plate tissue, originally thought to be an ideal representative model, was shown to pose several weaknesses including; difficulty in assuring the consistent number of chondrocytes in biopsy slices, alterations in gene expression levels when establishing cultures, adaptability to plastic cultures dishes, biopsy survival time *ex vivo* etc. Furthermore, it may be criticised that a higher concentration of recombinant FGF21 and GH were used in the experimental set-up than typically seen physiologically. Often this is widely accepted as it is well known that *in vitro* cellular model systems can respond differently to trigger biological responses. Moreover, studies have shown that biologically active FGF21 exists as a dimer (~50KDa), while recombinant FGF21 is found as a monomer (~25kDa) which is shown to have a lower bioactivity (Guasti et al., 2014). Lastly, the clinical evaluation in our VPT cohort posed some difficulty, particularly whilst evaluating nutritional levels, where our findings were inconclusive. A drawback with our clinical investigation, was the limitation to the data available of the VPT cohort. In this setting it is important to consider further evaluating other underlying co-factors/ co-morbidities (i.e. liver dysfunction, inflammatory markers) which may potentially affect hormonal levels.

Furthermore, the findings in this PhD thesis have opened new avenues for the consideration of future experimental designs and an opportunity to advance our knowledge in the field of GH resistance particularly with an association to underlying chronic conditions. With a rare opportunity to work with human growth plate tissue, an obvious choice would be to further optimise the experimental set-up, having already described the original drawbacks in using this

tissue type. A future experimental design would incorporate the establishment of a 3D growth plate biopsy culture, as well as the generation of a growth plate-like structure from embryonic stem cells or inducible pluripotent stem cells; both advances have still to be achieved. This would allow key experiments investigating the effect of chronic FGF21 on the direct expression of GHR and downstream events of the JAK/STAT cascade in a donor-specific manner. These models in addition to the established HEK-293 GHR system would offer stronger evidence to support the findings in this study.

In addition, to excel our knowledge in the field of GH resistance, greater emphasis will be placed on evaluating the root cause for elevated FGF21 expression. In this thesis the effect of chronic undernutrition on FGF21 circulatory levels was assessed as a clinical evaluation in VPT infants. To further enhance our understanding in this area using an *in vitro* experimental set-up would involve treatment of e.g. 3D human biopsy cultures with various macronutrients (protein, lipids, carbohydrates, minerals, vitamins etc.) to measure its effect on GHR activity and downstream events. Alternatively, a comparative *in vivo* chronic undernutrition animal model could also be considered. An *in vivo* model for chronic undernutrition would allow for an evaluation of macronutrient composition and circulatory FGF21 and IGF-1 levels, in addition to other suitable expression markers e.g. IGF-2, that may potentially affect growth outcomes. Furthermore, this would also open an opportunity to excise the metatarsal bone, to evaluate localised FGF21 levels within the growth plate, as well as the expression of GHR and downstream targets of the cascade.

The long-term considerations in advancing research in the field on GH resistance would incorporate an evaluation of potential drug targets to achieve localised reduction in chronic FGF21 levels. Initially, an *in vitro* cell system e.g. HEK-293 GHR, 3D human growth plate cultures would be used to first select drug targets and optimise dosage conditions. These experiments would have a large impact in enhancing paediatric therapeutic management in the cases of growth failure associated with GH resistance. Moreover, a continuation in stretching our knowledge in the field of GH resistance through key experimental investigations as discussed, may further offer a chance to consider FGF21 as a key biomarker measure in routine growth

evaluation for clinical paediatric endocrinology practice. This has the potential to act as an effective early biomarker diagnostic test to offer more tailored treatment strategies in children with debilitating chronic conditions. Thus, these novel approaches will aid to not only progress therapeutic management, but to also have a significant cost saving effect for failed GH treatment in the healthcare system. Ultimately, the advancement in clinical outcomes associated with GH resistance will improve the overall quality of life of infants in both the short and long-term.

References

Abad, V., J.L. Meyers, M. Weise, R.I. Gafni, K.M. Barnes, O. Nilsson, J.D. Bacher, and J. Baron. 2002. The role of the resting zone in growth plate chondrogenesis. *Endocrinology*. 143:1851-1857.

Abbassi, V. 1998. Growth and normal puberty. *Pediatrics*. 102:507-511.

Ahmed, S.F., and C. Farquharson. 2010. The effect of GH and IGF1 on linear growth and skeletal development and their modulation by SOCS proteins. *J Endocrinol*. 206:249-259.

Alves dos Santos, C.M., T. ten Broeke, and G.J. Strous. 2001. Growth hormone receptor ubiquitination, endocytosis, and degradation are independent of signal transduction via Janus kinase 2. *J Biol Chem*. 276:32635-32641.

Angelin, B., T.E. Larsson, and M. Rudling. 2012. Circulating fibroblast growth factors as metabolic regulators--a critical appraisal. *Cell Metab*. 16:693-705.

Armelin, H.A. 1973. Pituitary extracts and steroid hormones in the control of 3T3 cell growth. *Proc Natl Acad Sci U S A*. 70:2702-2706.

Arya, M., I.S. Shergill, M. Williamson, L. Gommersall, N. Arya, and H.R. Patel. 2005. Basic principles of real-time quantitative PCR. *Expert Rev Mol Diagn*. 5:209-219.

Aydin, S. 2015. A short history, principles, and types of ELISA, and our laboratory experience with peptide/protein analyses using ELISA. *Peptides*. 72:4-15.

Bae, K.H., J.G. Kim, and K.G. Park. 2014. Transcriptional regulation of fibroblast growth factor 21 expression. *Endocrinol Metab (Seoul)*. 29:105-111.

Bajpai, A., and P.S. Menon. 2006. Insulin like growth factors axis and growth disorders. *Indian J Pediatr*. 73:67-71.

Ballock, R.T., and R.J. O'Keefe. 2003. The biology of the growth plate. *J Bone Joint Surg Am*. 85-A:715-726.

Bang, P., R. Bjerknes, J. Dahlgren, L. Dunkel, J. Gustafsson, A. Juul, B. Kristrom, P. Tapanainen, and V. Aberg. 2011. A comparison of different definitions of growth response in short prepubertal children treated with growth hormone. *Horm Res Paediatr*. 75:335-345.

Barber, R.D., D.W. Harmer, R.A. Coleman, and B.J. Clark. 2005. GAPDH as a housekeeping gene: analysis of GAPDH mRNA expression in a panel of 72 human tissues. *Physiol Genomics*. 21:389-395.

Baron, R. 2000. Anatomy and Ultrastructure of Bone - Histogenesis, Growth and Remodeling. *In* Endotext. L.J. De Groot, P. Beck-Peccoz, G. Chrousos, K. Dungan, A. Grossman, J.M. Hershman, C. Koch, R. McLachlan, M. New, R. Rebar, F. Singer, A. Vinik, and M.O. Weickert, editors, South Dartmouth (MA).

Bartolo, M. 2014. Nutrition in childhood. *The Journal of the Malta College of Family Doctors*. 03.

Baxter, R.C. 1985. Measurement of growth hormone and prolactin receptor turnover in rat liver. *Endocrinology*. 117:650-655.

Beenken, A., and M. Mohammadi. 2009. The FGF family: biology, pathophysiology and therapy. *Nat Rev Drug Discov*. 8:235-253.

Beenken, A., and M. Mohammadi. 2012. The structural biology of the FGF19 subfamily. *Adv Exp Med Biol*. 728:1-24.

Belov, A.A., and M. Mohammadi. 2013. Molecular mechanisms of fibroblast growth factor signaling in physiology and pathology. *Cold Spring Harb Perspect Biol*. 5.

Bikle, D., S. Majumdar, A. Laib, L. Powell-Braxton, C. Rosen, W. Beamer, E. Nauman, C. Leary, and B. Halloran. 2001. The skeletal structure of insulin-like growth factor I-deficient mice. *J Bone Miner Res*. 16:2320-2329.

Blake, R.A., S. Park, P. Baltazar, E.B. Ayaso, D.B. Monterde, L.P. Acosta, R.M. Olveda, V. Tallo, and J.F. Friedman. 2016. LBW and SGA Impact Longitudinal Growth and Nutritional Status of Filipino Infants. *PLoS One*. 11:e0159461.

Breitling, J., and M. Aebi. 2013. N-linked protein glycosylation in the endoplasmic reticulum. *Cold Spring Harb Perspect Biol*. 5:a013359.

Brito, I., H. Gil-Pena, I. Molinos, V. Loredo, T. Henriques-Coelho, A. Caldas-Afonso, and F. Santos. 2012. Growth cartilage expression of growth hormone/insulin-like growth factor I axis in spontaneous and growth hormone induced catch-up growth. *Growth Horm IGF Res*. 22:129-133.

Brooks, A.J., J.W. Wooh, K.A. Tunny, and M.J. Waters. 2008. Growth hormone receptor; mechanism of action. *Int J Biochem Cell Biol*. 40:1984-1989.

Bullock, A.N., J.E. Debreczeni, A.M. Edwards, M. Sundstrom, and S. Knapp. 2006. Crystal structure of the SOCS2-elongin C-elongin B complex defines a prototypical SOCS box ubiquitin ligase. *Proc Natl Acad Sci U S A*. 103:7637-7642.

Carter-Su, C., J. Schwartz, and L.S. Argetsinger. 2016. Growth hormone signaling pathways. *Growth Horm IGF Res*. 28:11-15.

Chagin, A.S., and L. Savendahl. 2009. Genes of importance in the hormonal regulation of growth plate cartilage. *Horm Res*. 71 Suppl 2:41-47.

Cho, S.Y., and D.K. Jin. 2015. Guidelines for genetic skeletal dysplasias for pediatricians. *Ann Pediatr Endocrinol Metab*. 20:187-191.

Christmann, V., M.E. van der Putten, L. Rodwell, K. Steiner, M. Gotthardt, J.B. van Goudoever, and A.F.J. van Heijst. 2018. Effect of early nutritional intake on long-term growth and bone mineralization of former very low birth weight infants. *Bone*. 108:89-97.

Clarke, B. 2008. Normal bone anatomy and physiology. *Clin J Am Soc Nephrol*. 3 Suppl 3:S131-139.

Cole, T.J., Y. Statnikov, S. Santhakumaran, H. Pan, N. Modi, U. Neonatal Data Analysis, and G. the Preterm Growth Investigator. 2014. Birth weight and longitudinal growth in infants born below 32 weeks' gestation: a UK population study. *Arch Dis Child Fetal Neonatal Ed*. 99:F34-40.

Cuevas-Ramos, D., C.A. Aguilar-Salinas, and F.J. Gomez-Perez. 2012. Metabolic actions of fibroblast growth factor 21. *Curr Opin Pediatr*. 24:523-529.

David, A., V. Hwa, L.A. Metherell, I. Netchine, C. Camacho-Hubner, A.J. Clark, R.G. Rosenfeld, and M.O. Savage. 2011. Evidence for a continuum of genetic, phenotypic, and biochemical abnormalities in children with growth hormone insensitivity. *Endocr Rev*. 32:472-497.

de Jong, M., A. Cranendonk, J.W. Twisk, and M.M. van Weissenbruch. 2017. IGF-I and relation to growth in infancy and early childhood in very-low-birth-weight infants and term born infants. *PLoS One*. 12:e0171650.

Deng, L., K. He, X. Wang, N. Yang, C. Thangavel, J. Jiang, S.Y. Fuchs, and S.J. Frank. 2007. Determinants of growth hormone receptor down-regulation. *Mol Endocrinol*. 21:1537-1551.

Ding, X., J. Boney-Montoya, B.M. Owen, A.L. Bookout, K.C. Coate, D.J. Mangelsdorf, and S.A. Kliewer. 2012. betaKlotho is required for fibroblast growth factor 21 effects on growth and metabolism. *Cell Metab*. 16:387-393.

Doyle, D.A. 2012. Physical Growth of Infants and Children.

Doyle, L.W. 2015. Growth of preterm babies after birth. *Lancet Glob Health*. 3:e655-656.

Emons, J., A.S. Chagin, L. Savendahl, M. Karperien, and J.M. Wit. 2011. Mechanisms of growth plate maturation and epiphyseal fusion. *Horm Res Paediatr*. 75:383-391.

Erickson, A., and R. Moreau. 2016. The regulation of FGF21 gene expression by metabolic factors and nutrients. *Horm Mol Biol Clin Investig*.

Eswarakumar, V.P., I. Lax, and J. Schlessinger. 2005. Cellular signaling by fibroblast growth factor receptors. *Cytokine Growth Factor Rev*. 16:139-149.

Euser, A.M., C.C. de Wit, M.J. Finken, M. Rijken, and J.M. Wit. 2008. Growth of preterm born children. *Horm Res*. 70:319-328.

Fazeli, P.K., and A. Klibanski. 2014. Determinants of GH resistance in malnutrition. *J Endocrinol*. 220:R57-65.

Fernandez-Perez, L., B. Guerra, J.C. Diaz-Chico, and A. Flores-Morales. 2013. Estrogens regulate the hepatic effects of growth hormone, a hormonal interplay with multiple fates. *Front Endocrinol (Lausanne)*. 4:66.

Fisher, F.M., and E. Maratos-Flier. 2016. Understanding the Physiology of FGF21. *Annu Rev Physiol*. 78:223-241.

Fontenele, E.G., M.E. Moraes, C.B. d'Alva, D.P. Pinheiro, S.A. Landim, F.A. Barros, E.B. Trarbach, B.B. Mendonca, and A.A. Jorge. 2015. Association Study of GWAS-Derived

Loci with Height in Brazilian Children: Importance of MAP3K3, MMP24 and IGF1R Polymorphisms for Height Variation. *Horm Res Paediatr*. 84:248-253.

Frank, S.J. 2001. Growth hormone signalling and its regulation: preventing too much of a good thing. *Growth Horm IGF Res*. 11:201-212.

Frank, S.J., and S.Y. Fuchs. 2008. Modulation of growth hormone receptor abundance and function: roles for the ubiquitin-proteasome system. *Biochim Biophys Acta*. 1782:785-794.

Fukumoto, S. 2008. Actions and mode of actions of FGF19 subfamily members. *Endocr J*. 55:23-31.

Gasparetto, M., and G. Guariso. 2014. Crohn's disease and growth deficiency in children and adolescents. *World J Gastroenterol*. 20:13219-13233.

Gat-Yablonski, G., R. Pando, and M. Phillip. 2013. Nutritional catch-up growth. *World Rev Nutr Diet*. 106:83-89.

Gat-Yablonski, G., and M. Phillip. 2015. Nutritionally-induced catch-up growth. *Nutrients*. 7:517-551.

Ge, X., Y. Wang, S.K. Lam, and A. Xu. 2012. Metabolic actions of FGF21: molecular mechanisms and therapeutic implications. *Acta Pharmaceutica Sinica B*. 2:350-357.

Gent, J., P. van Kerkhof, M. Roza, G. Bu, and G.J. Strous. 2002. Ligand-independent growth hormone receptor dimerization occurs in the endoplasmic reticulum and is required for ubiquitin system-dependent endocytosis. *Proc Natl Acad Sci U S A*. 99:9858-9863.

Gevers, E.F., M.J. Hannah, M.J. Waters, and I.C. Robinson. 2009. Regulation of rapid signal transducer and activator of transcription-5 phosphorylation in the resting cells of the growth plate and in the liver by growth hormone and feeding. *Endocrinology*. 150:3627-3636.

Giustina, A., and J.D. Veldhuis. 1998. Pathophysiology of the neuroregulation of growth hormone secretion in experimental animals and the human. *Endocr Rev*. 19:717-797.

Goffin, V., and P.A. Kelly. 1997. The prolactin/growth hormone receptor family: structure/function relationships. *J Mammary Gland Biol Neoplasia*. 2:7-17.

Goldring, M.B., J.R. Birkhead, L.F. Suen, R. Yamin, S. Mizuno, J. Glowacki, J.L. Arbiser, and J.F. Apperley. 1994. Interleukin-1 beta-modulated gene expression in immortalized human chondrocytes. *J Clin Invest*. 94:2307-2316.

Govers, R., T. ten Broeke, P. van Kerkhof, A.L. Schwartz, and G.J. Strous. 1999. Identification of a novel ubiquitin conjugation motif, required for ligand-induced internalization of the growth hormone receptor. *EMBO J*. 18:28-36.

Greenhalgh, C.J., and W.S. Alexander. 2004. Suppressors of cytokine signalling and regulation of growth hormone action. *Growth Horm IGF Res*. 14:200-206.

Greenhalgh, C.J., E. Rico-Bautista, M. Lorentzon, A.L. Thaus, P.O. Morgan, T.A. Willson, P. Zervoudakis, D. Metcalf, I. Street, N.A. Nicola, A.D. Nash, L.J. Fabri, G. Norstedt, C.

Ohlsson, A. Flores-Morales, W.S. Alexander, and D.J. Hilton. 2005. SOCS2 negatively regulates growth hormone action in vitro and in vivo. *J Clin Invest*. 115:397-406.

Guasti, L., S. Silvennoinen, N.W. Bulstrode, P. Ferretti, U. Sankilampi, and L. Dunkel. 2014. Elevated FGF21 leads to attenuated postnatal linear growth in preterm infants through GH resistance in chondrocytes. *J Clin Endocrinol Metab*. 99:E2198-2206.

Gunawardane, K., T. Krarup Hansen, J. Sandahl Christiansen, and J.O. Lunde Jorgensen. 2000. Normal Physiology of Growth Hormone in Adults. *In* Endotext. L.J. De Groot, G. Chrousos, K. Dungan, K.R. Feingold, A. Grossman, J.M. Hershman, C. Koch, M. Korbonits, R. McLachlan, M. New, J. Purnell, R. Rebar, F. Singer, and A. Vinik, editors, South Dartmouth (MA).

Hall, B.K., and T. Miyake. 2000. All for one and one for all: condensations and the initiation of skeletal development. *Bioessays*. 22:138-147.

Harris, M., P.L. Hofman, and W.S. Cutfield. 2004. Growth hormone treatment in children: review of safety and efficacy. *Paediatr Drugs*. 6:93-106.

Hataya, Y., T. Akamizu, K. Takaya, N. Kanamoto, H. Ariyasu, M. Saijo, K. Moriyama, A. Shimatsu, M. Kojima, K. Kangawa, and K. Nakao. 2001. A low dose of ghrelin stimulates growth hormone (GH) release synergistically with GH-releasing hormone in humans. *J Clin Endocrinol Metab*. 86:4552.

Hawkes, C.P., and A. Grimberg. 2015. Insulin-Like Growth Factor-I is a Marker for the Nutritional State. *Pediatr Endocrinol Rev*. 13:499-511.

Haymond, M., A.M. Kappelgaard, P. Czernichow, B.M. Biller, K. Takano, W. Kiess, and H. Global Advisory Panel Meeting on the Effects of Growth. 2013. Early recognition of growth abnormalities permitting early intervention. *Acta Paediatr*. 102:787-796.

Heird, W.C. 2001. Determination of nutritional requirements in preterm infants, with special reference to 'catch-up' growth. *Semin Neonatol*. 6:365-375.

Herrington, J., and C. Carter-Su. 2001. Signaling pathways activated by the growth hormone receptor. *Trends Endocrinol Metab*. 12:252-257.

Hiltunen, H., E. Loyttyniemi, E. Isolauri, and S. Rautava. 2018. Early Nutrition and Growth until the Corrected Age of 2 Years in Extremely Preterm Infants. *Neonatology*. 113:100-107.

Hollanders, J.J., S.M. van der Pal, P. van Dommelen, J. Rotteveel, and M.J.J. Finken. 2017. Growth pattern and final height of very preterm vs. very low birth weight infants. *Pediatr Res*. 82:317-323.

Iglesias, P., R. Selgas, S. Romero, and J.J. Diez. 2012. Biological role, clinical significance, and therapeutic possibilities of the recently discovered metabolic hormone fibroblastic growth factor 21. *Eur J Endocrinol*. 167:301-309.

Inagaki, T. 2015. Research Perspectives on the Regulation and Physiological Functions of FGF21 and its Association with NAFLD. *Front Endocrinol (Lausanne)*. 6:147.

Inagaki, T., V.Y. Lin, R. Goetz, M. Mohammadi, D.J. Mangelsdorf, and S.A. Kliewer. 2008. Inhibition of growth hormone signaling by the fasting-induced hormone FGF21. *Cell Metab*. 8:77-83.

Kadakia, R., and J. Josefson. 2016. The Relationship of Insulin-Like Growth Factor 2 to Fetal Growth and Adiposity. *Horm Res Paediatr*. 85:75-82.

Karimian, E., A.S. Chagin, and L. Savendahl. 2011. Genetic regulation of the growth plate. *Front Endocrinol (Lausanne)*. 2:113.

Kato, Y., Y. Murakami, M. Sohmiya, and M. Nishiki. 2002. Regulation of human growth hormone secretion and its disorders. *Intern Med*. 41:7-13.

Kharitonenkov, A., and P. Larsen. 2011. FGF21 reloaded: challenges of a rapidly growing field. *Trends Endocrinol Metab*. 22:81-86.

Kile, B.T., and W.S. Alexander. 2001. The suppressors of cytokine signalling (SOCS). *Cell Mol Life Sci*. 58:1627-1635.

Kilkenny, D.M., and J.V. Rocheleau. 2016. The FGF21 Receptor Signaling Complex: Klothobeta, FGFR1c, and Other Regulatory Interactions. *Vitam Horm*. 101:17-58.

Kim, K.H., and M.S. Lee. 2015. FGF21 as a mediator of adaptive responses to stress and metabolic benefits of anti-diabetic drugs. *J Endocrinol*. 226:R1-16.

Kim, T.K., and J.H. Eberwine. 2010. Mammalian cell transfection: the present and the future. *Anal Bioanal Chem*. 397:3173-3178.

Knops, N.B., K.C. Sneeuw, R. Brand, E.T. Hille, A.L. den Ouden, J.M. Wit, and S.P. Verloove-Vanhorick. 2005. Catch-up growth up to ten years of age in children born very preterm or with very low birth weight. *BMC Pediatr*. 5:26.

Krebs, D.L., and D.J. Hilton. 2001. SOCS proteins: negative regulators of cytokine signaling. *Stem Cells*. 19:378-387.

Kronenberg, H.M. 2003. Developmental regulation of the growth plate. *Nature*. 423:332-336.

Kubicky, R.A., S. Wu, A. Kharitonenkov, and F. De Luca. 2012. Role of fibroblast growth factor 21 (FGF21) in undernutrition-related attenuation of growth in mice. *Endocrinology*. 153:2287-2295.

Kubista, M., J.M. Andrade, M. Bengtsson, A. Forootan, J. Jonak, K. Lind, R. Sindelka, R. Sjoback, B. Sjogreen, L. Strombom, A. Stahlberg, and N. Zoric. 2006. The real-time polymerase chain reaction. *Mol Aspects Med*. 27:95-125.

Laestander, C., and W. Engstrom. 2014. Role of fibroblast growth factors in elicitation of cell responses. *Cell Prolif*. 47:3-11.

Laron, Z. 2001. Insulin-like growth factor 1 (IGF-1): a growth hormone. *Mol Pathol*. 54:311-316.

Legato, M.J. 2004. Principles of Gender-Specific Medicine.

Letellier, E., and S. Haan. 2016. SOCS2: physiological and pathological functions. *Front Biosci (Elite Ed)*. 8:189-204.

Li, H., J. Zhang, and W. Jia. 2013. Fibroblast growth factor 21: a novel metabolic regulator from pharmacology to physiology. *Front Med*. 7:25-30.

Livak, K.J., and T.D. Schmittgen. 2001. Analysis of relative gene expression data using real-time quantitative PCR and the 2(-Delta Delta C(T)) Method. *Methods*. 25:402-408.

Locatelli, V., and V.E. Bianchi. 2014. Effect of GH/IGF-1 on Bone Metabolism and Osteoporsosis. *Int J Endocrinol*. 2014:235060.

Lui, J.C., O. Nilsson, and J. Baron. 2011. Growth plate senescence and catch-up growth. *Endocr Dev*. 21:23-29.

Lupu, F., J.D. Terwilliger, K. Lee, G.V. Segre, and A. Efstratiadis. 2001. Roles of growth hormone and insulin-like growth factor 1 in mouse postnatal growth. *Dev Biol*. 229:141-162.

Mackie, E.J., Y.A. Ahmed, L. Tatarczuch, K.S. Chen, and M. Mirams. 2007. Endochondral ossification: how cartilage is converted into bone in the developing skeleton. *Int J Biochem Cell Biol*. 40:46-62.

Mackie, E.J., L. Tatarczuch, and M. Mirams. 2011. The skeleton: a multi-functional complex organ: the growth plate chondrocyte and endochondral ossification. *J Endocrinol*. 211:109-121.

Marino, R. 2011. Growth plate biology: new insights. *Curr Opin Endocrinol Diabetes Obes*. 18:9-13.

Martinez, C.S., V.G. Piazza, M.E. Diaz, R.K. Boparai, O. Arum, M.C. Ramirez, L. Gonzalez, D. Becu-Villalobos, A. Bartke, D. Turyn, J.G. Miquet, and A.I. Sotelo. 2015. GH/STAT5 signaling during the growth period in livers of mice overexpressing GH. *J Mol Endocrinol*. 54:171-184.

Mellis, D.J., C. Itzstein, M.H. Helfrich, and J.C. Crockett. 2011. The skeleton: a multi-functional complex organ: the role of key signalling pathways in osteoclast differentiation and in bone resorption. *J Endocrinol*. 211:131-143.

Mericq, V., F. De Luca, M.I. Hernandez, V. Pena, K. Rossel, M. Garcia, A. Avila, G. Cavada, and G. Iniguez. 2014. Serum fibroblast growth factor 21 levels are inversely associated with growth rates in infancy. *Horm Res Paediatr*. 82:324-331.

Mohammadi, M., S.K. Olsen, and O.A. Ibrahimi. 2005. Structural basis for fibroblast growth factor receptor activation. *Cytokine Growth Factor Rev*. 16:107-137.

Moller, N., and J.O. Jorgensen. 2009. Effects of growth hormone on glucose, lipid, and protein metabolism in human subjects. *Endocr Rev*. 30:152-177.

Murata, Y., M. Konishi, and N. Itoh. 2011. FGF21 as an Endocrine Regulator in Lipid Metabolism: From Molecular Evolution to Physiology and Pathophysiology. *J Nutr Metab*. 2011:981315.

Nichols, J. 2016. Normal growth patterns in infants and prepubertal children.

Niklasson, A., E. Engstrom, A.L. Hard, K.A. Wikland, and A. Hellstrom. 2003. Growth in very preterm children: a longitudinal study. *Pediatr Res*. 54:899-905.

Nilsson, O., and J. Baron. 2004. Fundamental limits on longitudinal bone growth: growth plate senescence and epiphyseal fusion. *Trends Endocrinol Metab*. 15:370-374.

Nilsson, O., and J. Baron. 2005. Impact of growth plate senescence on catch-up growth and epiphyseal fusion. *Pediatr Nephrol*. 20:319-322.

Olsen, B.R., A.M. Reginato, and W. Wang. 2000. Bone development. *Annu Rev Cell Dev Biol*. 16:191-220.

Oostdijk, W., F.K. Grote, S.M. de Muinck Keizer-Schrama, and J.M. Wit. 2009. Diagnostic approach in children with short stature. *Horm Res*. 72:206-217.

Ornitz, D.M., and N. Itoh. 2015. The Fibroblast Growth Factor signaling pathway. *Wiley Interdiscip Rev Dev Biol*. 4:215-266.

Ortega, N., D.J. Behonick, and Z. Werb. 2004. Matrix remodeling during endochondral ossification. *Trends Cell Biol*. 14:86-93.

Pass, C., V.E. MacRae, S.F. Ahmed, and C. Farquharson. 2009. Inflammatory cytokines and the GH/IGF-I axis: novel actions on bone growth. *Cell Biochem Funct*. 27:119-127.

Pass, C., V.E. MacRae, C. Huesa, S. Faisal Ahmed, and C. Farquharson. 2012. SOCS2 is the critical regulator of GH action in murine growth plate chondrogenesis. *J Bone Miner Res*. 27:1055-1066.

Patel, Y.C. 1999. Somatostatin and its receptor family. *Front Neuroendocrinol*. 20:157-198.

Perez-Marti, A., V. Sandoval, P.F. Marrero, D. Haro, and J. Relat. 2016. Nutritional regulation of fibroblast growth factor 21: from macronutrients to bioactive dietary compounds. *Horm Mol Biol Clin Investig*. 30.

Pfeifer, A.C., J. Timmer, and U. Klingmuller. 2008. Systems biology of JAK/STAT signalling. *Essays Biochem*. 45:109-120.

Pinney, D.F., and C.P. Emerson, Jr. 1989. 10T1/2 cells: an in vitro model for molecular genetic analysis of mesodermal determination and differentiation. *Environ Health Perspect*. 80:221-227.

Prentice, A., I. Schoenmakers, M.A. Laskey, S. de Bono, F. Ginty, and G.R. Goldberg. 2006. Nutrition and bone growth and development. *Proc Nutr Soc*. 65:348-360.

Rawlings, J.S., K.M. Rosler, and D.A. Harrison. 2004. The JAK/STAT signaling pathway. *J Cell Sci*. 117:1281-1283.

Robson, H., T. Siebler, S.M. Shalet, and G.R. Williams. 2002. Interactions between GH, IGF-I, glucocorticoids, and thyroid hormones during skeletal growth. *Pediatr Res*. 52:137-147.

Rochira, V., E. Kara, and C. Carani. 2015. The endocrine role of estrogens on human male skeleton. *Int J Endocrinol*. 2015:165215.

Roelfsema, V., and R.G. Clark. 2001. The growth hormone and insulin-like growth factor axis: its manipulation for the benefit of growth disorders in renal failure. *J Am Soc Nephrol*. 12:1297-1306.

Rogol, A.D., P.A. Clark, and J.N. Roemmich. 2000. Growth and pubertal development in children and adolescents: effects of diet and physical activity. *Am J Clin Nutr*. 72:521S-528S.

Rosenbloom, A.L. 1997. Growth Hormone Insensitivity.

Rosenbloom, A.L. 2000. Physiology and disorders of the growth hormone receptor (GHR) and GH-GHR signal transduction. *Endocrine*. 12:107-119.

Rotwein, P. 2012. Mapping the growth hormone--Stat5b--IGF-I transcriptional circuit. *Trends Endocrinol Metab*. 23:186-193.

Rotwein, P., and D.J. Chia. 2010. Gene regulation by growth hormone. *Pediatr Nephrol*. 25:651-658.

Rozario, K.S., C. Lloyd, and F. Ryan. 2000. Gh and Igf-1 Physiology in Childhood. *In* Endotext. L.J. De Groot, G. Chrousos, K. Dungan, K.R. Feingold, A. Grossman, J.M. Hershman, C. Koch, M. Korbonits, R. McLachlan, M. New, J. Purnell, R. Rebar, F. Singer, and A. Vinik, editors, South Dartmouth (MA).

Saegusa, J., S. Yamaji, K. Ieguchi, C.Y. Wu, K.S. Lam, F.T. Liu, Y.K. Takada, and Y. Takada. 2009. The direct binding of insulin-like growth factor-1 (IGF-1) to integrin alphavbeta3 is involved in IGF-1 signaling. *J Biol Chem*. 284:24106-24114.

Sandberg, D.E. 2011. Short stature: psychosocial interventions. *Horm Res Paediatr*. 76 Suppl 3:29-32.

Sankilampi, U., M.L. Hannila, A. Saari, M. Gissler, and L. Dunkel. 2013. New population-based references for birth weight, length, and head circumference in singletons and twins from 23 to 43 gestation weeks. *Ann Med*. 45:446-454.

Sarabipour, S., and K. Hristova. 2016. Mechanism of FGF receptor dimerization and activation. *Nat Commun*. 7:10262.

Sedek, M., L.M. van der Velden, and G.J. Strous. 2014. Multimeric growth hormone receptor complexes serve as signaling platforms. *J Biol Chem*. 289:65-73.

Smith, R., A. Duguay, A. Bakker, P. Li, J. Weiszmann, M.R. Thomas, B.M. Alba, X. Wu, J. Gupte, L. Yang, J. Stevens, A. Hamburger, S. Smith, J. Chen, R. Komorowski, K.W. Moore, M.M. Veniant, and Y. Li. 2013. FGF21 can be mimicked in vitro and in vivo by a novel anti-FGFR1c/beta-Klotho bispecific protein. *PLoS One*. 8:e61432.

Solon-Biet, S.M., V.C. Cogger, T. Pulpitel, M. Heblinski, D. Wahl, A.C. McMahon, A. Warren, J. Durrant-Whyte, K.A. Walters, J.R. Krycer, F. Ponton, R. Gokarn, J.A. Wali, K. Ruohonen, A.D. Conigrave, D.E. James, D. Raubenheimer, C.D. Morrison, D.G. Le Couteur, and S.J. Simpson. 2016. Defining the Nutritional and Metabolic Context of FGF21 Using the Geometric Framework. *Cell Metab*. 24:555-565.

Stang, J., and Story, M. 2005. Adolescent Growth and Development. *Guidelines for Adolescent Nutrition Services*.

Stanley, T. 2012. Diagnosis of growth hormone deficiency in childhood. *Curr Opin Endocrinol Diabetes Obes*. 19:47-52.

Stevens, D.G., M.I. Boyer, and C.V. Bowen. 1999. Transplantation of epiphyseal plate allografts between animals of different ages. *J Pediatr Orthop*. 19:398-403.

Strous, G.J., and P. van Kerkhof. 2002. The ubiquitin-proteasome pathway and the regulation of growth hormone receptor availability. *Mol Cell Endocrinol*. 197:143-151.

Strous, G.J., P. van Kerkhof, R. Govers, A. Ciechanover, and A.L. Schwartz. 1996. The ubiquitin conjugation system is required for ligand-induced endocytosis and degradation of the growth hormone receptor. *EMBO J*. 15:3806-3812.

Su, B.H. 2014. Optimizing nutrition in preterm infants. *Pediatr Neonatol*. 55:5-13.

Suzuki, M., Y. Uehara, K. Motomura-Matsuzaka, J. Oki, Y. Koyama, M. Kimura, M. Asada, A. Komi-Kuramochi, S. Oka, and T. Imamura. 2008. betaKlotho is required for fibroblast growth factor (FGF) 21 signaling through FGF receptor (FGFR) 1c and FGFR3c. *Mol Endocrinol*. 22:1006-1014.

Thomas, P., and T.G. Smart. 2005. HEK293 cell line: a vehicle for the expression of recombinant proteins. *J Pharmacol Toxicol Methods*. 51:187-200.

Tiong, K.H., L.Y. Mah, and C.O. Leong. 2013. Functional roles of fibroblast growth factor receptors (FGFRs) signaling in human cancers. *Apoptosis*. 18:1447-1468.

Tollet-Egnell, P., A. Flores-Morales, A. Stavreus-Evers, L. Sahlin, and G. Norstedt. 1999. Growth hormone regulation of SOCS-2, SOCS-3, and CIS messenger ribonucleic acid expression in the rat. *Endocrinology*. 140:3693-3704.

Tse, W.Y., P.C. Hindmarsh, and C.G. Brook. 1989. The infancy-childhood-puberty model of growth: clinical aspects. *Acta Paediatr Scand Suppl*. 356:38-43; discussion 44-35.

Turnley, A.M. 2005. Role of SOCS2 in growth hormone actions. *Trends Endocrinol Metab*. 16:53-58.

Uauy, R., C.E. Mize, and C. Castillo-Duran. 2000. Fat intake during childhood: metabolic responses and effects on growth. *Am J Clin Nutr*. 72:1354S-1360S.

van den Eijnden, M.J., L.L. Lahaye, and G.J. Strous. 2006. Disulfide bonds determine growth hormone receptor folding, dimerisation and ligand binding. *J Cell Sci*. 119:3078-3086.

van den Eijnden, M.J., and G.J. Strous. 2007. Autocrine growth hormone: effects on growth hormone receptor trafficking and signaling. *Mol Endocrinol*. 21:2832-2846.

van der Eerden, B.C., M. Karperien, and J.M. Wit. 2003. Systemic and local regulation of the growth plate. *Endocr Rev*. 24:782-801.

van Kerkhof, P., R. Govers, C.M. Alves dos Santos, and G.J. Strous. 2000. Endocytosis and degradation of the growth hormone receptor are proteasome-dependent. *J Biol Chem*. 275:1575-1580.

van Kerkhof, P., M. Sachse, J. Klumperman, and G.J. Strous. 2001. Growth hormone receptor ubiquitination coincides with recruitment to clathrin-coated membrane domains. *J Biol Chem*. 276:3778-3784.

Vesterlund, M., F. Zadjali, T. Persson, M.L. Nielsen, B.M. Kessler, G. Norstedt, and A. Flores-Morales. 2011. The SOCS2 ubiquitin ligase complex regulates growth hormone receptor levels. *PLoS One*. 6:e25358.

Vijayakumar, A., S. Yakar, and D. Leroith. 2011. The intricate role of growth hormone in metabolism. *Front Endocrinol (Lausanne)*. 2:32.

Villar, J., F. Giuliani, Z.A. Bhutta, E. Bertino, E.O. Ohuma, L.C. Ismail, F.C. Barros, D.G. Altman, C. Victora, J.A. Noble, M.G. Gravett, M. Purwar, R. Pang, A. Lambert, A.T. Papageorghiou, R. Ochieng, Y.A. Jaffer, S.H. Kennedy, F. International, and C. Newborn Growth Consortium for the. 2015. Postnatal growth standards for preterm infants: the Preterm Postnatal Follow-up Study of the INTERGROWTH-21(st) Project. *Lancet Glob Health*. 3:e681-691.

Voller, A., A. Bartlett, and D.E. Bidwell. 1978. Enzyme immunoassays with special reference to ELISA techniques. *J Clin Pathol*. 31:507-520.

Walenkamp, M.J., and J.M. Wit. 2007. Genetic disorders in the GH IGF-I axis in mouse and man. *Eur J Endocrinol*. 157 Suppl 1:S15-26.

Walters, T.D., and A.M. Griffiths. 2009. Mechanisms of growth impairment in pediatric Crohn's disease. *Nat Rev Gastroenterol Hepatol*. 6:513-523.

Wang, X., K. He, M. Gerhart, Y. Huang, J. Jiang, R.J. Paxton, S. Yang, C. Lu, R.K. Menon, R.A. Black, G. Baumann, and S.J. Frank. 2002. Metalloprotease-mediated GH receptor proteolysis and GHBP shedding. Determination of extracellular domain stem region cleavage site. *J Biol Chem*. 277:50510-50519.

Waters, M.J. 2016. The growth hormone receptor. *Growth Horm IGF Res*. 28:6-10.

Weise, M., S. De-Levi, K.M. Barnes, R.I. Gafni, V. Abad, and J. Baron. 2001. Effects of estrogen on growth plate senescence and epiphyseal fusion. *Proc Natl Acad Sci U S A*. 98:6871-6876.

Wheeler, P.G., K. Bresnahan, B.A. Shephard, J. Lau, and E.M. Balk. 2004. Short stature and functional impairment: a systematic review. *Arch Pediatr Adolesc Med*. 158:236-243.

WHO. 2009. Infant and Young Child Feeding: Model Chapter for Textbooks for Medical Students and Allied Health Professionals. *In* Infant and Young Child Feeding: Model Chapter for Textbooks for Medical Students and Allied Health Professionals, Geneva.

Wit, J.M., P.E. Clayton, A.D. Rogol, M.O. Savage, P.H. Saenger, and P. Cohen. 2008. Idiopathic short stature: definition, epidemiology, and diagnostic evaluation. *Growth Horm IGF Res*. 18:89-110.

Wit, J.M., M.B. Ranke, and C. Kelnar. 2007. ESPE Classification of Paediatric Endocrine Diagnoses. *Hormone Research*. 68.

Wong, S.C., A.G. Catto-Smith, and M. Zacharin. 2014. Pathological fractures in paediatric patients with inflammatory bowel disease. *Eur J Pediatr*. 173:141-151.

Wong, S.C., A. Smyth, E. McNeill, P.J. Galloway, K. Hassan, P. McGrogan, and S.F. Ahmed. 2010. The growth hormone insulin-like growth factor 1 axis in children and adolescents with inflammatory bowel disease and growth retardation. *Clin Endocrinol (Oxf)*. 73:220-228.

Woo, Y.C., A. Xu, Y. Wang, and K.S. Lam. 2013. Fibroblast growth factor 21 as an emerging metabolic regulator: clinical perspectives. *Clin Endocrinol (Oxf)*. 78:489-496.

Woods, K. 2007. Genetic defects of the growth-hormone-IGF axis associated with growth hormone insensitivity. *Endocr Dev*. 11:6-15.

Wu, S., A. Levenson, A. Kharitonenkov, and F. De Luca. 2012. Fibroblast growth factor 21 (FGF21) inhibits chondrocyte function and growth hormone action directly at the growth plate. *J Biol Chem*. 287:26060-26067.

Xu, G., and S.R. Jaffrey. 2013. Proteomic identification of protein ubiquitination events. *Biotechnol Genet Eng Rev*. 29:73-109.

Xu, J., A.B. Keeton, J.L. Franklin, X. Li, D.Y. Venable, S.J. Frank, and J.L. Messina. 2006. Insulin enhances growth hormone induction of the MEK/ERK signaling pathway. *J Biol Chem*. 281:982-992.

Yadav, S., and A. Dabas. 2015. Approach to short stature. *Indian J Pediatr*. 82:462-470.

Yakar, S., C.J. Rosen, W.G. Beamer, C.L. Ackert-Bicknell, Y. Wu, J.L. Liu, G.T. Ooi, J. Setser, J. Frystyk, Y.R. Boisclair, and D. LeRoith. 2002. Circulating levels of IGF-1 directly regulate bone growth and density. *J Clin Invest*. 110:771-781.

Yang, C., C. Jin, X. Li, F. Wang, W.L. McKeehan, and Y. Luo. 2012. Differential specificity of endocrine FGF19 and FGF21 to FGFR1 and FGFR4 in complex with KLB. *PLoS One*. 7:e33870.

Yie, J., R. Hecht, J. Patel, J. Stevens, W. Wang, N. Hawkins, S. Steavenson, S. Smith, D. Winters, S. Fisher, L. Cai, E. Belouski, C. Chen, M.L. Michaels, Y.S. Li, R. Lindberg, M. Wang, M. Veniant, and J. Xu. 2009. FGF21 N- and C-termini play different roles in receptor interaction and activation. *FEBS Lett*. 583:19-24.

Yie, J., W. Wang, L. Deng, L.T. Tam, J. Stevens, M.M. Chen, Y. Li, J. Xu, R. Lindberg, R. Hecht, M. Veniant, C. Chen, and M. Wang. 2012. Understanding the physical interactions in the FGF21/FGFR/beta-Klotho complex: structural requirements and implications in FGF21 signaling. *Chem Biol Drug Des*. 79:398-410.

Yoshimura, A., and H. Yasukawa. 2012. JAK's SOCS: a mechanism of inhibition. *Immunity*. 36:157-159.

Yu, J., L. Zhao, A. Wang, S. Eleswarapu, X. Ge, D. Chen, and H. Jiang. 2012. Growth hormone stimulates transcription of the fibroblast growth factor 21 gene in the liver through the signal transducer and activator of transcription 5. *Endocrinology*. 153:750-758.

Zaman, F., D. Chrysis, K. Huntjens, A. Chagin, M. Takigawa, B. Fadeel, and L. Savendahl. 2014. Dexamethasone differentially regulates Bcl-2 family proteins in human proliferative chondrocytes: role of pro-apoptotic Bid. *Toxicol Lett*. 224:196-200.

Zhu, T., E.L. Goh, R. Graichen, L. Ling, and P.E. Lobie. 2001. Signal transduction via the growth hormone receptor. *Cell Signal*. 13:599-616.

Zuscik, M.J., M.J. Hilton, X. Zhang, D. Chen, and R.J. O'Keefe. 2008. Regulation of chondrogenesis and chondrocyte differentiation by stress. *J Clin Invest*. 118:429-438.

Appendix 7.

Table 7.1 PCR thermocycler reaction cycle conditions and primer sequence. Thermocycler RT-PCR reaction cycle conditions for *(GHR, Ghr, FGF21, FGFR1 β-KLOTHO and GAPDH)*: polymerase activation for 3 minutes at 95°C, followed by 35 cycles of denaturation for 3 seconds at 95°C, 30 seconds annealing temperature (see table below for specific temperatures) and extension for 20 seconds 72°C. Extra-extension was for 3 minutes at 72°C. PCR reaction cycle conditions for *(FGFR1 IIIC* isoform*)*: polymerase activation 5 minutes 95°C, followed by 35 cycles denaturation for 1 minute at 95°C, annealing for 1 minute at 65°C and extension for 1 minute at 72°C). Extra-extension was for 10 minutes at 72°C. PCR reaction cycle conditions for *(SOCS1, SOCS2* and *SOCS3)*: polymerase activation 3 seconds 95°C, followed by 35 cycles denaturation for 3 minutes at 95°C, annealing for 50 seconds at 63°C and extension for 45 seconds at 72°C). Extra-extension was for 3 minutes at 72°C.

Name Forward (F) Reverse (R)	**Species Human (H) Mouse (M)**	**Forward primer sequence in 5'-3' orientation**	**Reverse primer sequence in 5'-3' orientation**
PCR			
GHR	H	GGTATGGATCTCTGGCAGCTG	GAGGGCAATGGGTGGATCTG
Ghr	M	TGCTGCCTGCTGTTTGTATC	TTCCAGAAAATGTGCTGCTG
FGF21	H	ACCTGGAGATCAGGGAGGA	AGTGGAGCGATCCATACAGG
FGFR1	H	GAAGTTCAAATGCCCTTCCA	CCAGCTGGTATGTGTGGTTG
FGFR-IIIC	H	ACCACCGACAAAGAGATGGA	GCAGAGTGATGGGAGAGTCC
β-KLOTHO	H	GCTCTCAAAGCCCACATAC	GCAGCATAACGATAGAGGCC
SOCS1	H	GACGCCTGCGGATTCTACT	TAAGGGCGAAAAAGCAGTTC
SOCS2	H	GAGCTCGGTCAGACAGGATG	GTCCGCTTATCCTTGCACAT
SOCS3	H	GCCACCTACTGAACCCTCCT	AACACCAGGGGGATCTTCTC
GAPDH	H	GAAGGTGAAGGTCGGAGT	GAAGATGGTGATGGGATTTC

Table 7.2 RT-qPCR cycle conditions and primer sequences. Mx3000 Thermocycler reaction conditions: polymerase activation at 95˚C for 15 minutes, followed by 40 cycles of denaturation at 95˚C for 15 seconds, annealing at 60˚C for 30 seconds and extension at 72˚C for 30 seconds.

Name Forward (F) Reverse (R)	**Species Human (H) Mouse (M)**	**Forward primer sequence in 5'-3' orientation**	**Reverse primer sequence in 5'-3' orientation**
RT-qPCR			
FGF21	H	QuantiTect Primer Assay purchased from Qiagen.	
Fgf21	M		
GAPDH	H		
Gapdh	M		
SOCS2	H	GGTCGAGGCGATCAGTG	TCCTTGAAGTCAGTGCGAA
IGF-1	H	TGGTGGATGCTCTTCAGTTC	GACAGAGCGAGCTGACTTG
GHR	H	GTGATGCTTTTTCTGGAAGTGA	TCAGGGCATTCTTTCCATTC
FGFR1	H	GAAGTTCAAATGCCCTTCCA	CCAGCTGGTATGTGTGGTTG
FGFR1-IIIC	H	ACCACCGACAAAGAGATGGA	GCAGAGTGATGGGAGAGTCC
β-KLOTHO	H	GCTCTCAAAGCCCACATAC	GCAGCATAACGATAGAGGC

Table 7.3 Primary antibody list for western blot analysis.

Antibody	Source (code), species	Dilution
GHR (B-10)	Santa Cruz Biotechnology (sc-137185), mouse	1:500
Stat5 (C-17)	Santa Cruz Biotechnology (sc-835), rabbit	1:500
Phospho-Stat5 (Tyr 694) (C11C5)	Cell Signaling Technology (9359), rabbit	1:500
Jak2 (D2E12)	Cell Signaling Technology (3230), rabbit	1:500
Phospho-Jak2 (Tyr1007/1008)	Cell Signaling Technology (3771), rabbit	1:500
SOCS2	Abcam (ab3692), rabbit	1:500
Ubiquitin (Ubi-1)	Abcam (ab7254), mouse	1:500
GAPDH (G9)	Santa Cruz Biotechnology (sc-365062), mouse	1:10,000
Beta Actin (AC-15)	Abcam (ab6276), mouse	1:10,000

Table 7.4 Primary antibody list for immunohistochemistry.

Antibody	Source (code), species	Dilution
GHR (B-10)	Santa Cruz Biotechnology (sc-137185), mouse	1:25
FGF21	Abcam (ab66564), rabbit	1:100
FGFR1	Abcam (ab63601), rabbit	1:50
β-Klotho	Abcam (ab106794), rabbit	1:300

Table 7.5 Number of observations *n*=(x) for length SDS and weight SDS per sub-group of postmenstrual age (weeks) to assess mean growth patterns in 64 VPT infants.

	Number of observations *n*=(x)	
Postmenstrual age (weeks)	**Length SDS**	**Weight SDS**
22 – 24.99	9	8
25 – 27.99	25	24
28 – 30.99	52	52
31 – 33.99	64	64
34 – 36.99	64	64
37 – 39.99	58	58
40 – 42.99	55	55
43 – 45.99	51	51
46 – 48.99	27	29
49 – 51.99	36	38
52 – 54.99	44	44
55 – 57.99	26	26
58 – 60.99	30	31
61 – 72.99	114	114
73 – 84.99	104	103
85 – 96.99	81	81
97 – 108.99	48	47
109 – 120.99	32	32
121 – 132.99	9	9
133 – 141.99	26	26

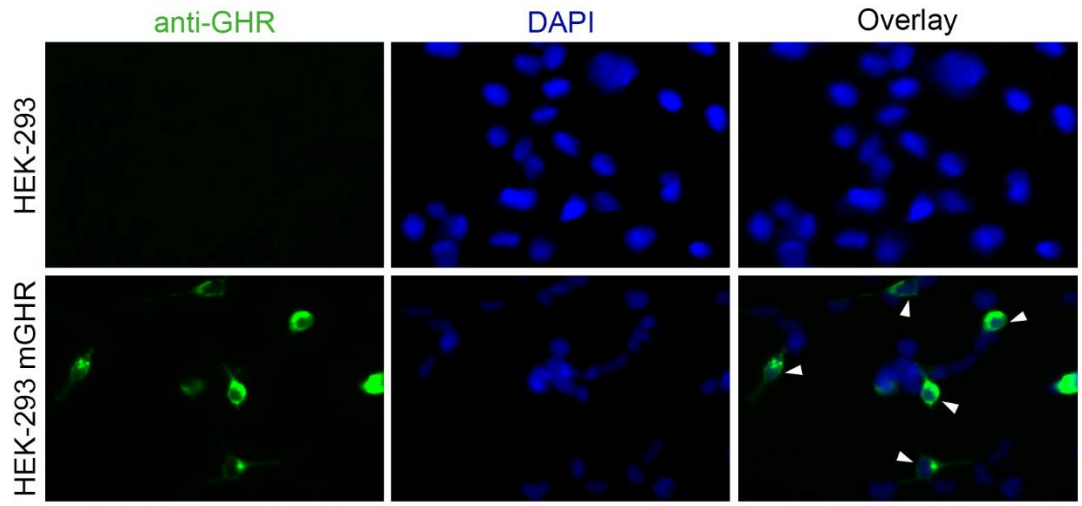

Figure 7.1 Immunofluorescent staining verifies GHR expression in HEK-293 mGHR stable cell line model. Fluorescent microscopic analysis of GHR (Alex 488, green) in HEK-293 (control) and HEK-293 mGHR stable line. Nuclei are labelled with DAPI (blue). White arrows indicate clear points of GHR expression. Representative images were taken at x40 magnification.

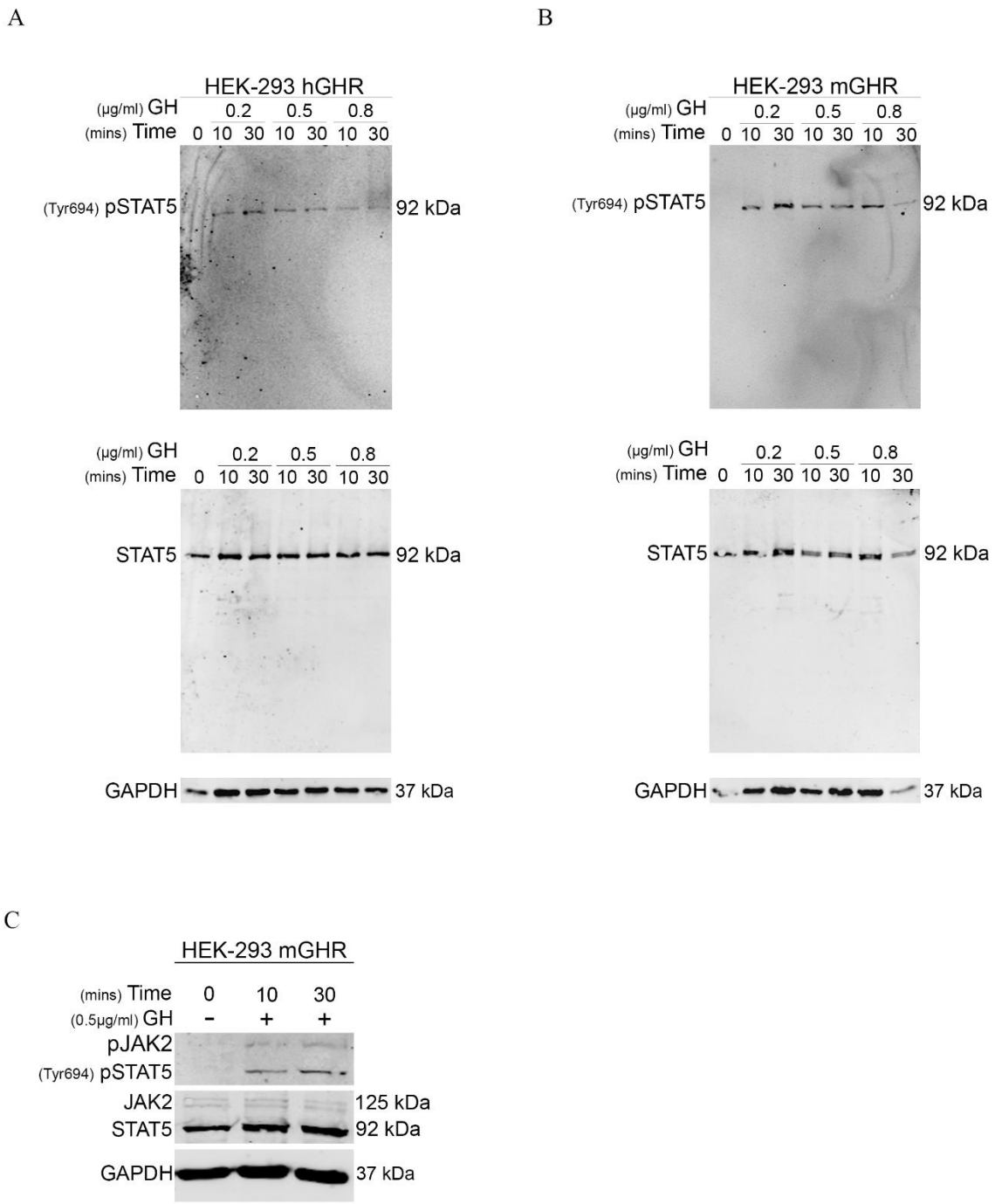

Figure 7.2 Optimisation of recombinant Growth hormone dosage and assessment of early downstream mediators of the JAK/STAT cascade. (A) HEK-293 hGHR and **(B)** HEK-293 mGHR stable lines were serum starved overnight and challenged with recombinant human GH at 0.2, 0.5 and 0.8 µg/ml for 10 or 30 minutes. Whole cell lysates were extracted and size-separated onto a 10% SDS-PAGE and assessed for the expression of STAT5 (92kDa) and pSTAT5(Tyr694) using western blot analysis. **(C)** HEK-293 mGHR cells were serum starved as previously described and treated with recombinant human GH (0.5µg/ml) for 10 or 30 minutes. Lysates were examined for the protein expression of JAK (125kDa), STAT5 (92kDa), pJAK2 and pSTAT5(Tyr694). GAPDH (37kDa) was used as a loading control.

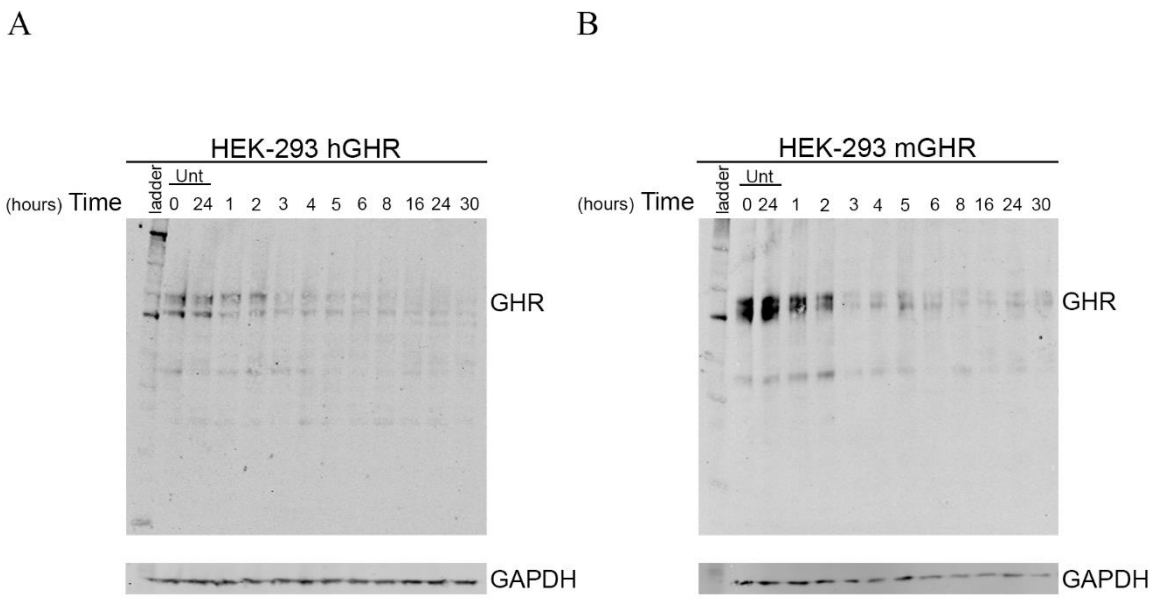

Figure 7.3 Assessment of the optimum time duration of Cycloheximide treatment to determine GHR half-life. (A) HEK-293 hGHR **(B)** HEK-293 mGHR stable lines were serum starved overnight before the addition of Cycloheximide (100µg/ml) for 0 to 30 hours. Whole cell lysates were extracted at indicated time intervals before the assessment of GHR (~110 – 140 kDa) expression using western blot analysis. Housekeeping GAPDH (37 kDa) was used as a loading control. Unt: Untreated.

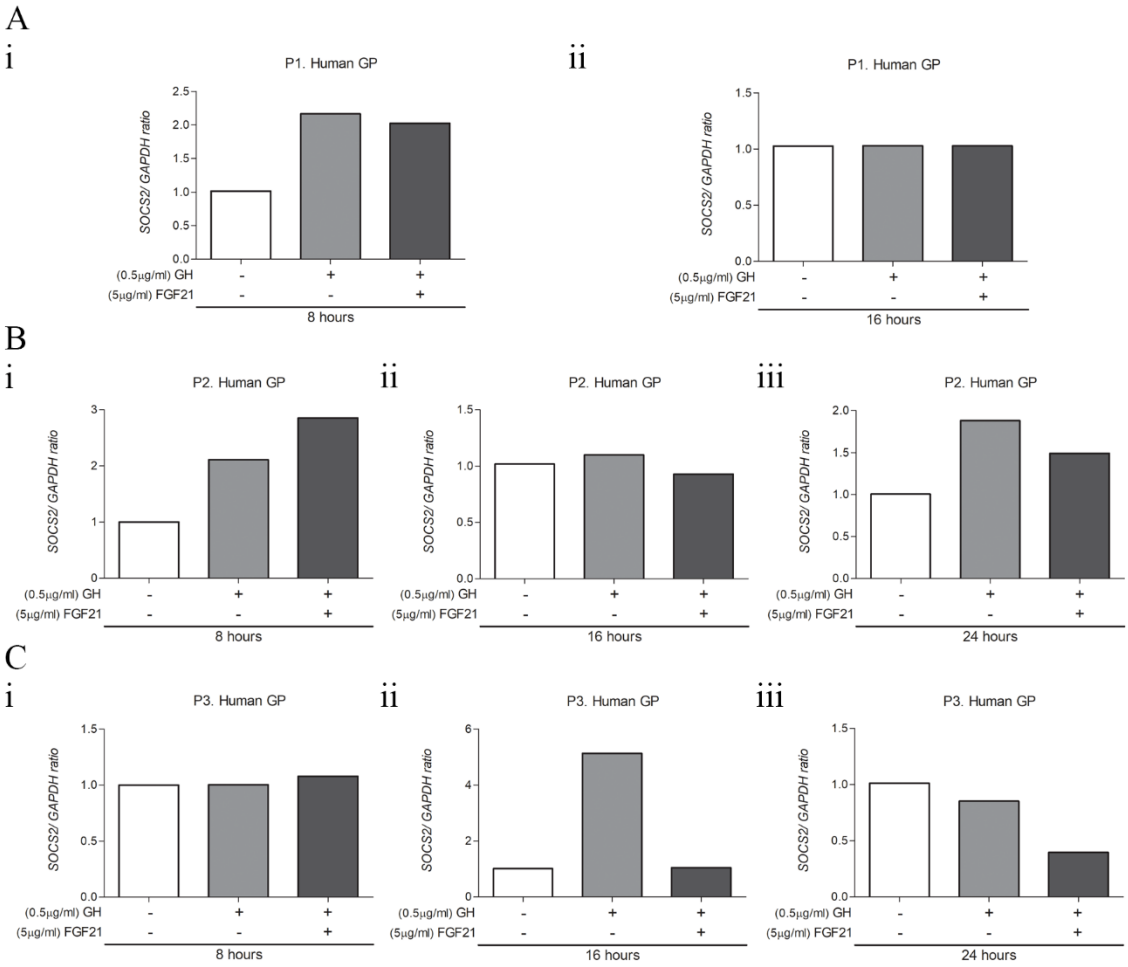

Figure 7.4 RT-qPCR of *SOCS2* expression in primary cultures of human growth plate biopsies. Human growth plate biopsies were serum starved and treated with or without recombinant human FGF21 (5µg/ml) overnight, followed by treatment with human recombinant GH (0.5µg/ml) for 8, 16 or 24 hours. Collection of RNA extracts were examined for their expression of *SOCS2* using RT-qPCR. **(A)** Patient 1 human growth plate biopsies, **(i)** 8 hours, **(ii)** 16 hours. **(B)** Patient 2 human growth plate biopsies, **(i)** 8 hours, **(ii)** 16 hours, **(iii)** 24 hours. **(C)** Patient 3 human growth plate biopsies, **(i)** 8 hours, **(ii)** 16 hours, **(iii)** 24 hours. All comparisons were made to control (untreated) and normalised to *GAPDH* (housekeeping gene).

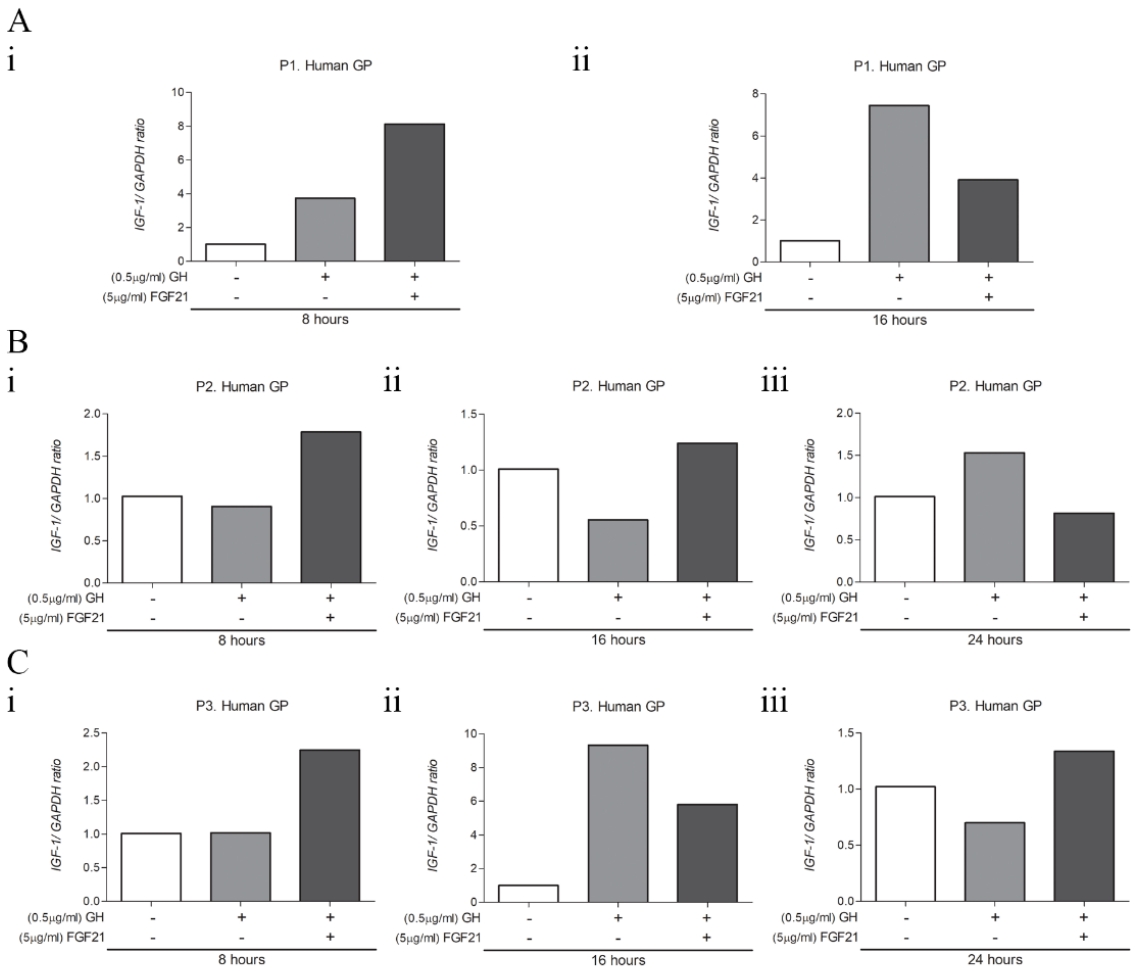

Figure 7.5 RT-qPCR of *IGF-1* expression in primary cultures of human growth plate biopsies. Human growth plate biopsies were serum starved and treated with or without recombinant human FGF21 (5µg/ml) overnight. The next day cultures were treated with human recombinant GH (0.5µg/ml) for 8, 16 or 24 hours. Collection of RNA extracts were examined for their expression of *IGF-1* using RT-qPCR. **(A)** Patient 1 human growth plate biopsies, **(i)** 8 hours, **(ii)** 16 hours. **(B)** Patient 2 human growth plate biopsies, **(i)** 8 hours, **(ii)** 16 hours, **(iii)** 24 hours. **(C)** Patient 3 human growth plate biopsies, **(i)** 8 hours, **(ii)** 16 hours, **(iii)** 24 hours. All comparisons were made to control (untreated) and normalised to *GAPDH* (housekeeping gene).

A

i hβ-KLOTHO

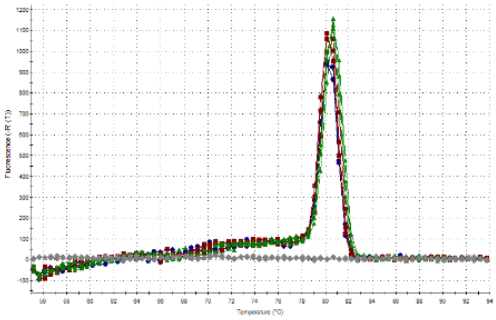

ii hFGFR1

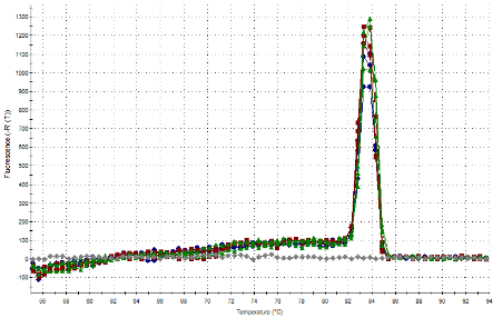

iii hFGFR1-IIIC

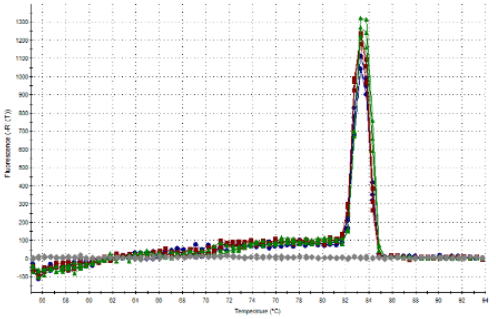

iv hGHR

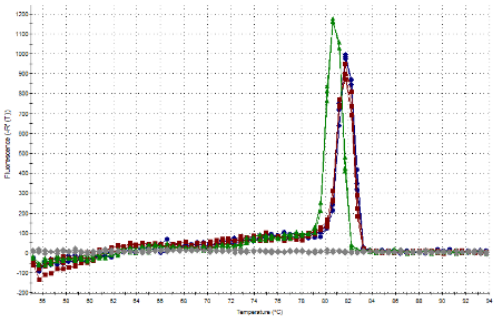

v hGAPDH

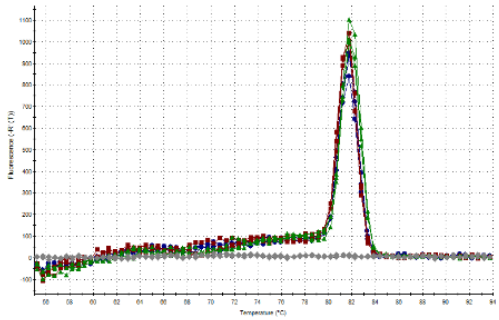

B

i

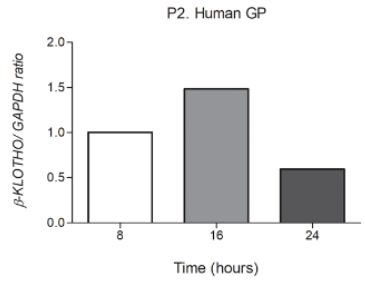

ii

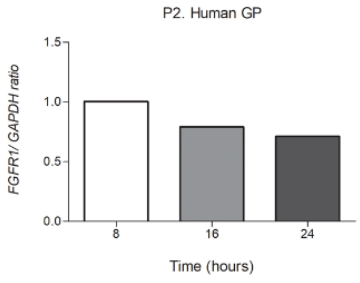

iii

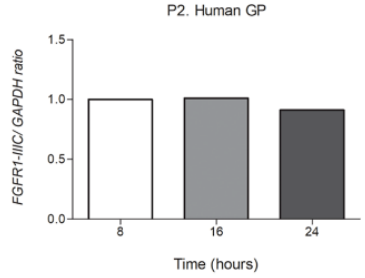

iv

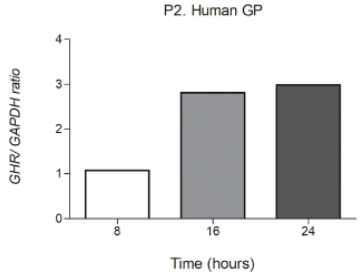

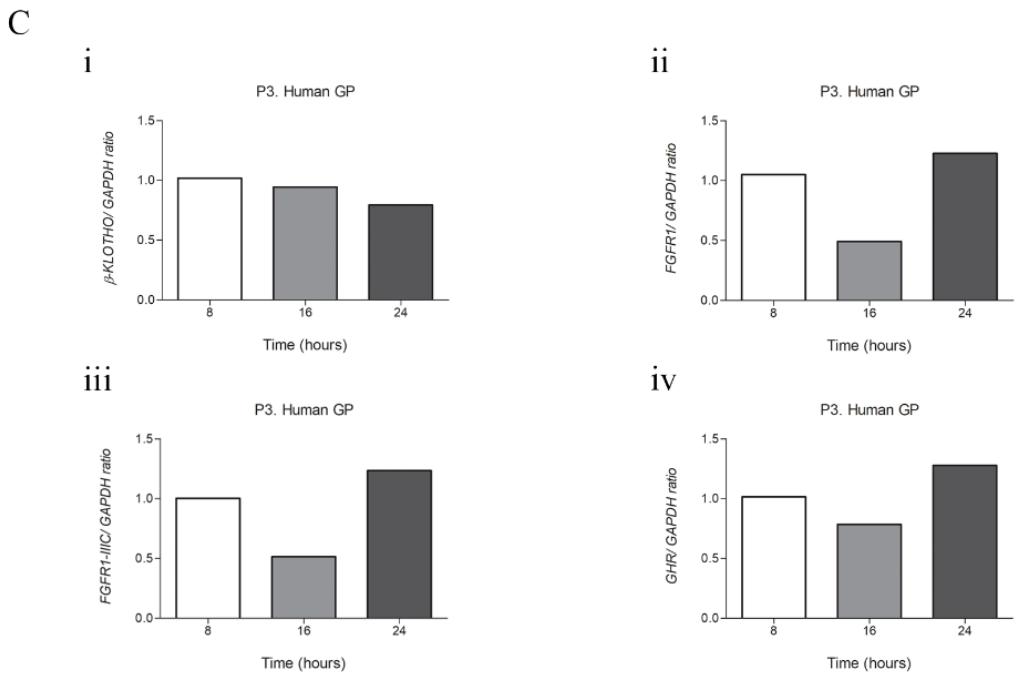

Figure 7.6 RT-qPCR of the endogenous expression of *FGF21* receptors and *GHR* expression in primary cultures of human growth plate biopsies. RNA extracts of Human growth plate biopsies control (untreated) at 8, 16 and 24 hours were assessed their expression of FGF21 receptor (human *β-KLOTHO, FGFR1, FGFR1-IIIC*) and *GHR* using RT-qPCR. **(A)** Representative dissociation curve from RT-qPCR **(i)** human *β-KLOTHO*, **(ii)** human *FGFR1,* **(iii)** human *FGFR1-IIIC*, **(iv)** human *GHR*, **(v)** human *GAPDH*. X-axes: temperature ˚C, Y-axes: first negative derivative of the change in fluorescence. **(B)** RT-qPCR analysis in Patient 2 human growth plate biopsies **(i)** *β-KLOTHO*, **(ii)** *FGFR1*, **(iii)** *FGFR1-IIIC* **(iv)** *GHR*. **(C)** RT-qPCR analysis in Patient 3 human growth plate biopsies **(i)** *β-KLOTHO*, **(ii)** *FGFR1*, **(iii)** *FGFR1-IIIC* **(iv)** *GHR*. All comparisons were made to 8 hour time point, normalised to *GAPDH* (housekeeping gene).

A

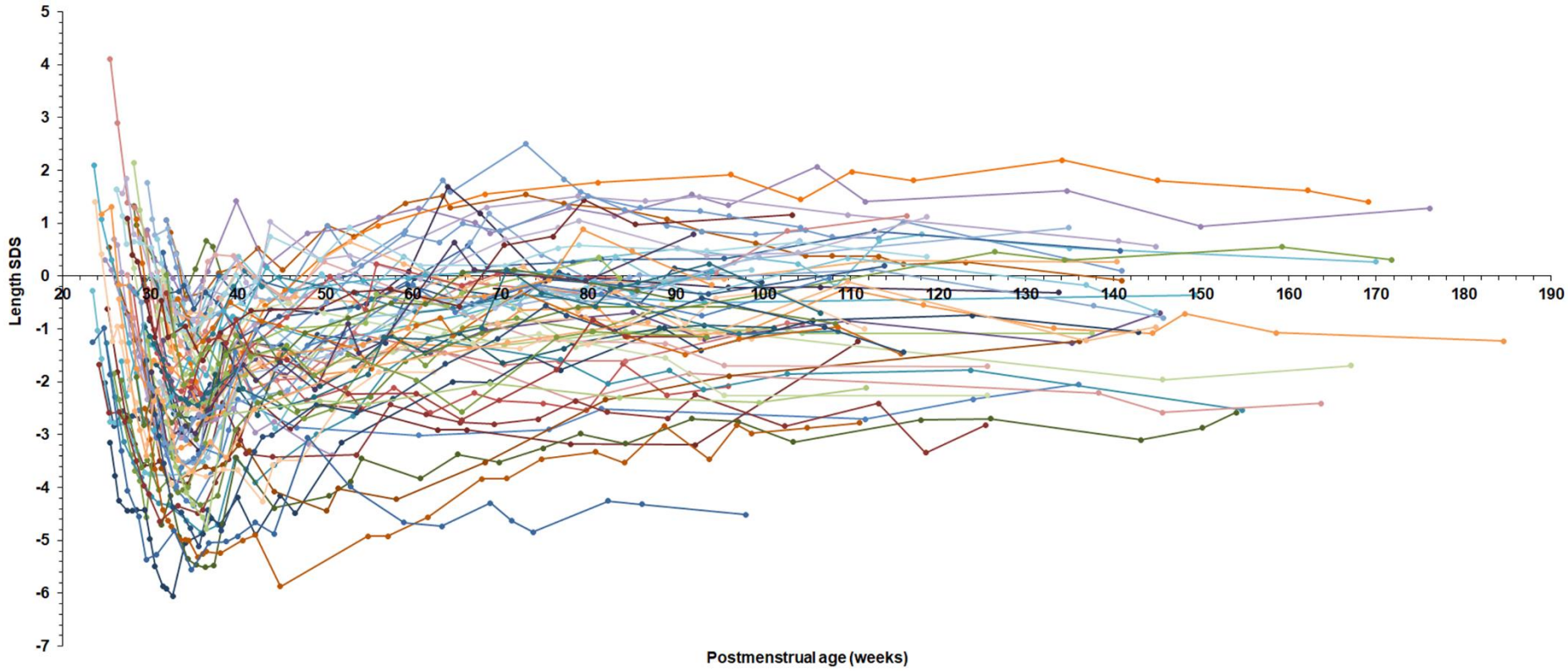
Length SDS
5
4
3
2
1
0
-1
-2
-3
-4
-5
-6
-7
20
30
40
50
60
70
80
90
100
110
120
130
140
150
160
170
180
190
Postmenstrual age (weeks)

B

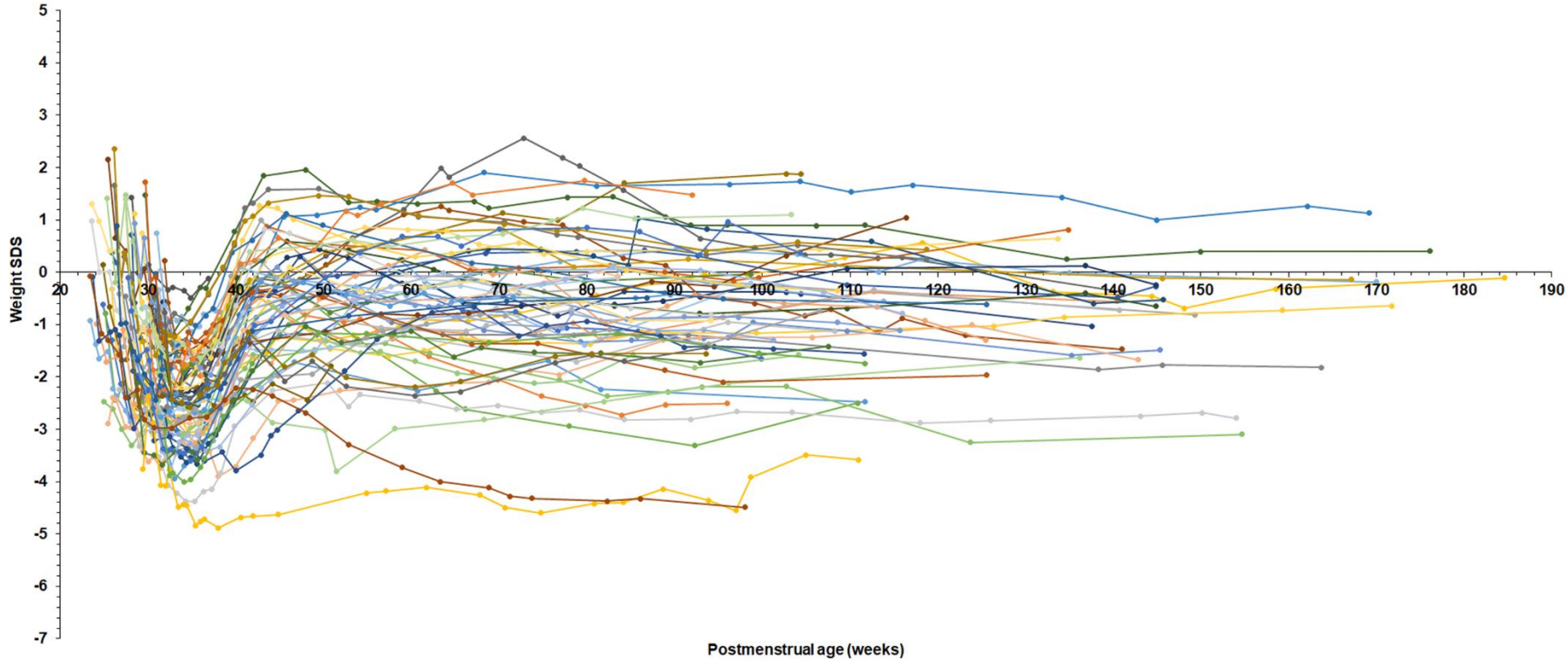
Weight SDS
5
4
3
2
1
0
-1
-2
-3
-4
-5
-6
-7
20
30
40
50
60
70
80
90
100
110
120
130
140
150
160
170
180
190
Postmenstrual age (weeks)

C

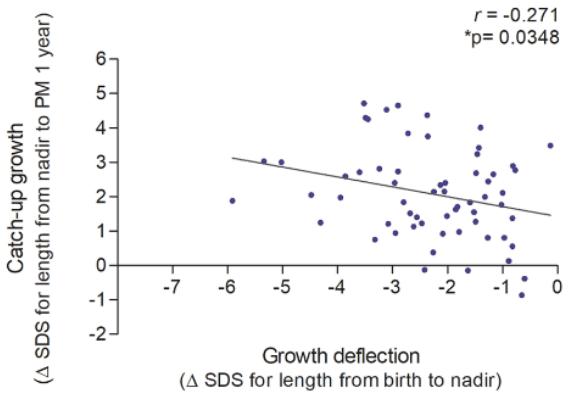

Figure 7.7 Assessment of growth patterns in very pre-term infants. (A) Representative growth charts for length SDS or **(B)** weight SDS of individual VPT patients from birth to total growth follow-up in PM age (weeks). **(C)** Magnitude of growth deflection (Δ SDS for length from birth to nadir) vs Catch-up growth (Δ SDS for length from nadir to PM 1 year months). Pearson's R correlation (*r*) and *p* values were obtained from Bivariate correlation analyses.

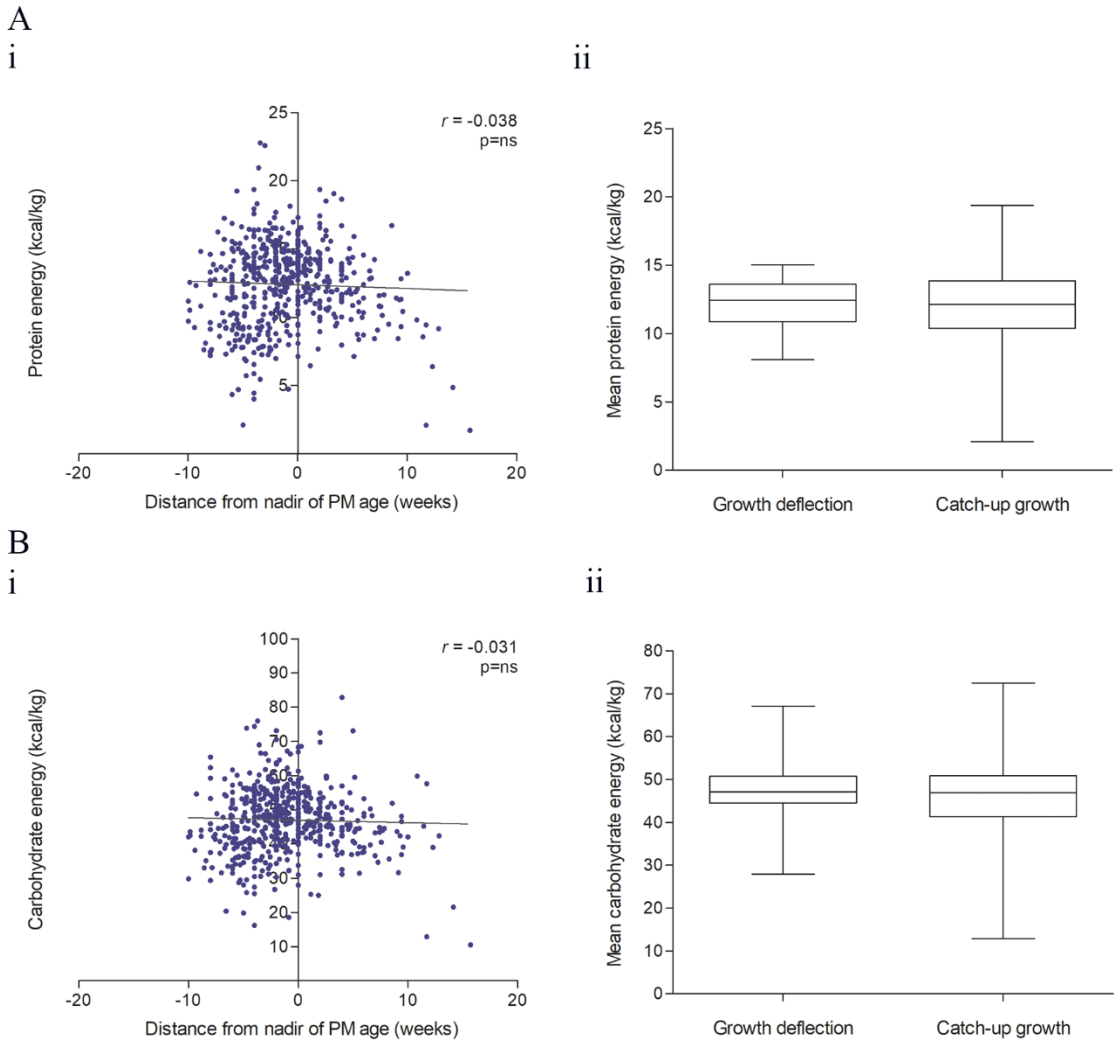

Figure 7.8 Protein and carbohydrate availability was not associated with very pre-term infant growth patterns. Assesment of macronutritent energy availability during growth deflection vs catch-up growth. **(Ai)** Protein (kcal/kg), **(Bi)** Carbohydrate (kcal/kg) energy vs distance from nadir of postmenstrual age (weeks). Pearson's R correlation (*r*) and *p* values were obtained from Bivariate correlation analyses. Mean **(Aii)** Protein (kcal/kg), **(Bii)** Carbohydrate (kcal/kg), energy was evealuated seperately during periods of deflection and catch-up growth. *p* values were obtained from Paried *t*-test analysis.

A

i

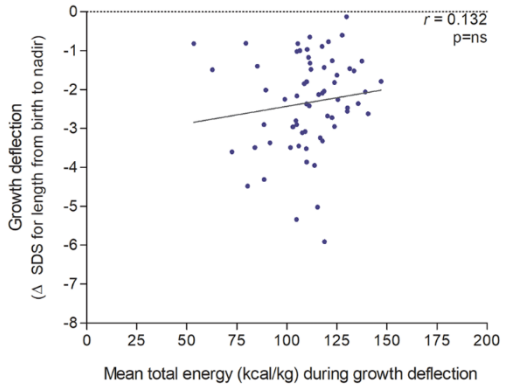

ii

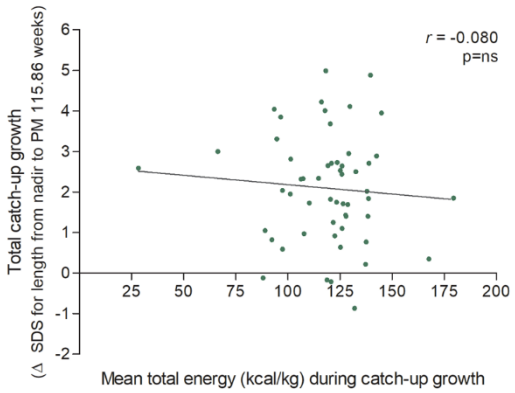

B

i

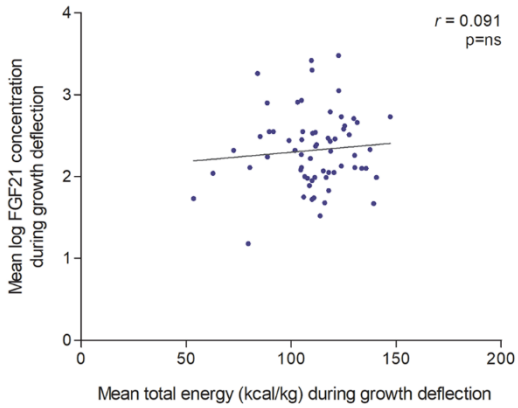

ii

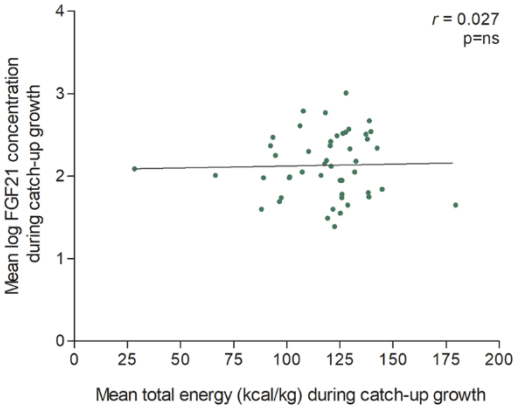

C

i

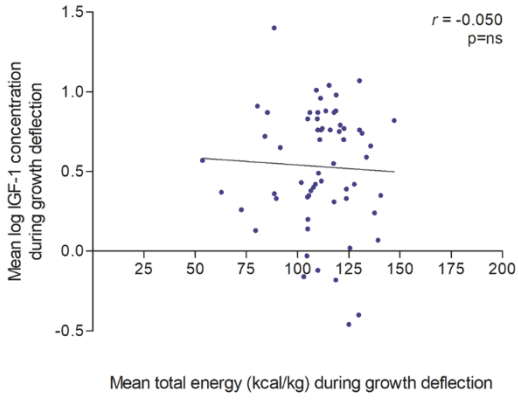

ii

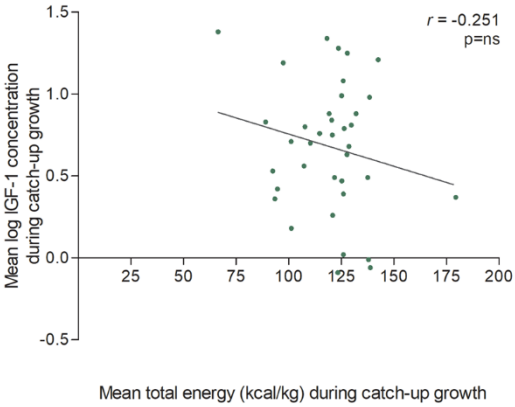

D

i

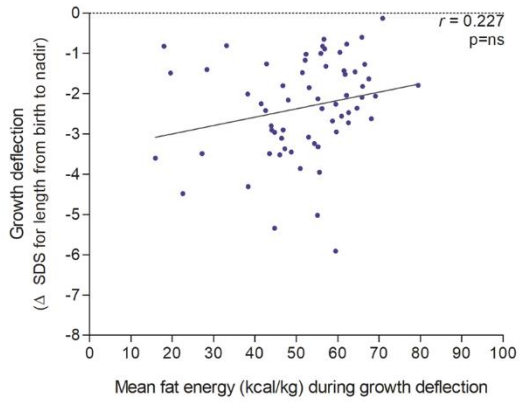

ii

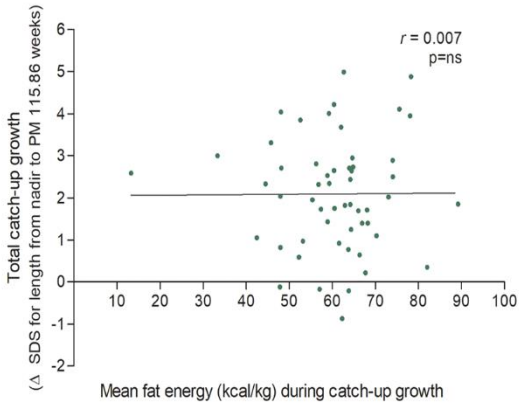

E

i

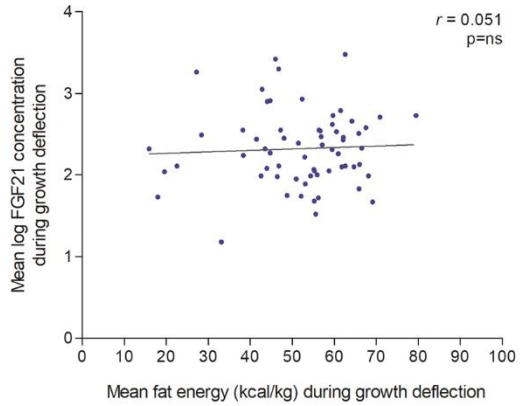

ii

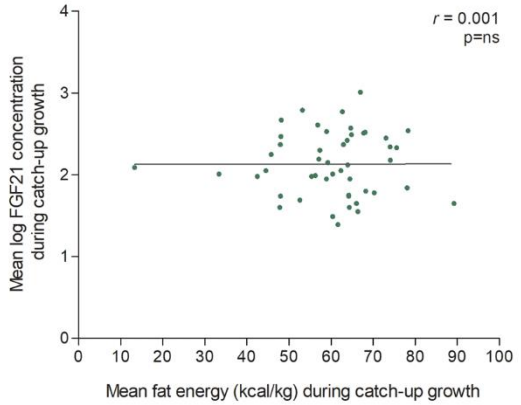

F

i

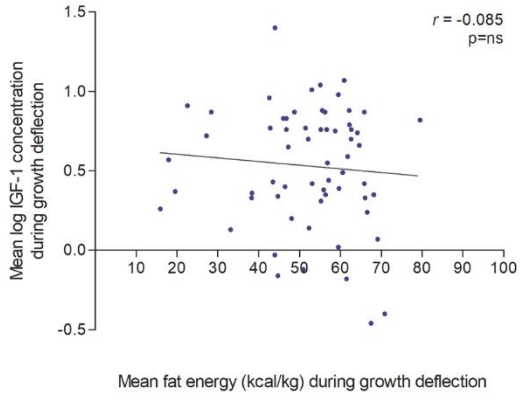

ii

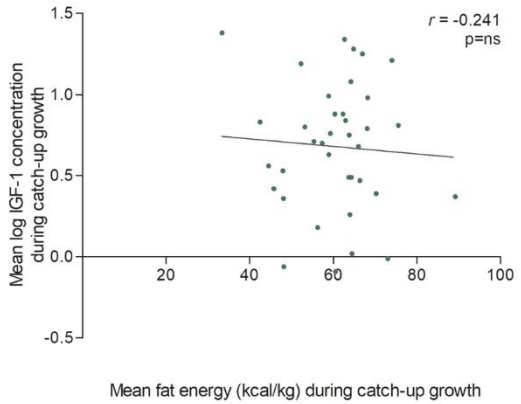

G

i

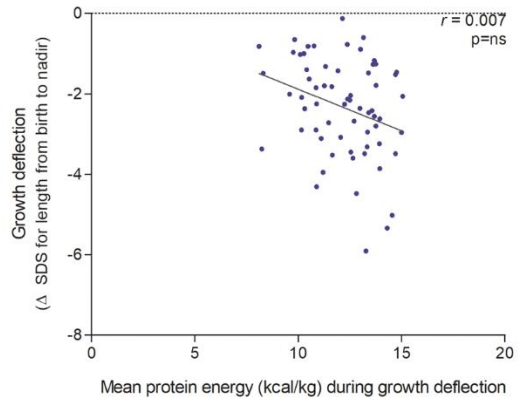

ii

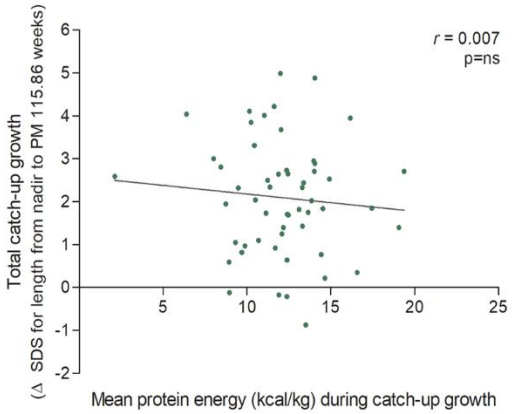

H

i

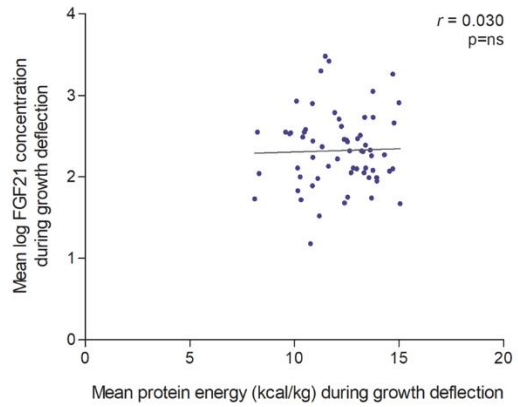

ii

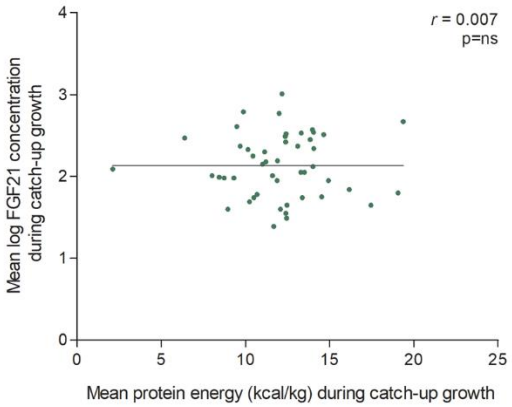

I

i

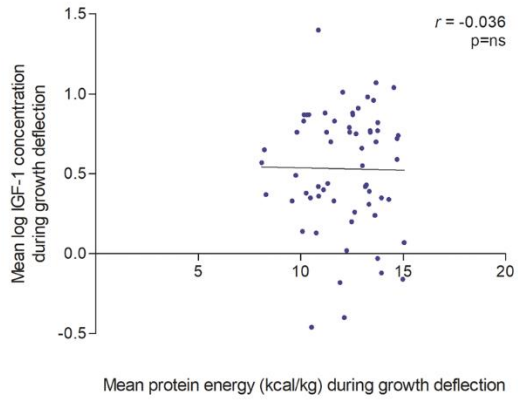

ii

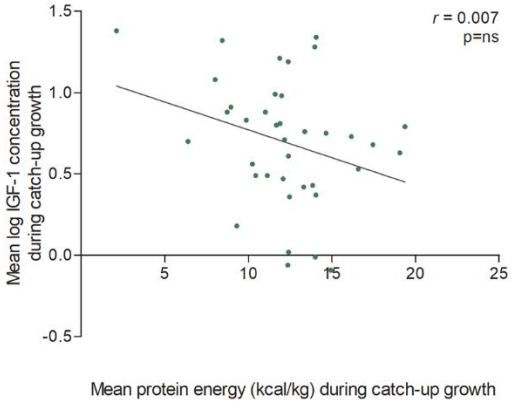

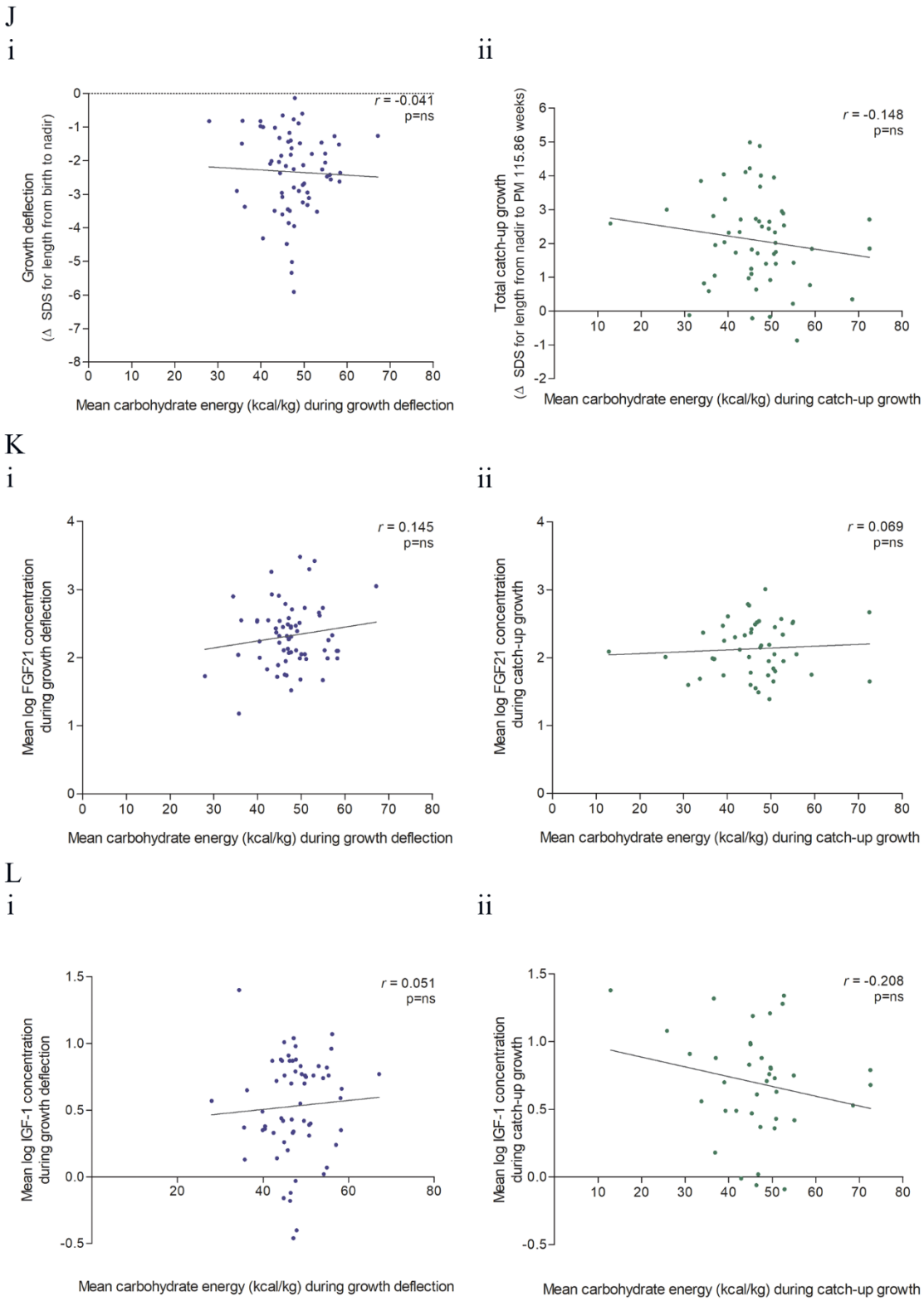

Figure 7.9 Hormonal levels and the magnitude of linear growth deflection or catch-up growth were not dependent on the availability of total, protein and carbohydrate energy. **(A) (i)** Growth deflection (Δ SDS for length from birth to nadir), **(ii)** Total catch-up (Δ SDS for length from nadir to PM 115.86 weeks) vs mean total energy (kcal/kg) during deflection/ catch-up growth. **(B)** Mean FGF21 (pg/ml), **(C)** Mean IGF-1 (ng/ml) vs mean total energy (kcal/kg) during **(i)** deflection and **(ii)** catch-up growth. **(D) (i)** Growth deflection (Δ SDS for length from birth to nadir), **(ii)** Total catch-up (Δ SDS for length from nadir to PM 115.86 weeks) vs mean fat energy (kcal/kg) during deflection/ catch-up growth. **(E)** Mean FGF21 (pg/ml), **(F)** Mean IGF-1

(ng/ml) vs mean fat energy (kcal/kg) during **(i)** deflection and **(ii)** catch-up growth. **(G) (i)** Growth deflection (Δ SDS for length from birth to nadir), **(ii)** Total catch-up (Δ SDS for length from nadir to PM 115.86 weeks) vs mean protein energy (kcal/kg) during deflection/ catch-up growth. **(H)** Mean FGF21 (pg/ml), **(I)** Mean IGF-1 (ng/ml) vs mean protein energy (kcal/kg) during **(i)** deflection and **(ii)** catch-up growth. **(J) (i)** Growth deflection (Δ SDS for length from birth to nadir), **(ii)** Total catch-up (Δ SDS for length from nadir to PM 115.86 weeks) vs mean carbohydrate energy (kcal/kg) during deflection/ catch-up growth. **(K)** Mean FGF21 (pg/ml), **(L)** Mean IGF-1 (ng/ml) vs mean carbohydrate energy (kcal/kg) during **(i)** deflection and **(ii)** catch-up growth. Pearson's R correlation (*r*) and *p* values were obtained from Bivariate correlation analyses.